

Investigation of the Combinations of Loading and Facet Joint Contributions in Lumbar Disc Herniation

By Bethany Kamitakahara

Masters Thesis

Supervisor: Associate Professor John Costi

*Submitted to the School of Computer Science, Engineering and Mathematics in the Faculty of
Science and Engineering in partial fulfilment of the requirements for the degree of Master of
Engineering (Biomedical) at Flinders University – Adelaide, Australia.*

Declaration

I certify that this work does not incorporate without acknowledgment any material previously submitted for a degree or diploma in any university; and that to the best of my knowledge and belief it does not contain any material previously published or written by another person except where due reference is made in the text.

Signed (October 2017)



Bethany Kamitakahara

Abstract

Intervertebral disc herniation can compress nerve roots, cause a localised inflammatory response and consequently lead to sciatica or low back pain (LBP). These conditions significantly decrease quality of life, limit activity and impose a large socio-economic burden on the individual and community (Duthey 2013). Disc herniations occur most frequently at the L4-L5 or L5-S1 disc levels in the postero-lateral region (Rajasekaran et al. 2013; Marshall & McGill 2010). Certain risk factors such as age, disc degeneration and sudden or repetitive mechanical loading can predispose the disc to herniation.

Numerous in vitro mechanical tests have been conducted in an attempt to characterise and simulate intervertebral disc herniation. Functional spinal units (FSUs) have been loaded under physiological conditions of fatigue loading or sudden overloading. Previous findings have clearly demonstrated that disc herniation can be achieved by fatigue or sudden overload in healthy, or mildly degenerated, discs (Adams & Hutton 1982). However, several studies have removed the facet joints during testing to improve visibility of the failure event (Wilke et al. 2016; Veres et al. 2010). The facet joints are imperative in restricting axial rotation, forward sliding and extension. Consequently, removing facet joints may compromise the physiological conditions that would be experienced in vivo. These studies have primarily focussed on characterising the specimen's mechanical properties at failure. To the author's knowledge, no work has been conducted to compare the six degree of freedom (6DOF) behaviour of the disc before and after a herniation event.

This study primarily aimed to develop a protocol to herniate sheep intact FSUs and isolated discs under varying directions of sudden overload in the hexapod robot and to investigate modes of failure between test groups. Twenty-nine sheep L4-L5 FSUs were used to model the human lumbar spine. Each specimen was rotated in flexion, lateral bending and axial rotation and loaded in compression at 6.67 mm/s. A 6DOF loading protocol was conducted to compare the mechanical properties of the specimens before and after the failure event.

Herniation was observed in 61.5% of intact FSUs, while 68.8% of isolated discs failed by nuclear extrusion and endplate-vertebral fracture. Two-way univariate ANOVAs revealed a significant difference in stress, modulus and toughness between intact and isolated discs. Evidently, the facet joints contribute significantly to an FSUs compressive stiffness and mechanical behaviour during failure. The findings also suggest that intact FSUs in lateral bending are least susceptible to injury in sudden overload, while combined flexion and lateral bending is the most at risk.

Acknowledgments

I would like to acknowledge and sincerely thank my supervisor, John Costi. Not only for his guidance and continual support throughout the course of the project, but for his enthusiasm and passion in my project and all things spine-related. I must also acknowledge Dhara Amin for her support, wealth of knowledge and sixth sense when working with the hexapod. I would also like to thank Michael Russo for his significant contribution, many early mornings and countless hours spent testing specimens in the hexapod. I would like to acknowledge Javad Tavakoli and Scott Maney for their assistance in the Biomechanics Laboratory. Finally, I'd like to thank my friends and family for their continual support throughout a stressful, challenging and rewarding year.

Table of Contents

Declaration.....	2
Abstract.....	3
Acknowledgments	4
Table of Figures.....	8
Table of Tables	10
1 Introduction.....	11
2 Functional Anatomy of the Lumbar Spine.....	13
2.1 Lumbar Vertebrae	13
2.2 The Intervertebral Disc.....	15
2.2.1 Nucleus Pulposus.....	16
2.2.2 Annulus Fibrosus	16
2.2.3 Vertebral Endplate	17
2.3 Muscles of the Lumbar Spine.....	17
2.4 Ligaments of the Lumbar Spine.....	18
2.5 Joints of the Lumbar Spine	19
2.6 Comparison of Sheep and Human Lumbar Anatomy	19
3 Biomechanics of the Intervertebral Disc.....	21
3.1 Biomechanical Properties	21
3.1.1 Non-Linearity	21
3.1.2 Time-Dependent Behaviour.....	22
3.1.2.1 Creep.....	23
3.1.2.2 Stress Relaxation	24
3.1.2.3 Hysteresis.....	25
3.1.2.4 Neutral Zone Theory.....	25
3.1.3 Anisotropy	26
3.2 Movement at the Intervertebral Disc	27
3.3 Biomechanics of the Sheep Lumbar Spine.....	29
4 Intervertebral Disc Herniation	30
4.1 Risk Factors of Intervertebral Disc Herniation.....	32
4.1.1 Ageing.....	32
4.1.2 Intervertebral Disc Degeneration.....	34

4.1.3	Mechanical and Occupational Hazards	36
4.2	Complications of Intervertebral Disc Herniation.....	37
4.2.1.1	Sciatica and Low Back Pain	38
5	Literature Review: In Vitro Mechanical Testing of the Intervertebral Disc	40
5.1	Testing Systems.....	40
5.2	Specimen Type.....	42
5.2.1	Age and Disc Degeneration	43
5.3	Mechanical Loading.....	44
5.3.1	Fatigue Loading	44
5.3.2	Sudden Overloading	50
5.3.3	Facet Joints in Mechanical Testing of the Disc	54
5.4	Mechanical Properties of a Herniated Disc.....	55
6	Project Aims & Hypotheses	56
6.1	Aims	56
6.2	Hypotheses	57
7	Methods.....	58
7.1	Specimen Preparation.....	59
7.2	Potting.....	61
7.3	Geometric Centre Measurements	62
7.4	Hydration & Preloading	62
7.5	Mechanical Testing.....	63
7.5.1	The Flinders University Hexapod Robot.....	63
7.5.2	Pilot Mechanical Testing	64
7.5.3	Mechanical Testing.....	68
7.6	Data Analysis	71
7.7	Assessing Failure Mode.....	72
8	Results	73
8.1	Hydration Data Analysis.....	73
8.2	Modes of Failure	74
8.2.1	Herniation	75
8.2.2	Endplate-Vertebral Shear Fracture	77
8.2.3	Vertebral Damage.....	77
8.2.4	No Damage	78
8.2.5	Mode of Failure and Mechanical Behaviour Comparisons	78
8.3	Loading Direction Mechanical Behaviour Comparisons.....	81

8.3.1	Stress-Strain Curves.....	81
8.3.2	Stress.....	85
8.3.3	Strain.....	86
8.3.4	Modulus.....	87
8.3.5	Toughness.....	88
9	Discussion	90
9.1	Limitations	90
9.2	Physiological Conditions in the Hexapod.....	91
9.3	Modes of Failure.....	92
9.4	Effect of FSU Type and Loading Direction.....	94
10	Conclusions.....	97
10.1	Future Work.....	97
11	References.....	99
12	Appendices.....	104
12.1	Appendix 1: Sheep Sudden Overload Protocol	104
12.2	Appendix 2: Geometric Centre Data Sheet.....	110
12.3	Appendix 3: Pilot Testing Results.....	114
12.4	Appendix 4: Matlab Code.....	121
12.5	Appendix 5: Assessing Modes of Failure.....	128
12.6	Appendix 6: Specimen Results	129
12.7	Appendix 7: Results Summary.....	232
12.8	Appendix 8: Modes of Failure Statistics.....	234
12.9	Appendix 9: Failure Parameters Statistics.....	235

Table of Figures

Figure 1. Right lateral view of the vertebrae of the lumbar spine	13
Figure 2. Lateral and superior view of vertebral anatomy	14
Figure 3. Trabecular bone arrangement of vertebral body	14
Figure 4. Transverse and coronal images of the anatomy of the intervertebral disc	15
Figure 5. Annulus fibrosus lamellae orientation.....	16
Figure 6. Medial sagittal section of lumbar spine illustrating ligaments.....	18
Figure 7. Posterior illustration of the facet joints.....	19
Figure 8. Right lateral view of FSU.....	21
Figure 9. Typical stress-strain curve for collagen-rich material.....	22
Figure 10. Creep response of viscoelastic materials.....	23
Figure 11. Stress relaxation response.....	24
Figure 12. Hysteresis curve where energy is lost with loading and unloading cycles.....	25
Figure 13. Load-deformation curve illustrating the neutral and elastic zones.....	26
Figure 14. 6DOF behaviour of lumbar intervertebral disc FSU	26
Figure 15. Illustration of the orientation of the vertebral axes and 6DOF movement.....	27
Figure 16. Load carrying capacity of the intervertebral disc in compression.....	28
Figure 17. Bending of lumbar FSU.....	28
Figure 18. Axial Rotation of the Lumbar FSU.....	29
Figure 19. Histological sections and diagrams of a healthy disc and in states of failure	31
Figure 20. Types of herniation.....	32
Figure 21. Comparison of young and old human lumbar intervertebral discs.....	33
Figure 22. Sagittal sections of disc degeneration.....	34
Figure 23. Illustration of three types of annular tears.....	35
Figure 24. Stress concentrations across the mid-sagittal distance of the disc.....	36
Figure 25. Comparison of occupational hazards associated to herniation.....	37
Figure 26. Image of dermatomes innervated by spinal nerves in the human body.....	38
Figure 27. Custom built rig for mechanical testing of the intervertebral disc.....	41
Figure 28. Load-displacement curve for three FSUs.....	51
Figure 29. Effect of rate of pressurisation on mode of failure.....	52
Figure 30. Flow chart summarising the main steps involved in the protocol.....	58
Figure 31. Image of sheep lumbar spine before dissection.....	59

Figure 32. Image of dissected sheep lumbar spine (L1-L6)	59
Figure 33. Lateral view of FSU.	60
Figure 34. Image of intact FSU taken from five views.....	60
Figure 35. Image of isolated disc taken from five views.....	61
Figure 36. Image of potting alignment rig and attached base cup.....	61
Figure 37. Image of the hexapod robot with a specimen mounted on X-Y table.....	63
Figure 38. Left posterior view of SSO4 herniation in flexion and lateral bending.	66
Figure 39. Images of inferior vertebral fracture in pilot test FSUs.....	66
Figure 40. Plot of x, y and z-axis forces recorded for specimen SSO3 during failure.....	67
Figure 41. Image of the X-Y table.....	68
Figure 42. Plot of force the in x, y and z-axes for specimen SO12 with the X-Y table.	68
Figure 43. Example of LVDT hydration equilibrium (SSO6).....	73
Figure 44. Left postero-lateral herniation in lateral bend (SO6).	75
Figure 45. Posterior view of inferior endplate-vertebra fracture	75
Figure 46. View of the inferior endplate of superior vertebra failed at endplate-vertebra	76
Figure 47. Images of endplate-vertebral failure (arrows) on left side	76
Figure 48. Image of SO23 failed at inferior endplate-vertebral interface.....	77
Figure 49. Image of vertebral fracture	78
Figure 50. Anterior (a) and posterior (b) images of an intact FSU (SO5).....	78
Figure 51. Comparison of load-displacement curves between intact and isolated discs.	80
Figure 52. Stress-strain curves for intact FSUs in flexion.....	81
Figure 53. Stress-strain curves for isolated discs in flexion	82
Figure 54. Stress-strain curves for intact FSUs in lateral bend.....	82
Figure 55. Stress-strain curves for isolated discs in lateral bend.....	83
Figure 56. Stress-strain curves for intact FSUs in flexion and lateral bend	83
Figure 57. Stress-strain curves for isolated discs in flexion and lateral bend.....	84
Figure 58. Stress-strain curves for intact FSUs in lateral bend and axial rotation.....	84
Figure 59. Stress-strain curves for isolated discs in lateral bend and axial rotation.....	85
Figure 60. Bar graph of average stress at failure in intact and isolated discs.....	85
Figure 61. Bar graph of average stress between directions of loading.....	86
Figure 62. Bar graph comparing average maximum strain at failure between groups.	87
Figure 63. Bar graph of average modulus at between intact and isolated discs.	87
Figure 64. Bar graph of average modulus between directions of loading.	88
Figure 65. Bar graph of average toughness between intact and isolated discs.....	89

Table of Tables

Table 1. Range of motion of each DOF29

Table 2. Comparison of fatigue loading studies49

Table 3. Comparison of fatigue loading studies.53

Table 4. Pilot testing parameters, aims and observations.65

Table 5. Identification of testing groups by combinations of loading70

Table 6. Load cell limits70

Table 7. Classifications of failure modes.....72

Table 8. Summary of failure modes by specimen group and direction of loading.....74

Table 9. Average load, moment, stress, strain, modulus and toughness by group79

1 Introduction

The intervertebral disc is an essential structure within the spine that fundamentally acts to transfer loads and enable movement of the vertebrae. This tissue is composed of the nucleus pulposus, annulus fibrosus and vertebral endplates, which ultimately provide the disc with unique viscoelastic and anisotropic properties. Certain risk factors such as age, disc degeneration and sudden or repetitive mechanical loading can predispose the disc to intervertebral disc herniation, or the '*displacement of disc material beyond the limits of the intervertebral disc space*' (Fardon et al. 2014). *In vitro*, herniations occur most frequently in discs aged 40 – 50 years at the L4-L5 or L5-S1 disc levels in the postero-lateral region (Adams & Hutton 1982). Extruded disc material can subsequently compress nerve roots, trigger an inflammatory response and result in symptoms of LBP or sciatica. Sciatica and LBP significantly decrease quality of life, limit activity and impose a large socio-economic burden on the individual and the community (Duthey 2013).

Extensive research has been conducted to characterise factors involved in intervertebral disc herniation. *In vitro* mechanical loading of FSUs has attempted to simulate physiological conditions present in repetitive lifting tasks (i.e. fatigue) or conditions experienced by the disc at a sudden and high rate of loading (i.e. sudden overload). Previous work has proven that fatigue or sudden overload can effectively cause herniation by annular rupture or annular-endplate junction failure in young and mildly degenerated discs (Wade et al. 2014; Wade et al. 2015; Adams & Hutton 1982). Despite the facet joints significant role in restricting certain movements, several studies have removed the posterior elements prior to mechanical testing. It is unknown whether removing these joints compromises the physiological conditions that would be experienced *in vivo* during intervertebral disc herniation. To the author's knowledge, there is little knowledge on the 6DOF mechanical properties of the disc before and after herniation.

This study primarily aimed to develop a protocol to herniate sheep intact FSUs and isolated discs under several directions of sudden overload in the hexapod robot for the first time and subsequently, investigate modes of failure between test groups.

Chapter 2 provides a brief overview of the vertebral and soft tissue anatomy of the lumbar spine, with a specific focus on the microstructure and functional anatomy of the intervertebral disc in humans and sheep.

Chapter 3 describes how the intervertebral disc structure relates to its time-dependent and anisotropic biomechanical function in humans and sheep.

Intervertebral disc herniation is defined in chapter 4. The pathogenesis, associated risk factors and the consequent symptoms are also briefly described.

Chapter 5 provides a detailed analysis and review of previous literature on in vitro mechanical simulation of intervertebral disc herniation by fatigue and sudden overload. This chapter establishes the primary reasoning for undertaking this project.

Chapter 6 outlines the primary objectives and hypotheses of the project.

The methods of the project have been described in chapter 7 and includes a brief description of the hexapod robot, specimen preparation, potting, hydration, pilot testing, mechanical testing, data analysis and assessing failure modes.

Chapter 8 presents the main findings and results of the project. Mechanical parameters used to assess mode of failure include stress, strain, modulus and toughness.

Chapter 9 discusses the results; identifying comparisons with previous research and trends between intact and isolated discs in different directions of loading.

Finally, chapter 10 summarises the main findings of the study and identifies areas requiring further work.

2 Functional Anatomy of the Lumbar Spine

The vertebral column is comprised of 33 vertebrae, which can be classified by region from superior to inferior as cervical, thoracic, lumbar, sacral and coccyx. The human lumbar region, or lower back, includes five vertebrae that connect proximally to the thoracic spine and distally to the sacrum. These vertebrae are named numerically superiorly to inferiorly as L1, L2, L3, L4, L5 (Figure 1).

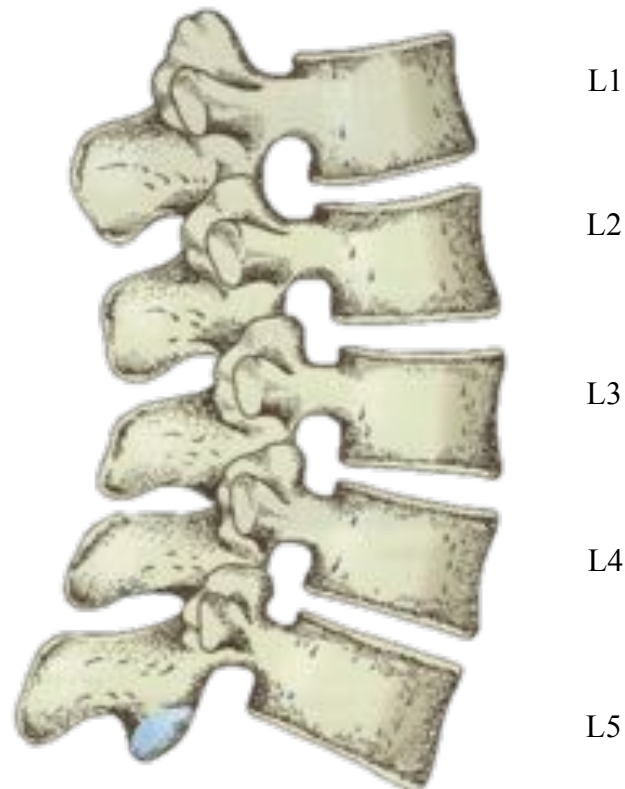


Figure 1. Right lateral view of the vertebrae of the lumbar spine (Adams et al. 2013)

Adjacent lumbar vertebrae are adjoined by an intervertebral disc, ligaments, muscles and joints. These structures ultimately provide the vertebral column with rigidity, mobility, protection of the spinal canal and resistance to compressive loads (Adams et al. 2013).

2.1 Lumbar Vertebrae

The lumbar vertebrae are irregular bones comprised of an anterior vertebral body and posterior elements separated by pedicles (Figure 2).

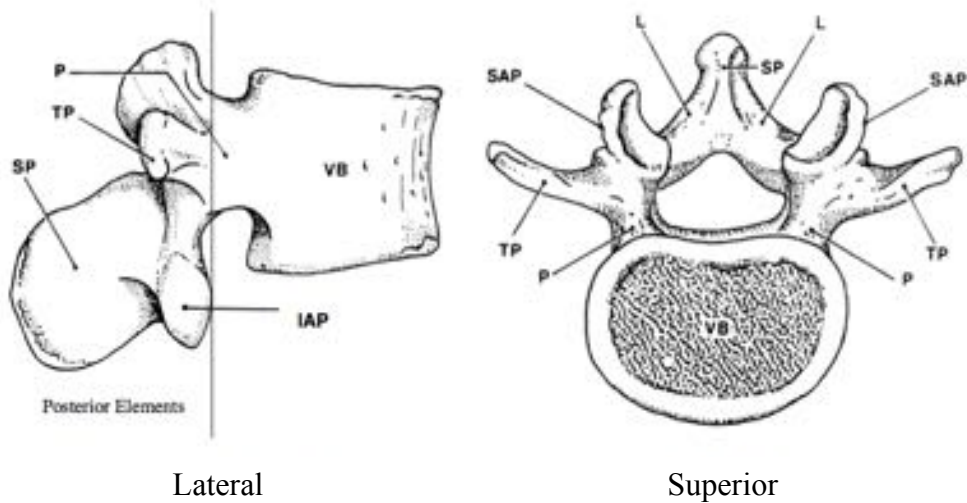


Figure 2. Lateral and superior view of vertebral anatomy, P: pedicle, VB: vertebral body, TP: Transverse process, SP: Spinous process, SAP: Superior articular process, IAP: Inferior articular process, L: Lamina (Adams et al. 2013).

The vertebral body is primarily involved in withstanding compressive loads. It consists of an inner cancellous cavity surrounded by a shell of cortical bone. The internal structure of the cancellous bone is arranged in vertical and transverse trabeculae, which provides the vertebrae with a strong, yet lightweight load-bearing structure (Figure 3).

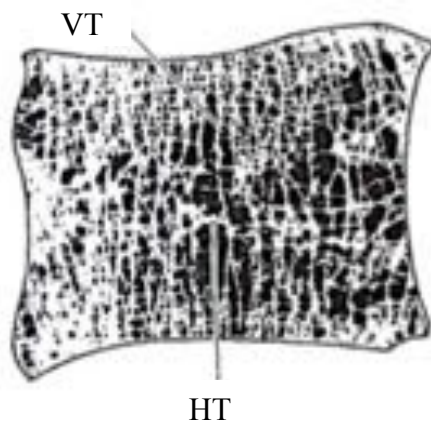


Figure 3. Trabecular bone arrangement of vertebral body, VT: vertical trabecula, HT: horizontal trabecula (Bogduk 1997).

The posterior elements of a vertebra include the laminae, the superior and inferior articular processes, the spinous processes and the left and right transverse processes. The laminae transmit force between the posterior elements and the vertebral body, joined at a central midline (Adams et al. 2013). At this

junction, the spinous process projects dorsally. The left and right transverse processes project laterally from the pedicles, which also have accessory processes projecting from their posterior surface (Adams et al. 2013). These processes act as sites of attachment for muscles that control movement of the lumbar vertebral column. The laminae also give rise to left and right superior and inferior articular processes. The superior articular processes articulate with the inferior articular processes forming the facet joints. Finally, the pedicles are small regions of bone that connect the posterior elements to the vertebral bodies (Adams et al. 2013). Therefore, all forces sustained by the posterior elements are transmitted to the vertebral body via the pedicles, and vice versa. The pedicles, laminae and posterior surface of the vertebral body enclose the spinal canal, which contains and protects the spinal cord (Adams et al. 2013).

2.2 The Intervertebral Disc

The intervertebral disc is a strong yet deformable soft tissue that separates and binds adjacent vertebral bodies. The intervertebral disc enables rocking movement of the vertebrae and plays a significant role in sustaining and transferring compressive loads in the spine. The disc is composed of three distinct tissues including the central nucleus pulposus, peripheral annulus fibrosus and superior and inferior vertebral endplates as illustrated in Figure 4. The composition and microstructure of these tissues ultimately provide the intervertebral disc with its unique mechanical and functional properties.

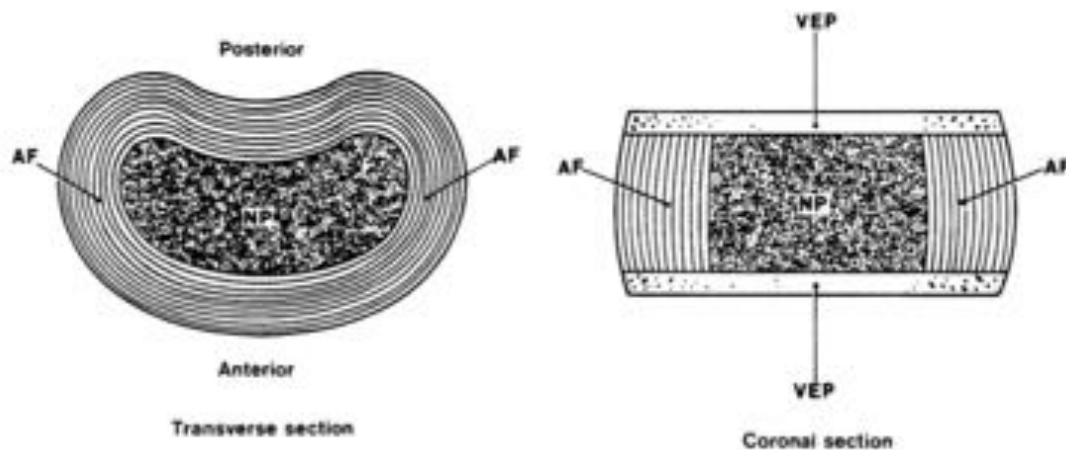


Figure 4. Transverse and coronal images of the anatomy of the intervertebral disc, AF: annulus fibrosus, NP: nucleus pulposus, VEP: vertebral endplate (Adams et al. 2013).

2.2.1 Nucleus Pulposus

The nucleus pulposus is the gelatinous core of the intervertebral disc and is composed primarily of water, proteoglycans and collagen. These components ultimately enable the nucleus to support mechanical loads through hydrostatic pressure. Water constitutes approximately 70-90% of the intervertebral disc's total weight, which varies significantly with age, degeneration and loading (Adams & Hutton 1983; Kraemer et al. 1985). Proteoglycans are very large molecules that contribute approximately 30-50% of the dry weight (Adams & Muir 1976). Proteoglycans play a significant role within the nucleus due to their strong electrostatic attraction to water. Therefore, a linear correlation exists between proteoglycan content and osmotic swelling pressure such that the disc is kept hydrated. Finally, collagen also contributes to the composition of the nucleus pulposus at approximately 20% of the dry weight (Eyre & Muir 1976). Collagen type II is the most abundant collagen present in the nucleus, followed by collagen type I.

2.2.2 Annulus Fibrosus

The annulus fibrosus is made up of 15-25 concentric lamellae around the nucleus pulposus (Marchand & Ahmed 1990). Each lamella is comprised of parallel type I collagen fibres, which are arranged obliquely at an angle of approximately 45-65° from the spine's longitudinal axis (Hickey & Hukins 1980). The orientation of consecutive lamellae alternates from positive to negative with respect to the longitudinal axis (Figure 5).

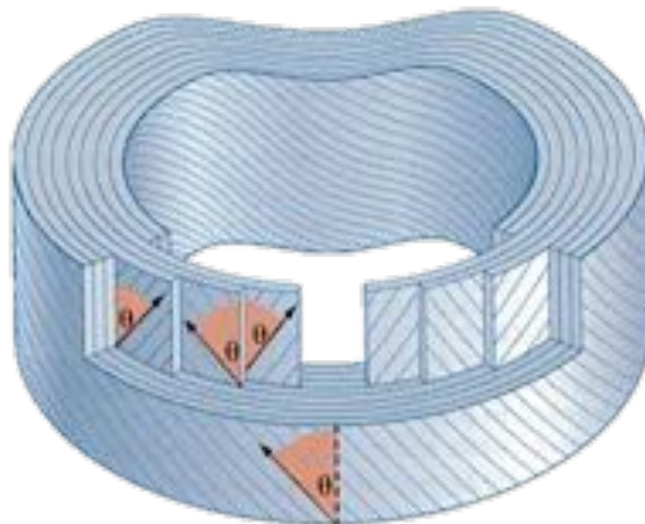


Figure 5. Annulus fibrosus lamellae orientation. Collagen fibres are organised in concentric lamellae, where the orientation or angle of fibres (θ) alternates with each lamella (Adams et al. 2013).

This arrangement of fibres provides the annulus with anisotropic properties. Similar to the nucleus pulposus, water is the most abundant component in the annulus, contributing approximately 60-80% of the weight (Kraemer et al. 1985). The annulus has a much larger proportion of collagen fibres in comparison to the nucleus, making up about 70% of the dry weight (Eyre & Muir 1976). A gradient of collagen exists within the annulus fibrosus such that type I collagen content increases from inner to outer annulus, while type II collagen decreases (Eyre & Muir 1976). This change in collagen distribution reflects the mechanical role of the tissue, where the outer annulus withstands tension, while the inner annulus exhibits behaviour more closely associated to the nucleus under compression. Finally, proteoglycans contribute approximately 10% of the dry weight. Similar to collagen type II, the relative content increases from outer annulus to inner, which also reflects water content at 60% outer to 80% inner annulus (Eyre & Muir 1976).

2.2.3 Vertebral Endplate

The endplates are thin layers of cartilage that provide an interface between the vertebral bodies and the intervertebral disc. The endplates are made up of hyaline cartilage and thus, have a high collagen type II (60-80% dry weight) content, proteoglycans (17% dry weight) and water (58% wet weight) (Roberts et al. 1989). The endplates are porous to facilitate the exchange of nutrients, waste products and other metabolites from the vertebral bodies to the avascular disc.

2.3 Muscles of the Lumbar Spine

The vertebral muscles stabilise and enable movement, while also exerting a compressive force on the lumbar spine. The activation of these muscles also exerts a significant compressive force on the lumbar spine. The major muscles that contribute to movements of flexion/extension, right/left axial rotation and right/left lateral bending have been briefly outlined.

❖ Flexion/Extension:

Little muscle innervation is required to produce flexion of the lumbar spine. Flexion can be caused by gravity, relaxation of extensor muscles of the spine and indirectly through contraction of psoas major and rectus abdominis (Adams et al. 2013). The posterior muscles of the lumbar spine include multifidus, longissimus thoracis and iliocostalis lumborum and are involved in extension (Adams et al. 2013).

❖ Left/Right Lateral Bending:

Unilateral contraction of right or left longissimus thoracis contributes to lateral bending of the lumbar spine. Lateral bending is also generated by contraction of the iliocostalis lumborum and quadratus lumborum (Adams et al. 2013).

❖ Left/Right Axial Rotation:

Axial rotation of the lumbar spine is a relatively passive process caused by movement of the thorax. The obliquus externus, obliquus internus and iliocostalis lumborum muscles may contribute to axial rotation (Adams et al. 2013).

2.4 Ligaments of the Lumbar Spine

Fundamentally, ligaments act to limit and stabilise a joint's range of motion. There are five ligaments of the lumbar spine including the anterior longitudinal ligament, posterior longitudinal ligament, ligamentum flavum, interspinous ligaments and supraspinous ligaments (Adams et al. 2013) (Figure 6). These ligaments fundamentally act to limit and stabilise the joints in the lumbar spine.

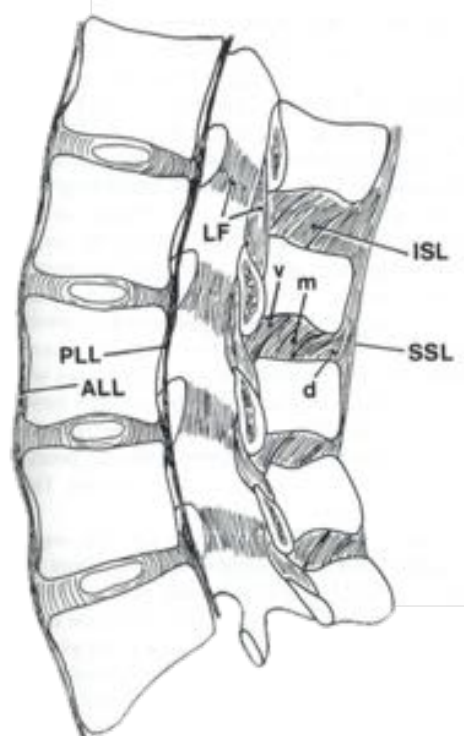


Figure 6. Medial sagittal section of lumbar spine illustrating ligaments. PLL: posterior longitudinal ligament, ALL: Anterior longitudinal ligament, LF: ligamentum flavum, ISL: interspinous ligament, SSL: supraspinous ligament, v: ventral, m: middle, d: dorsal (Adams et al. 2002).

This study only looks at the mechanical involvement of the anterior and posterior longitudinal ligaments in loading, where the ligamentum flavum, interspinous ligament and supraspinous ligaments are removed in both the intact FSUs and isolated discs. The anterior longitudinal ligament attaches to the anterior surface of all vertebral bodies and intervertebral discs (Adams et al. 2013). This ligament acts to limit anterior separation of vertebral bodies during extension. Conversely, the posterior longitudinal ligament extends over the posterior surface of the vertebral bodies and discs, restricting flexion of the spine (Adams et al. 2013).

2.5 Joints of the Lumbar Spine

Each motion segment has one anterior joint and two posterior joints. Anteriorly, the disc connects two adjacent vertebral bodies and acts as a limited range universal joint that can move in 6DOFs. Posteriorly, there are two synovial plane joints between the superior and inferior articular processes that are interchangeably known as zygapophysial joints, apophysial joints or facet joints (Figure 7). These facet joints provide an important locking mechanism between adjacent vertebrae, limiting axial rotation, extension and forward sliding (Adams et al. 2013).

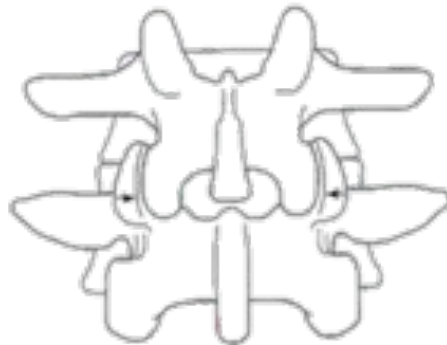


Figure 7. Posterior illustration of the facet joints. Arrows indicating the left and right facet joints between superior and inferior articular processes (Adams et al. 2002).

2.6 Comparison of Sheep and Human Lumbar Anatomy

Cadaver tissue is difficult to obtain, expensive and can be complicated by significant biological variability between gender, genetics, disease and age. Therefore, the mechanical tests in this thesis have used sheep lumbar spines to model the human spine. Human and sheep lumbar spines share similar gross anatomical structure. The most significant differences between these species can be found in the number of lumbar vertebrae, geometry of vertebrae and discs, bone mineral density, curvature of the spine and loading patterns.

Sheep spines have 6-7 lumbar vertebrae, while humans have only 5 (Wilke et al. 1997a). The lumbar vertebrae and intervertebral discs are much smaller in sheep in comparison to human spines. Wilke et al. (1997a) also found that the human vertebra is typically wider than tall, while sheep vertebrae are taller than they are wide. However, both sheep and human vertebra width is greater than depth, such that the vertebral bodies and discs share a characteristically oval shape (Wilke et al. 1997a). Finally, the anterior disc height in sheep lumbar spines is significantly less than in humans (Wilke et al. 1997a).

Sheep and human lumbar spines share similar biochemical composition. Water content of the nucleus pulposus is approximately 80-86% in sheep (Leahy & Hukins 2001; Reid et al. 2002) and 83% in healthy human discs (Lyons et al. 1981). The collagen content in the outer annulus is also very similar between sheep and humans at 30% (Reid et al. 2002) and 33% (Lyons et al. 1981), respectively. Bone mineral density can be up to four times higher in sheep lumbar vertebrae in comparison to humans (Alini et al. 2008). This significant difference in bone density may be attributed to the fact that sheep are quadrupeds, while humans are bipeds. The curvature of the lumbar spine also differs between these species, where sheep spines are kyphotic and human spines exhibit lumbar lordosis (Wilke et al. 1997a). However, it was reported that the quadruped spine is mainly loaded along its long axis, similar to that of humans (Smit 2002).

Despite small disparities in anatomy; the gross anatomical structure and composition of the intervertebral discs in sheep are comparable to those of humans. Furthermore, sheep represent an appropriate model for the human lumbar spine. This chapter has provided a brief overview of the anatomy of the human and sheep lumbar spines. The structure of the lumbar spine is closely linked to its function. The unique microstructure of the intervertebral disc ultimately gives rise to its biomechanical properties.

3 Biomechanics of the Intervertebral Disc

A functional spinal unit, or motion segment, is the smallest physiological motion unit of the spine and thus, exhibits movement in 6DOFs and biomechanical properties similar to that of the lumbar spine. Therefore, the mechanical properties of the FSU will be considered representative of the lumbar spine. An FSU includes the two adjacent vertebrae, the intervening intervertebral disc and the anterior and posterior longitudinal ligaments (Figure 8).

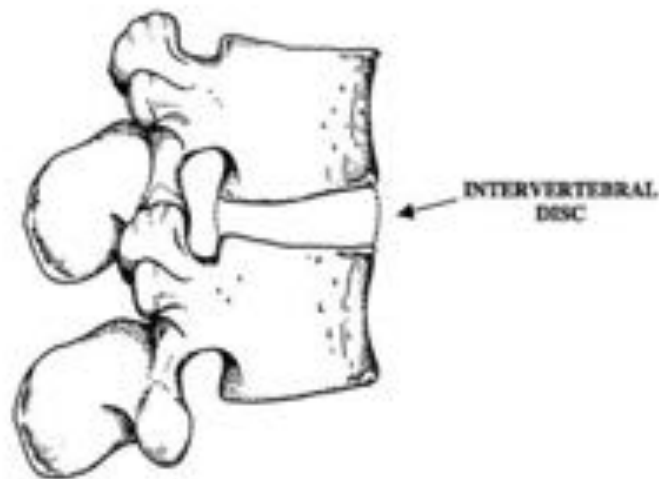


Figure 8. Right lateral view of FSU (Thompson 2002).

3.1 Biomechanical Properties

The intervertebral disc is a complex tissue that exhibits elastic, non-linear, anisotropic, biphasic and viscoelastic behaviour. Having a thorough understanding of these mechanical properties is essential in assessing the aetiology of injury and disease in response to loading.

3.1.1 Non-Linearity

The intervertebral disc is a collagenous tissue. Collagen-rich tissues are mechanically strong and organised into hierarchical structures, which provides these tissues with high stiffness and non-linear behaviour (Korhonen & Saarakkala 2011). These mechanical properties can be presented in a stress-strain curve, which illustrates the strain induced in a material when a stress is applied. The stress-strain curve of a collagenous structure, such as the intervertebral disc, exhibits distinct behaviour across four regions 1) toe region 2) elastic region 3) plastic region 4) failure region (Figure 9).

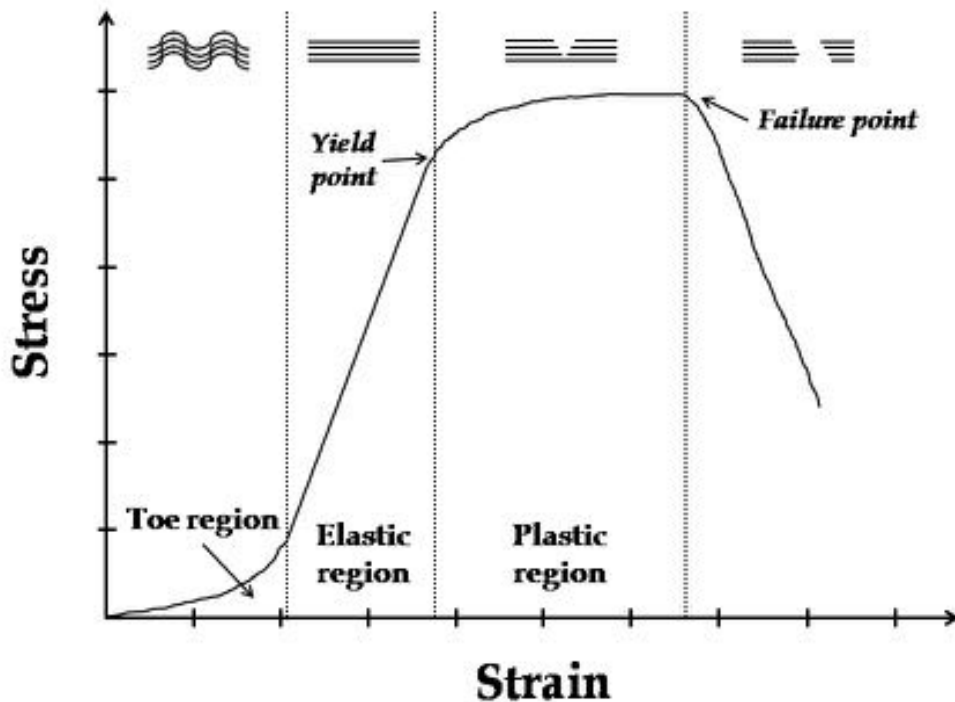


Figure 9. Typical stress-strain curve for collagen-rich material. The curve is divided into the toe region, elastic region, plastic region and failure with illustrations of the collagen fibre behaviour in each region (Korhonen & Saarakkala 2011).

The initial toe region is a non-linear region that represents the alignment and straightening of the crimped collagen fibres at low strains (Park & Lakes 2007). This is followed by a stiffer, elastic region where the fibres are strained and there is a linear relationship between stress and strain. The slope of the linear region is known as the modulus of elasticity and is directly proportional to the stiffness of the material. The end of the elastic region occurs when the yield point is reached and deformation is no longer reversible. In the plastic region, collagen fibres may begin to fail and consequently, become permanently deformed. Finally, if continued stress is applied, the material reaches a failure point and catastrophic irreversible failure occurs (Park & Lakes 2007).

3.1.2 Time-Dependent Behaviour

The intervertebral disc also exhibits time-dependent properties. Varying the rate of loading will ultimately influence the mechanical properties of the tissue. This time-dependent nature of the disc is fundamentally due to its viscoelastic and poroelastic nature (Cohen et al. 1976). A viscoelastic response is where the relationship between stress and strain depends on time. In such cases, the stiffness depends on the rate of loading. At high rates of loading, a viscoelastic material acts like a viscoelastic fluid with high stiffness, while low rates of loading will cause the material to act like a viscoelastic solid with lower stiffness.

The intervertebral disc exhibits these time-dependent viscoelastic properties as it is a poroelastic biphasic material (Costi et al. 2008). A biphasic material has a porous solid phase, which is permeable to the fluid phase. Therefore, when loaded, the solid phase is immediately deformed, increasing pore pressure and driving fluid through the solid phase to regions of lower pressure. However, there may be drag between the fluid and solid phase, resulting in slow fluid movement and the continual deformation of the disc until pressure equilibrium is reached. Therefore, high rates of loading do not allow enough time for the fluid to diffuse and consequently, the solid phase withstands the load. Conversely, a slow rate of loading will allow the fluid to diffuse out of the solid. Furthermore, viscoelastic materials such as the intervertebral disc, typically exhibit creep, stress relaxation and hysteresis.

3.1.2.1 Creep

Creep has been defined as the slow, progressive deformation of a material under constant stress until equilibrium is reached (Twomey & Taylor 1982). When the load is removed, the material will exhibit creep recovery, whereby the strain is gradually reduced to its original value (Figure 10). Creep and creep recovery play a significant role in the diurnal variation in human stature.

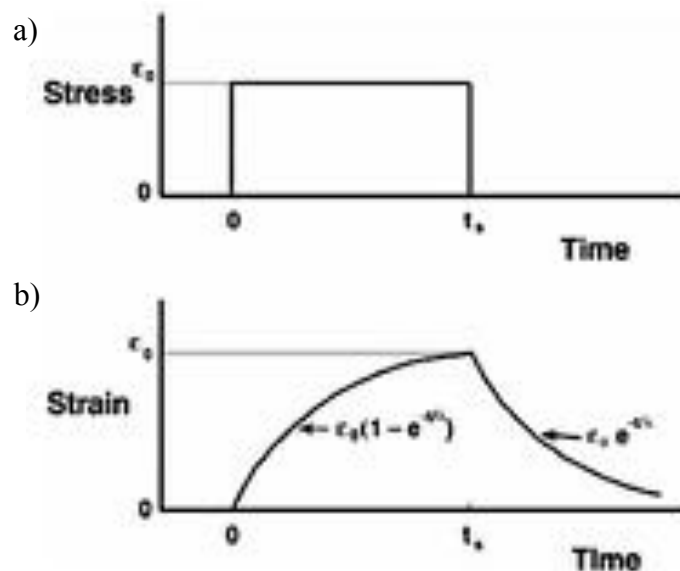


Figure 10. Creep response of viscoelastic materials (a) stress is applied (b) gradual increase in strain (ϵ_0) until stress is removed at t_s (Park & Lakes 2007)

3.1.2.1.1 Diurnal Variation

Throughout the day, the intervertebral disc is exposed to varying compressive forces, which result in radial bulging and loss of water content and disc height (Adams et al. 1987). Decreased disc height can be attributed to both the elastic and time-dependent properties of the disc. Under a compressive load, the collagen fibres in the lamellae of the annulus have an elastic response, which enables the annulus to bulge outwards, reducing disc height. The compressive load also overcomes the hydrostatic pressure in the nucleus, forcing water out of the disc. As a result, the disc experiences creep, decreased disc height and reduced stature. Removal of this compressive force when supine decreases the hydrostatic pressure in the nucleus, enabling water to travel back into the disc, restoring disc height (Adams et al. 1987). Ultimately, creep causes water content of the nucleus to vary diurnally by 20% where it is highest in the morning after rest and lowest following day-time activity (Botsford et al. 1994). This diurnal variation in water content of the nucleus has led to the postulation that lumbar discs are at greater risk of injury in the morning due to higher hydrostatic pressure (Adams et al. 1987; Adams et al. 1990).

3.1.2.2 Stress Relaxation

As the intervertebral disc is a viscoelastic material, it exhibits stress relaxation. Stress relaxation occurs when a constant strain is applied and the resultant stress decreases with time until equilibrium is reached (Figure 11). At this point of equilibrium, stress becomes constant.

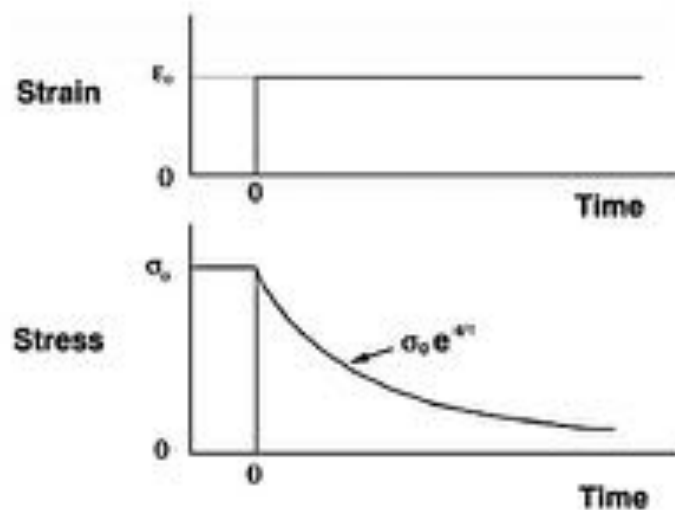


Figure 11. Stress relaxation response(a) constant strain (ϵ_0) applied (b) resultant stress (σ_0) decreasing with time (t) (Park & Lakes 2007)

3.1.2.3 Hysteresis

Due to the viscoelastic behaviour of the intervertebral disc, the loading and unloading stress-strain curves do not follow the same path. When a disc is loaded, it stores energy to be able to return to its original state. The amount of energy stored is equivalent to energy required to displace the disc. When unloaded, the disc experiences creep relaxation and disc height is restored. However, the energy required to restore the disc to its original shape is less than that required to displace it, and thus, there is energy lost. The difference between the loading and unloading curves represents the amount of energy lost and is known as 'hysteresis' (Figure 12).

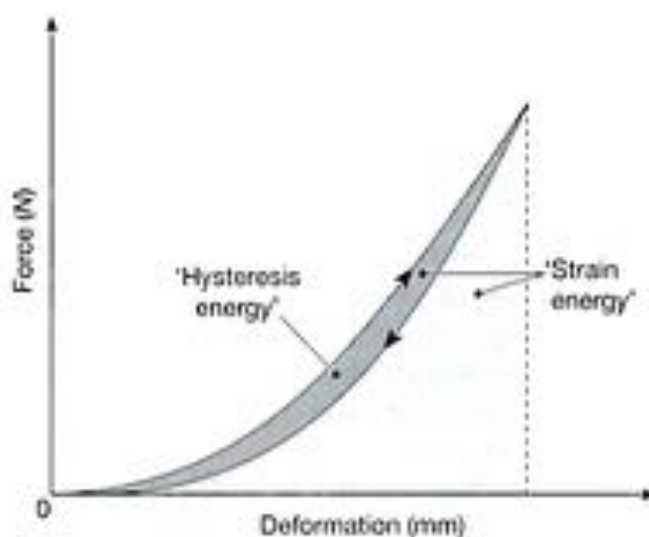


Figure 12. Hysteresis curve where energy is lost with loading and unloading cycles (Adams et al. 2002).

3.1.2.4 Neutral Zone Theory

It has been suggested that many studies have minimised the viscoelastic effect of the spine to achieve more repeatable results (Panjabi 1992). Consequently, the initial non-linear region of the load-displacement curve has not been included and the output appears as just the linear elastic region of the curve. However, it is believed that this non-linear region is of clinical importance as it may indicate spinal instability (Panjabi 1992). Therefore, Panjabi (1992) proposed the 'neutral zone' theory, which suggests that the range of motion of the spine can be divided into a neutral zone and an elastic zone. The neutral zone represents the spinal range of motion near the neutral position, where there is little resistance to movement (Oxland & Panjabi 1992; Panjabi 1992). The end of the neutral zone indicates the start of the elastic zone. Panjabi (1992) defines the elastic zone as the range of spinal motion that is produced against significant resistance (Figure 13).

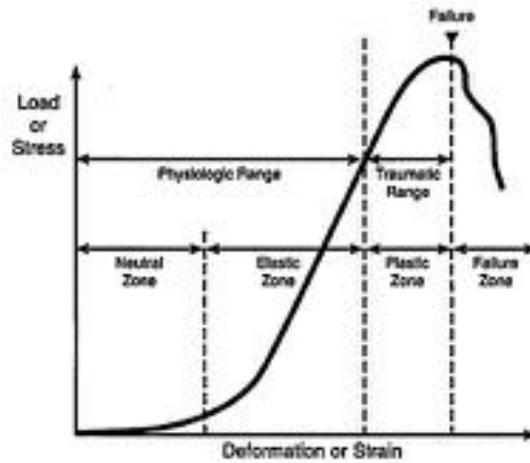


Figure 13. Load-deformation curve illustrating the neutral and elastic zones (Panjabi 1992)

3.1.3 Anisotropy

The intervertebral disc exhibits anisotropic, or direction-dependent behaviour. It has been suggested that compression, flexion and lateral bending generates an internal pressure gradient, fluid flow and poroelastic behaviour of the disc, while there is little change in volume of the disc in directions of axial rotation, anterior-posterior shear and lateral shear (Costi et al. 2008). Costi et al. (2008) conducted a 6DOF test at four frequencies and demonstrated different stiffness of the disc for different directions of loading (Figure 14).

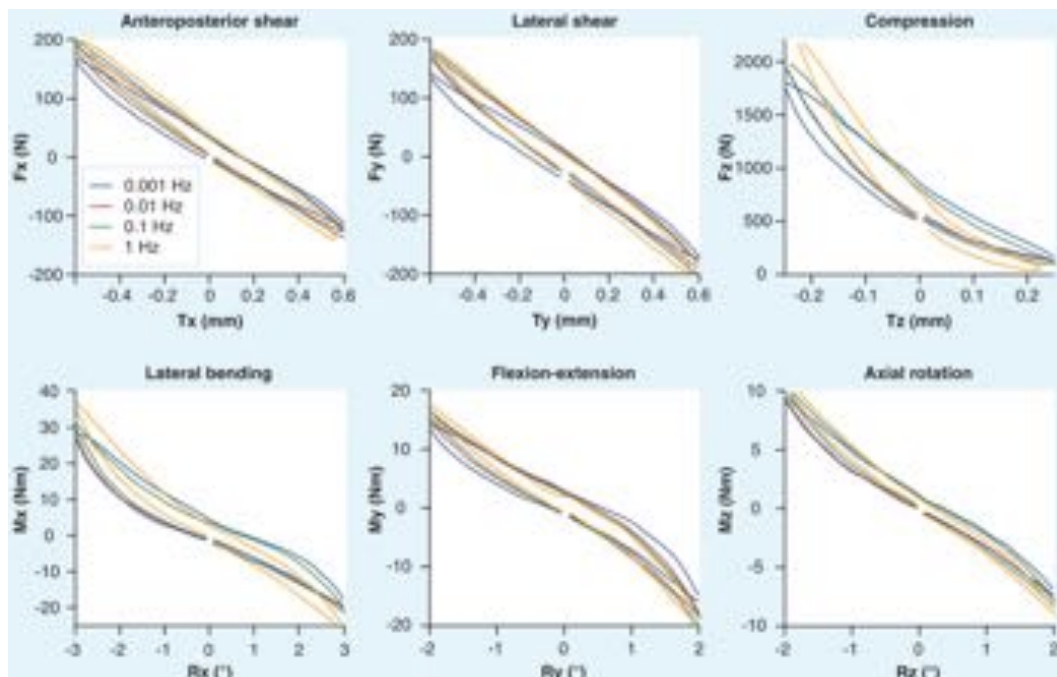


Figure 14. 6DOF behaviour of lumbar intervertebral disc FSU at 0.001 Hz, 0.01 Hz, 0.1 Hz and 1 Hz illustrating frequency and direction dependent behaviour (Costi et al. 2008).

3.2 Movement at the Intervertebral Disc

The lumbar spine is able to move in 6DOFs about three axes (x-axis, y-axis, z-axis) in translation and rotation. These movements include right/left shear (negative/positive x-axis translation), anterior/posterior shear (positive/negative z-axis translation), compression and tension (negative/positive y-axis translation), flexion/extension (positive/negative x-axis rotation), right/left lateral bending (positive/negative z-axis rotation) and right/left axial rotation (negative/positive y-axis rotation) (Figure 15).

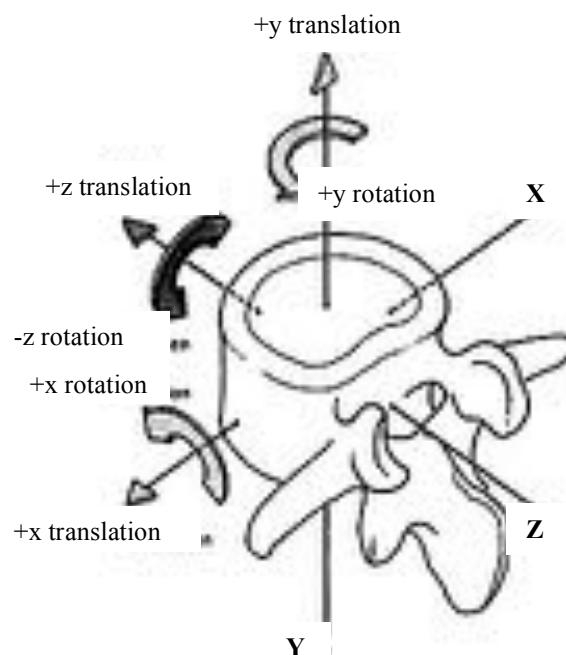


Figure 15. Illustration of the orientation of the vertebral axes and 6DOF movement (Bogduk 1997).

The unique microstructure of the intervertebral disc enables it to carry various types of physiological loads, while also allowing movement. These physiological loads fundamentally employ the intervertebral disc in compression and in tension. When a compressive load is applied, it is transmitted between adjacent vertebrae via the intervertebral disc. A compressive load increases intradiscal pressure in the nucleus, causing it to expand radially and exert a force on the annulus and endplates (Adams et al. 2013). This outward force causes radial bulging of the annulus, consequently stretching the lamellae collagen fibres in tension. Similarly, the outward force from the nucleus deforms the endplates such that the compressive load is transmitted to the adjacent vertebra (Adams et al. 2013). Therefore, the annulus acts to contain the nucleus pulposus in compression (Figure 16).

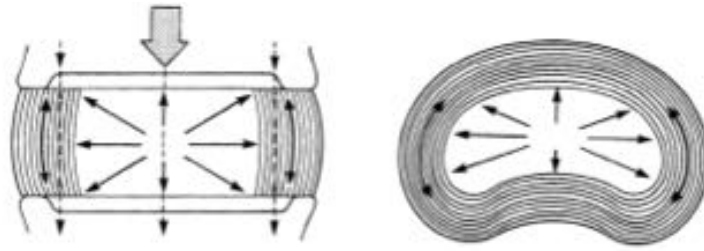


Figure 16. Load carrying capacity of the intervertebral disc in compression. Arrow indicates compressive load applied to the disc, which exerts a force outward on the annulus and endplates (Adams et al. 2013).

On the other hand, when a tensile load is exerted on a motion segment, the annular fibres in line with direction of the force, are employed in tension. These compressive and tensile forces experienced within the disc vary with position of the lumbar spine in flexion/extension, lateral bending, axial rotation, anterior/posterior and lateral shear movements. Flexion/extension and lateral bending are rotational movements that cause compression in the direction of movement and tension in the direction opposite to movement (Figure 17).

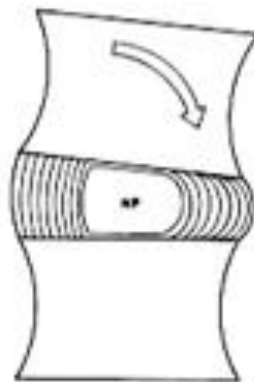


Figure 17. Bending of lumbar FSU. NP: Nucleus pulposus. Arrow indicates direction of load (Adams et al. 2013).

Axial rotation involves the twisting motion of one vertebra relative to another. This movement employs annular fibres in the direction of motion (Figure 18).



Figure 18. Axial Rotation of the Lumbar FSU. Arrow indicates direction of movement (Adams et al. 2013).

Anterior-posterior and right/left lateral shear movements involve parallel plane movement of one vertebra with respect to the other. However, due to the orientation of the collagen fibres in the annulus, the disc is unable to resist significant shear force. The range of motion of these 6DOFs are restricted by physiological limits (Table 1) (Pearcy & Tibrewal 1984; Costi et al. 2011).

Table 1. Range of motion of each DOF. Compression (Brinckmann et al. 1983), anterior-posterior shears (Lu et al. 2005), lateral shear estimated (Costi et al. 2011), flexion (Stokes & Frymoyer 1987; Pearcy et al. 1984), extension (Pearcy et al. 1984), lateral bending (Pearcy & Tibrewal 1984), axial rotation (Pearcy & Tibrewal 1984).

DOF	Physiological range of motion limit
Compression	1.4mm
Anterior shear	1.4mm
Posterior shear	1.5mm
Right/left lateral shear	1.5mm
Flexion	13°
Extension	5°
Right/left lateral bending	10°
Right/left axial rotation	4°

3.3 Biomechanics of the Sheep Lumbar Spine

For sheep lumbar spines to be an appropriate model of the human lumbar spine, they must be both anatomically and biomechanically comparable. Sheep intervertebral discs share similar anatomical

and biochemical composition to humans (Section 2.6). Therefore, it can be expected that sheep discs also have viscoelastic, time-dependent anisotropic behaviour as seen in human lumbar discs. The most significant differences between sheep and human lumbar mechanical properties include stiffness, physiological range of motion and differences in loading experienced by the quadruped and biped.

Previous research has shown that human intervertebral discs are stiffer than sheep discs (Costi et al. 2009). However, human discs are also much larger in size. Normalisation of the stiffness results excludes the effect of disc size and shows that at a certain loading frequency, differences in stiffness are proportional between human and sheep discs (Costi et al. 2009). Similarities have also been found between energy absorption, of sheep and human discs, indicating similar viscoelastic properties (Costi et al. 2009).

Comparisons between the physiological range of motion between species has been difficult due to biological variability in humans and variance between studies (Wilke et al. 1997b). Wilke et al. (1997b) reported that sheep lumbar spines have a smaller range of motion in all DOFs in comparison to the human lumbar spine. However, the overall trends suggest that loading directions are largely similar to those of human spines (Wilke et al. 1997b). Finally, although both quadrupeds and bipeds are loaded along the long axis of the spine, disparities in vertebral bone density indicate that sheep spines have to withstand higher axial compressive stresses (Smit 2002).

The underlying biomechanical properties of human and sheep intervertebral discs has been described in this chapter. Certain risk factors can inhibit this mechanical behaviour and predispose the intervertebral disc to injury and herniation. The biomechanical properties of the lumbar spine presented in this chapter were taken into consideration when mechanically testing sheep FSUs in this study.

4 Intervertebral Disc Herniation

The combined task forces of the North American Spine Society, the American Society of Spine Radiology and the American Society of Neuroradiology have defined intervertebral disc herniation as “*localised or focal displacement of disc material beyond the limits of the intervertebral disc space*” resulting in pain, weakness or numbness in a myotomal or dermatomal distribution (Fardon et al. 2014). Herniation is a serious problem as it can cause sciatica or LBP, consequently reducing an

individual's quality of life. It has also largely been agreed upon that the lower lumbar regions including L4-L5 and L5-S1 are the most common disc levels that experience herniation, while the posterior-postero-lateral regions of the disc are most vulnerable to injury (Rajasekaran et al. 2013; Marshall & McGill 2010; Adams & Hutton 1982).

Lumbar disc herniation has generally been associated to rupture of the annulus fibrosus. However, recent studies have implicated disruption of the endplate junction as an additional mode of failure in herniation (Rajasekaran et al. 2013). Annular rupture typically occurs when the annulus is weakened in tension, while it has been hypothesised that annular-endplate junction rupture occurs as a result of a high rate of loading and mechanical imbalance between the soft tissue of the annulus and hard vertebral endplate (Figure 19) (Wade et al. 2015).

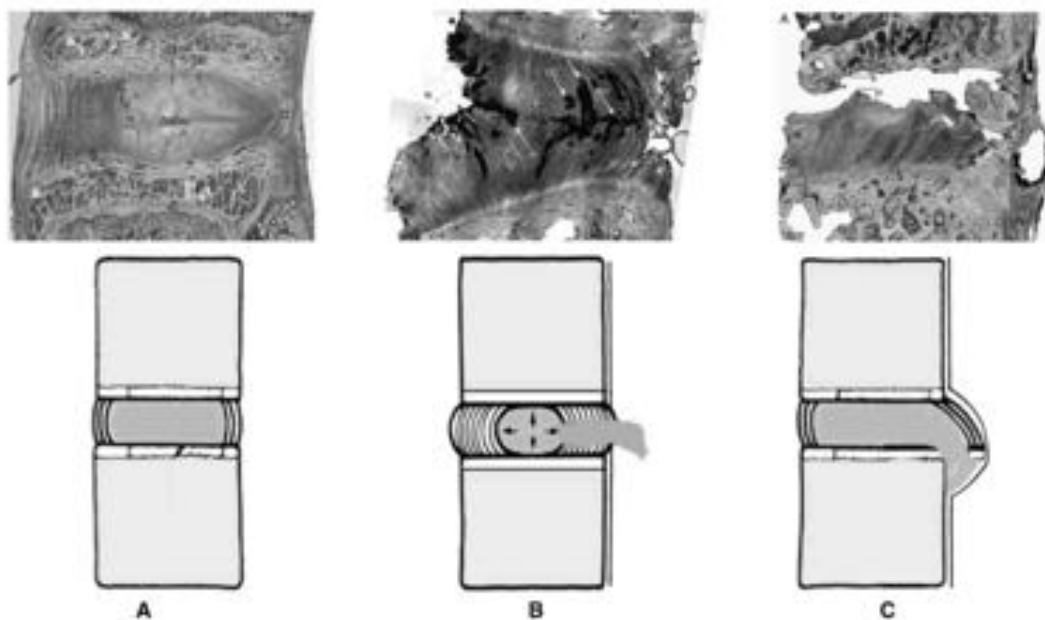


Figure 19. Histological sections and diagrams of a healthy disc and in states of failure (A) normal disc (B) failure by rupture of the annulus fibrosus (C) failure by avulsion of the endplate junction (Rajasekaran et al. 2013).

Depending on the extent of nucleus migration, herniated discs can be categorised as a protrusion, extrusion or sequestration (Figure 20).

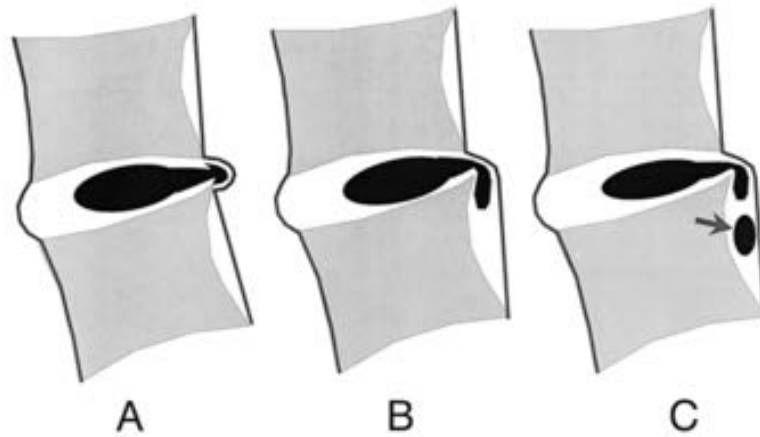


Figure 20. Types of herniation A) Protrusion B) Extrusion C) Sequestration (Schroeder et al. 2016).

A protrusion is where there is significant bulging of the annulus, but the annulus is not ruptured. Therefore, the nucleus does not migrate into the extra-discal space. Rupture of the annulus with little nucleus migration is known as an extrusion. In extrusions, the nucleus is still attached to the disc (Schroeder et al. 2016). Finally, a sequestration is known as a ‘complete’ herniation as the disc tissue is no longer attached and is expelled out of the disc space. Protrusions are commonly found in asymptomatic individuals, while extrusions and sequestrations may present with symptoms of sciatica and LBP (Stafford et al. 2007).

4.1 Risk Factors of Intervertebral Disc Herniation

Herniation has been associated to several key risk factors including ageing, disc degeneration, mechanical loading hazards (e.g. occupational, driving cars, sport), genetic inheritance, gender, obesity, diabetes and smoking. Of these risk factors, the involvement of ageing, disc degeneration and mechanical loading hazards will be considered in this thesis. These factors significantly influence the mechanical integrity of the disc and may consequently contribute to lumbar disc herniation.

4.1.1 Ageing

The intervertebral disc is the largest avascular structure in the human body and is therefore, particularly susceptible to ageing, degeneration and damage. Unlike disc degeneration, ageing of the disc is a natural process that occurs inevitably with age. These age-related changes may include biochemical, histological and metabolic changes that can impact structure and function of the intervertebral disc (Adams & Roughley 2006). With increasing age, the nucleus becomes dry, fibrous and stiff (Adams et al. 1986). Biochemical changes include a decrease of proteoglycan and water

content, an increase in protein cross-linking and changes in the collagen type and distribution (Figure 21) (Adams & Roughley 2006).

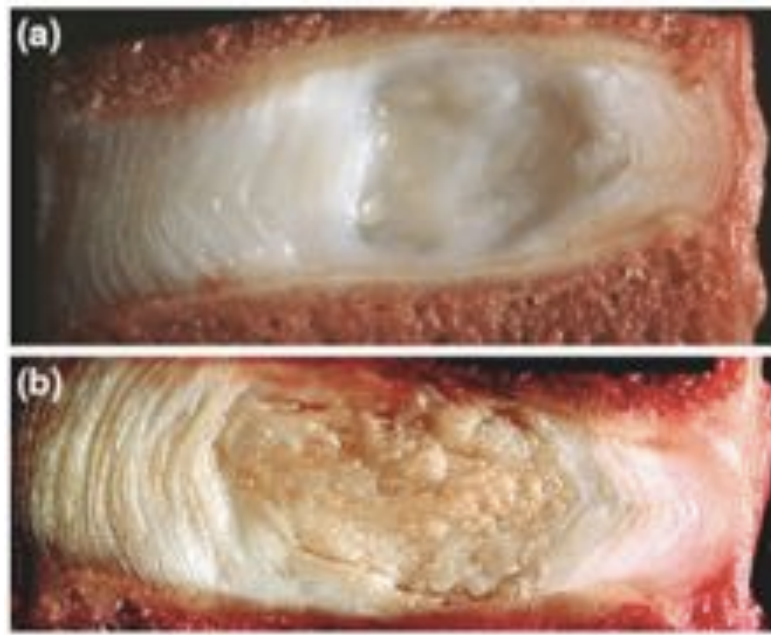


Figure 21. Comparison of young and old human lumbar intervertebral discs sectioned in the mid-sagittal plane (a) Healthy young disc (b) Healthy disc showing signs of biochemical ageing from middle-aged adult (Adams 2015).

Proteoglycan fragmentation can occur as early as childhood (Buckwalter 1995). Although loss of proteoglycan fragments from the nucleus is a slow process, it ultimately results in decreased number of proteoglycans and hence, water content in the disc (Adams & Hutton 1980). Older discs also have reduced matrix turnover, which enables collagen to become increasingly cross-linked, further reducing turnover and inhibiting repair in old discs (Duance et al. 1998). Despite increased cross-linking, the overall content of collagen within the disc decreases with age (Singh et al. 2009). Type II collagen fibres in the inner annulus are also replaced with type I fibres, exhibiting mechanical properties more comparable to those of the annulus.

With increasing age, co-morbidities may also exist. Osteoporosis may weaken the vertebral bodies adjacent to the intervertebral disc, whereby the disc pushes into the vertebra causing the endplates to curve (Pfirrmann et al. 2006). Functionally, increased nuclear volume causes a decrease in hydrostatic pressure and consequently, the annulus withstands more of the compressive load (Adams et al. 1996). These age-related changes ultimately influence the disc's mechanical function such that older discs tend to be stiffer and weaker in comparison to young discs.

4.1.2 Intervertebral Disc Degeneration

Intervertebral disc degeneration is an accelerated progressive process that inhibits normal mechanical function of the disc and has been defined as ‘*an aberrant cell-mediated response to progressive structural failure*’ (Adams & Roughley 2006). Although degeneration is more common in older discs, it is not an age-related process. Typically, disc degeneration is characterised by gross structural changes to the annulus. Degenerative structural changes to the disc can include loss of lamellar organization, annular tears, buckling of the annulus, decreased water content in the nucleus, reduced disc height, endplate defects and vertical bulging into the vertebral bodies (Adams et al. 2013). Disc degeneration is a progressive cascade of events that spreads rapidly as damage to one part of the disc increases load-bearing requirements of an adjacent tissue (Figure 22).

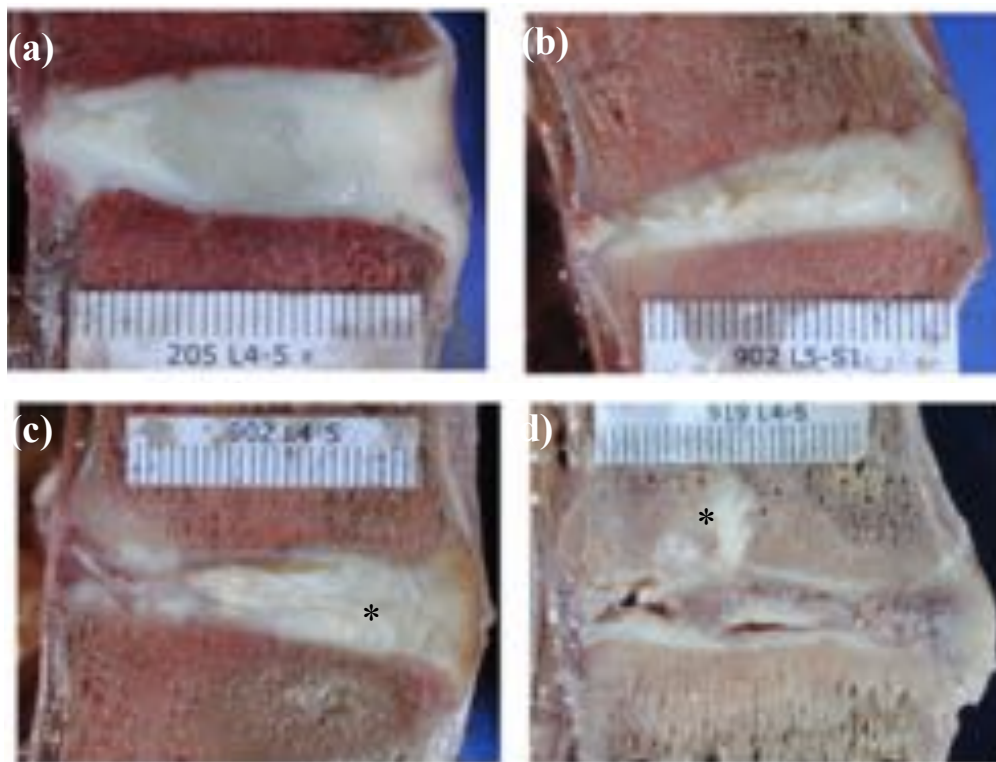


Figure 22. Sagittal sections of disc degeneration (a) healthy disc (b) mild degeneration and significant disc height loss (c) moderate degeneration, asterisks: annular tears visible (d) severe degeneration – asterisks: disc disruption into superior vertebral body (Galbusera et al. 2014).

4.1.2.1 Annular Tears

Intervertebral disc degeneration can present macroscopically with annular tears. Annular tears can be defined as disruptions to the arrangement of collagen fibres in the lamellae of the annulus and can be classified as concentric tears, radial tears or rim lesions (Figure 23).

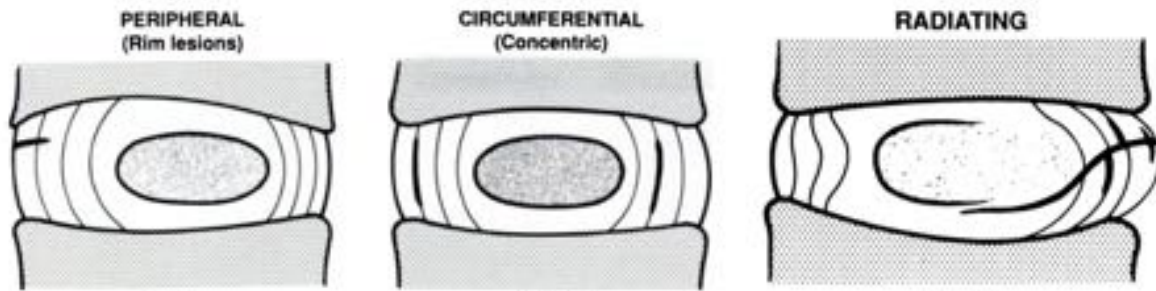


Figure 23. Illustration of three types of annular tears (Osti et al. 1992).

❖ Circumferential Tears

Circumferential tears appear as separations of the lamellae that occur consequent to delamination, or the loss of normal adhesion between lamellae (Vernon-Roberts et al. 1997). Evidence suggests that circumferential tears may propagate from high interlamellar shear strains and stresses. Circumferential tears are the most common type of annular lesion in both the anterior and posterior regions of the annulus (Osti et al. 1992).

❖ Radial Fissures

Radial fissures typically extend outward from the nucleus pulposus in the posterior or posterolateral regions of the disc (Osti et al. 1990; Vernon-Roberts et al. 1997). In comparison to circumferential tears, radial fissures typically occur in the inner region of the posterior annulus, while circumferential tears occur in the middle and outer regions of the anterior annulus (Vernon-Roberts et al. 1997).

❖ Peripheral Rim Tears

Peripheral rim tears have been defined as the separation of the outer layers of the annulus from the vertebral body. These tears predominantly occur in the anterior region of the disc (Hilton et al. 1980). It has been suggested that these tears could be the result of direct trauma to the disc rather than degeneration (Hilton et al. 1980).

No correlation has been found between radial fissures, concentric tears or rim lesions, which suggests that they occur independent of each other (Vernon-Roberts et al. 1997). Similar to ageing, these degenerative structural changes ultimately impact the biomechanical behaviour of the disc. Decreased proteoglycan and hence, water content in the disc results in a decrease in intradiscal pressure and disc height (Vergroesen et al. 2015). Reduced intradiscal pressure in the disc can also result in high stress concentrations in the annulus in comparison to healthy non-degenerated discs (Figure 24). These stress concentrations may increase the risk of further damage in adjacent tissues.

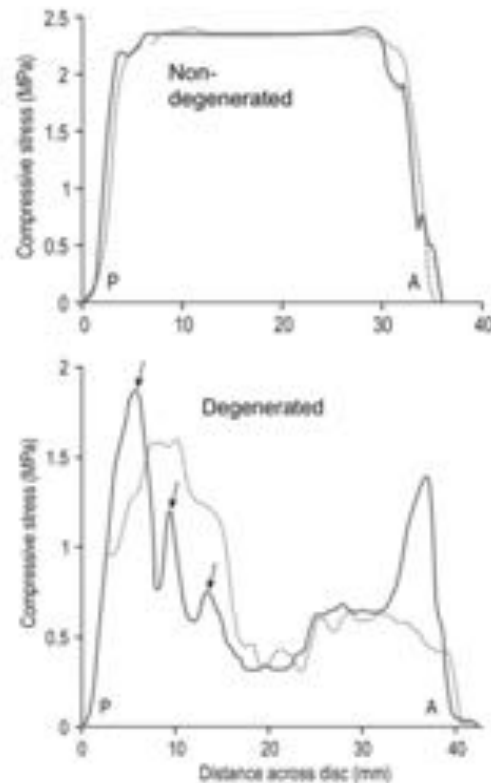


Figure 24. Stress concentrations across the mid-sagittal distance of the disc. (a) Healthy young disc, stress varies little with location or direction, indicating fluid-like properties (b) Degenerated disc, nucleus pressure is low, high stress concentrations and gradients in the annulus (arrows).

P=posterior, A=Anterior (Adams et al. 2013).

4.1.3 Mechanical and Occupational Hazards

Lumbar disc herniation has been associated with excessive or repetitive mechanical loading that can be classified as sudden overload or fatigue loading, respectively. Sudden overload refers to an incident where a high rate of loading is applied to the disc, resulting in immediate catastrophic injury. For example, when someone trips, the muscles in the spine generate a large force to counteract this motion. On the other hand, fatigue loading refers to tasks that involve repetitive bending, twisting and lifting as required in certain occupations (Kelsey et al. 1984).

Epidemiologic studies have found that individuals with jobs that require heavy lifting at least 25 times a day were three times more likely to develop herniations in comparison to those who were not required to repetitively lift heavy objects (Kelsey et al. 1984). Similarly, Heliovaara (1987) found an increased risk of disc herniation leading to hospitalisation in drivers, wood workers, metal workers and construction workers in comparison to professional and white collar workers (Figure 25).

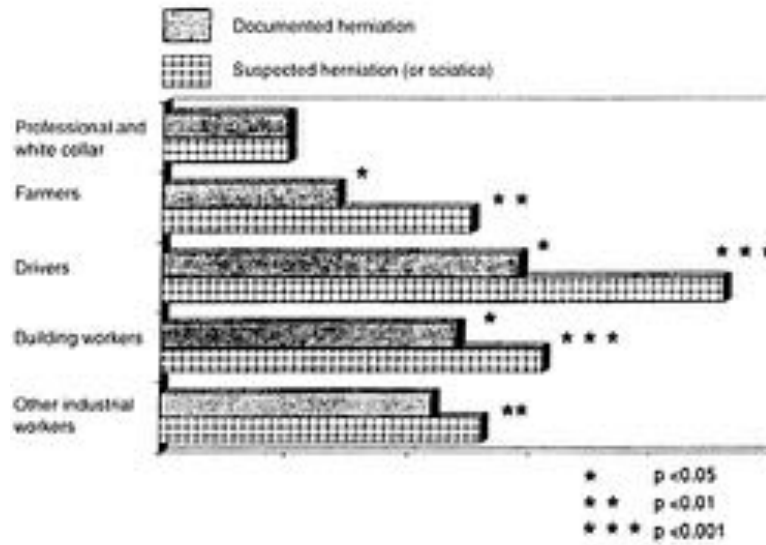


Figure 25. Comparison of occupational hazards associated to herniation. Data from: Heliovaara et al. 1987 (Postacchini & Cinotti 1999)

Fundamentally, these tasks involve repetitive actions of flexion, lateral bending or axial rotation. These postures recruit the posterior lamellae in tension while compressing the anterior fibres of the disc. Consequently, the posterior region of the disc is predisposed to excessive mechanical strain, which can result in an accumulation of microscopic damage to the disc. Posterior or postero-lateral herniations may cause compression of nerve endings in the spinal canal and ultimately lead to dysfunction, sciatica and LBP (Porchet et al. 2002).

4.2 Complications of Intervertebral Disc Herniation

Symptoms of lumbar disc herniation typically arise consequent to compression of spinal nerve roots or an immunologic reaction leading to inflammation, nerve dysfunction and pain. It has been found that pressure on nerve roots results in loss of function and is rarely associated with pain (Takahashi et al. 2006). This is further supported by the fact that removal of herniated disc material compressing nerves does not necessarily relieve pain. On the other hand, evidence has suggested a larger inflammatory role in nerve root pain (Lindahl & Rexed 1951; McCarron et al. 1987). The severity of pain has been correlated with the severity of herniation, where individuals with extrusions and sequestrations reported higher levels of leg pain in comparison to those with protrusions (Porchet et al. 2002). Therefore, symptoms present will vary depending on the disc level (i.e. L1-S1), anatomical site and severity of herniation (i.e. protrusion, extrusion, sequestration). Each spinal nerve innervates and supplies a specific dermatome and myotome (Figure 26).

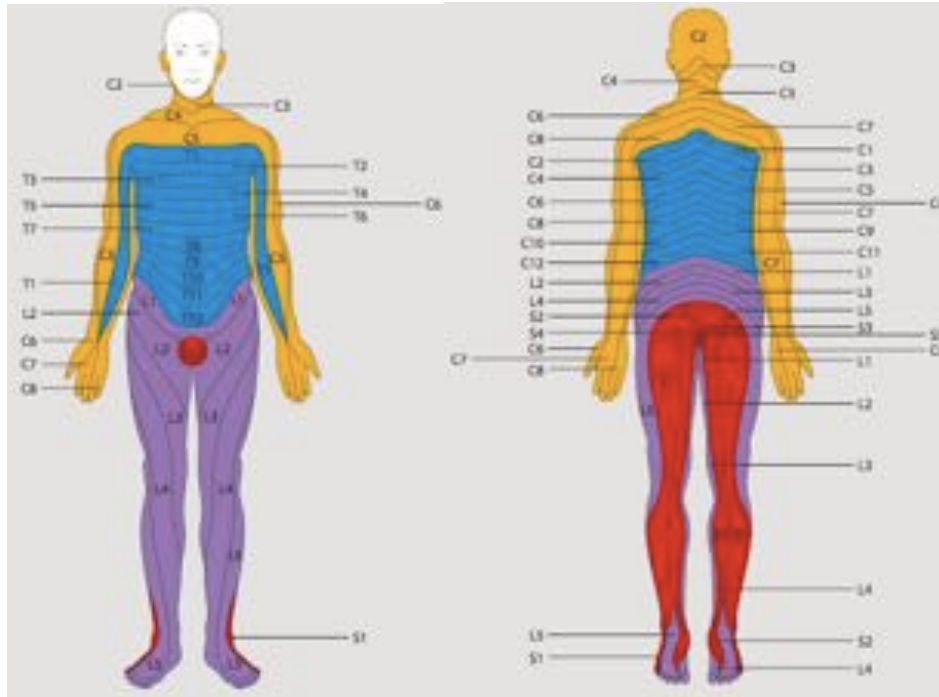


Figure 26. Image of dermatomes innervated by spinal nerves in the human body. Each colour corresponds to different vertebral levels. Dermatomal areas that may be affected by lumbar disc herniation are depicted in purple and red (Hernández et al. 2013).

The lumbar spinal nerves predominantly innervate the low back and the lower limbs of the body. Impingement of a lumbar spinal nerve will subsequently produce pain or dysfunction in the dermatome or myotome innervated by that nerve. Therefore, sciatica and LBP are common symptoms of intervertebral disc herniation.

4.2.1.1 Sciatica and Low Back Pain

Sciatica is defined as ‘*pain in the distribution of the sciatic nerve due to pathology of the nerve itself*’ (Stafford et al. 2007). The lifetime prevalence of sciatica has been estimated to be between 13% and 40%, while annual incidence is approximately 1-5% (Stafford et al. 2007). A Finnish population of 57,000 subjects were followed for 11 years to assess the incidence of herniation or sciatica requiring hospitalisation (Heliovaara et al. 1987). Of these patients, 1537 presented with symptoms and 24% of these patients were diagnosed clinically with intervertebral disc herniation (Heliovaara et al. 1987). The global socio-economic burden of sciatica remains unclear as there is no distinction between the impact of LBP conditions. Therefore, the burden of LBP and sciatica will be considered together.

LBP has been defined as ‘*pain or discomfort localised below the costal margin and above the inferior gluteal folds, with or without leg pain*’ (Duthey 2013). Although LBP isn’t as common as sciatica in individuals with a herniated disc, it should still be noted due to its global impact. LBP is a leading

cause of disability, reducing quality of life, limiting work performance, and causing a large economic burden through direct and indirect costs. The Global Burden of Disease 2010 study estimated the point prevalence of low back pain to be 9.4%. It was also found that out of the 291 conditions investigated, LBP had the highest number of years lived with disability (YLDs) and ranked sixth in terms of overall burden (Hoy et al. 2014). Prevalence of LBP also increases with age, peaking at 80 years of age (Hoy et al. 2014). Therefore, with an ageing population, it is expected that LBP will continue to be a serious issue in coming decades.

LBP causes a serious economic burden due to both direct (e.g. hospitalisation, physician visits, medical devices, medication, diagnostic tests) and indirect (e.g. lost wages due to absence from work, reduced productivity) costs. Approximately 72.3% of US workers with back pain reported significant functional impairment (Ricci et al. 2006). In the United States of America (USA), total direct and indirect costs associated to low back pain were estimated to be \$100-\$200 billion per year (Katz 2006). Evidently, LBP and sciatica present a serious problem for patients, family and society. As lumbar disc herniation is a significant cause of sciatica and LBP, there is a need for a thorough understanding of the aetiology of disease. Therefore, extensive research has been conducted into in vitro mechanical testing of FSUs in an attempt to simulate herniation and characterise mechanical properties at failure.

5 Literature Review: In Vitro Mechanical Testing of the Intervertebral Disc

Extensive research has been conducted to gain a thorough understanding of factors involved in lumbar disc herniation and the consequent modes of failure. To quantify the association of risk factors to disc herniation, in vitro mechanical testing has attempted to simulate physiological conditions in fatigue loading (e.g. repetitive lifting) and sudden overloading (e.g. car crash, falls). As previously mentioned, fatigue loading is where the lumbar intervertebral disc is loaded repetitively at relatively low magnitudes of load, while sudden overloading refers to a high load applied at a fast rate. Variables that have been assessed and factors that have differed between studies include the testing system used, specimen type, age and degenerative stage of the disc, direction of loading and the mechanical loading regime.

5.1 Testing Systems

To simulate physiological conditions, specimens have been tested in a mechanical loading system to induce herniation (Wade et al. 2014; Wade et al. 2015; Gordon et al. 1991; Adams & Hutton 1982; Marshall & McGill 2010; Callaghan & McGill 2001) and by nuclear pressurisation in an attempt to develop an understanding of the mechanical disruption of the disc in response to increased intradiscal pressure (Veres et al. 2010; Veres et al. 2009; Veres et al. 2008). Nuclear pressurisation primarily aims to simulate increased hydrostatic intradiscal pressure that is experienced during compression in vivo. In this process, the inferior vertebra of each FSU was fit with an injection screw. A piston-cylinder device was then used to inject a viscous gel into the nucleus to increase pressure (Veres et al. 2008). Although this method of nuclear pressurisation has been proven to effectively characterise factors involved in disc failure mechanics, induce annular tears and cause herniation, it is limited by the inability to remove pressure once it has been applied (Veres et al. 2009; Veres et al. 2008; Veres et al. 2010). This process may also negatively impact the physiological conditions and integrity of the disc as the injection screw is inserted from the inferior vertebra into the disc.

On the other hand, mechanical testing systems have proven to be a more common means of testing and simulating intervertebral disc herniation. These systems benefit greatly from their ability to statically or dynamically replicate movements experienced in vivo. Mechanical testing systems have generally been single-axis or multi-axis hydraulic servo-controlled machines that apply loads or moments to a specimen. Pioneering studies investigating failure mechanisms of the disc primarily used uniaxial testing devices (Virgin 1951). However, movements in real life are rarely restricted to a

single axis. As such, these uniaxial testing systems have been improved upon to include custom rigs that allow combinations of compression with torsion, flexion or lateral bending (Adams & Hutton 1982; Adams & Hutton 1981; Adams & Hutton 1985; Wade et al. 2014; Wade et al. 2015; Gordon et al. 1991). To implement this, various studies have utilised a roller system that sets the specimen in a certain degree of flexion (Figure 27).

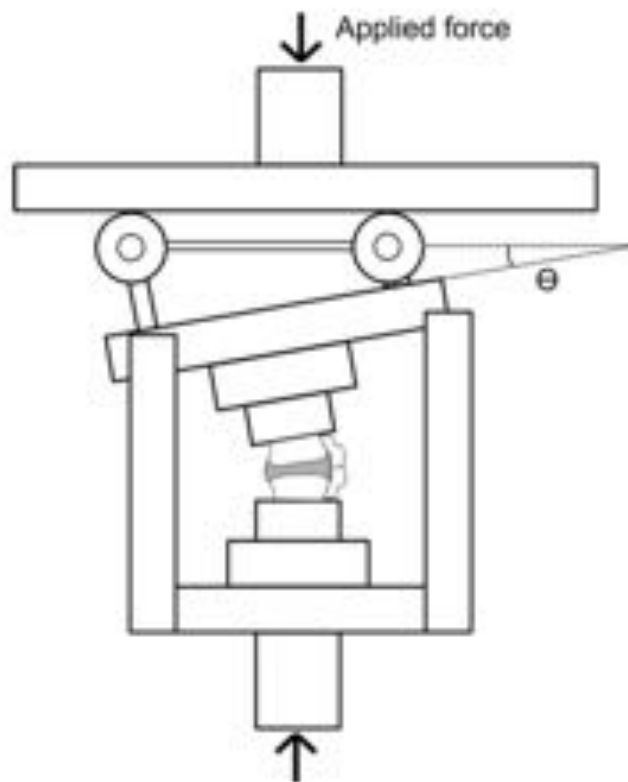


Figure 27. Custom built rig for mechanical testing of the intervertebral disc. This rig is used to compress motion segments in flexion as set by a roller height difference. Vertical pillars constrain the upper plate to a single plane of motion, eliminating torsion (Wade et al. 2015)

Callaghan & McGill (2001) later developed apparatus to test specimens in two dynamic axes in flexion/extension and compression. This testing system also included an X-Y table mounted beneath the specimen to enable translation in the horizontal plane (Callaghan & McGill 2001). Drake et al. (2005) made alterations to this testing apparatus to not only include dynamic loads in two DOFs but also, a static load applied to a third DOF. Overall, these mechanical testing systems have been limited by the number of DOFs that the system can control or by the rate of loading.

To the author's knowledge, only three 6DOF systems have been developed for the use of biomechanical simulation of complex loading and measurement of joint kinematics (Ding et al. 2011; Wilke et al. 2016; Schulte et al. 2008). However, very few studies have been conducted using these

6DOF systems to investigate and attempt to simulate intervertebral disc herniation (Wilke et al. 2016; Berger-Roscher et al. 2017). 6DOF testing systems benefit significantly from the ability to control and record movement in 6DOFs, which is closer to movement seen in vivo. Although a 6DOF hexapod robot developed at Flinders University has been used to characterise properties of the disc, it is yet to be used to simulate intervertebral disc herniation by sudden overload (Amin et al., 2016a; Amin et al., 2016b).

5.2 Specimen Type

The specimen type used in mechanical testing of the disc has varied significantly between species, from cadaveric motion segments (Gordon et al. 1991) to ovine (Wade et al. 2015; Wade et al. 2014; Berger-Roscher et al. 2017), bovine (Simunic et al. 2004; Race et al. 2000; Simunic et al. 2001) and porcine (Drake et al. 2005; Tampier et al. 2007; Marshall & McGill 2010; Callaghan & McGill 2001). Although ovine, bovine and porcine specimens have been found to be comparable models to the human spine (Reid et al. 2002; Wilke et al. 1996; Alini et al. 2008), there will always be some disparities between species. Cadaver specimens are the most desirable specimen type when attempting to characterise herniation in humans. However, cadaver specimens can be fraught with significant variation in age, degeneration, disease and genetic factors.

There has also been significant variation between disc levels tested, ranging from cervical (C3-C4) in porcine (Tampier et al. 2007; Callaghan & McGill 2001) and caudal in bovine (Simunic et al. 2004; Race et al. 2000; Simunic et al. 2001), to lumbar segments (L1-2, L2-L3, L3-L4, L4-5, L5-S1) in ovine (Wade et al. 2015; Wade et al. 2014; Berger-Roscher et al. 2017), and human specimens. Conclusive findings have reported L4-L5 and L5-S1 disc levels to be most likely to herniate (Adams & Hutton 1982; Willburger et al. 2004; Rajasekaran et al. 2013). Adams & Hutton (1982) loaded 61 lumbar cadaver FSUs in hyperflexion and compression. It was found that 54% of L4-L5 and 50% of L5-S1 specimens failed by herniation, respectively. Conversely, the proportion of L3-L4 (31%), L2-L3 (33%) and L1-L2 (38%) specimens that failed by herniation was much lower (Adams & Hutton 1982). This has been supported by Rajasekaran et al. (2013) who conducted a prospective study of 181 subjects requiring microdiscectomy. L4-L5 was the most common site of herniation (49%), followed by L5-S1 (43%), L3-L4 (6%) and L2-L3 (2%) (Rajasekaran et al. 2013). This suggests that in vitro mechanical tests attempting to simulate herniation should use L4-L5 or L5-S1 specimens, or disc levels in an animal model that share similar characteristics. Furthermore, there has been significant variation in specimen types used, which should be noted when making comparisons between findings of different species.

5.2.1 Age and Disc Degeneration

The question of whether ageing and disc degeneration precedes herniation or whether degenerative structural changes develop subsequent to herniation, has been widely debated (Adams & Hutton 1982; Lama et al. 2013; Adams et al. 2015). Clinically, it is believed that degeneration precedes herniation, while in vitro mechanical studies have reported findings that oppose this. Therefore, various mathematical models (Schmidt et al. 2007), in vitro tests (Simunic et al. 2004; Adams & Hutton 1982) and clinical studies (Willburger et al. 2004) have focused on the effect of specimen age and degenerative grade in causing herniation.

Adams & Hutton (1982) tested motion segments ranging from 14 to 78 years in acute hyperflexion. Of the 8 specimens older than 59 years, 0% failed by intervertebral disc herniation. Instead, discs tend to herniate more commonly in slightly degenerated discs at 40-49 years with 78% of specimens within this age range failing by herniation (Adams & Hutton 1982). Both the 30-39 and 50-59 age groups reported 50% failing by herniation, while only 31% of the <30 years group failed by herniation (Adams & Hutton 1982). This correlates well with findings of a prospective observational study that found the average age in 743 patients with herniation was 41 years (Cummins et al. 2006) and a clinical study of 55 patients requiring microdiscectomy where the mean age was 43 years (Willburger et al. 2004). These findings suggest that discs with extensive age-related change may be less prone to herniation due to decreased water content and hence, decreased intradiscal pressure exerted on the annulus. Therefore, when simulating herniation by in vitro mechanical testing, cadaver specimens should ideally be 40-49 years, while animal models should also be representative of this age. However, it is important to note that with increasing age, there may also be concurrent disc degeneration influencing the discs mechanical behaviour.

The relationship between disc degeneration and intervertebral disc herniation is still unknown and has been largely disagreed upon. The extent of disc degeneration can be graded from 1 (normal healthy disc) to 4 (severe changes) (Galante 1967). Following mechanical testing by acute hyperflexion, Adams & Hutton (1982) macroscopically examined and classified cadaver specimens based on the degree of degeneration. The proportion of grade 1 degeneration specimens that failed by herniation was 33%, while 71% of grade 2 degenerated discs herniated, 38% of grade 3 herniated and 0% of grade 4 failed by herniation (Adams & Hutton 1982). Similarly, Gordon et al. (1991) tested 14 cadaver FSUs under cyclic loading in combinations of flexion and axial rotation at 1.5 Hz. Of these specimens, 10 failed by protrusion, while 4 failed by nuclear extrusion. There was a statistically significant correlation between specimens that failed by nuclear extrusion and grade 2 degeneration (Gordon et al. 1991). Lama et al. (2013) compared 21 herniated discs with 11 non-herniated discs that showed similar degrees of degeneration, histologically. It was found that changes to the annulus were

significantly different between herniated and degenerated discs (Lama et al. 2013). On the other hand, no significant degenerative differences were observed in the nucleus between herniated and degenerated discs. Typically, degeneration begins in the nucleus. Therefore, Lama et al. (2013) concluded that it is unlikely that degeneration caused herniation in 21 of the 32 discs. Furthermore, it has been hypothesised that slightly degenerated discs are more susceptible to herniation as there is evidence of annular degeneration, while the nucleus still exhibits hydrostatic pressure (Adams & Hutton 1982). Conversely, severely degenerated discs do not herniate as the nucleus is stiffer with no hydrostatic properties. As such, all in vitro mechanical tests attempting to simulate herniation should be conducted on non-degenerated or mildly degenerated discs.

5.3 Mechanical Loading

Mechanical loading of the intervertebral disc has predominantly been carried out as either fatigue or sudden overloading. It should be noted that in vivo, the disc experiences various types of loading. Therefore, it may be more accurate to hypothesise that fatigue loading weakens the disc so that an event of sudden overload consequently ruptures the disc, or vice versa. Very few studies have focused on the combination of fatigue and sudden overload (Adams & Hutton 1983; Adams & Hutton 1985). Interestingly, a specimen subjected to fatigue loading followed by hyperflexion sustained a herniation down a radial fissure (Adams & Hutton 1985). However, the ensuing literature review on fatigue and sudden overload has largely separated these loading conditions.

5.3.1 Fatigue Loading

In vivo, fatigue loading of the spine typically occurs in manual handling, industrial labour, exposure to vibration or athletic exercise that occurs over time. Key factors that must be taken into consideration and that have varied between studies when simulating fatigue loading include; the number and frequency of loading cycles, the magnitude of load and direction of loading. Fatigue loading is out of the scope of this project and will not be part of the mechanical loading protocol. However, current research in the area will be presented to provide a complete review of testing methods conducted to simulate intervertebral disc herniation.

5.3.1.1 Number of Cycles

Essentially, in vitro fatigue loading is attempting to simulate a realistic accumulation of micro-damage to the intervertebral disc as seen in vivo. The number and frequency of load cycles applied must therefore take into consideration, the rate of tissue repair. The intervertebral disc is an avascular material and consequently has poor and slow means for tissue repair. Due to very slow turnover rates,

it can take years to replace damaged proteoglycans and collagen in the intervertebral disc (Sivan et al. 2008). As such, the number of uninterrupted load cycles has ranged significantly from 1000 to 86,400 cycles conducted over several hours (Liu et al. 1985; Wilke et al. 2016; Callaghan & McGill 2001; Gordon et al. 1991). Evidently, repair of the intervertebral disc within this short period of time would not occur in vivo by cell or tissue repair. However, the intervertebral disc is rarely loaded continuously until failure in vivo. Instead, loading is intermittent with periods of rest where the body is supine. As previously described, the intervertebral disc experiences creep due to high compressive loads, forcing fluid out of the nucleus and decreasing disc height. When supine, the compressive load is significantly reduced, which allows for the resorption of water into the nucleus pulposus. As such, previous in vitro testing fails to accommodate for the diurnal fluid flow of the disc. In vivo, this would delay the process of annular tear formation so that herniation may occur over weeks, months or years rather than just hours as seen in mechanical tests.

5.3.1.2 Magnitude of Compressive Load

The magnitude of compressive load experienced by the lumbar spine varies significantly depending on posture and activity. Therefore, several studies have focussed on determining the intradiscal pressure during various conditions of loading (Nachemson 1981). Nachemson (1981) findings indicate that compressive force on the lumbar spine is 150-250 N when supine, 500-800 N when standing erect, 700-1000 N when sitting erect and 1900 N when lifting a 10 kg weight. This pioneering work has provided a basis for the magnitude of load that should be applied during cyclic loading of the disc. Typically, the magnitude of the compressive load has ranged between 260 N to 6000 N (Drake et al. 2005; Callaghan & McGill 2001). This significant variation in compressive load is an indicator of the type of task being simulated, where higher loads are representative of more strenuous lifting. Fatigue loading is attempting to replicate loads that occur in occupations that involve bending and lifting. Therefore, it is within reason to test different magnitudes of compressive loading. Callaghan & McGill (2001) found that increasing axial compressive forces from 260 N to 1472 N resulted in more frequent and severe injuries to the disc. Adams & Hutton (1983) applied much larger compressive loads up to 6000 N that resulted in the majority of specimens failing by endplate fracture. This suggests that the upper limit of compressive load required to induce herniation had been exceeded in this study. Clinically, this means that the two ends of the spectrum, very light repetitive lifting or very heavy repetitive lifting, will not necessarily cause an intervertebral disc herniation. The specific range of compressive loading in which herniation occurs remains undefined.

5.3.1.3 Direction of Loading

The direction of loading has also varied significantly between in vitro mechanical fatigue loading studies with combinations of axial compression, flexion, lateral bending and axial rotation reported in

the literature. Lumbar motion segments have been tested extensively in static pure axial compression (Brinckmann et al. 1988). It has been concluded that motion segments repetitively loaded in axial compression alone fail almost exclusively by endplate fracture or vertebral body compression (Brinckmann et al. 1987; Gallagher et al. 2005). Vertebral fractures were observed in 16 of 17 cadaver FSUs cyclically tested in compression by Hansson et al. (1987) and 52 of 70 cadaver FSUs tested by Brinckmann et al. (1988). The likelihood of simulating a vertebral fracture increases with the number of load cycles and the magnitude of the cyclic compressive load (Brinckmann et al. 1987; Callaghan & McGill 2001).

During compression, the nucleus withstands the load by exerting an omni-directional force outwards on the annulus and the endplates. Consequently, the endplates bulge into the adjacent vertebra (Brinckmann et al. 1983; Hansson 1983). The vertebral endplates are particularly susceptible to damage due to their thin structure, which is required for efficient exchange of nutrients and waste between the vertebra and the avascular disc. Furthermore, it has been concluded that pure compressive loading of the lumbar motion segment does not directly damage the intervertebral disc (Brinckmann et al. 1989; Hutton & Adams 1982). However, compression and vertebral fracture may lead indirectly to disc failure. Vertebral endplate fracture increases the volume of the disc occupied by the nucleus, which consequently decreases hydrostatic pressure in the nucleus and its ability to resist compression such that the annulus withstands compression instead. Although pure compression does not directly damage the intervertebral disc, compressive forces in conjunction with flexion, axial rotation or lateral bending may cause more significant damage to the disc.

Flexion of the lumbar spine has been recognised as a common movement involved in repetitive bending and lifting of objects. Flexion of a motion segment results in compression anteriorly, while posteriorly, collagen fibres in the lamellae of the annulus are stretched and weakened in tension. However, flexion alone, without a compressive load, shows no damage to the disc (Wade et al. 2014). Therefore, it has been postulated that compression of the disc in this vulnerable position can cause annular tears and subsequently lead to intervertebral disc herniation predominantly in the posterior or postero-lateral region of the annulus (Callaghan & McGill 2001). Various studies have focussed on mechanically simulating intervertebral disc herniation in flexed motion segments (Gallagher et al. 2005; Callaghan & McGill 2001; Parkinson & Callaghan 2009). A low magnitude of flexion moment and small compressive load induces little injury to the disc injury, while increasing flexion moment and magnitude increases risk of injury to the disc (Callaghan & McGill 2001).

Axial rotation is not considered a primary movement of the lumbar spine and its role in producing herniation in non-degenerated discs has drawn mixed conclusions. Compression and rotation employ

the lamellae collagen fibres in tension. Pioneering research conducted by Adams & Hutton (1981) found that more axial rotation is required to damage the intervertebral disc than required to damage the facet joints. Adams & Hutton (1981) found facet joints fail at the physiological limit of torsion at 1-2°, while much greater angles are required to damage the disc. Therefore, Adams and Hutton (1981) concluded that axial rotation was not a major factor in the aetiology of disc herniation. Several research groups have also found that axial torque repetitively loaded in compression damages the facet joints and is not compromising to the structural integrity of the intervertebral disc (Marshall & McGill 2010; Pearcy & Hindle 1991; Drake et al. 2005), thus supporting the findings of Adams & Hutton (1981). It has therefore been found that facet joints protect the intervertebral disc from excessive axial rotation.

Conversely, epidemiological studies have found an association between lifting during axial rotation with an increased incidence of disc herniation (Kelsey et al. 1984; Mundt et al. 1993). It has been suggested that combinations of loading involving axial rotation could enhance the vulnerability of the disc (Marshall & McGill 2010). Combinations of axial torque/twist with repetitive flexion have successfully simulated disc damage and herniation (Marshall & McGill 2010; Drake et al. 2005; Gordon et al. 1991). It has been hypothesised that in flexion, the facet geometry allows for an increase in axial rotation, ultimately resulting in overstraining of the annular fibres (Pearcy & Hindle 1991). This theory was supported by research conducted by Marshall & McGill (2010) who reported axial torque and repetitive flexion initiated delamination within the annulus and was present in 67.5% of FSUs tested. Similarly, Drake et al. (2005) found that the inclusion of axial torque to repetitive flexion-extension motions in compression contributed to earlier initiation of disc herniation. The occurrence of facet fractures was also higher in the axial torque group compared to the no torque group. As the facet joints begin to fail, the FSU is able to rotate further, which further increases the tensile strain on the annulus (Drake et al. 2005). Furthermore, it can be concluded that while axial rotation alone does not damage the disc, combinations of loading may enable rotation beyond the physiological limit, consequently increasing the tensile strain of the annulus fibrosus.

The combination of lateral bending and flexion frequently occurs in situations where people bend to reach an object not directly in front of them (Adams & Hutton 1981). This motion is common in manual handling tasks and plays a significant role in causing posterior intervertebral disc herniation (Pearcy & Tibrewal 1984). This combination of loading may be the most susceptible to damage as it produces maximum stretching and high shear strains in the posterolateral annulus opposite to the side of bending, which may ultimately contribute to delamination of the annulus fibrosus (Costi et al. 2007). This hypothesis has been supported by a study recently conducted by Berger-Roscher et al. (2017). This study tested several complex combinations of loading that involved flexion, axial

rotation, lateral bending and compression, and concluded that both flexion and lateral bending are crucial in generation of failure (Berger-Roscher et al. 2017). Cadaveric experiments in cyclic loading of flexion combined with lateral bending have also demonstrated that physiologically reasonable repetitive loads can lead to posterolateral herniation (Adams & Hutton 1985).

5.3.1.4 Failure Modes

In vitro mechanical fatigue loading has successfully simulated intervertebral disc herniation (**Error! Reference source not found.**). However, studies have varied in specimen type, number of cycles, compressive load and direction of loading, making it challenging to accurately identify and define which factors are having a significant effect in causing herniation. Adams and Hutton (1983) reported three herniations by protrusion out of the forty-one specimens tested in flexion and cyclic axial compression, while the remaining specimens failed predominantly by endplate fracture. Conversely, Gordon et al. (1991) reported herniation in all fourteen specimens tested. While the incidence of herniation has varied between studies, the mechanism of failure has been largely agreed upon. Adams and Hutton (1985) identified five stages involved in gradual disc herniation, including self-selection of the disc, distortion of lamellae and development of postero-lateral radial fissures, lamellae rupture, extrusion of small amounts of nucleus and finally, the disc reaches a ruptured but stable state. This theory has been supported by several studies that have reported distortion of the lamellae and nuclear extrusion through annular tears (Gordon et al. 1991; Adams & Hutton 1983). However, recent findings have also implicated the annular-endplate junction as a possible site of failure in fatigue loading (Wilke et al. 2016).

Table 2. Comparison of fatigue loading studies

Author	Specimen Type	Number of Load Cycles	Frequency	Load Magnitude	Posture	Findings & Failure type
Adams & Hutton (1983)	41 cadaver	9600	1.5 Hz	1500 N – 6000 N	Flexion (specific to subject and disc level)	11 endplate fracture/vertebral body compression 20 loaded in sudden overload (3 protrusions, 17 endplate fracture)
Adams & Hutton (1985)	55 cadaver	9600	1.5 Hz	500 N - 4000 N	Flexion 15°	Ruptured discs don't herniate 6 herniated in group B, 1 herniated in group D Vertebral damage in remaining specimens
Callaghan & McGill (2001)	26 porcine (C3-C4)	Up to 86,400	1 Hz	260 N – 1472 N	Flexion/extension torque	15 herniated Increased likelihood with higher compression
Drake et al. (2005)	18 porcine (C3-C4)	Up to 6000	1 Hz	1472 N	Axial torque: 5Nm Flexion	AT group 7/9 facet fractures compared to no AT group at 2/9 facet fractures. After 3000 cycles 71% AT group herniated, while 29% no AT group herniated
Gordon et al. (1991)	14 cadaver	Average 40,000	1.5 Hz	1334 N	Flexion: 7° Axial rotation: 3°	10 annular protrusion 4 nuclear extrusion
Wilke et al. (2016)	8 ovine	1200	0.5 Hz	800 N	Flexion – 0-12° Right lateral bend: 0-9° Axial rotation: 0-4°	4 herniations, 2 protrusions, 2 delaminations. Of herniations and protrusions, 2 annular failure, 4 endplate junction failure,

5.3.2 Sudden Overloading

Sudden overloading refers to an incident of bending where a high compressive load is applied at a high rate, consequently causing immediate injury to the disc. In vivo, this may include slips, trips or falls, which can generate high and sudden forces to the lumbar spine. Although it can be difficult to link an event of sudden overload to sciatica and symptoms of herniation, it could play a large role in the initial development of tears and damage to the disc. It has been suggested that the stiffness and ultimate strength of biological tissues varies with loading rate. Sudden overloading imposes an unexpected high force to the lumbar spine that results in immediate injury to the intervertebral disc. In vitro testing of FSUs in sudden overload has primarily taken into consideration the rate of loading in neutral, flexed and hyperflexed discs and the influence these factors have on failure of the disc.

5.3.2.1 *Rate of Loading*

As previously described, the intervertebral disc is as a biphasic material with time-dependent properties that experiences creep over time. When a specimen is compressed with a slow rate of loading, the fluid phase gradually diffuses through the solid phase to regions of lower pressure, consequently resulting in creep of the tissue. However, when a high rate of load is applied, the fluid phase does not have enough time to diffuse out due to drag between the fluid and solid phases and no creep occurs. Therefore, to generate sudden and traumatic physiological loading, the rate must ultimately minimise the effect of creep (Race et al., 2000). The extensor muscles of the spine are generally slow postural muscles. Therefore, in cases of sudden overloading, these muscles may be unable to generate the required force rapidly enough to prevent excessive movement of the spine. Rapid and unexpected loading may also increase the compressive force acting on the spine (Mannion et al. 2000). Therefore, various electromyographic studies have focussed on identifying rates of loading that are physiologically possible in the lumbar spine (Dolan & Adams 1993). These studies have shown that the maximum rate at which the muscles of the spinal column can generate a force sufficient to lift or catch a significant weight in response to a 'surprise' load is around 0.75 seconds, requiring a compression rate of 400mm/min (Dolan & Adams 1993; Mannion et al. 2000). Adams and Hutton (1982) tested 61 cadaver FSUs in hyperflexion where the load applied increased at 3000 N/s, resulting in 42.6% failing by herniation. Wade et al. (2014; 2015) loaded ovine lumbar FSUs in a neutral posture and in flexion at velocities classified as low (2mm/min), high (40mm/min) and surprise (400mm/min) rates. At the high rate of loading, 58% of specimens failed by herniation while 83% of specimens loaded at the surprise rate herniated. Evidently, the incidence of damage to the disc appears to increase with increasing rates of loading. Interestingly, there is little variation in load at failure between specimens loaded at different rates. Typically, load at failure has ranged between 5 – 14.2 kN for each rate of loading (Wade et al. 2015; Wade et al. 2014). Wade et al. (2014, 2015) also

found that a significantly lower load was required to induce disc failure compared with that required for endplate fracture at the higher rate of compression when combined with flexion (Figure 28). Therefore, the load at failure may aid the interpretation of events and classification of mode of failure.

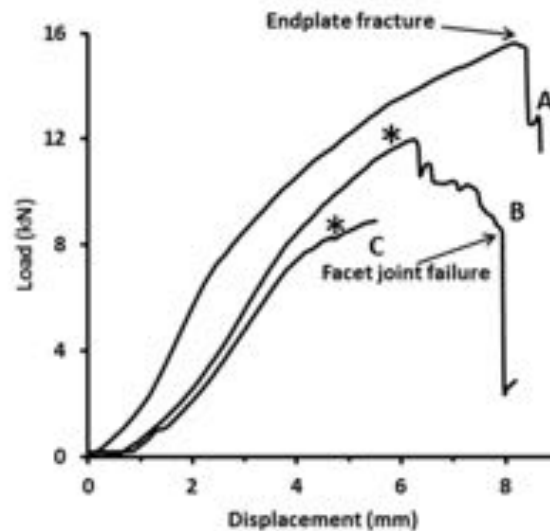


Figure 28. Load-displacement curve for three FSUs. One specimen was tested in a neutral posture and failed by endplate fracture (curve A). The remaining two specimens failed by disc wall failure (curve B) and the other test was stopped at the first indication of failure (curve C). Asterisks indicate audible fibre rupture (Wade et al. 2014).

5.3.2.1 Direction of Loading

Several studies have proven that the rate of loading, or pressurisation, applied to the disc influences the failure mode in herniation (Wade et al. 2014; Wade et al. 2015; Veres et al. 2010). Unlike fatigue loading studies, in vitro mechanical tests by sudden overload have predominantly focused on failure in a neutral posture, flexion or hyperflexion (Wade et al. 2014; Wade et al. 2015; Adams & Hutton 1982; Veres et al. 2010). Similar to fatigue loading, it has been proven that specimens in a neutral posture fail by vertebral or endplate fracture. Flexion decreases the disc's ability to withstand high nuclear pressure. Veres et al. (2010) tested sheep by nuclear pressurisation and found that flexed discs suffered tears adjacent to the outer annulus at the cartilaginous/vertebral endplate junction. Wade et al. (2014; 2015) also tested specimens in neutral and flexed postures at different rates of loading and found that specimens loaded at low and high rates in neutral postures invariably resulted in endplate fracture. Interestingly, flexed specimens at a low rate of loading failed by endplate fracture, while a high rate of loading caused disc failure in approximately 50% of specimens (Wade et al. 2014). Evidently, the direction of loading and the rate of loading contribute to the incidence of damage to the disc. To the authors knowledge, specimens have not been tested by sudden overload in other directions of loading.

5.3.2.2 Modes of Failure

The rate of loading ultimately influences the mode of failure observed in the disc. At the surprise rate of loading (400 mm/min), Wade et al. (2015) found that 83% of specimens failed by herniation, while only 17% suffered endplate fracture. Of these herniations, 25% were mid-span annular rupture and 58% were annular endplate rupture (Wade et al. 2015). When tested at the lower rate (40 mm/min), only 58% herniated. Of these specimens that herniated, 42% were annular rupture, while 16% failed by annular-endplate rupture (Wade et al. 2014). Therefore, these findings indicate that the rate at which the flexed motion segment is compressed will determine which intervertebral disc tissue is vulnerable to damage. It has been theorised that during a low rate of loading, increased nucleus pressure allows sufficient time for fluid flow and creep to occur. As a result, the pressure is localised to the mid-disc and little pressure is applied to the adjacent endplates. On the other hand, high rates of loading do not allow fluid flow to occur. Consequently, pressure is transferred to the endplates causing an imbalance in micromechanical compliance between the soft disc and hard endplates (Figure 29) (Wade et al. 2015).

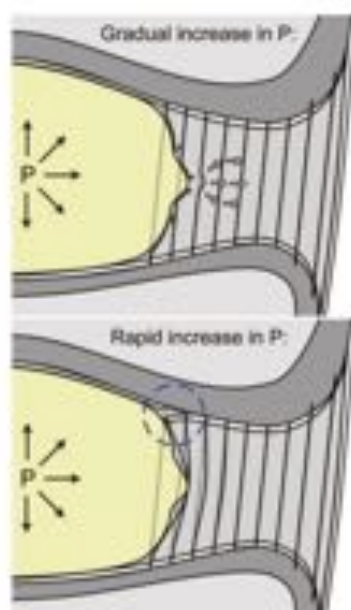


Figure 29. Effect of rate of pressurisation on mode of failure. During a slow rate of loading, fluid has time to diffuse, consequently stretching and causing disruption to annular fibres. On the other hand, high rates of pressurisation does not allow enough time for fluid flow to occur resulting in tearing of cartilaginous endplate in neutral posture. (Veres et al. 2010)

Furthermore, differences in rates of loading, direction of loading and modes of failure have been identified in cases of sudden overload by axial compression and nuclear pressurisation (**Error! Reference source not found.**).

Table 3. Comparison of fatigue loading studies.

Author	Specimens	Rates of loading	Posture	Findings / Failure type
Adams (1982)	61 cadaver (intact)	3000 N/s	Hyperflexion (6-18°)	26 herniated
Saiee et al. (2017)	33 ovine (Intact and isolated discs)	400 mm/min	Flexion (10°)	All herniated
Simunic et al. (2004)	96 Bovine	0.004MPa/sec 4MPa/sec	Flexion	Average damage weighting – Fully flexed fully hydrated with high rate of load (4MPa/sec) had highest weighting
Veres et al. (2010)	27 ovine (isolated discs) – nuclear pressurisation	4x 12 MPa impulses 2x 14 MPa impulses 16 MPa impulses to fail	Neutral Flexion (7°)	Neutral 89% disc failure Flexed 43% vertebral failure Radial tears most common
Wade et al. (2014)	72 Ovine (intact)	2mm/min 40mm/min	Neutral Flexion (10°)	40mm/min – 42% endplate fracture, 58% herniation (42% mid-span annular rupture, 16% annular endplate rupture)
Wade et al. (2015)	74 Ovine (intact)	400mm/min	Flexion (10°)	17% endplate fracture 83% herniation (25% mid-span annular rupture, 58% annular endplate rupture)

5.3.3 Facet Joints in Mechanical Testing of the Disc

The facet joints play a significant role in limiting axial rotation, extension and forward sliding of the disc while also withstanding compressive loads. However, the inclusion of the posterior elements during mechanical testing of the disc has varied between studies. In several cases, the facet joints have been removed to provide a clear view of the posterior annulus during failure (Berger-Roscher et al. 2017; Wilke et al. 2016; Veres et al. 2010; Veres et al. 2009). Conversely, other research groups have included posterior elements to preserve physiological constraints during compressive testing (Wade et al. 2015; Wade et al. 2014; Adams & Hutton 1982). Although removing the posterior elements may aid visual detection of failure, it fails to meet physiologically similar conditions that would occur in vivo.

Berger-Roscher et al. (2017) tested thirty ovine specimens in combinations of flexion, lateral bending and axial rotation without facet joints. This group reported 76% endplate junction and 24% annular failures with combinations of lateral bending and flexion having the highest degree of risk. The exclusion of facet joints may have exposed the disc to increased anterior shear load bearing, increased axial rotation and decreased ability to withstand high loads. As this fatigue loading study was carried out over 1,000 cycles, there was the potential for water to diffuse out of the disc, resulting in reduced disc height. Under physiological circumstances, the facet joints would be required to withstand more of the compressive load as disc height decreases. As such, removal of the posterior elements during testing may expose the disc to increased loads that would have otherwise been supported by the facet joints. Additionally, this study reported failure events after just 1000 cycles. This differs significantly to studies that included facet joints that varied between 6,000 and 40,000 cycles at higher compressive loads of 1334 N – 1472 N (Gordon et al. 1991; Drake et al. 2005). This suggests that without facets, the disc is susceptible to injury with fewer cycles and lower loads. Furthermore, it is important to identify exactly how the facet joints contribute towards protecting the disc and what disparities in failure and herniation would be expected between the two groups.

Previous research has found that the facet joints play a significant role in withstanding loads, while also limiting movement. The intervertebral disc supports the majority of posterior shear loading, while the facet joints contribute significantly to anterior shear loading (Skrzypiec et al. 2013; Lu et al. 2005). Skrzypiec et al. (2013) found that the intervertebral disc contributes approximately 38% to initial anterior shear load-bearing, while the facet joints contribute significantly at approximately 55-66%. Previous findings have also found that isolated discs are 66% less stiff than intact FSUs in anterior shear, while all isolated discs loaded in anterior and posterior shear presented with damage at the interface between the endplates and the disc (Skrzypiec et al. 2013). The failure load of the human

disc in anterior shear is estimated to be 77% of the failure load of the intact motion segment (Cripton et al. 1995). Evidently, the posterior elements play a significant role in withstanding anterior shear forces to protect the disc.

Load sharing between the intervertebral disc and facet joints has been described in detail for axial compression (Adams & Hutton 1980; Dunlop et al. 1984). Under normal physiological conditions, the facet joints do not contribute to load sharing in compression and hence, the compressive mechanical properties of the intact FSU do not differ to those of an isolated disc (Adams & Hutton 1980).

However, narrowing of the disc can result in up to 70% of the compressive load being transferred to the facet joints (Dunlop et al. 1984; Adams & Hutton 1983). The facet joints also play a significant role in restricting excessive axial rotation. Sawa & Crawford (2008) found that the greatest facet load occurred during axial rotation followed by extension, flexion and lateral bending. The involvement of facet joints in supporting loads during flexion has drawn mixed conclusions. Although the facet joints do not contribute towards withstanding compressive loads during flexion, they prevent excessive forward flexion (Schendel et al. 1993). It has been proposed that the facet capsule ligaments play a significant role in resisting flexion of the intervertebral joint. Similar to forward flexion, lateral bending can tension and damage the contralateral capsule ligaments. This suggests that when present, the spinal ligaments will fail prior to nuclear herniation such that the disc is protected by the facet joints (Adams & Hutton 1983). Finally, Saipee et al. (2017) recently reported no difference in mode of failure experienced by intact and isolated discs failed by sudden overload in flexion. However, there is a significant difference in load at failure and hence, stiffness of the FSU (Saipee et al. 2017). Therefore, further work is required to investigate whether different directions of loading in intact FSUs and isolated discs will result in different modes of failure.

5.4 Mechanical Properties of a Herniated Disc

Previous research has predominantly focussed on simulating the herniation event itself. Therefore, fatigue and sudden overloading studies have primarily assessed load, stress, moments, specimen damage at failure and conditions required to induce herniation. To the author's knowledge, no research has been conducted to investigate the 6DOF mechanical properties of a specimen before and after a herniation event. This information would provide valuable insight into how the intervertebral disc is mechanically and functionally inhibited by herniation in different directions of loading.

6 Project Aims & Hypotheses

Numerous biomechanical tests have been undertaken in an attempt to simulate *in vivo* conditions and cause herniation in lumbar motion segments. However, several limitations and gaps have led to inconclusive results.

- ❖ Significant variation between experimental testing conditions, making it difficult to compare findings (i.e. specimen type, load, number of cycles, direction of loading, testing system).
- ❖ Very few studies have implemented a dynamic 6DOF mechanical testing system in simulating intervertebral disc herniation (Berger-Roscher et al. 2017; Wilke et al. 2016).
- ❖ Inclusion of the facet joints in previous studies has varied. The facet joints play a significant role in limiting axial rotation, extension and anterior shear of the disc. Therefore, it would be more desirable to keep the facets intact to more accurately represent *in vivo* conditions. Failure modes of intact FSUs and isolated discs have recently been compared in flexion (Saipae et al. 2017). However, this has not been attempted with different combinations of loading.
- ❖ Few studies have looked at the effect of combined loading in sudden overload in comparison to fatigue loading. It has been suggested that three axes of combined loading could increase the vulnerability of the intervertebral disc to injury (Pearcy & Hindle 1991; Costi et al. 2007). Therefore, complex motions could more closely represent *in vivo* loading conditions (Pearcy & Tibrewal 1984).
- ❖ Previous work has not characterised 6DOF mechanical properties of the FSU before and after the failure event.

6.1 Aims

To address these gaps and limitations in previous research, this study primarily aimed to:

- 1) Develop a sudden overload protocol that applies a high rate of axial compression in various combinations of loading directions to simulate herniation for the first time in the Flinders University hexapod robot.
- 2) Compare and identify the influence of facet joints on the failure mode experienced by sheep FSUs during sudden axial compressive overload in several directions of loading.
- 3) Investigate the modes of failure in varying combinations of loading conditions (i.e. flexion, lateral bend, axial rotation).
- 4) Compare the 6DOF mechanical properties of intact and isolated disc FSUs before and after a failure event.

6.2 Hypotheses

The following hypotheses have been made in regards to the results of this study. These hypotheses were tested with two-way univariate tests, non-parametric Kruskal-Wallis H tests and categorical Chi-Squared tests in SPSS.

- 1) There will be a significant difference between axial compressive failure stress and modulus of intact and isolated disc specimens.
- 2) Maximum axial compressive stress at failure will be higher in intact specimens in comparison to isolated discs.
- 3) Specimens tested in flexion and lateral bending will be most susceptible to injury and have the lowest axial compressive stress at failure.
- 4) Initial compressive stiffness of intact and isolated discs will be significantly greater than compressive stiffness quantified after the failure event.
- 5) Modes of failure between intact and isolated discs will be significantly different.

7 Methods

This study primarily involved specimen preparation, potting, hydration and mechanical testing in the hexapod (Appendix 1). Pilot testing was required to develop the hexapod protocol. The overall process carried out for each specimen was executed over two days (Figure 30).

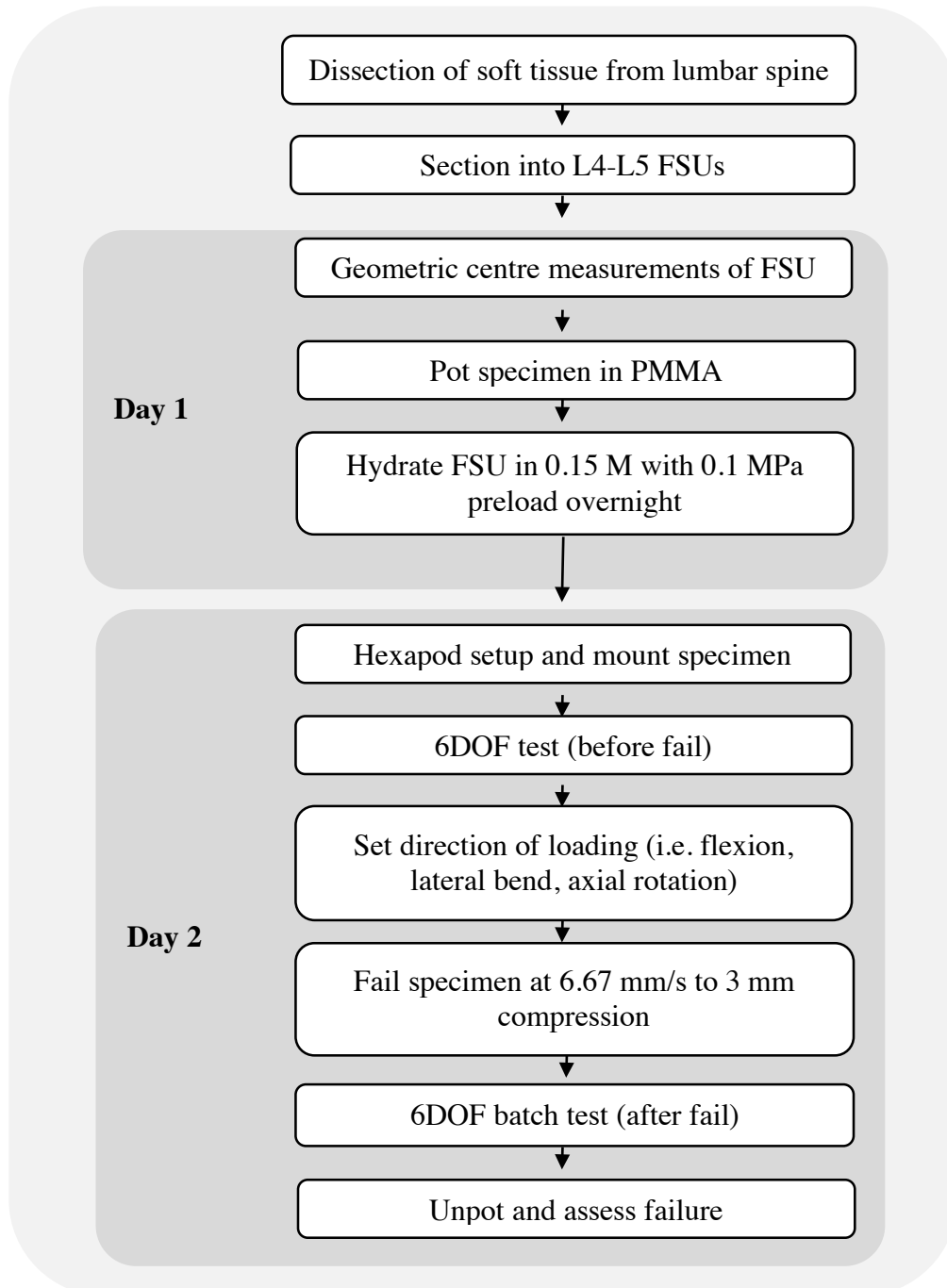


Figure 30. Flow chart summarising the main steps involved in the protocol.

7.1 Specimen Preparation

Thirty-two lumbar spines from sheep aged 12-24 months were sourced and collected from Austral Meats Adelaide Wholesale Meat (16 Main North Road, Gepps Cross SA 5094) and stored at -20°C (Figure 31).



Figure 31. Image of sheep lumbar spine before dissection

Specimens with visible macroscopic damage to the intervertebral disc were not included. Several steps were taken to prepare these specimens for mechanical testing, including the dissection of extraneous soft tissue, sectioning of the spine into FSUs and classification as intact or isolated disc specimens. Prior to dissection, the lumbar spines were thawed at room temperature for at least three hours. Careful dissection of soft tissue surrounding the vertebrae and discs was conducted using a scalpel and forceps (Figure 32).



Figure 32. Image of dissected sheep lumbar spine (L1-L6)

Preservation of the intervertebral disc, anterior longitudinal ligament, posterior longitudinal ligament and facet joint capsule was essential to accurately represent physiological FSUs. Dissected lumbar spines were individually wrapped in saline soaked gauze, sealed in plastic bags and re-frozen. This process was carried out over a period of four weeks prior to mechanical testing.

Following the completion of lumbar spine dissection, they were cut into FSUs. In preparation for sectioning FSUs, the lumbar spines were thawed at room temperature for at least three hours. A bandsaw was used to extract the L4-L5 FSU from each lumbar spine. These FSUs were sectioned such that the superior and inferior vertebral surfaces were cut parallel to the mid-transverse plane of the intervertebral disc. The transverse processes were removed and these L4-L5 FSUs were randomly assigned to the 'intact FSU' or 'isolated disc' groups. A hacksaw was used to cut down the coronal plane of the spinal canal and remove the posterior elements of the isolated disc group (Figure 33).



Figure 33. Lateral view of FSU. Dashed line indicates location of cut to remove facet joints

The spinal cord and any remaining soft tissue were removed for both groups. At this stage, the intact (Figure 34) and isolated disc (Figure 35) specimens had been prepared.

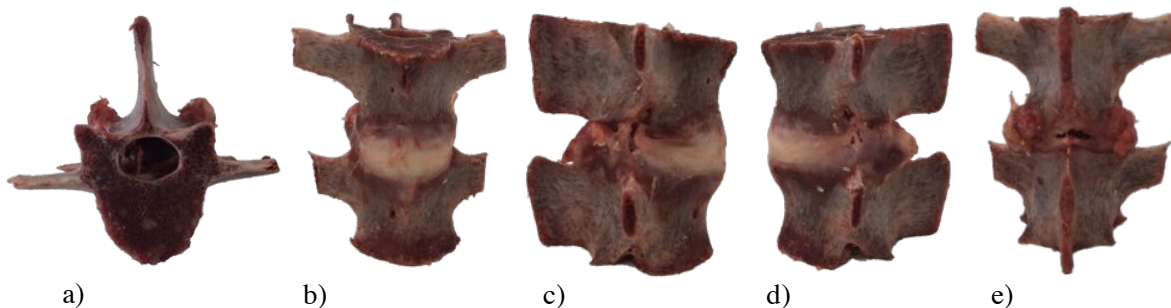


Figure 34. Image of intact FSU taken from five views a) Superior b) Anterior c) Right lateral d) Left lateral e) Posterior.

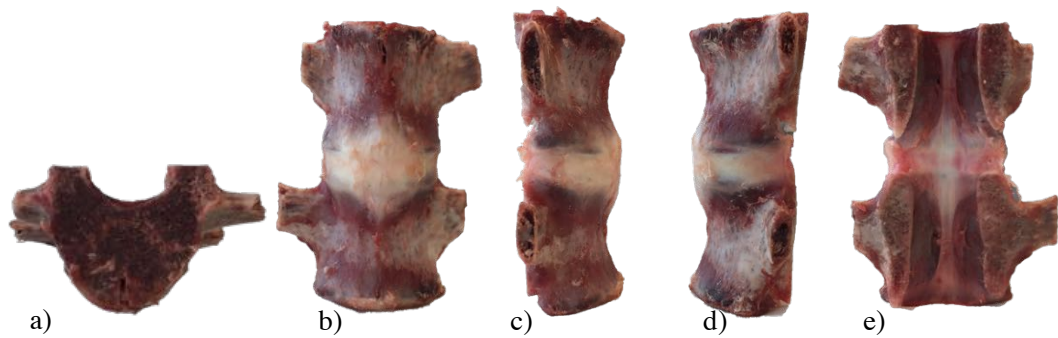


Figure 35. Image of isolated disc taken from five views a) Superior b) Anterior c) Right lateral d) Left lateral e) Posterior.

7.2 Potting

Potting was conducted the day prior to mechanical testing. Potting is a process involved in fixing the specimen in a top and bottom cup (stainless steel or aluminium) to provide a stable platform for the specimen to be mounted on in the hexapod. Specimens were potted in polymethyl methacrylate (PMMA) and aligned with a custom built alignment rig. PMMA is composed of a powder and liquid methyl methacrylate monomer and was combined at a ratio of 2.5 mL to 1mL, respectively. Enough PMMA was used to cover the majority of the inferior and superior vertebrae, while avoiding the disc. When these components are combined, an exothermic free-radical polymerisation is induced, producing a hard material. The alignment rig ultimately ensures that the top and bottom cups are parallel to each other and therefore, to the mid-transverse plane of the disc (Figure 36).

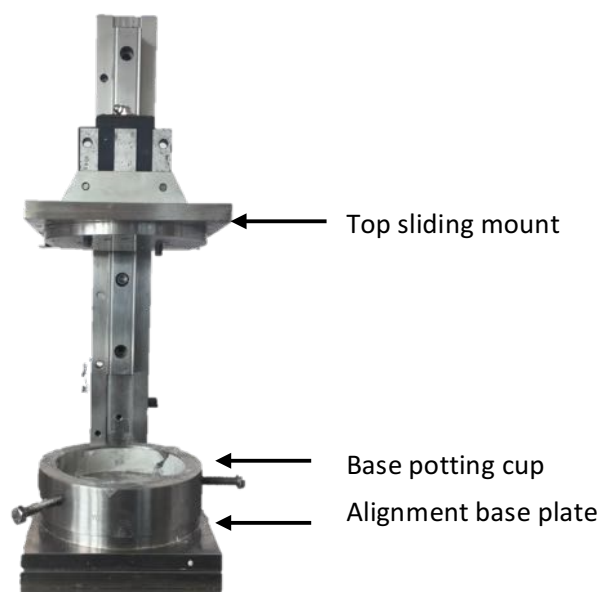


Figure 36. Image of potting alignment rig and attached base cup.

7.3 Geometric Centre Measurements

The hexapod robot rotates about a centre of rotation in the x-, y- and z-axes. When an FSU is mounted in the hexapod, it's geometric centre may differ to the centre of the hexapod. Therefore, measurements were taken once the inferior vertebra was potted in the base cup to determine the x-, y- and z-offsets required to align the geometric centre of the disc with the centre of the hexapod (Appendix 2). The x-offset and y-offset refers to the distance from the centre of the disc to the anterior edge of the cup and the left lateral side of the cup, respectively. The z-offset refers to the distance from the centre of the disc to the load cell of the hexapod.

7.4 Hydration & Preloading

To simulate physiological conditions, each specimen was hydrated and preloaded the day prior to mechanical testing. When in vivo, the intervertebral disc is exposed to diurnal changes of pressure, which varies with the sleep-wake cycle. When active, the intradiscal pressure experienced by the disc can range from 400 N -1900 N depending on how strenuous the task is (Nachemson 1964). Due to the disc's viscoelastic properties, these external loads applied to the disc throughout the day cause the disc to become dehydrated and consequently result in decreased disc height. When at rest and supine, the intradiscal pressure of the disc is much lower at 0.1 MPa (Nachemson et al. 1964). This allows water to move back into the disc and reach a steady state of hydration equilibrium. To simulate these conditions in vitro, each potted specimen was immersed in a 0.15 M phosphate buffered saline (PBS) bath overnight, or at least 4 hours, and the calculated preload force, or weight, was applied.

Disc area was estimated based on the formula, $Area = AP \times LAT \times 0.84$ (Nachemson et al. 1964), where AP is the anterior-posterior width and LAT is the right-left lateral width of the superior and inferior endplates and was used to calculate preload force necessary to produce 0.1 MPa pressure on the disc. The following formula was used, where P is intradiscal pressure, F is preload force and A is area.

$$P = \frac{F}{A}$$
$$F = P \times A$$

The relationship between the external compressive stress applied to the FSU and nucleus pressure is linear, where nuclear pressure is greater by a factor of approximately 1.5 (Nachemson et al. 1964).

$$F = \frac{0.1 \text{ MPa} \times A}{1.5}$$

Over time, water diffuses into the nucleus pulposus and the disc height increases. Hydration of the disc reaches a plateau, or steady state of equilibrium after approximately 3-4 hours, with the largest increase in hydration occurring in the first hour (Costi et al. 2002). To assess and validate the efficacy of this method of hydration, linear variable differential transformers (LVDTs) were set up to measure the displacement of the loading platform and thus, the displacement of the disc during hydration.

7.5 Mechanical Testing

7.5.1 The Flinders University Hexapod Robot

The Flinders University hexapod is a 6DOF mechanical testing robot based on the Stewart platform. The hexapod can function in single-axis or multi-axis displacement or rotations and is capable of reproducing 3D kinematics. Therefore, the hexapod is an ideal tool for testing and simulating intervertebral disc herniation by applying physiological rotations and forces to the disc. The hexapod is constructed of six servo-controlled ball screw driven actuators that position the mobile upper plate with respect to a fixed base plate (Figure 37).

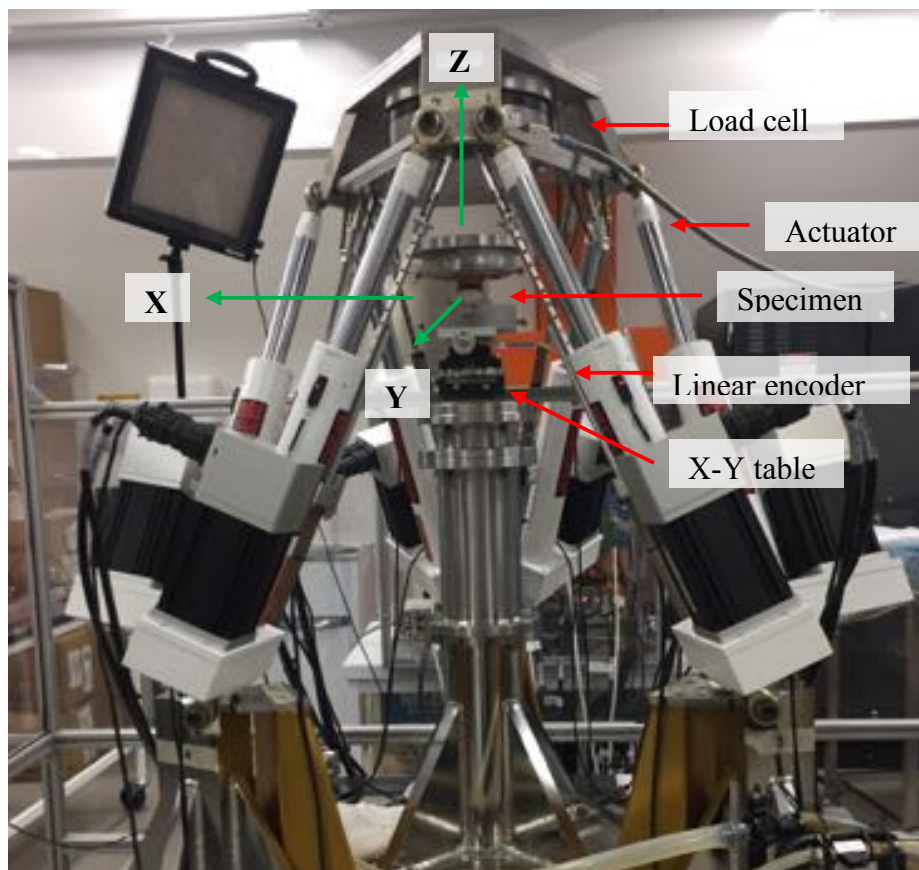


Figure 37. Image of the hexapod robot with a specimen mounted on X-Y table. Green arrows indicate the axis coordinate system of the hexapod, where the Y-axis is coming out of the page.

The specimen being tested is bolted to the upper and base plates. As such, any displacement, rotation, moment or force experienced at the upper plate will also correspond to those at the specimen if the potting is perfect. Six linear optical incremental encoders (B366784180185, LDM54, MicroE Systems, Inc., Brillerica, MA) are coupled with each hexapod leg to measure leg length. The resultant displacement and rotations can then be calculated about a fixed centre point. Forces and moments are measured by a load cell (MC3A-6-1000, AMTI, Watertown, MA), having a maximum axial compressive force limit of 20 kN and moment of 1500 Nm.

The hexapod is capable of being driven in 6DOF load control, 1 DOF position control or hybrid control (1DOF position control and 5DOF load control). The load control system allows for the application of dynamic loading either as pure forces/moments with real-time minimisation of all off-axis forces/moments, while position control sets the displacement or rotation of an axis while the other axes are controlled. Finally, hybrid control implements both features of load and position control by applying a load and position in an axis and minimising all off-axis forces, moments, displacements and rotations.

7.5.2 Pilot Mechanical Testing

As the first study of its kind in the hexapod, pilot testing was required to ensure the protocol was capable of meeting the objectives of the project (Section 6.1). The pilot protocol was developed based upon findings from the literature review (Section 5). Sheep L4-L5 FSUs were tested in sudden overload at 6.67mm/s (Wade et al. 2015) until 3mm of compression was reached. These tests were conducted in combinations of flexion (FL), right lateral bending (LB) and right axial rotation (AR), it has been hypothesised that flexion in combination with lateral bending will be most susceptible to injury (Berger-Roscher et al. 2017; Costi et al. 2007).

The primary objectives of pilot testing were to:

- ❖ Test FSUs in sudden overload at 6.67mm/s until 3mm of compression was reached.
- ❖ Ensure 3mm of compression was sufficient to produce failure.
- ❖ Simulate intervertebral disc herniation and ensure specimens are not failing by vertebral fracture or by other unexpected modes of failure.
- ❖ Become familiar with the hexapod and the protocol.
- ❖ Identify the most appropriate control mode as load control, position control or hybrid control.

Eight intact FSUs were tested (5xFL, 1xFL+LB, 1xLB, 1xC+Ramp FL). Each FSU was prepared (Section 7.1), potted (Section 7.2) and hydrated overnight (Section 7.4) as previously described. The

following day, specimens were mechanically tested in the hexapod where direction of loading, hexapod control mode and axis of ramp loading were tested (Table 4). Hexapod data was collected at 100 Hz for 20-30 seconds.

Table 4. Pilot testing parameters, aims and observations. SSO= Sheep sudden overload, FL=Flexion, LB=Right lateral bend, C=Compression.

ID	Disc Level	Control Mode	Test Group	Aim	Vertebral	Herniation
SSO1	L4-L5	Hybrid	FL + C	Practice with Hexapod	Inferior vertebra fracture	-
SSO2	L4-L5	Hybrid	LB + C	Practice with Hexapod	Inferior vertebra fracture	-
SSO3	L4-L5	Hybrid	C + FL	High compressive force causing vertebra fracture?	-	-
SSO4	L4-L5	Hybrid	FL + LB + C	Test new direction of loading (FL+LB)	Anterior bleeding	Posterior
SSO5	L4-L5	Position	FL + C	Test position control	Anterior inferior vertebra	-
SSO6	L4-L5	Load	FL + C	Test load control	Inferior vertebra & Facet failure	-
SSO7	L4-L5	Hybrid	FL + C	Validate need for XY table	-	-
SSO8	L4-L5	Hybrid	FL + C	Validate need for XY table	-	-

7.5.2.1 Pilot Testing Results

The compression and ramp flexion specimen (SSO3) will be excluded from analysis as the hexapod was unable to rotate at the specified rate, consequently triggering a fault flag before test completion. Of the pilot tests ramped to failure in compression, 12.5% failed by left postero-lateral herniation, 12.5% showed no visible damage to the disc or vertebrae, while 75% failed by inferior vertebral fracture with no evidence of damage to the disc. The specimen that failed by herniation was tested in flexion and lateral bending and nucleus was extruded posteriorly into the spinal canal (Figure 38).

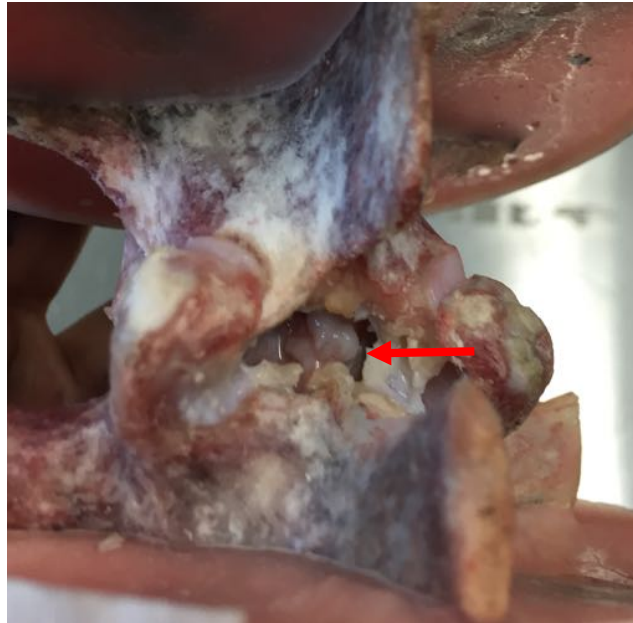


Figure 38. Left posterior view of SSO4 herniation in flexion and lateral bending. Arrow indicates white nuclear material extruded into the spinal canal of the FSU.

These findings supported the hypothesis that the combination of flexion and lateral bending poses the highest degree of risk to injury of the disc. This also significantly contributed towards validating the protocol as herniation was achieved in hybrid control by sudden overload at 6.67 mm/s to 3 mm of compression. However, many specimens failed by inferior vertebral damage (Figure 39).



Figure 39. Images of inferior vertebral fracture in pilot test FSUs. (a) Left anterior view of SSO5 (arrow: inferior vertebral shear fracture on right side). (b) View from left side of SSO6 (arrow: endplate junction failure and left facet failure).

To assess mechanisms of failure, each specimen's load-displacement, stress-strain, force-time, moment-time, displacement-time and rotation-time figures were plot for each test (Appendix 3). The sampling frequency when collecting data from the hexapod may have been too slow and future testing

would benefit from a higher sampling rate. However, the most notable finding of this analysis was the significant anterior-posterior (y-axis) and right-left lateral (x-axis) shear forces recorded at failure (Figure 40).

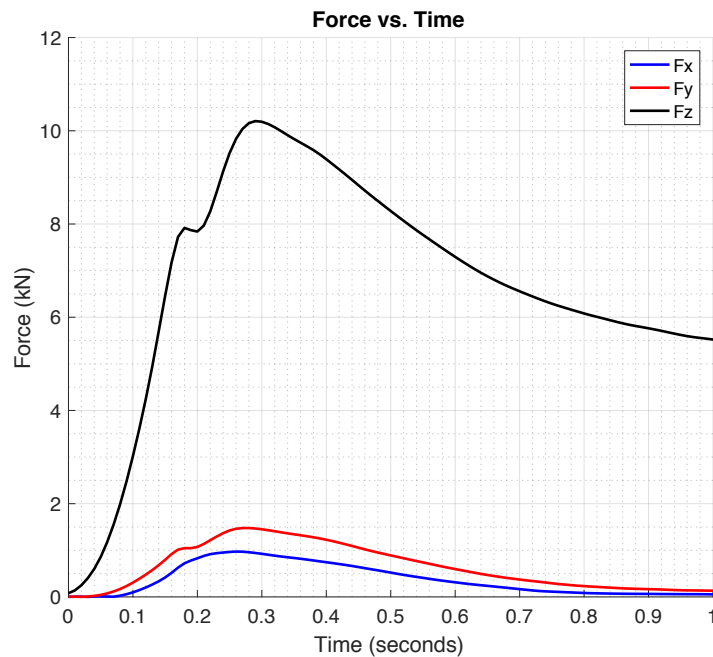


Figure 40. Plot of x, y and z-axes forces recorded for specimen SSO3 during failure. The z-axis is the primary axis of loading in compression and a high force is expected, while the x- and y-axes forces should be minimised to zero.

Many of these pilot tests were conducted in hybrid control (75%) or load control (12.5%), while only one was tested in position control. In hybrid or load control, the hexapod was driven in the primary z-axis, while attempting to minimise off-axes forces and moments to zero. However, the hexapod was unable to achieve this (Figure 40). In load and hybrid control, the hexapod receives force feedback at 0.3 Hz so that the force can be adjusted or minimised to the desired level (Lawless et al. 2014). However, this feedback loop was too slow to compensate for off-axes forces generated in sudden overload at 6.67 mm/s and thus, the shear forces were not minimised. It is also reasonable to assume that these unexpectedly high shear forces generated high shear strain and consequently resulted in anterior shear fracture of the inferior vertebra in 71.4% of specimens tested.

7.5.2.2 X-Y Table

Based upon the pilot testing findings, no system, including the hexapod robot, is capable of controlling load or position at the desired rate of 6.67 mm/s. Therefore, to physically minimise these forces, specimens must be allowed to translate in the anterior-posterior and right-left lateral directions. To achieve this, an X-Y table was developed. The X-Y table has two ball bearing rails in

the X and Y directions and a platform for the potted specimen to be mounted on (Figure 41). Similar approaches have been used in previous studies to enable shear movement (Callaghan & McGill 2001).

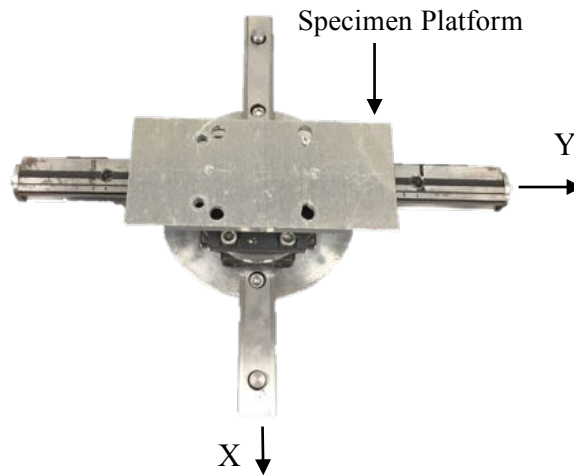


Figure 41. Image of the X-Y table. Arrows indicate the direction of X-axis and Y-axis translation.

Mounting the X-Y table underneath the potted specimen in the hexapod appeared to effectively enabled shear translation and thus, reduced anterior-posterior and lateral shear forces (Figure 42).

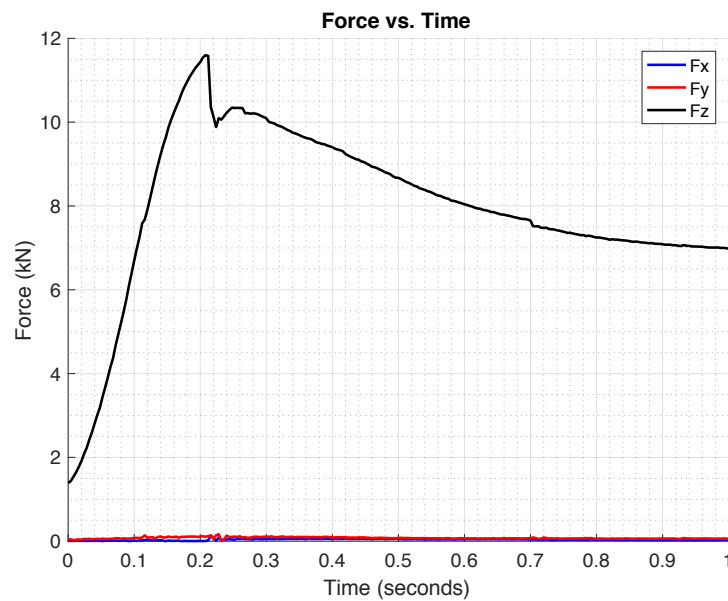


Figure 42. Plot of force the in x, y and z-axes for specimen SO12 with the X-Y table. This plot illustrates that the x- and y-axes forces are small and hence, the X-Y table is reducing shear forces.

7.5.3 Mechanical Testing

Mechanical testing of the specimen was carried out the day following potting and hydration of the specimen. This process primarily involved hexapod setup, 6DOF batch test before fail, setting the

specified posture, failure of the specimen, 6DOF batch test after fail and removing and unpotting the specimen.

7.5.3.1 Six Degrees of Freedom Test

The intervertebral disc is an anisotropic material and thus exhibits mechanical properties unique to the direction of loading. To quantify these mechanical properties in each DOF, specimens underwent a 6DOF sinusoidal loading regime at 0.1 Hz for five cycles. A frequency of 0.1 Hz was used as it is similar to that of walking and hence poses no risk of injury to the specimen. A compressive follower preload of 0.5 MPa was applied during each DOF in an attempt to mimic physiological conditions experienced by the disc (Patwardhan et al. 1999). To ensure the specimen returns to initial conditions between loading directions and to prevent inter-test variation, each DOF was followed by 5 minutes of creep recovery at 0.1 MPa (Amin et al. 2016).

Due to the biphasic behaviour of the disc, the sequence of tests was chosen to minimise fluid exudation. Bending and compression were found to promote the most significant degree of fluid flow, ultimately reducing volume and disc height of the specimen, while torsion and shear movements result in minimal changes to disc volume and fluid flow (Costi et al. 2008). Therefore, testing was conducted in the following order and the magnitude of each test was kept within a normal physiological range to prevent injury (Costi et al. 2008; Lu et al. 2005; Pearcy & Tibrewal 1984).

6DOF loading sequence:

1. Lateral shear (± 0.6 mm)
2. Anterior-posterior shear (± 0.6 mm)
3. Axial rotation ($\pm 2^\circ$)
4. Lateral bending ($\pm 5^\circ$)
5. Flexion-extension ($\pm 5^\circ$)
6. Axial compression (0.6 MPa + 0.5 MPa follower preload)

7.5.3.2 Direction of Loading

Prior to final catastrophic failure, the hexapod was driven in position control to rotate the FSU to the desired position relative to the geometric centre of the disc. The direction of rotation of the superior vertebra with respect to the inferior vertebra varied between four combinations of flexion, right lateral bending and right axial rotation (Table 5).

Table 5. Identification of testing groups by combinations of loading

	Flexion (13°)	Right Lateral Bend (10°)	Right Axial Rotation (4°)
Group 1	✓		
Group 2	✓	✓	
Group 3		✓	
Group 4		✓	✓

Therefore, rotation in the x, y and z axes (Rx: flexion/extension, Ry: right/left lateral bending, Rz: right/left axial rotation) were set according to the group being tested. Leg length, force and moment data was collected at 100 Hz for 75 seconds to confirm the specimen had reached the desired degree of rotation.

7.5.3.3 Sudden Overload

Once the specimen had been rotated to the desired position, the hexapod was set up for sudden overload failure in position control. To prevent triggering a load cell fault during failure, the load cell limits were increased (Table 6). Rx and Ry position control were enabled to minimise rotation of the specimen during failure.

Table 6. Load cell limits

	Fx	Fy	Fz	Mx	My	Mz
Load cell limit	6000 N	6000 N	17000 N	1000 Nm	1000 Nm	1000 Nm

A ramp velocity of 6.67 mm/s was applied to the specimen until a maximum compressive displacement of 3 mm in the primary z-axis was reached. Failure of the specimen was filmed and photographed. The raw hexapod data was collected at 250 Hz for 20 seconds. Following the failure event, each specimen underwent another 6DOF loading protocol to characterise the failed specimen's mechanical properties, as previously described (Section 7.5.3.1). The specimen was then removed from the hexapod, unpotted and observations were taken to determine the mode of failure.

7.6 Data Analysis

Hexapod leg lengths, loads and moments were collected during each test and formatted into two files. This data was then transformed using a previously constructed LabView program to account for the axis offsets and determine axial positions and rotations. Data from each sudden overload and 6DOF test was processed and analysed using code developed in Matlab (2016b, the Mathworks Inc.) (Appendix 4).

Analysis of the failure data involved adjusting the data to the start point of the test, plotting load-displacement curves, plotting displacement, rotation, force and moment against time. Stress, strain, stiffness and toughness throughout the test were also calculated. Axial compressive stress (σ) was determined using the following formulae, given the force (F) and intervertebral disc area (A).

$$\sigma = \frac{F}{A}$$

Strain (ε) was calculated using the following formulae, given the initial (l_o) and final (l) height of the disc.

$$\varepsilon = \frac{l_o - l}{l} \times 100\%$$

Failure was identified as the first peak of the stress-strain curve. Modulus was calculated along the linear elastic region of the stress-strain curves. The linear elastic region was identified as the region of the curve where stress was between 30% and 50% of the maximum stress. A linear regression function was used in Matlab to determine the slope of the curve (Matlab POLYVAL.m and POLYFIT.m having an order of 1). Finally, toughness or energy absorption at failure was calculated by integrating the area under the curve to the point of maximum stress (Matlab TRAPZ.m).

Statistical analysis was conducted in SPSS to test the project hypotheses (Section 6.2). Chi-squared likelihood ratio tests were conducted for assessing categorical data (e.g. modes of failure, direction of loading), while two-way univariate tests and non-parametric Kruskal-Wallis H tests were used to test the significance of variance between categorical and parametric data. Where necessary, Bonferroni post-hoc analyses were conducted. The significance level, or alpha value, was 0.05 such that a difference in means was deemed significant when $p < 0.05$ (2-tailed). For this study, marginal significance has been identified as $0.05 > p < 0.08$. The author acknowledges, that this is not a valid indication of significant variance between means. Instead, it provides an avenue for discussion and future work in the area to clarify the degree of significance.

7.7 Assessing Failure Mode

During sudden overload testing, a specimen can fail at various sites including annular rupture herniation, annular-endplate junction failure, endplate-vertebral shear fracture, endplate fracture, facet joint failure (dislocation or fracture), anterior vertebral body fracture or pedicle fracture. To simplify classifications, these modes of failure have been separated into four groups (Table 7).

Table 7. Classifications of failure modes

	Classification	Sites of failure
1	Herniation	<ul style="list-style-type: none"> - Annular herniation - Annular Endplate-junction failure
2	Herniation and endplate vertebral shear fracture	<ul style="list-style-type: none"> - Nuclear extrusion and endplate-vertebral shear fracture - Order or sequence of events may be inconclusive
3	Endplate-vertebral shear fracture	<ul style="list-style-type: none"> - Endplate-vertebral shear fracture
4	Vertebral Damage	<ul style="list-style-type: none"> - Endplate fracture - Facet joint failure - Anterior vertebral body fracture - Pedicle fracture
5	No damage	<ul style="list-style-type: none"> - No visible evidence of damage to the exterior surfaces

The occurrence and order in which structures fail may not necessarily be clear. Therefore, a protocol for classifying failure has been developed that involves analysis of failure videos, observations, load-displacement curves and moment-time curves (Appendix 5). Each specimen was filmed from the left-posterolateral region. This footage was analysed in iMovie 10.1.6 in slow motion at 5% of the original speed. Significant events (e.g. disc bulging, vertebral fracture, nuclear extrusion or spikes in sound) and time of occurrence were noted. These events were then matched to events on the load-displacement curves at the corresponding times. The load-displacement curve provides an indication of the type of failure event that has occurred. Typically, a load-displacement curve has a linear elastic region prior to catastrophic failure. It has been proposed that small changes in slope to the load-displacement curve, or small plateaus, are indicators of either a) gradual nuclear extrusion or b) gradual shear translation of the vertebra. In such a case, the displacement is increasing while the load remains relatively constant, indicating less resistance to force applied. On the other hand, a peak followed by a steep decline in load may indicate catastrophic vertebral failure as there is significant displacement. This may occur in cases of vertebral endplate fracture, shear fracture, pedicle fracture or facet failure. Overall, this process aided identification and sequence of failure events.

8 Results

This chapter presents and analyses data gathered from hydration equilibrium, modes of failure and the hexapod data to assess load, displacement, stress, strain, modulus and toughness at failure. Of the desired forty-eight specimens, thirty-two were mechanically loaded to failure in the hexapod robot. However, three specimens were excluded from statistical analysis due to technical complications with the hexapod during testing (SO10) and pre-existing damage to the specimen, inhibiting physiologically representative conditions in vitro (SO7, SO12). Therefore, twenty-nine specimens were successfully tested for analysis (Intact FSUs: 4xFL, 4xLB, 4xFL+LB, 1xLB+AR, Isolated Discs: 5xFL, 5xLB, 5xFL+LB, 1xLB+AR). However, it should be noted that no statistical analyses of the combined lateral bending and axial rotation group was conducted as only one specimen was tested for each group.

8.1 Hydration Data Analysis

Each specimen was hydrated in 0.15 M PBS for an average of 8.5 hours ranging from 4.5 to 12 hours. The hydration equilibrium of these specimens was measured using LVDTs. Due to the high sensitivity of the LVDTs, many of the measurements were not included as the LVDTs detected external displacements in addition to the change in disc height (e.g. table being knocked). However, the general trend showed that the change in disc height, or steady state equilibrium, was reached after approximately 4 hours (Figure 43).

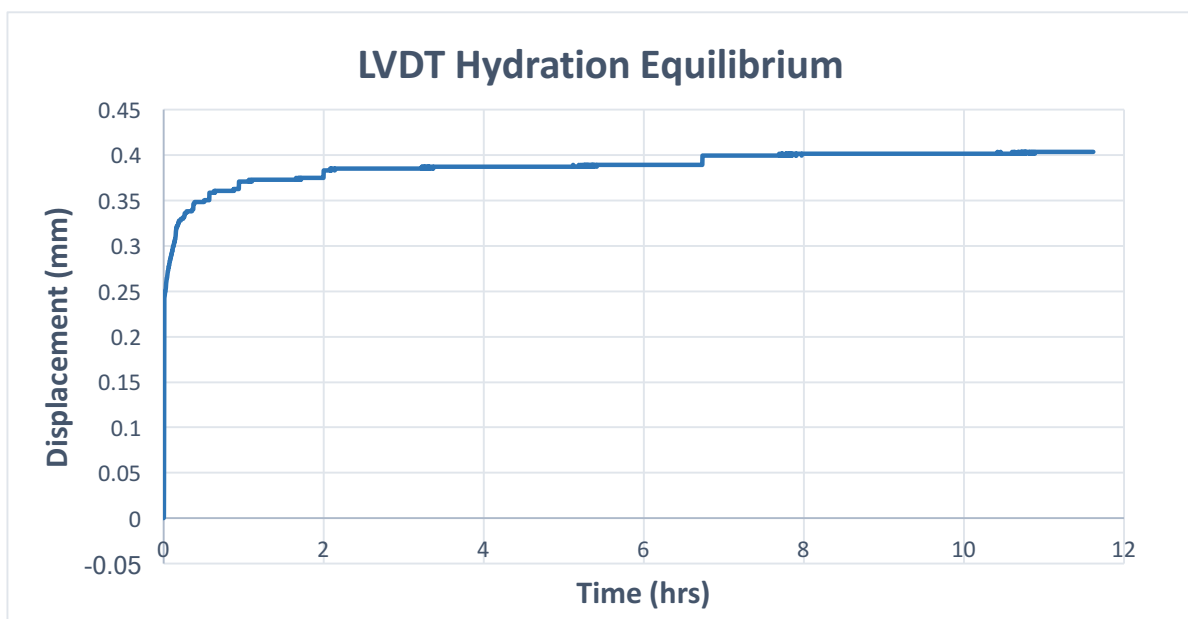


Figure 43. Example of LVDT hydration equilibrium (SSO6). Increase in disc height with time as water content of the disc increases.

8.2 Modes of Failure

Classification of modes of failure seen in the FSUs has been made based primarily on photographic evidence, video capture of the failure event and the corresponding load-displacement curves (Appendix 6 and Appendix 7). Of the twenty-nine specimens successfully tested, sufficient evidence for classification was present in twenty-eight specimens (Intact: 4xFL, 4xLB, 3xFL+LB, 1xLB+AR, Isolated disc: 5xFL, 5xLB, 5xFL+LB, 1xLB+AR). The correlation between test groups and modes of failure was conducted with Chi-Square Likelihood Ratio tests. Modes of failure were grouped by specimen type and direction of loading (Table 8).

Table 8. Summary of failure modes by specimen group and direction of loading

	Direction of Loading	Herniation	Herniation & Endplate-Vertebra	Endplate-Vertebral Shear	Vertebral damage	No damage
Intact	Flexion	50%	0%	0%	25%	25%
	Lateral Bend	100%	0%	0%	0%	0 %
	Flexion and Lateral Bend	25%	50%	0%	0%	25%
	Lateral Bend and Axial Rotation	100%	0%	0%	0%	0 %
Disc	Flexion	0%	40%	40%	20%	0 %
	Lateral Bend	0%	80%	20%	0%	0%
	Flexion and Lateral Bend	0%	80%	20%	0%	0%
	Lateral Bend and Axial Rotation	0%	100%	0%	0%	0%

There was a statistically significant difference between modes of failure seen in intact and isolated disc specimens ($p=0.001$). Of intact specimens, 76.9% had nucleus extruded (i.e. herniation, herniation & endplate-vertebral shear). Although none of the isolated disc specimens failed by herniation alone, 68.8% had evidence of nuclear extrusion as well as endplate-vertebral shear fracture. There were significant differences in modes of failure between intact and isolated discs that were in flexion ($p=0.05$) or lateral bend ($p=0.002$). Interestingly, there was no significant difference between mode of failure between intact and isolated discs in flexion and lateral bending ($p=0.229$). Finally, there was no significant difference between failure modes in different directions of loading in isolated discs ($p=0.471$) or intact FSUs ($p=0.078$).

8.2.1 Herniation

Of all specimens tested, 75.0% reported evidence of nuclear extrusion. These specimens were classified as herniation alone or as herniation in combination with endplate-vertebral shear fracture. The most prevalent mode of failure seen in intact FSUs was by herniation (61.5%). Intact FSUs loaded in combined lateral bend and axial rotation and in pure lateral bend all failed by herniation, while only 50% and 25% of intact specimens loaded in pure flexion and combined flexion and lateral bending herniated, respectively. The sites of annular herniation in intact FSUs included right-posterolateral (15.4%), left-postero-lateral (61.5%) and posterior (23.1%). As expected, the site of annular herniation was correlated with the direction of loading with marginal significance ($p=0.055$), where left posterolateral herniations were observed in tests involving right lateral bending (Figure 44).



Figure 44. Left postero-lateral herniation in lateral bend (SO6). Arrow indicates nucleus extruded.

Isolated discs did not fail by herniation alone. Instead, nuclear extrusion in addition to catastrophic inferior endplate-vertebral shear fracture were observed in 68.8% of isolated discs (Figure 45).



Figure 45. Posterior view of inferior endplate-vertebra fracture with nucleus extruded (arrow) in SO16 loaded in flexion and lateral bending.

Evidence suggests that these fractures were initiating and propagating from the inferior surface of the vertebral endplates. When separated from its inferior vertebra, endplate fractures and nuclear material can be seen extruding (Figure 46).



Figure 46. View of the inferior endplate of superior vertebra failed at endplate-vertebra interface with nucleus extruded (arrow) in SO27 tested in flexion and lateral bend.

A similar mode of failure was seen in two of the intact FSUs loaded in flexion and lateral bending (15.4%), although not to the same extent. Inferior endplate-vertebral shear fracture and nuclear extrusion was observed at the left postero-lateral side of the specimen at the inferior endplate-vertebral interface. Despite the presence of facet joints, the endplate appears to be torn away from the inferior vertebra (Figure 47).

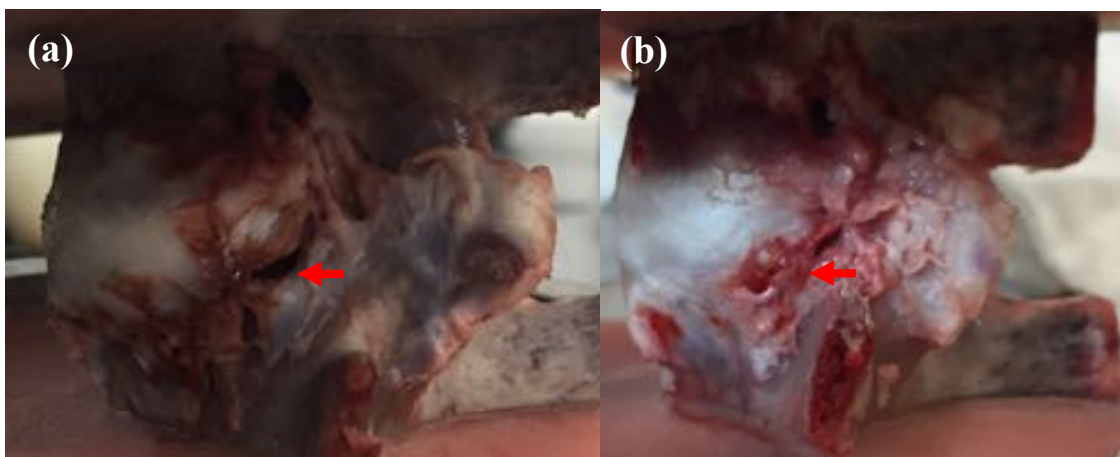


Figure 47. Images of endplate-vertebral failure (arrows) on left side in (a) SO3 and (b) SO8 in flexion and right lateral bending.

Interestingly, there was a significant difference in stress ($p=0.020$) and toughness ($p=0.016$) between intact and isolated discs that were loaded in flexion and lateral bend and failed by herniation and endplate-vertebral shear.

8.2.2 Endplate-Vertebral Shear Fracture

Observations show that 60.7% of all specimens had an element of endplate-vertebral shear fracture at the inferior vertebra, where 88.2% were isolated discs and 11.8% were intact FSUs. Specimens that failed by endplate-vertebral shear fracture alone showed no evidence of nuclear extrusion. It is believed that failure typically propagated from the right inferior-endplate surface (Figure 48). Of specimens that had an element of endplate-vertebral shear fracture, 73.3% had nucleus extruded.



Figure 48. Image of SO23 failed at inferior endplate-vertebral interface (arrow) with no nucleus extruded. Loaded in flexion and lateral bending

8.2.3 Vertebral Damage

Vertebral damage was not a major mode of failure observed in any of the testing groups. One intact FSU (6.25%) and one isolated disc (7.7%) failed by vertebral damage alone. Both vertebral fractures were loaded in flexion. The type of vertebral damage differed between intact and isolated disc specimens. The intact FSU fractured along the right-anterior surface of the inferior vertebra, while the isolated disc specimen failed at the inferior vertebra (Figure 49).



Figure 49. Image of vertebral fracture on the right side of the inferior vertebra in SO30 loaded in flexion

8.2.4 No Damage

There was no apparent damage observed in 15.4% of intact FSUs. However, it has been noted, that possible damage may simply be internal (Figure 50).

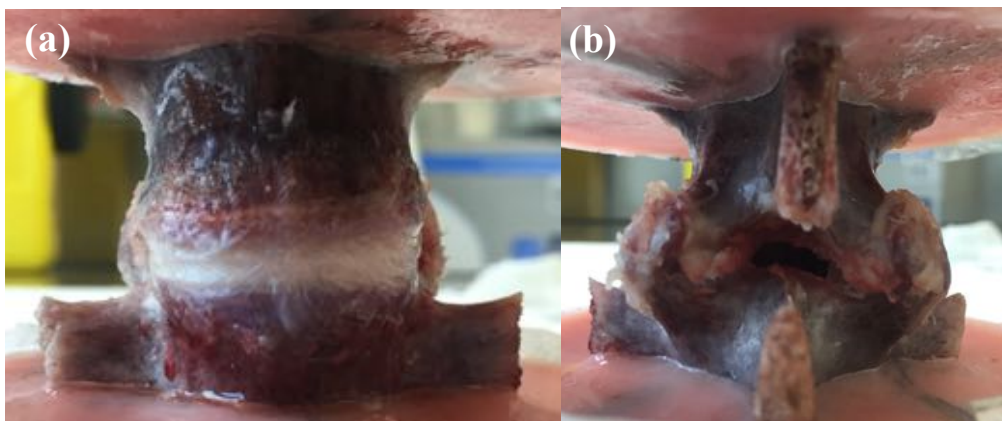


Figure 50. Anterior (a) and posterior (b) images of an intact FSU (SO5) with no visible damage to the disc or vertebrae.

8.2.5 Mode of Failure and Mechanical Behaviour Comparisons

The first peak load, moments, stress, strain, modulus and toughness were averaged across testing groups and within modes of failure (Table 9).

Table 9. Average load, moment, stress, strain, modulus and toughness by group (HER: Herniation, VER: vertebral fracture, EP-VER: endplate-vertebral shear fracture, Mx: Flexion moment, My: Lateral bend moment, Mz: Axial rotation moment, SD: standard deviation). Note: SD not included for groups with one specimen.

			Averages \pm SD							
	Posture	Mode of Failure	Load (kN)	Mx (Nm)	My (Nm)	Mz (Nm)	Stress (MPa)	Strain (%)	Modulus (MPa)	Toughness (MJ/m ³)
Intact FSU	FL	HER	12.8 \pm 0.7	25.5 \pm 15.5	9.8 \pm 7.5	2.96 \pm 3.0	25.9 \pm 1.8	63.7 \pm 21.1	58.1 \pm 10.7	7.3 \pm 1.7
		VER	8.2	24.1	3.0	5.6	17.6	60.6	37.8	4.7
	LB	HER	11.9 \pm 2.6	65.0 \pm 40.3	76.8 \pm 16.7	8.0 \pm 6.0	30.2 \pm 3.6	50.9 \pm 26.7	70.8 \pm 20.8	8.8 \pm 5.2
	FL + LB	HER	5.5	12.7	46.3	5.2	12.6	32.8	25.2	3.0
		HER + EP-VER	8.2 \pm 0.1	2.6 \pm 2.8	53.6 \pm 12.4	12.7 \pm 2.1	18.1 \pm 0.03	46.1 \pm 1.8	45.9 \pm 2.8	4.9 \pm 9.5
	LB + AR	HER	8.26	56.6	6.6	28.6	19.99	54.12	48.0	5.1
Isolated Discs	FL	VER	4.9	3.3	2.4	0.3	13.3	69.6	24.1	4.2
		EP-VER	6.7 \pm 1.3	6.5 \pm 8.0	6.1 \pm 7.3	1.9 \pm 2.2	14.6 \pm 0.4	49.6 \pm 3.1	40.4 \pm 3.2	3.1 \pm 0.7
		HER + EP-VER	5.1	17.4	11	0.5	11.0	49.3	45.0	2.3
	LB	HER + EP-VER	5.8 \pm 1.7	21.4 \pm 18.9	36.8 \pm 15.8	2.8 \pm 0.8	13.3 \pm 4.6	33.1 \pm 17.5	44.6 \pm 8.9	2.7 \pm 2.0
		EP-VER	4.3	9.4	27.1	3.0	11.0	29.4	37.0	1.9
	FL + LB	HER + EP-VER	4.6 \pm 1.1	10.5 \pm 3.8	25.4 \pm 6.3	1.3 \pm 0.5	10.3 \pm 2.8	27.6 \pm 14.9	37.3 \pm 6.0	1.7 \pm 9.1
		EP-VER	4.8	2.4	25.5	1.0	10.1	52.2	23.1	2.5
	LB + AR	HER + EP-VER	3.6	19.3	21.3	6.5	9.3	55.36	18.7	2.9

Peak flexion, lateral bend and axial rotation moments were averaged for each failure group. Many of these peak moments were greater than physiological limits. However, no clear trend could be associated to failure mode due to significant variance between specimens. The load-displacement curves of intact FSUs and isolated discs show disparities between herniated, herniated and endplate-vertebral shear fracture and pure endplate-vertebral shear damage (Figure 51).

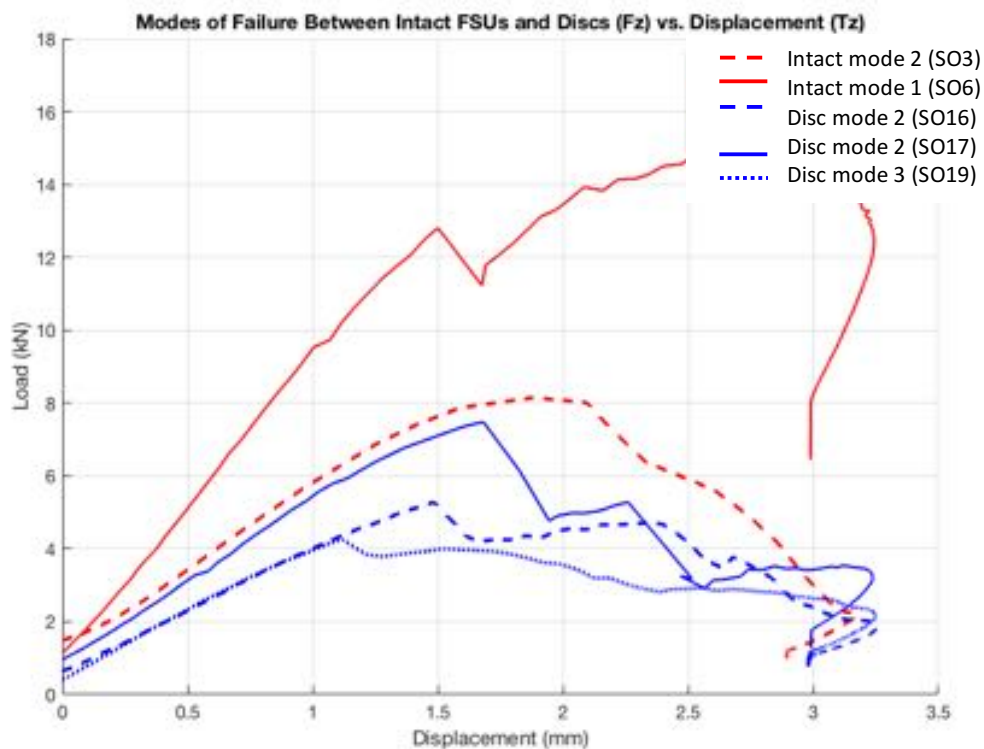


Figure 51. Comparison of load-displacement curves between intact and isolated discs. Loads at failure in intact herniated specimen (SO6) tested in lateral bend greater than intact specimen tested in flexion and lateral bend (SO3) that failed by herniation and endplate-vertebral shear. Intact FSUs loads at failure both greater than isolated discs tested in lateral bend (SO17, SO19) and flexion and lateral bend (SO16).

Statistical comparisons between modes of failure could only be made between test groups that reported multiple types of failure within or between test (Appendix 8). The main findings from these analyses were that there were no significant differences in failure parameters (i.e. stress, strain, modulus, toughness) between modes of failure in specimens tested in the isolated flexion lateral bend group, the isolated lateral bend group or the intact flexion group. However, there was a statistically significant difference in stress ($p=0.005$) and strain ($p=0.045$) between intact specimens that failed by herniation and by herniation and endplate-vertebral shear in the flexion and lateral bend group.

8.3 Loading Direction Mechanical Behaviour Comparisons

Twenty-nine specimens (Intact: 4xFL, 4xLB, 4xFL+LB, 1xLB+AR, Isolated discs: 5xFL, 5xLB, 5xFL+LB, 1xLB+AR) were successfully rotated and loaded at 6.67 mm/s until 3 mm of compression was reached. Two-way univariate ANOVAs and non-parametric Kruskal-Wallis tests were conducted to assess variance of stress, strain, modulus and toughness between specimen type and between direction of loading (Appendix 9).

8.3.1 Stress-Strain Curves

The stress-strain curves were plotted by FSU group (intact or isolated) and by direction of loading (Figure 52-Figure 59). These stress-strain curves were used to derive the modulus and toughness at failure for each specimen, while also visually illustrating underlying trends within groups. The stress-strain curves have the same x- and y- scales for comparisons between groups. It should be noted that the stress at the beginning of each test differs according to the load applied to the specimen when mounted to the hexapod.

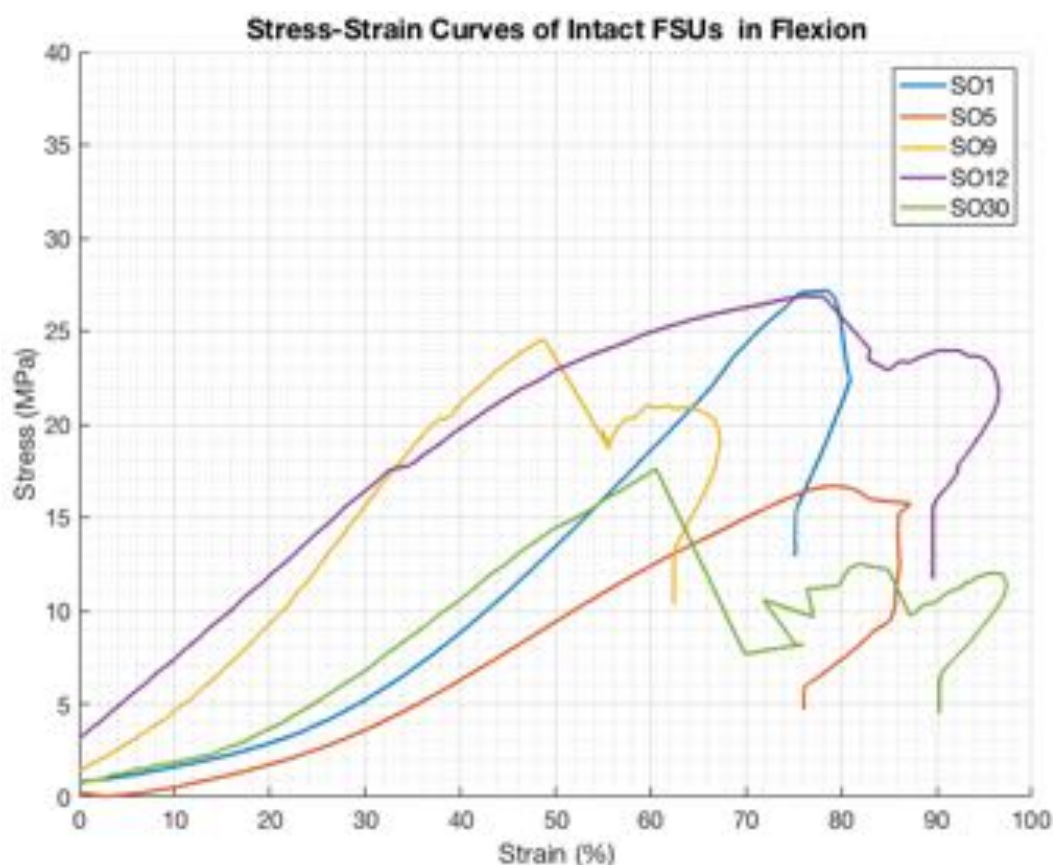


Figure 52. Stress-strain curves for intact FSUs in flexion

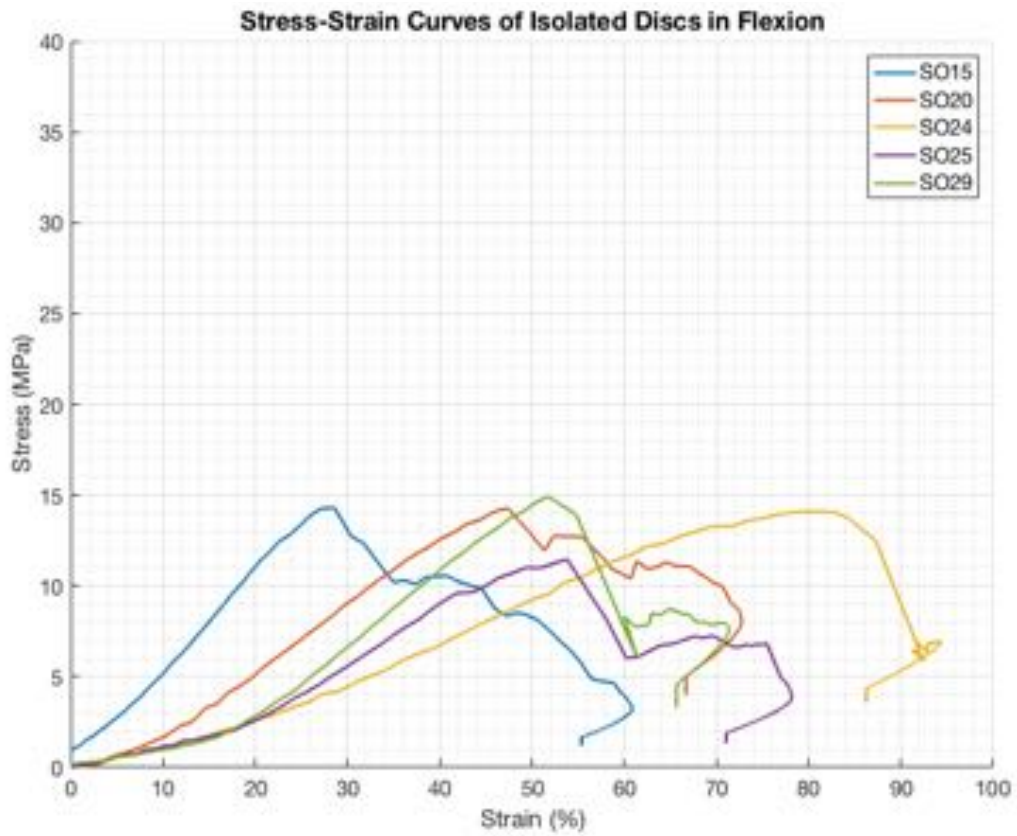


Figure 53. Stress-strain curves for isolated discs in flexion

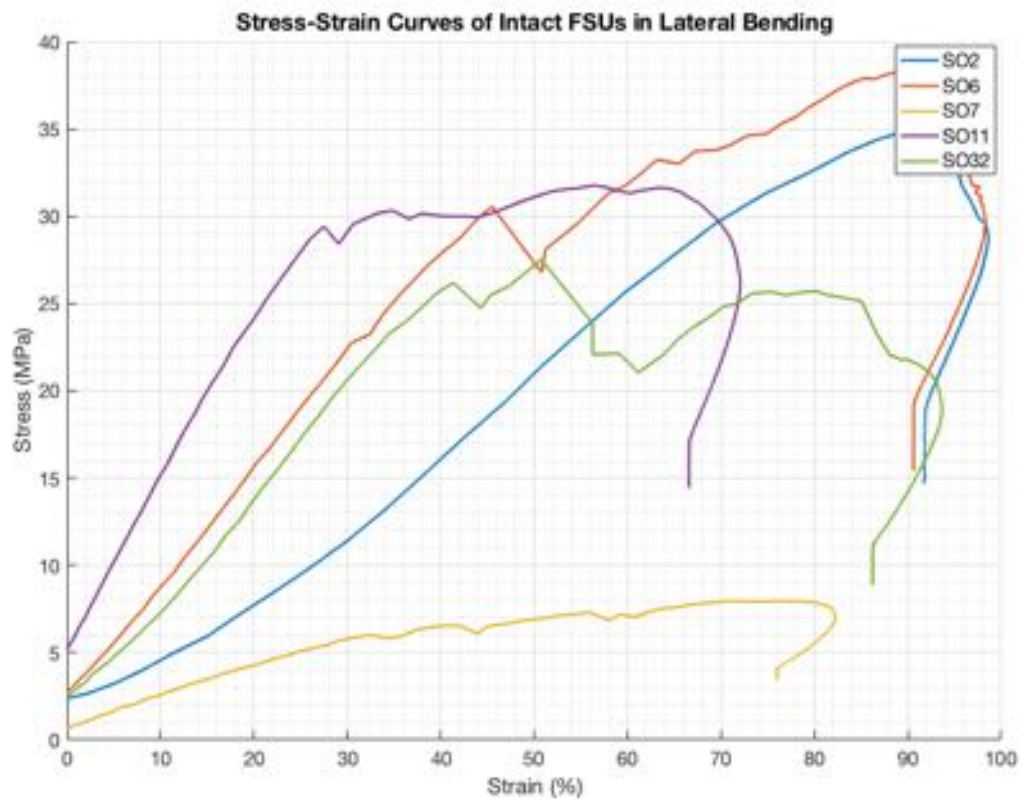


Figure 54. Stress-strain curves for intact FSUs in lateral bend

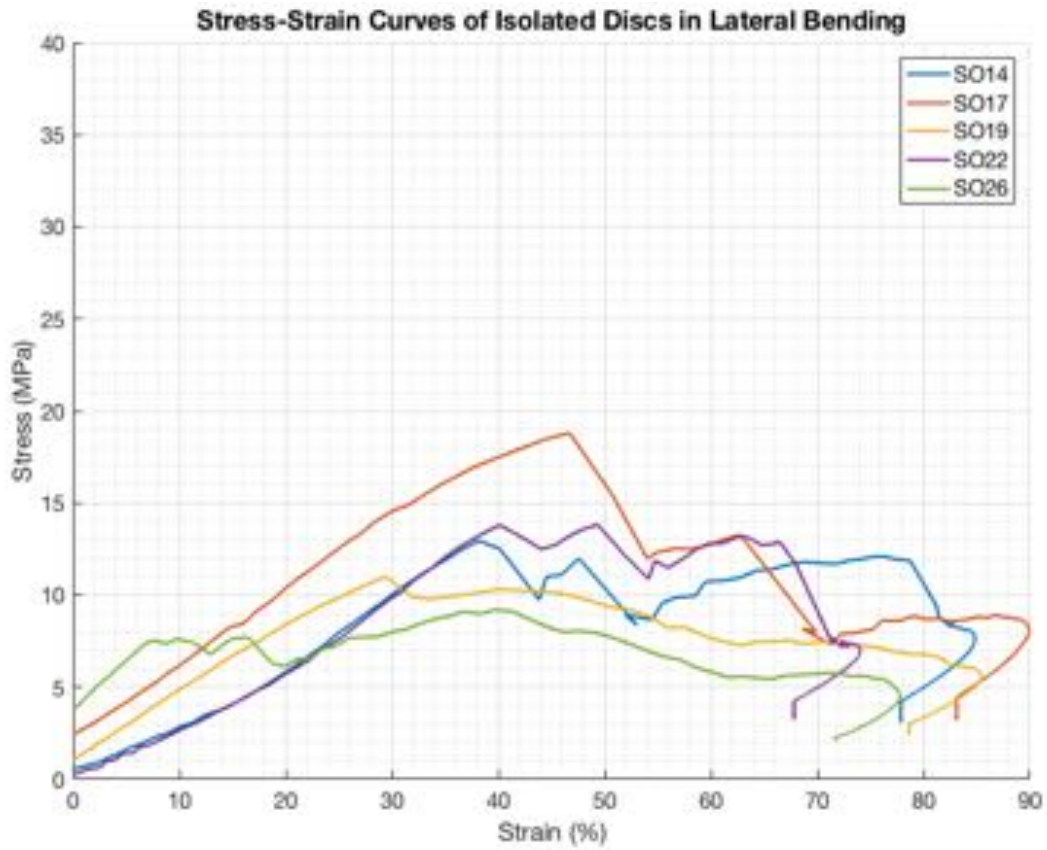


Figure 55. Stress-strain curves for isolated discs in lateral bend

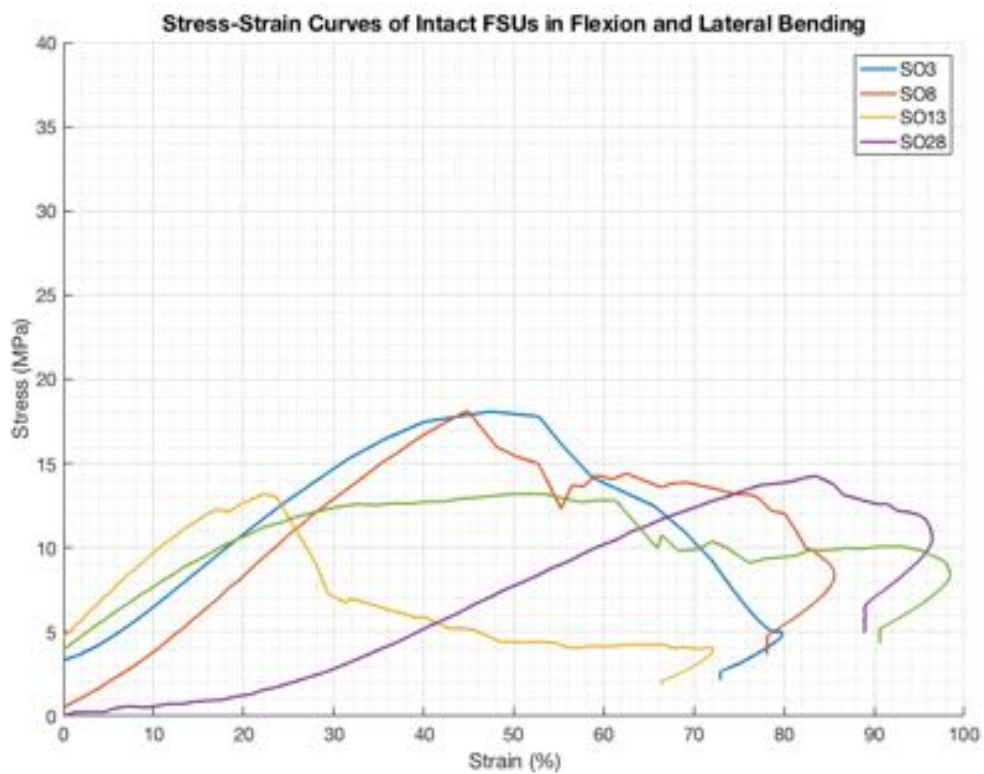


Figure 56. Stress-strain curves for intact FSUs in flexion and lateral bend

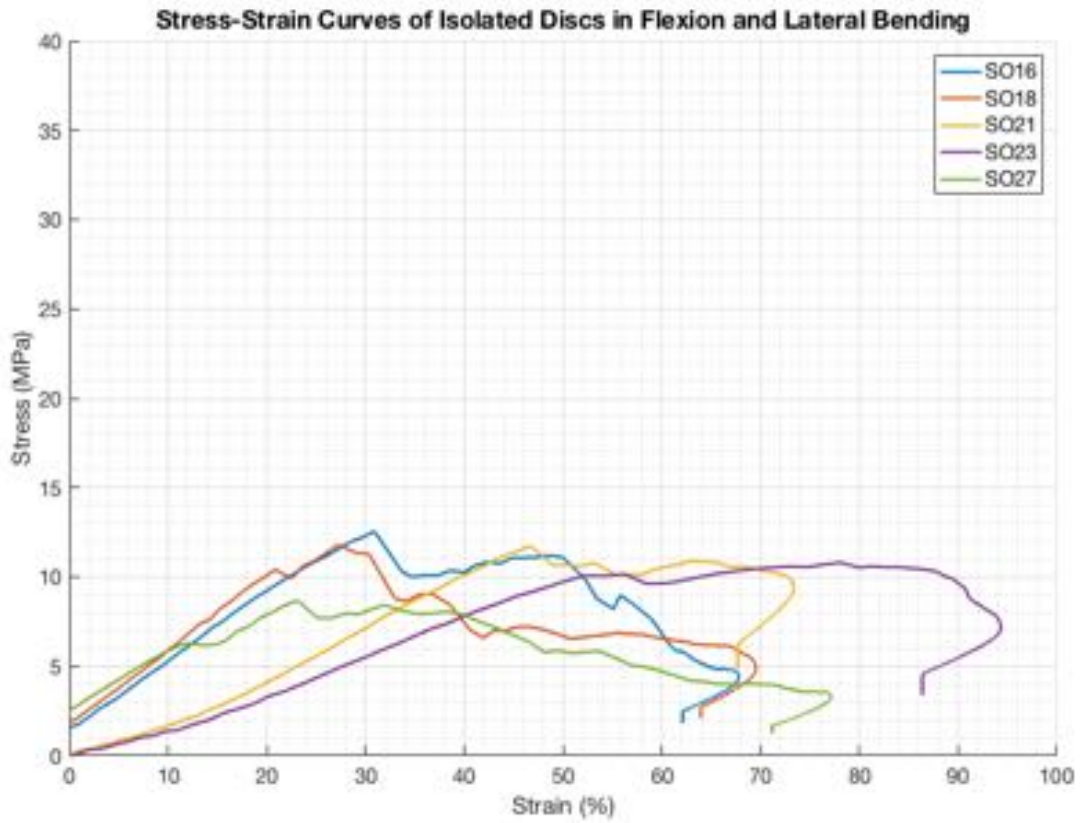


Figure 57. Stress-strain curves for isolated discs in flexion and lateral bend

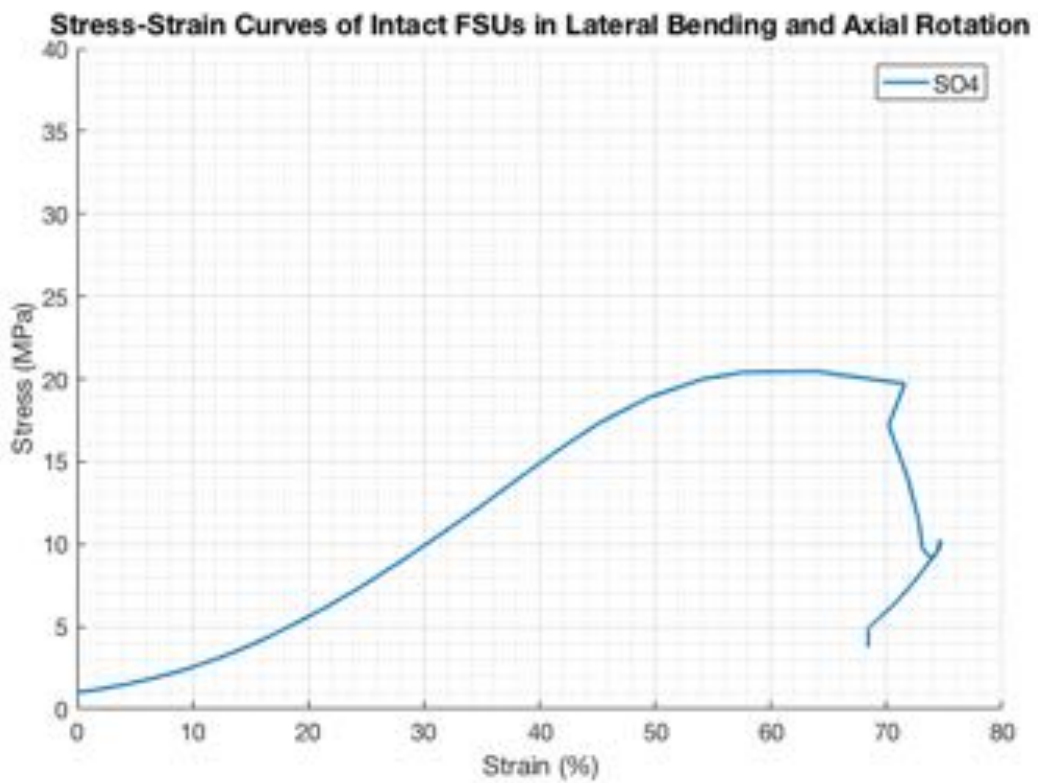


Figure 58. Stress-strain curves for intact FSUs in lateral bend and axial rotation

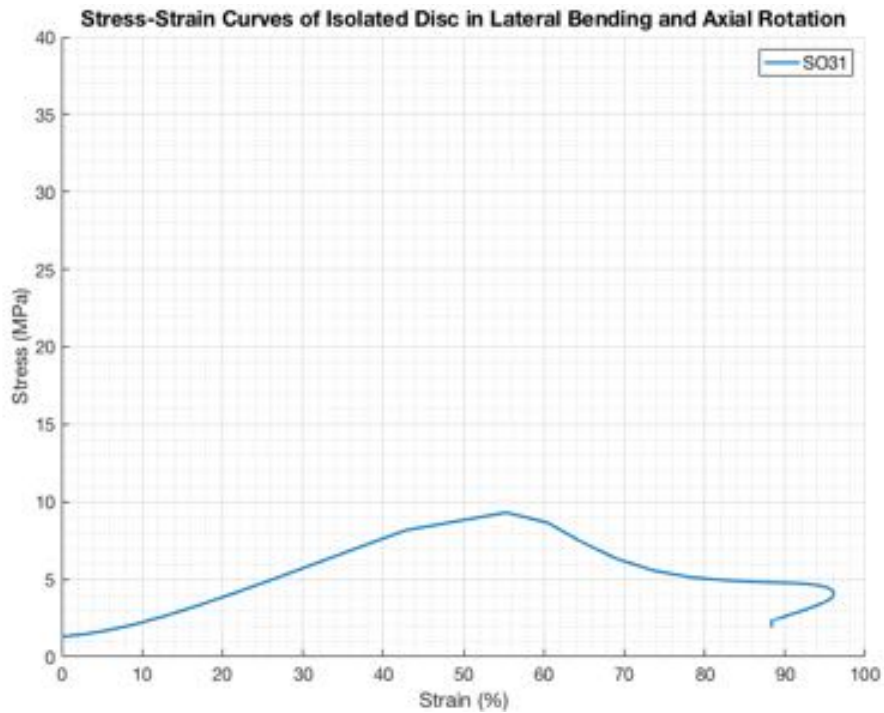


Figure 59. Stress-strain curves for isolated discs in lateral bend and axial rotation

8.3.2 Stress

Overall, there was a significant difference in stress at failure between intact FSUs and isolated discs ($p < 0.001$). The results from the two-way univariate ANOVA indicate that there was an interaction between FSU type and direction of loading ($p < 0.001$). Further analysis revealed significant differences between intact and isolated discs in flexion ($p = 0.003$), lateral bend ($p < 0.001$) and flexion and lateral bend ($p = 0.027$) (Figure 60).

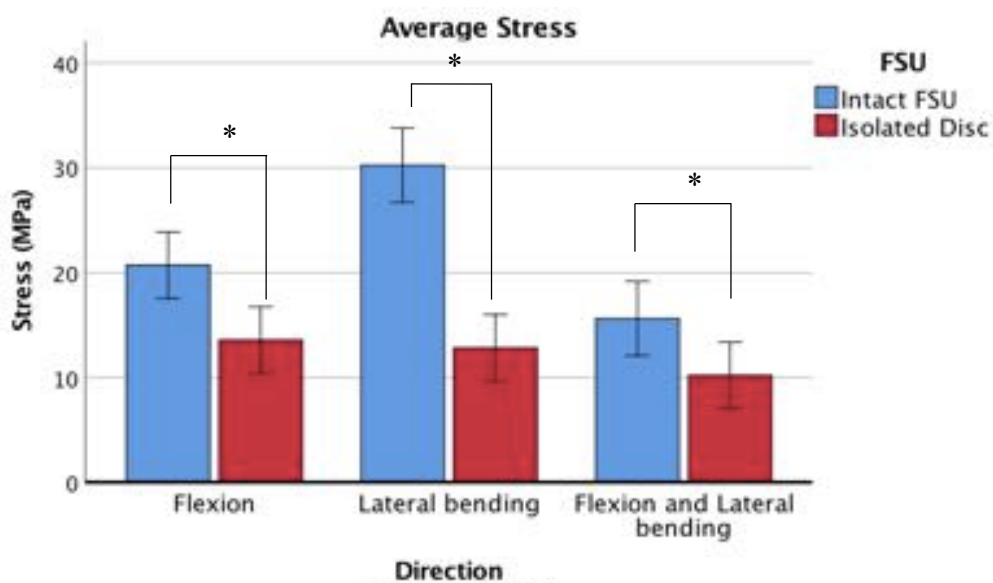


Figure 60. Bar graph of average stress at failure in intact and isolated discs. Error bars: 95% confidence interval. Asterisk: $p < 0.05$

Pairwise comparisons of the interaction between FSU type and direction of loading showed a significant difference in stress between intact flexion and intact lateral bend ($p=0.001$), intact lateral bend and combined flexion and lateral bend ($p=0.000$), but no significant difference between intact flexion and combined flexion and lateral bending ($p=0.11$) (Figure 61).

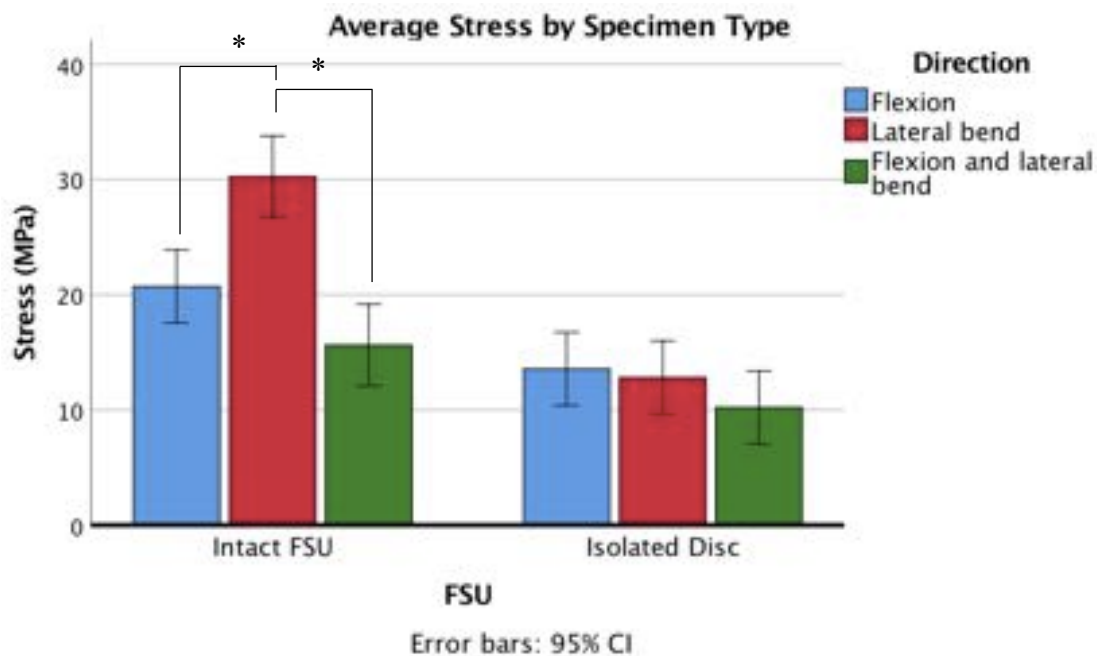


Figure 61. Bar graph of average stress between directions of loading. Error bars: 95% confidence interval. Asterisk: $p < 0.05$

This supports the finding that the lowest average stress at failure in intact specimens occurred in flexion and lateral bend (15.6 MPa), while the highest average stress was in pure lateral bend (30.2 MPa). Interestingly, there were no significant differences between directions of loading in isolated discs.

8.3.3 Strain

Mean strain at failure was calculated and grouped according to specimen type and direction of loading (Figure 62). A two-way univariate ANOVA test reported a significant difference in strain between intact and isolated discs ($p=0.038$). However, there was no significant difference between directions of loading. These results suggest that intact FSUs were typically strained in compression by approximately 50 – 67%, while isolated discs were strained by 32 – 55% at failure.

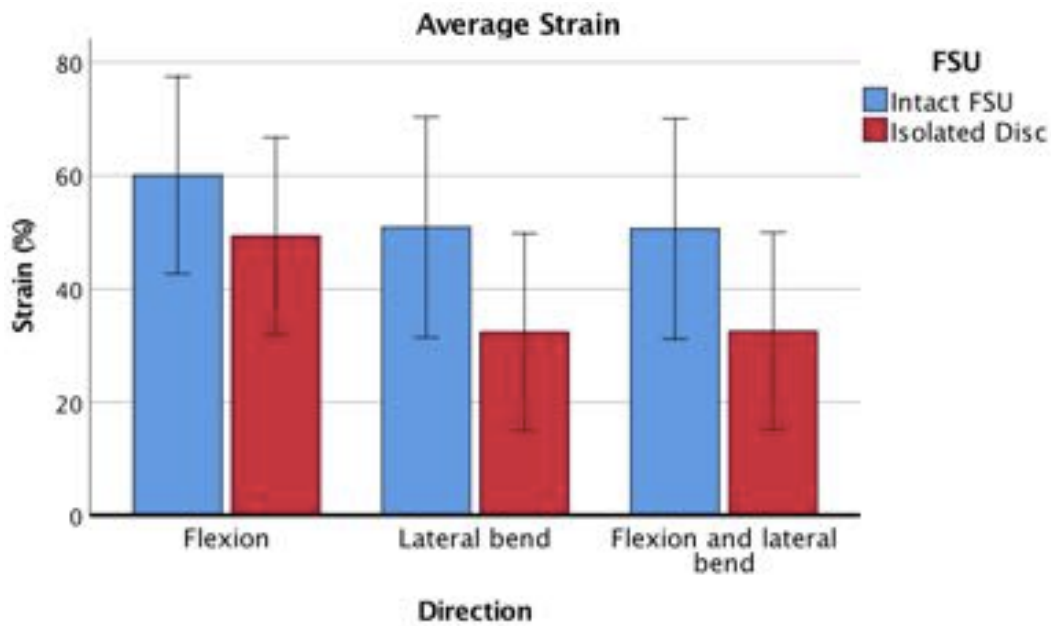


Figure 62. Bar graph comparing average maximum strain at failure between groups. Error bars: 95% confidence interval.

8.3.4 Modulus

Overall, there was a significant difference in modulus between intact and isolated discs ($p=0.012$). There was also a significant difference in modulus between directions of loading ($p=0.007$). Pairwise comparisons revealed a significant difference in modulus between intact and isolated discs ($p=0.003$) in lateral bend (Figure 63).

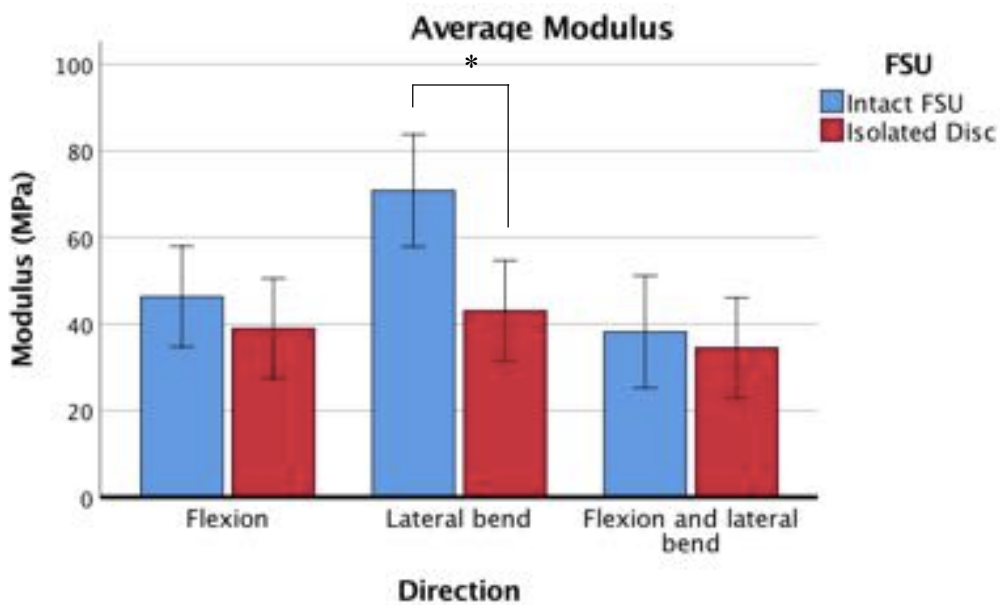


Figure 63. Bar graph of average modulus at between intact and isolated discs. Error bars: 95% confidence interval. Asterisk: $p < 0.05$

There was a significant difference between flexion and lateral bend ($p=0.024$) in intact specimens and a difference between flexion and combined flexion and lateral bend ($p=0.004$) in intact specimens (Figure 64). No other significant differences were found.

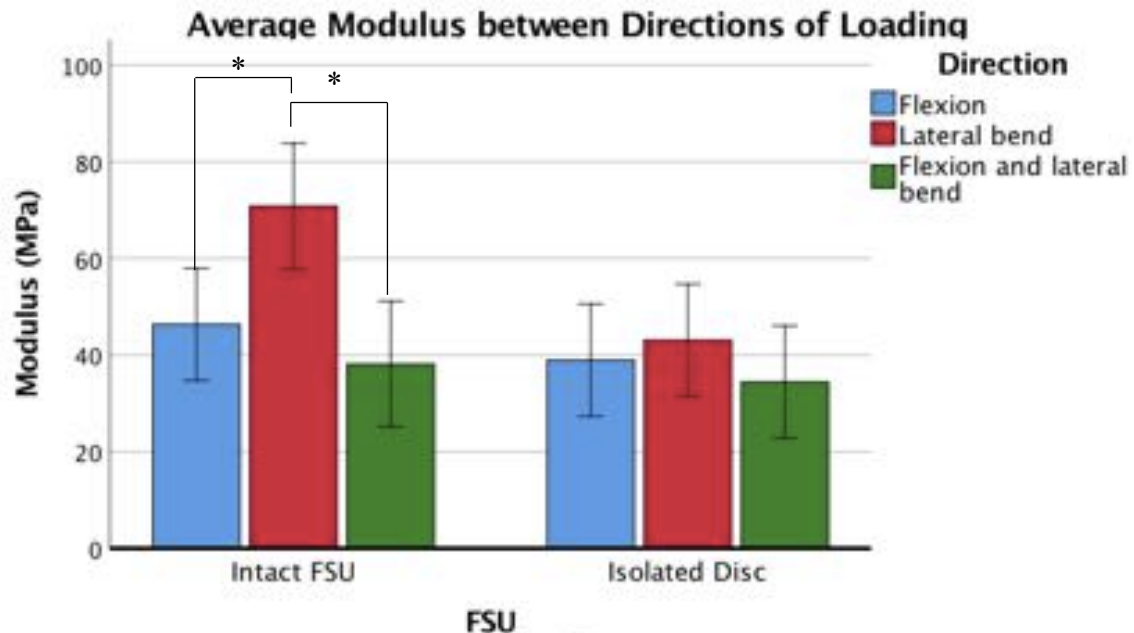


Figure 64. Bar graph of average modulus between directions of loading. Error bars: 95% confidence interval. Asterisk: $p < 0.05$

8.3.5 Toughness

Average toughness or energy absorption of the specimen at failure shows that intact FSUs had a much higher toughness in comparison to their isolated disc counterparts. On the other hand, toughness differences between the combinations of loading in isolated discs is relatively small. Due to failure to meet the Levene's test of equal variance, a Kruskal-Wallis analysis of the data was conducted. This test reported a significant difference between intact FSUs and isolated disc toughness ($p < 0.001$). As expected, statistical significance was found for each combination of loading between intact and isolated discs. There was a significant difference in toughness between lateral bend and combined flexion and lateral bend in intact specimens ($p=0.043$). No other significant differences were found between directions of loading in intact or isolated discs. Specimens in pure lateral bend absorbed the most energy (8.8 MJ/m^3), while the least amount of energy was absorbed in the flexion and lateral bend group (4.3 MJ/m^3). No significant differences were found between loading combinations for isolated discs (Figure 65).

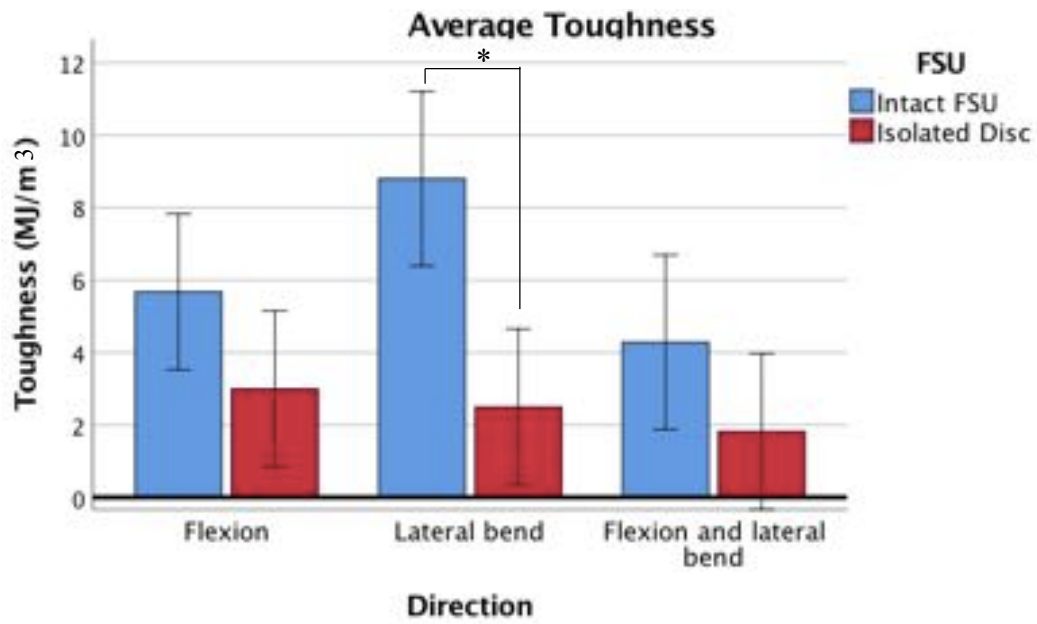


Figure 65. Bar graph of average toughness between intact and isolated discs. Error bars: 95% confidence interval. Asterisk: $p < 0.05$

The results presented in this chapter have outlined the modes of failure and average mechanical properties of intact FSUs and isolated discs in varying combinations of loading. It is also important to discuss the relevance of the findings and how they address limitations in previous research.

9 Discussion

This study aimed to develop a protocol to herniate sheep intact FSUs and isolated discs under varying directions of sudden overload in the hexapod robot and subsequently, investigate modes of failure between test groups. The facet joints prevent excessive axial rotation, forward sliding of the disc and extension (Adams et al. 2013). Therefore, it was hypothesised that there would be significant differences between intact FSUs and isolated disc specimen failure stress and modes of failure. Previous research has also reported that the combination of flexion and lateral bending is most susceptible to disc injury (Berger-Roscher et al. 2017; Costi et al. 2007). As such, it was hypothesised that the intact and isolated discs tested in flexion and lateral bend would fail at the lowest compressive load and stress. Another aim of this project was to characterise and compare the specimen's mechanical properties before and after herniation. However, due to time restrictions, this objective was not met and will not be discussed in this chapter. Twenty-nine sheep specimens were successfully tested in the hexapod for analysis. However, the protocol used to induce failure by sudden overload in sheep FSUs had not previously been attempted in the hexapod and thus, there were several limitations that should be acknowledged.

9.1 Limitations

The most significant limitation of this study was the use of young sheep spines to model the human spine. Numerous similarities have been reported between the species anatomy (Wilke et al. 1997a), biochemical composition (Reid et al. 2002) and biomechanical behaviour (Costi et al. 2009; Wilke et al. 1997b) in 3 – 4 year old sheep lumbar spines. However, the FSUs used in this study were from 1 – 2 year old sheep. Although the gross anatomical structures of young sheep lumbar spine would be comparable to the human lumbar spine, the integrity and mechanical similarity has not previously been reported. This study was also limited by a relatively small sample size of specimens successfully tested ($n=1$ to 5 per test group). In particular, a larger sample size in the lateral bend and axial rotation groups ($n=1$) would be required to derive meaningful statistics. Mechanical testing of this direction of loading was restricted by the hexapod graphical user interface (GUI), which only permitted rotations of flexion (R_x) and lateral bending (R_y). The two specimens tested in lateral bend and axial rotation were conducted in a different GUI that was capable of axial rotation (R_z). However, use of this GUI compromised the 6DOF loading protocol and was not used for further tests. However, to evaluate the effect of certain movements in causing herniation, it is important to characterise *all* directions of loading.

Testing in the hexapod was limited by the inclusion of the X-Y table during the 6DOF loading protocol. Translation of the X-Y table on the inferior surface of the specimen was not recorded by the superior load cell and linear encoders. Consequently, data gathered on anterior-posterior and lateral shears were not representative of actual translation. In future, this could be avoided by mounting the X-Y table superior to the specimen. During the failure test, isolated disc specimens frequently experienced catastrophic damage to the endplate-vertebra interface. Such catastrophic failure makes it difficult to interpret the results and identify the precise sequence of events that led to failure of the specimen. Again, the absence of shear translations also makes it challenging to determine whether or not catastrophic failure occurred within physiological limits of shear translation. Finally, this study was also limited by the method for determining the mode of failure. Due to time restrictions and project budget, the only analysis made was by visual inspection of the FSU. Failure events were recorded from the left postero-lateral side. Consequently, damage outside of this field of view was not captured. This identification process would also benefit from additional modalities (e.g. MRI, x-rays and macroscopic dissection) to more accurately interpret the mechanism of failure.

9.2 Physiological Conditions in the Hexapod

To achieve *in vivo* conditions, each specimen was hydrated in 0.15 M PBS and subjected to an axial compressive preload of 0.1 MPa for an average of 8.5 hours to simulate the unloaded disc during rest (Wilke et al. 1999). Steady state equilibrium was reached after approximately 4 hours of hydration. This supports previous findings that found the disc reached a plateau in hydration after 3 – 4 hours (Costi et al. 2002). It has also been suggested that discs are at greater risks of injury in the morning due to high water content and thus, high hydrostatic pressure (Adams et al. 1987; Adams et al. 1990). Specimens were rotated in combinations of 13° flexion, 10° lateral bend, or 4° axial rotation, showing no disruption to the disc. This is consistent with earlier findings that applied 10° of flexion and reported no initial damage (Veres et al. 2009; Wade et al. 2014). Similar to previous studies, an elevated rate of compression was applied in combination with flexion, lateral bend or axial rotation to promote annular wall disruption and herniation (Adams & Hutton 1982; Wade et al. 2014; Wade et al. 2015). Without this combination of loading, specimens invariably fail via endplate or vertebral fracture (Wade et al. 2014). Damage to the vertebrae itself was only reported in two cases, indicating the compressive load applied and rate of loading was such that it minimised failure by vertebral fracture and was within a physiological limit. Furthermore, this protocol has successfully simulated physiological conditions in the hexapod that put the disc most at risk of herniating by sudden overload.

9.3 Modes of Failure

Specimens failed by herniation alone (27.6%), herniation and endplate-vertebral shear fracture (44.8%), endplate-vertebral shear fracture alone (13.8%) or vertebral fracture (6.9%). Nucleus extrusion was observed in 72.4% of specimens within the ‘herniation alone’ and ‘herniation and endplate-vertebral shear fracture’ groups. Two intact specimens (SO5, SO28) were classified as ‘no damage’ due to no visible damage to the exterior surface of the disc or vertebrae, despite a ‘cracking’ sound noted at failure and 3 mm of compression. Further macroscopic and imaging analysis of the specimens was out of the scope of this project. Consequently, classification of failure modes remains speculative. In particular, no conclusive classification has been given to the ‘herniation and endplate-vertebral shear fracture’ group as the sequence of events could not be determined. In addition, it was not possible to determine whether specimens failed by annular rupture or annular endplate-junction failure as previously described. Wade et al. (2015) conducted a very similar study, loading flexed specimens at 400 mm/min and found that 83% herniated. Of these herniated specimens, 58% failed by annular-endplate junction rupture, while 25% failed by annular rupture (Wade et al. 2015). Rajasekaran et al. (2013) also reported 65% of 181 herniated discs failed by annular-endplate junction rupture. Testing conditions were similar to those of previous studies, it would be reasonable to hypothesise that approximately 50 – 70% of specimens tested in the current study failed at the annular-endplate junction. At this interface, there is a significant difference in material stiffness between the annulus and endplate, putting this region at risk of high stress concentrations (Wade et al. 2014). Previous studies have reported tearing of the annulus/cartilaginous endplate such that these fragments are extruded with nuclear material in approximately 49% of herniated specimens (Wade et al. 2014; Moore et al. 1996). However, no fragments of endplate were observed in the extruded material for any of the specimens that herniated. The site of annular herniation was correlated with the direction of loading with marginal significance ($p=0.055$). Of intact specimens tested in flexion and right lateral bending that herniated, 100% occurred in the left postero-lateral region of the disc, while 80% of intact specimens tested in lateral bend herniated on the left postero-lateral side. This is consistent with previous findings that indicate the contralateral side of the disc to bending is most susceptible to damage (Rajasekaran et al. 2013; Berger-Roscher et al. 2017)

Many specimens failed by endplate-vertebral shear fracture (58.6%) with or without nuclear extrusion. In many cases, this failure mode appeared as catastrophic damage to the inferior endplate-vertebral interface, where the superior vertebra and intervertebral disc were completely torn from the inferior vertebra. To the author’s knowledge, this type of catastrophic failure where the FSU components have been completely sheared apart, has not previously been reported by in vitro mechanical studies attempting to simulate herniation. However, Veres et al. (2010) identified a cartilaginous/vertebral endplate junction failure type in flexed specimens tested by nuclear

pressurisation. This failure type was characterised by ‘*tears adjacent to the outer annulus at the cartilaginous/vertebral endplate junction*’ that typically occurred at the inferior interface (Veres et al. 2010). A similar mode of failure was reported by Wade et al. (2014; 2015) and was then classified as annular-endplate junction rupture. Based upon these similarities between current findings and previous research, it could be hypothesised that specimens that were classified as ‘endplate-vertebral shear fracture’ were instead failing by annular-endplate junction failure. Catastrophic damage of these specimens complicated the classification process as specimens appeared to be failing by fracture of the inferior vertebra. However, many specimens showed evidence of nuclear extrusion. Several theories have been developed in an attempt to justify and explain how isolated discs failed. All specimens were displaced to 3 mm of compression. However, the average displacement at failure in isolated discs was 1.6 mm. This suggests that there was 1.4 mm of displacement that occurred subsequent to the initial failure event. Therefore, it is possible that isolated discs initially failed at the annular-endplate junction at approximately 1.6 mm, followed by further catastrophic failure for the remaining 1.4 mm. This implies that herniation occurs at much smaller displacements than previously indicated (Wade et al. 2014; Wade et al. 2015). Wade et al. (2015) previously tested sheep FSUs to 5 mm of compressive displacement or when the load decreased by 20%. It is assumed that most of the specimens tested in this study were stopped at the 20% load threshold rather than 5 mm displacement, thereby preventing catastrophic failure and purely capturing the herniation event. If instead, these specimens had been taken to 5 mm of compression, it is hypothesised that similar catastrophic damage would have been observed. However, it should also be noted that this type of failure may be the result of the specimen type used. The sheep FSUs were 1 – 2 years, while previous studies have used 4 – 6 year old sheep FSUs (Wade et al. 2015; Wade et al. 2014; Veres et al. 2010).

Comparisons between failure modes were limited to test groups that had specimens fail by more than one mode. No significant differences in failure mode mechanical parameters (i.e. stress, strain, modulus, toughness) were found in isolated discs between the herniation and endplate-vertebral shear fracture group and the endplate-vertebral shear groups. This suggests that similar modes of failure are in fact occurring, whereby nucleus has not yet been extruded in the ‘endplate-vertebral shear’ group. On the other hand, there was a significant difference in stress and modulus between herniation alone and herniation and endplate-vertebral shear fracture in intact FSUs in flexion and lateral bending. Interestingly, the flexion and lateral bending group was the only intact direction of loading that failed by herniation and endplate-vertebral shear fracture. If the theory that the ‘endplate-vertebral shear fracture’ failure type is an end-stage of annular-endplate rupture, this indicates that the flexion and lateral bending group is most susceptible to this type of herniation, while the remaining intact groups are susceptible to annular herniation. The herniation and endplate-vertebral shear fracture group had a higher stress and strain at failure in comparison to herniation alone. This differs to results of previous

findings that reported very similar load-displacement curves between annular rupture and annular-endplate junction herniations (Wade et al. 2015).

9.4 Effect of FSU Type and Loading Direction

As expected, intact FSUs and isolated discs had very different modes of failure, stress, modulus and toughness at failure. Chi-squared likelihood ratio tests showed a significant difference between modes of failure in intact and isolated discs ($p=0.001$). Nuclear material was extruded in 76.9% of intact FSUs (i.e. herniated or herniation and endplate-vertebral shear fracture), while nucleus was only evident in 68.8% of isolated discs. Instead, isolated discs typically experienced catastrophic failure at the inferior endplate-vertebral interface as previously described (93.8%). This mode of failure was only reported in 15.4% of intact FSUs. These findings differ significantly to previous studies that reported no significant difference in structural failure between intact FSUs and specimens with defunctioned posterior elements of sheep FSUs (Saipiee et al. 2017). Saipiee et al. (2017) reported gross extrusion of nuclear material or combined extrusion and endplate failure in both the intact group ($n=8$) and in the isolated disc group ($n=25$). This significant disagreement with previous research presents two possible paths for interpretation of the results in regards to the testing systems used and the role of the facet joints.

Pilot testing revealed that the hexapod is unable to minimise shear forces during axial compression at 6.67 mm/s and thus, an X-Y table was implemented on the inferior surface of the specimen to allow for shear translation. Although shear translation was not measured during testing, it has been hypothesised that excessive anterior-posterior or lateral translation was involved in the high incidence of endplate-vertebra damage in the isolated discs. This type of damage was also reported in two intact FSUs. This was unexpected as the facet joints should restrict excessive forward sliding of the disc. This suggests that shear translation was exceeding the physiological limit of 1.5 mm in anterior-posterior and lateral directions. On the other hand, assuming that the testing system had simulated physiological conditions similar to previous studies, these results indicate a significant difference between modes of failure between intact and isolated disc specimens. Facet joints support the majority of anterior shear loads (Tencer et al. 1982; Skrzypiec et al. 2013; Lu et al. 2005). Skrzypiec et al. (2013) found that the intervertebral disc contributes 38% to initial anterior shear loading while the facet joints contribute 55-66%. Interestingly, Skrzypiec et al. (2013) reported similar patterns in failure, where all disc-segment specimens presented with damage at the interface between the endplates and the disc. Furthermore, supporting the hypothesis that intact FSUs and isolated discs experience different modes of failure.

Two-way univariate tests and non-parametric Kruskal-Wallis tests also revealed significant differences between intact FSUs and isolated disc's stress ($p < 0.001$), strain, ($p = 0.038$), modulus ($p = 0.012$) and toughness ($p < 0.001$) at failure. Overall, intact FSUs had an initial failure stress of 21.9 ± 6.8 MPa compared to 12.0 ± 3.0 MPa for the isolated disc group. Saipiee et al. (2017) reported very similar results where failure stress was 23.6 ± 5.8 MPa for intact FSUs and 14.8 ± 3.3 MPa in isolated discs. Given the different stress at failure, this indicates a significant difference in stiffness of the intact FSUs and isolated discs. Skrzypiec et al. (2013) found that specimens with no facet joints were 66% less stiff than specimens with facets in anterior shear. This relationship has been supported by the current findings, where isolated discs (0.38 ± 0.11 MPa) were 74.5% less stiff than the intact FSUs (0.51 ± 0.19 MPa).

This study also looked at the effect of varying the combination of loading applied to the motion segment. No significant difference was found between the modes of failure experienced between loading directions in intact FSUs ($p = 0.558$) or isolated discs ($p = 0.275$). One-way univariate tests reported significant difference in stress between intact and isolated discs in flexion ($p = 0.003$), lateral bend ($p < 0.001$) and flexion and lateral bend ($p = 0.027$). Interestingly, a significant difference in modulus ($p = 0.003$) and toughness ($p = 0.043$) between intact and isolated discs was only reported in the lateral bending group, while modulus and toughness between intact and isolated flexion and combined flexion and lateral bending were very similar. However, pure lateral bending is the only direction of loading that has an increased stiffness in intact FSUs in comparison to isolated discs. In flexion, the superior vertebra is rotated anteriorly. As a result, there is little contact between the superior and inferior articular processes of the facet joints. On the other hand, as a specimen rotates in lateral bending, the ipsilateral superior and inferior articular processes of the facet joints come into contact. Therefore, it can be assumed that increased stiffness in the lateral bending group can be attributed to the involvement of the facet joints.

There was a significant difference in stress ($p = 0.001$) and modulus ($p = 0.024$) between intact FSUs in pure flexion and pure lateral bending. There was also a significant difference in stress ($p < 0.001$) and modulus ($p = 0.004$) between intact FSUs in pure lateral bending and combined flexion and lateral bending, while no significant difference was reported between intact flexion and combined flexion and lateral bending ($p = 0.110$). These findings have several implications. Firstly, flexion and lateral bending reaches the lowest load and stress at failure (15.6 MPa) in intact specimens, indicating increased susceptibility to injury. This agrees with previous research that identified this combination of loading as posing the highest degree of risk to injury of the disc (Costi et al. 2007; Berger-Roscher et al. 2017). This direction of loading also reported the lowest stress in isolated discs (10.2 MPa), suggesting its susceptibility with and without facet joints involved. As previously mentioned, these

significant differences in stress and modulus between directions of loading in intact FSUs may also be attributable to the involvement of the facet joints.

Unlike the intact FSUs, there were no significant differences in stress, strain, modulus or toughness between directions of loading in isolated discs. Isolated disc specimens typically failed by catastrophic rupture at the inferior endplate and vertebra interface. This reduced variation in results may be attributed to the reduced stiffness and toughness of the specimen.

10 Conclusions

This project has developed a repeatable protocol to successfully simulate intervertebral disc herniation in sheep FSUs by sudden overload in the hexapod robot. Modes of failure varied significantly between intact FSUs and isolated discs, while little variation was observed between directions of loading. The modes of failure identified in this study do not support previous findings (Saippee et al. 2017). This may be attributed to differences in specimens, mechanical testing systems or protocol. Intact FSUs failed predominantly by herniation, while isolated discs failed by a combination of herniation and endplate-vertebral shear fracture. Intact FSUs failed at much higher stresses in comparison to isolated discs. This suggests that facet joints contribute significantly to the specimen's stiffness at failure. The facet joints appear to play the largest role in pure lateral bending, which had the highest mean stress, modulus and toughness in intact FSUs. Conversely, combined flexion and lateral bending reported the lowest stress, modulus and toughness. In comparison to intact FSUs, there was little variation within and between isolated disc specimens in regards to axial compressive failure stress, modulus and toughness. Future work is required to further develop the sudden overload protocol and clearly identify the role of directions of loading in intervertebral disc herniation.

10.1 Future Work

Further work is required to develop a complete understanding of the failure mechanisms involved in intervertebral disc herniation. Several recommendations have been proposed based on the limitations and findings of the current study. Due to restrictions of the hexapod GUI, testing in combined axial rotation and lateral bending was only conducted in two specimens. Previous research has confirmed that the facet joints play a significant role in limiting axial rotation. In addition to this, the current study has identified lateral bending as having the highest modulus and stress at failure. Therefore, future work would benefit from completing this analysis of the lateral bend and axial rotation group to provide a complete analysis of these failure modes with intact FSUs. The current project also involved a 6DOF loading protocol in addition to the sudden overload protocol. However, only the sudden overload data has been analysed in this thesis. Therefore, future work will predominantly focus on analysing the stiffness and phase angles of each specimen before and after the failure event. This information will be useful in assessing how herniation can impact the mechanical integrity of the FSU.

The sudden overload protocol developed successfully produced nuclear extrusion in 72.4% of intact FSUs and isolated discs. However, for more consistent and repeatable results in future, several alterations to the protocol are recommended. The sheep specimens used in this study were relatively

young, aged between 12 – 24 months. To more accurately model the human disc, older sheep FSUs should be used instead. Each specimen failure was recorded by one camera from the left postero-lateral side of the disc. Consequently, other views of the specimen were not recorded, making it difficult to interpret the order in which failure occurred (e.g. right postero-lateral herniation or anterior vertebral fracture). Therefore, it would be highly recommended to film the failure events from at least two views (i.e. posterior and anterior). Adjustment to failure detection is also required, particularly when working with isolated discs. Severe and catastrophic failure in many of the isolated discs indicates that 3 mm of compression was too much displacement. Therefore, displacements of 1.5 – 2 mm may be more suitable for isolated sheep discs. An alternative to this would be to integrate a system into the hexapod GUI that sets a threshold and detects a certain decrease in load (e.g. 20%) to indicate failure. Development of a protocol to classify modes of failure would also be highly beneficial. To the authors knowledge, there are no structured guidelines for classifying modes of failure that encompass factors such as macroscopic appearance, microscopic appearance and mechanical properties at failure.

Few clinical findings have reported a sudden overloading event as immediately preceding herniation and sciatica. Therefore, several studies have implicated the joint contribution of a sudden overload event in addition to fatigue loading. Based on the current findings, the sudden overload event should be conducted in flexion and lateral bend as it poses the highest degree of risk to failure.

11 References

- Adams, M.A. 2013, *The Biomechanics of Back Pain*, 3rd edition, Edinburgh, Churchill Livingstone.
- Adams, M.A. et al., 1990. Diurnal changes in spinal mechanics and their clinical significance. *The Journal of bone and joint surgery*, 72-B(2), pp.266–270.
- Adams, M.A., 2015. Intervertebral disc tissues. In *Engineering Materials and Processes*. Bristol: Springer International Publishing Switzerland, pp. 7–35.
- Adams, M.A. et al., 1996. Sustained loading generates stress concentrations in lumbar intervertebral discs. *Spine*, 21, pp.434–438.
- Adams, M.A. et al., 2015. Why do some intervertebral discs degenerate, when others (in the same spine) do not? *Clinical Anatomy*, 28(2), pp.195–204.
- Adams, M.A., Dolan, P. & Hutton, W.C., 1986. The stages of disc degeneration as revealed by discograms. *The Journal of bone and joint surgery British volume*, 68(1), pp.36–41.
- Adams, M.A. & Hutton, W.C., 1985. Gradual disc prolapse. *Spine*, 10(6), pp.524–531.
- Adams, M.A. & Hutton, W.C., 1982. Prolapsed intervertebral disc: A hyperflexion injury. *Spine*, 7(3), pp.184–191.
- Adams, M.A. & Hutton, W.C., 1980. The effect of posture on the role of the apophysial joints in resisting intervertebral compressive forces. *The Journal of bone and joint surgery. British volume*, 62-B(3), pp.358–362.
- Adams, M.A. & Hutton, W.C., 1983. The mechanical function of the lumbar apophyseal joints. *Spine*, 8(3), pp.327–330.
- Adams, M.A. & Hutton, W.C., 1981. The Relevance of Torsion to the Mechanical Derangement of the Lumbar Spine. *Spine*, 6(3), pp.241–248.
- Adams, M.A. & Roughley, P.J., 2006. What is Intervertebral Disc Degeneration, and What Causes It? *Spine*, 31(18), pp.2151–2161.
- Adams, M. a & Hutton, W.C., 1983. The effect of fatigue on the lumbar intervertebral disc. *J Bone Joint Surg Br*, 65(2), pp.199–203.
- Adams, M., Dolan, P. & Hutton, W., 1987. Diurnal variations in the stresses on the lumbar spine. *Spine*, 12(2), pp.130–137.
- Adams, M. & Hutton, W., 1983. The effect of posture on the fluid content of lumbar intervertebral discs. *Spine*, 8(6), pp.665–671.
- Adams, P. & Muir, H., 1976. Qualitative changes with age of proteoglycans of human lumbar discs. *Annals of the rheumatic diseases*, 35(4), pp.289–96.
- Ahmed, A.M., Duncan, N.A. & Burke, D.L., 1990. The effect of facet geometry on the axial torque-rotation response of lumbar motion segments. *Spine*, 15(5), pp.391–401.
- Alini, M. et al., 2008. Are animal models useful for studying human disc disorders / degeneration ? *European Spine Journal*, 17, pp.2–19.
- Amin, D.B. et al., 2016. Effect of degeneration on the six degree of freedom mechanical properties of human lumbar spine segments. *Journal of Orthopaedic Research*, 34(8), pp.1399–1409.
- Amin, D.B. et al., 2016. The effect of six degree of freedom loading sequence on the in-vitro compressive properties of human lumbar spine segments. *Journal of Biomechanics*, 49(14), pp.3407–3414.
- Antoniou, J. et al., 1996. The human lumbar intervertebral disc: Evidence for changes in the biosynthesis and denaturation of the extracellular matrix with growth, maturation, ageing, and degeneration. *Journal of Clinical Investigation*, 98(4), pp.996–1003.
- Battié, M.C. et al., 2008. Genetic and environmental effects on disc degeneration by phenotype and spinal level: a multivariate twin study. *Spine*, 33(25), pp.2801–2808.

- Berger-Roscher, N. et al., 2017. Influence of Complex Loading Conditions on Intervertebral Disc Failure. *Spine*, 42(2), pp.E78–E85.
- Botsford, D.J., Esses, S.I. & Ogilvie-Harris, D.J., 1994. In vivo diurnal variation in intervertebral disc volume and morphology. *Spine*, 19(8), pp.935–940.
- Brinckmann, P. et al., 1983. Deformation of the vertebral end-plate under axial loading of the spine. *Spine*, 8(8), pp.851–856.
- Brinckmann, P. et al., 1987. Fatigue fracture of human lumbar vertebrae. *Clin Biomech (Bristol, Avon)*, 2, pp.94–96.
- Brinckmann, P., Biggemann, M. & Hilweg, D., 1988. Fatigue fracture of human lumbar vertebrae. *Clinical Biomechanics*, 3, p.i–ii, S1–S23.
- Brinckmann, P., Biggemann, M. & Hilweg, D., 1989. Prediction of the compressive strength of human lumbar vertebrae. *Clinical Biomechanics*, 4(SUPPL. 2).
- Buckwalter, J.A., 1995. Aging and degeneration of the human intervertebral disc. *Spine*, 20(11), pp.1307–14.
- Callaghan, J.P. & McGill, S.M., 2001. Intervertebral disc herniation: Studies on a porcine model exposed to highly repetitive flexion/extension motion with compressive force. *Clinical Biomechanics*, 16(1), pp.28–37.
- Cassidy, J.J., Hiltner, A. & Baer, E., 1989. Hierarchical Structure of the Intervertebral Disc. *Connective Tissue Research*, 23(1), pp.75–88.
- Cohen, R.E., Hooley, C.J. & McCrum, N.G., 1976. Viscoelastic creep of collagenous tissue. *Journal of Biomechanics*, 9(4), pp.175–184.
- Costi, J.J. et al., 2007. Direct measurement of intervertebral disc maximum shear strain in six degrees of freedom: Motions that place disc tissue at risk of injury. *Journal of Biomechanics*, 40(11), pp.2457–2466.
- Costi, J.J. et al., 2008. Frequency-Dependent Behavior of the Intervertebral Disc in Response to Each of Six Degree of Freedom Dynamic Loading. *Spine*, 33(16), pp.1731–1738.
- Costi, J.J. et al., 2009. Human versus sheep intervertebral disc mechanical and vertebral cortical bone strain properties.
- Costi, J.J., Freeman, B.J. & Elliott, D.M., 2011. Intervertebral disc properties: challenges for biodevices. *Expert Review of Medical Devices*, 8(3), pp.357–376.
- Costi, J.J., Hearn, T.C. & Fazzalari, N.L., 2002. The effect of hydration on the stiffness of intervertebral discs in an ovine model. *Clinical Biomechanics*, 17(6), pp.446–455.
- Crawford, N.R., Peles, J.D. & Dickman, C.A., 1998. The spinal lax zone and neutral zone: measurement techniques and parameter comparisons. *Journal of spinal disorders*, 11(5), pp.416–29.
- Cummins, J. et al., 2006. Descriptive Epidemiology and Prior Healthcare Utilization of Patients in the Spine Patient Outcomes Research Trial's (SPORT) Three Observational Cohorts. *Spine*, 31(7), pp.806–814.
- Ding, B. et al., 2011. Real-time FPGA Control of a Hexapod Robot for 6- DOF Biomechanical Testing. *IEEE*, pp.252–257.
- Dolan, P. & Adams, M.A., 1993. The relationship between EMG activity and extensor moment generation in the erector spinae muscles during bending and lifting activities. *Journal of Biomechanics*, 26(4–5), pp.513–522.
- Drake, J.D.M. et al., 2005. The influence of static axial torque in combined loading on intervertebral joint failure mechanics using a porcine model. *Clinical Biomechanics*, 20(10), pp.1038–1045.
- Duance, V.C. et al., 1998. Changes in. *Spine*, 23(23), pp.2545–2551.
- Dunlop, R.B., Hutton, W.C. & Adams, A., 1984. Disc space narrowing and the lumbar facet joints. *The Journal of bone and joint surgery*, 66B(5), pp.706–710.
- Duthey, B., 2013. Background Paper 6.24 Low back pain. Priority Medicines for Europe and the World. *Global Burden of Disease (2010)*, (March), pp.1–29.
- Ehlers, W., Karajan, N. & Markert, B., 2009. An extended biphasic model for charged hydrated

- tissues with application to the intervertebral disc. *Biomechanics and Modeling in Mechanobiology*, 8(3), pp.233–251.
- Eyre, D.R. & Muir, H., 1976. Types I and II collagens in intervertebral disc. Interchanging radial distributions in annulus fibrosus. *The Biochemical journal*, 157(1), pp.267–270.
- Fardon, D.F. et al., 2014. Lumbar disc nomenclature: Version 2.0 Recommendations of the combined task forces of the North American Spine Society, the American Society of Spine Radiology and the American Society of Neuroradiology. *Spine Journal*, 14(11), pp.2525–2545.
- Galante, J.O., 1967. Tensile Properties of the Human Lumbar Annulus Fibrosus. *Acta Orthopaedica Scandinavica*, 38(sup100), pp.1–91.
- Galbusera, F. et al., 2014. Ageing and degenerative changes of the intervertebral disc and their impact on spinal flexibility. *European Spine Journal*, 23(3), pp.324–333.
- Gallagher, S. et al., 2005. Torso flexion loads and the fatigue failure of human lumbosacral motion segments. *Spine*, 30(20), pp.2265–2273.
- Gordon, S.J. et al., 1991. Mechanism of Disc Rupture. *Spine*, 16(4), pp.450–456.
- Heliovaara, M., Knekt, P. & Aromaa, A., 1987. Incidence and risk factors of herniated lumbar intervertebral disc or sciatica leading to hospitalization. *Journal of Chronic Disease*, 40(3), pp.251–258.
- Hernández, C.P. et al., 2013. What is sciatica and radicular pain ? In *Pain in Primary Care Practice*. Springer Healthcare, pp. 1–15.
- Hickey, D.S. & Hukins, D.W., 1980. X-ray diffraction studies of the arrangement of collagenous fibres in human fetal intervertebral disc. *Journal of anatomy*, 131, pp.81–90.
- Hilton, R.C., Ball, J. & Benn, R.T., 1980. Annular tears in the dorsolumbar spine. *Annals of the rheumatic diseases*, 39(6), pp.533–8.
- Hoy, D. et al., 2014. The global burden of low back pain: estimates from the Global Burden of Disease 2010 study. *Annals of the Rheumatic Diseases*, 73(6), pp.968–974.
- Hutton, W.C. & Adams, M.A., 1982. Can the lumbar spine be crushed in heavy lifting? *Spine*, 7(6), pp.586–590.
- Iatridis, J.C. et al., 1996. Is the nucleus pulposus a solid or a fluid? Mechanical behaviors of the nucleus pulposus of the human intervertebral disc. *Spine*, 21(10), pp.1174–1184.
- Jager, M. et al., 2000. Evaluation and assessment of lumbar load during total shifts for occupational manual materials handling jobs within the Dortmund Lumbar Load Study - DOLLY. *International Journal of Industrial Ergonomics*, 25(6), pp.553–571.
- Katz, J.N., 2006. Lumbar Disc Disorders and Low-Back Pain: Socioeconomic Factors and Consequences. *The Journal of Bone and Joint Surgery*, 88A(2), pp.21–24.
- Keller, T.S., Spengler, D.M. & Hansson, T.H., 1987. Mechanical behavior of the human lumbar spine. I. Creep analysis during static compressive loading. *Journal of Orthopaedic Research*, 5(4), pp.467–478.
- Kelsey, J.L. et al., 1984. An epidemiologic study of lifting and twisting on the job and risk for acute prolapsed lumbar intervertebral disc. *Journal of Orthopaedic Research*, 2(1), pp.61–66.
- Korhonen, R.K. & Saarakkala, S., 2011. Biomechanics and Modeling of Skeletal Soft Tissues. In V. Klika, ed. *Theoretical Biomechanics*. InTech, pp. 113–132.
- Kraemer, J., Kolditz, D. & Gowin, R., 1985. Water and electrolyte content of human intervertebral discs under variable load. *Spine*, 10(1), pp.69–71.
- Lama, P. et al., 2013. Do intervertebral discs degenerate before they herniate, or after? *Bone and Joint Journal*, 95 B(8), pp.1127–1133.
- Lawless, I.M. et al., 2014. Adaptive velocity-based six degree of freedom load control for real-time unconstrained biomechanical testing. *Journal of Biomechanics*, 47(12), pp.3241–3247.
- Leahy, J.C. & Hukins, D.W., 2001. Viscoelastic Properties of the Nucleus Pulposus of the Intervertebral Disk in Compression. , 12(8), pp.689–692.
- Lindahl, O. & Rexed, B., 1951. Histologic Changes in Spinal Nerve Roots of Operated Cases of Sciatica. *Acta Orthopaedica Scandinavica*, 20(3), pp.215–225.

- Liu, Y., Goel, V. & Dejong, A., 1985. Torsional Fatigue Failure of Lumbar Intervertebral Joints. *Spine*, 10(10).
- Lu, W.W. et al., 2005. Pure Shear Properties of Lumbar Spinal Joints and the Effect of Tissue Sectioning on Load Sharing. *Spine*, 30(8), pp.204–209.
- Lyons, G., Eisenstein, S.M. & Sweet, M.B., 1981. Biochemical changes in intervertebral disc. *Biochimica et Biophysica Acta*, 673(4), pp.443–453.
- Mannion, A.F., Adams, M.A. & Dolan, P., 2000. Sudden and unexpected loading generates high forces on the lumbar spine. *Spine*, 25(7), pp.842–852.
- Marchand, F. & Ahmed, A., 1990. Investigation of the Laminate Structure of Lumbar Disc Anulus Fibrosus. *Spine*, 15(5), pp.402–410.
- Marras, W.S. et al., 1993. The role of dynamic three-dimensional trunk motion in occupationally-related low back disorders. *Spine*, 18(5), pp.617–628.
- Marshall, L.W. & McGill, S.M., 2010. The role of axial torque in disc herniation. *Clinical Biomechanics*, 25(1), pp.6–9.
- McCarron, R.F. et al., 1987. The inflammatory effect of nucleus pulposus. A possible element in the pathogenesis of low-back pain. *Spine*, 12(8), pp.760–4.
- Moore, R. et al., 1996. The Origin and Fate of Herniated Lumbar Intervertebral Disc Tissue. *Spine*, 21(18), pp.2149–2155.
- Mundt, D.J. et al., 1993. An Epidemiological Study of Non-Occupational Lifting as a Risk Factor for Herniated Lumbar Intervertebral Disc. *Spine*, 18(5), pp.595–602.
- Nachemson, A., 1959. Measurement of Intradiscal Pressure. *Acta Orthopaedica Scandinavica*, 28(4), pp.269–289.
- Nachemson, A., 1963. The Influence of Spinal Movements on the Lumbar Intradiscal Pressure and on the Tensile Stresses in the Annulus Fibrosus. *Acta Orthopaedica Scandinavica*, 33(1–4), pp.183–207.
- Nachemson, A.F., 1981. Disc Pressure Measurements. *Spine*, 6(1), pp.93–97.
- Norman, R. et al., 1998. A comparison of peak vs cumulative physical work exposure risk factors for the reporting of low back pain in the automotive industry. *Clinical Biomechanics*, 13(8), pp.561–573.
- Osti, O.L. et al., 1992. Annular tears and disc degeneration in the lumbar spine. A post-mortem study of 135 discs. *The Journal of bone and joint surgery. British volume*, 74(5), pp.678–682.
- Osti, O.L., Vernon-Roberts, B. & Fraser, R.D., 1990. 1990 Volvo Award in experimental studies. Anulus tears and intervertebral disc degeneration. An experimental study using an animal model. *Spine*, 15(8), pp.762–767.
- Oxland, T.R. & Panjabi, M.M., 1992. The onset and progression of spinal injury: A demonstration of neutral zone sensitivity. *Journal of Biomechanics*, 25(10), pp.1165–1172.
- Panagiotacopoulos, N.D. et al., 1987. Water content in human intervertebral discs. Part II. Viscoelastic behaviour. *Spine*, 12(9), pp.918–924.
- Panjabi, M.M., 1992. The Stabilizing System of the Spine. Part II. Neutral Zone and Instability Hypothesis. *Journal of Spinal Disorders*, 5(4), pp.390–397.
- Park, J. & Lakes, R.S., 2007. *Biomaterials* Third., Springer.
- Parkinson, R.J. & Callaghan, J.P., 2009. The role of dynamic flexion in spine injury is altered by increasing dynamic load magnitude. *Clinical Biomechanics*, 24(2), pp.148–154.
- Pearcy, M., Portek, I. & Shepherd, J., 1984. Three-dimensional x-ray analysis of normal movement in the lumbar spine. *Spine*, 9(3), pp.294–297.
- Pearcy, M.J., 1993. Twisting Mobility of the Human Back in Flexed Postures. *Spine*, 18(1), pp.114–9.
- Pearcy, M.J. & Hindle, R.J., 1991. Axial rotation of lumbar intervertebral joints in forward flexion. *Proceedings of the Institution of Mechanical Engineers. Part H, Journal of engineering in medicine*, 205(4), pp.205–9.
- Pearcy, M.J. & Tibrewal, S.B., 1984. Axial rotation and lateral bending in the normal lumbar spine measured by three-dimensional radiography. *Spine*, 9(6), pp.582–587.

- Pfirrmann, C.W.A. et al., 2006. Effect of Aging and Degeneration on Disc Volume and Shape: A Quantitative Study in Asymptomatic Volunteers. *Journal of Orthopaedic Research*, 24(5), pp.1086–1094.
- Porchet, F. et al., 2002. Relationship between severity of lumbar disc disease and disability scores in sciatica patients. *Neurosurgery*, 50(6), pp.1253–1260.
- Postacchini, F. & Cinotti, G., 1999. Etiopathogenesis. In F. Postacchini, ed. *Lumbar Disc Herniation*. Rome: Springer Verlag Wien, pp. 151–167.
- Race, A., Broom, N.D. & Robertson, P., 2000. Effect of loading rate and hydration on the mechanical properties of the disc. *Spine*, 25(6), pp.662–669.
- Rajasekaran, S. et al., 2013. ISSLS Prize Winner: The anatomy of failure in lumbar disc herniation. *Spine*, 38(17), pp.1491–1500.
- Reid, J.E. et al., 2002. Sheep lumbar intervertebral discs as models for human discs. *Clinical Biomechanics*, 17(4), pp.312–314.
- Ricci, J.A. et al., 2006. Back Pain Exacerbations and Lost Productive Time Costs in United States Workers. *Spine*, 31(26), pp.3052–3060.
- Roberts, S., Menage, J. & Urban, J.P.G., 1989. Biochemical and structural properties of the cartilage end-plate and its relation to the intervertebral disc. *Spine*, 14(2), pp.166–174.
- Schendel, M.J. et al., 1993. Experimental measurement of ligament force, facet force, and segment motion in the human lumbar spine. *Journal of Biomechanics*, 26(4–5), pp.427–438.
- Schmidt, H. et al., 2007. The risk of disc prolapses with complex loading in different degrees of disc degeneration - A finite element analysis. *Clinical Biomechanics*, 22(9), pp.988–998.
- Schroeder, G.D., Guyre, C.A. & Vaccaro, A.R., 2016. The epidemiology and pathophysiology of lumbar disc herniations. *Seminars in Spine Surgery*, 28(1), pp.2–7.
- Schulte, T. et al., 2008. The effect of dynamic , semi-rigid implants on the range of motion of lumbar motion segments after decompression. *European Spine Journal*, 17, pp.1057–1065.
- Shirazi-Adl, A., Ahmed, A.M. & Shrivastava, S.C., 1986. Mechanical Response of a Lumbar Motion Segment in Axial Torque Alone and Combined with Compression. *Spine*, 11(9), pp.914–927.
- Simunic, D.I., Broom, N.D. & Robertson, P. a, 2001. Biomechanical factors influencing nuclear disruption of the intervertebral disc. *Spine*, 26(11), pp.1223–1230.
- Simunic, D.I., Robertson, P. a & Broom, N.D., 2004. Mechanically induced disruption of the healthy bovine intervertebral disc. *Spine*, 29(9), pp.972–978.
- Singh, K. et al., 2009. Age-related changes in the extracellular matrix of nucleus pulposus and anulus fibrosus of human intervertebral disc. *Spine*, 34(1), pp.10–16.
- Sivan, S.S. et al., 2006. Aggrecan turnover in human intervertebral disc as determined by the racemization of aspartic acid. *Journal of Biological Chemistry*, 281(19), pp.13009–13014.
- Sivan, S.S. et al., 2008. Collagen turnover in normal and degenerate human intervertebral discs as determined by the racemization of aspartic acid. *Journal of Biological Chemistry*, 283(14), pp.8796–8801.
- Skrzypiec, D.M. et al., 2013. Estimation of shear load sharing in moderately degenerated human lumbar spine. *Journal of Biomechanics*, 46, pp.651–657.
- Smit, T.H., 2002. The use of a quadruped as an in vivo model for the study of the spine - Biomechanical considerations. *European Spine Journal*, 11(2), pp.137–144.
- Stafford, M.A., Peng, P. & Hill, D.A., 2007. Sciatica : a review of history , epidemiology , pathogenesis , and the role of epidural steroid injection in management. *British Journal of Anaesthesia*, 99(4), pp.461–473.
- Stokes, I.A. & Frymoyer, J., 1987. Segmental motion and instability. *Spine*, 12(7), pp.688–691.
- Takahashi, K., Shima, I. & Porter, R.W., 2006. Nerve Root Pressure in Lumbar Disc Herniation. *Spine*, 24(19), pp.2003–2006.
- Tampier, C. et al., 2007. Progressive disc herniation: an investigation of the mechanism using radiologic, histochemical, and microscopic dissection techniques on a porcine model. *Spine*, 32(25), pp.2869–2874.

- Twomey, L. & Taylor, J., 1982. Flexion creep deformation and hysteresis in the lumbar vertebral column. *Spine*, 7(2), pp.116–122.
- Umehara, S. et al., 1996. Effects of degeneration on the elastic modulus distribution in the lumbar intervertebral disc. *Spine*, 21(April 1996), p.811–819; discussion 820.
- Veres, S.P., Robertson, P.A. & Broom, N.D., 2010. ISSLS Prize Winner: How Loading Rate Influences Disc Failure Mechanics. *Spine*, 35(21), pp.1897–1908.
- Veres, S.P., Robertson, P. a & Broom, N.D., 2008. ISSLS Prize Winner: Microstructure and Mechanical Disruption of the Lumbar Disc Annulus. *Spine*, 33(25), pp.2702–2710.
- Veres, S.P., Robertson, P. a & Broom, N.D., 2009. The morphology of acute disc herniation: a clinically relevant model defining the role of flexion. *Spine*, 34(21), pp.2288–96.
- Vergroesen, P.P.A. et al., 2015. Mechanics and biology in intervertebral disc degeneration: A vicious circle. *Osteoarthritis and Cartilage*, 23(7), pp.1057–1070.
- Vernon-Roberts, B., Fazzalari, N.L. & Manthey, B.A., 1997. Pathogenesis of tears of the anulus investigated by multiple-level transaxial analysis of the T12-L1 disc. *Spine*, 22(22), pp.2641–2646.
- Virgin, W.J., 1951. Experimental investigations into the physical properties of the intervertebral disc. *The Journal of Bone and Joint Surgery*, 33B(4), pp.607–611.
- Wade, K.R. et al., 2014. How Healthy Discs Herniate. *Spine*, 39(13), pp.1018–1028.
- Wade, K.R. et al., 2015. “Surprise” Loading in Flexion Increases the Risk of Disc Herniation Due to Annulus-Endplate Junction Failure,
- Weber, H., 1983. Lumbar disc herniation. A controlled, prospective study with ten years of observation. *Spine*, 8(2), pp.131–140.
- Wilke, H.-J. et al., 1997. Anatomy of the sheep spine and its comparison to the human spine. *Anatomical Record*, 247(4), pp.542–555.
- Wilke, H.-J. et al., 1999. New in vivo measurements of pressures in the intervertebral disc in daily life. *Spine*, 24(8), pp.755–762.
- Wilke, H.-J., Kettler, A. & Claes, L.E., 1997. Are Sheep Spines a Valid Biomechanical Model for Human Spines? *Spine*, 22(20), pp.2365–2374.
- Wilke, H.J. et al., 2016. A new dynamic six degrees of freedom disc-loading simulator allows to provoke disc damage and herniation. *European Spine Journal*, 25(5), pp.1363–1372.
- Wilke, H.J., Geppert, J. & Kienle, A., 2011. Biomechanical in vitro evaluation of the complete porcine spine in comparison with data of the human spine. *European Spine Journal*, 20(11), pp.1859–1868.
- Wilke, H.J., Krischak, S. & Claes, L., 1996. Biomechanical comparison of calf and human spines. *Journal of Orthopaedic Research*, 14(3), pp.500–503.
- Willburger, R.E. et al., 2004. Clinical symptoms in lumbar disc herniations and their correlation to the histological composition of the extruded disc material. *Spine*, 29(15), pp.1655–1661.

12 Appendices

12.1 Appendix 1: Sheep Sudden Overload Protocol

Note: Lumbar spines have previously been dissected to remove extraneous soft tissue, sectioned into L4-L5 FSUs and classified as intact FSU or isolated disc specimens.

Day 1

➤ **Specimen Measurements**

1. Measure FSU height, superior vertebra height, inferior vertebra height, disc height, anterior-posterior endplate width, lateral endplate width dimensions as outlined in Appendix 2 to determine disc area, preloads and offset calculations.

➤ **Specimen Preparation**

1. Thaw specimens for testing for at least three hours at room temperature.
2. Using a scalpel and forceps, remove any remaining soft tissue or periosteum from FSU and thoroughly dry to ensure good fixation between the FSU vertebra and PMMA as depicted below.



Intact FSU



Isolated Disc

➤ **Potting**

Materials:

- 5 x stainless steel and aluminium potting cups



- 6x fixation screws
- Masking tape
- Clear acrylic packaging tape
- Molybond grease
- Mixing container and utensils
- Polymethyl methacrylate (PMMA): PMMA is composed of a powder (pre-polymerized PMMA, radio-opacifier and initiator) and a liquid methyl methacrylate monomer stabiliser and inhibitor. The two components are mixed together causing an exothermic free-radical polymerisation of the monomer causing the PMMA to heat up as it cures and hardens.
- Potting alignment rig: A stainless steel structure that has a plate that attaches to the base of the alignment rig and a top plate that can move up and down the ball bearing railing. This alignment device ensures the cups are parallel to each other and therefore, the mid-transverse plane of the disc.

1. Preparing potting cups

- a. Clean thoroughly with 70% ethanol solution
- b. Cover thru holes on the base of the cup with acrylic packaging tape to prevent PMMA from leaking.
- c. Cover fixation screw thru holes on the wall of the cups with masking tape to prevent PMMA from leaking
- d. Screw in 3 fixation bolts on walls of cup for both top and bottom cup so that it pierces the masking tape on the inner side of the cup
- e. Apply Molybond grease to the fixation screws



2. Potting base cup
 - a. Bolt base cup to alignment rig base plate so that the posterior side of the cup and base plate are aligned correctly.
 - b. Bolt the rig base plate to the alignment rig
 - c. Position the inferior surface of the inferior vertebra in the base cup, such that the centre of the disc is in the centre of the cup
 - d. Once in the desired position, tighten the fixation bolts until gripping the inferior vertebra and holding the FSU in place.
 - e. Measure out 80mL of PMMA powder and 32mL liquid at a ratio of 2.5mL powder to 1mL liquid. Make adjustments to reach the desired consistency
 - f. Mix PMMA powder and liquid in mixing container with mixing utensil
 - g. Pour the PMMA continuously into the bottom cup
 - h. Let set for 15-20 minutes

3. Geometric centre measurements
 - a. Once PMMA in the base cup has set, take the x- and y- geometric centre measurements as outlined in Appendix 2.

4. Potting top cup
 - a. Unbolt the alignment rig base plate from alignment rig
 - b. Unbolt base plate from base potting cup
 - c. Bolt top cup to base plate and to alignment rig
 - d. Bolt base cup upside down to alignment rig slide mount so that the superior vertebra is facing downward
 - e. Slowly lower base cup and attached slide mount into the top cup so that the superior surface of the superior vertebra comes into contact with the base of the top cup.
 - f. Once lowered, tighten the top cup fixation screws around the superior vertebra
 - g. Repeat steps 2e-h.

➤ **Hydration and Preload**

Materials:

- Potted specimens
 - Plastic hydration container
 - 0.15 M phosphate buffered saline (PBS)
 - Hydration rig
 - 9.8 N weights
 - Loading platform
 - Hydration rig clamps
 - Linear variable differential transformers (LVDTs)
1. Position the hydration container underneath the hydration rig.
 2. Place potted specimens in the plastic container with centre of the disc aligned with the centre of the loading platform.
 3. Fill the plastic container with PBS to sufficiently submerge and cover the discs.
 4. Lower hydration platform through respective hole of the hydration rig so that the tip of the loading platform comes into contact with the superior vertebra in line with the centre of the disc.
 5. Apply preload to specimen using 9.8N weights as calculated in Appendix 2.
 6. Insert LVDTs in hydration clamps so that the tip of the LVDT is in contact with the inferior side of the loading platform.
 7. The LVDT measures displacement of the loading platform and hence, displacement of the disc over time. This is output in Signal Express on the computer.
 8. Leave specimens to hydrate for at least 4 hours (preferably overnight)
 9. Following hydration, remove and dry specimens for testing in the hexapod.

Day 2

➤ **Hexapod Protocol**

Note: Hexapod protocol only includes steps specific to this test. More detailed description of how to use the hexapod has been previously outlined in a hexapod manual.

1. Mount specimen in the hexapod
 - a. Mount 300mm base pillar
 - b. Mount ...mm base pillar
 - c. Mount X-Y table on base pillar
 - d. Mount potted specimen on X-Y table
 - e. Upper adapter plate mounted on potted specimen

2. Hexapod jogged down to attach upper adapter plate, specimen coupling plate and load cell plate.
3. Specimen axis x, y, z offsets, recovery preload and follower preloads are entered into the host computer VI in LabView.
4. The 6DOF batch test file is read in and run (43 minutes).
5. Once the 6DOF batch is finished, the hexapod VI is setup for failure
 - a. Rotate specimen (i.e. flexion, lateral bend, flexion and lateral bend or lateral bend and axial rotation).
 - i. Enable position control
 - ii. Constrain Rx and Ry
 - iii. Set primary axis = 2
 - iv. Set sample rate = 100
 - v. Set time = 75
 - vi. Collect data and set Rx, Ry or Rz depending on the test being conducted

Test	Rx	Ry	Rz
Flexion	-13		
Lateral bend		-10	
Flexion and lateral bend	-13	-10	
Lateral bend and axial rotation		-10	-4

- b. Fail specimen by sudden overload with video recording from the left posterior side to capture failure events
 - i. Set sample rate = 250
 - ii. Set time = 20
 - iii. Under ramp testing
6. Set velocity = 6.67
7. Set displacement = -3
 - i. Collect data
 - ii. Start ramp test
- b. Return specimen to original position
 - i. Under ramp testing
8. Set velocity = 0.5
9. Set displacement = 0 and start ramp test
 - a. Depending on the test conducted, set Rx, Ry or Rz position control constrains back to 0
10. Run the second 6DOF batch test (43 minutes).

12.2 Appendix 2: Geometric Centre Data Sheet

SHEEP FSU SUDDEN OVERLOAD DATA SHEET 2017			
Specimen Prep Date		Testing Date	
Specimen ID		Specimen Number	
		Testing Conditions	
		Disc Level	
Day 1 Specimen Preloading & Hydration			
Prepping for overnight preload			
<ol style="list-style-type: none"> 1. Remove specimen from freezer 2. Thaw on bench for 2hrs 3. Take geometric centre measurements to calculate offsets 			
1. Measure the total height of the FSU			
1. FSU height height [mm]	1	2	3 Average 0.00
2. Measure the height of the superior (top) vertebra			
Superior height [mm]	1	2	3 Average 0.00
3. Measure the height of the inferior (bottom) vertebra			
Inferior height [mm]	1	2	3 Average 0.00
4. Measure the height of the disc			
Take three measurements at left lateral, right lateral and the center of the disc			
Disc height [mm]	1	2	3 Average 0.00

4. Calculate Z offset from the sum of specimen coupling plate, height of the top cup, superior vertebra and half the disc

Height of specimen Coupling plate [mm] 24

Height of Top Cup [mm]

Z offset [mm] 34.00

4. Measure endplate dimensions using caliper

Superior	1	2	3	Average
AP_S [mm]				#DIV/0!
LAT_S [mm]				#DIV/0!

Inferior	1	2	3	Average
AP_I [mm]				#DIV/0!
LAT_I [mm]				#DIV/0!

Combined Superior/Inferior Avg Dimensions		Disc Area		mm ²
Avg_AP =	#DIV/0!	0.84 x Avg_AP x Avg_LAT	#DIV/0!	#DIV/0!
Avg_LAT =	#DIV/0!			

After Potting Base Cup

5. Measure the X offset
 take this measurement once the specimen has been potted in the bottom cup
 measure from the center of the disc to the inside left edge of the cup
 or the outside of the cup and subtract the width of the cup wall



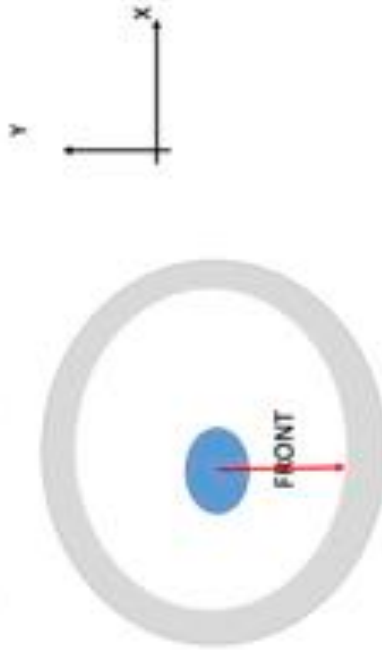
Y-Offset	1	2	Average
Length [mm]			0.00

Inner Radius of Cup [mm]	45
--------------------------	----

Y-Offset	-45.00
----------	--------

6. Measure the Y offset

take this measurement once the specimen has been potted in the bottom cup
measure from the center of the disc to the inside front edge of the cup or the outside of the cup and subtract the width of the cup wall



Y-Offset	1	2	Average
Length [mm]			0.00

Inner Radius of Cup [mm]	45
--------------------------	----

Y-Offset [mm]	-45.00
---------------	--------

7. Once potted, measure the height of the potted assembly

take one measurement and then rotate the assembly 90 degrees, repeat another three times

Height (mm)	1	2	3	4
-------------	---	---	---	---

5. Calculate testing parameters:

Preload (N)	Followup (N)	Reference (N)
0.1MPa $(Area \times 0.1/1.5)$	0.1MPa $(Area \times 0.5/1.5)$	0.6MPa $(Area \times 0.6/1.6)$
#DIV/0!	#DIV/0!	#DIV/0!

Compressive Loads

6. Take specimen photos

7. Preload outside of hexapod using weights

Preload weights	Start height	Start Time	End Height	End Time

8. Leave specimens in rig outside hexapod overnight

9. Set up LVDT for measuring displacements during preloading as

Hexapod Setup

USE HEXAPOD PROTOCOL

GOOD TESTING

File Name:

Start Time
End Time

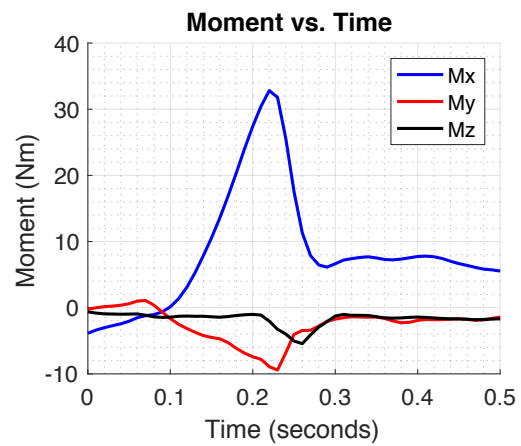
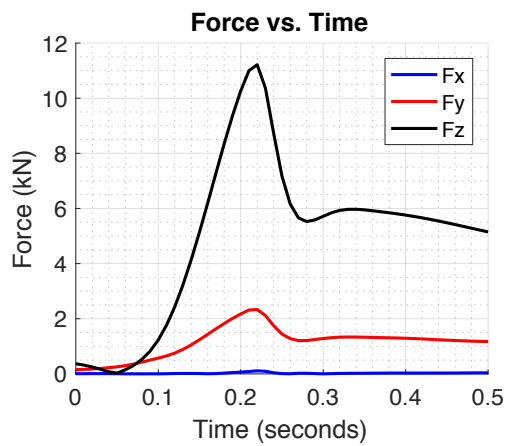
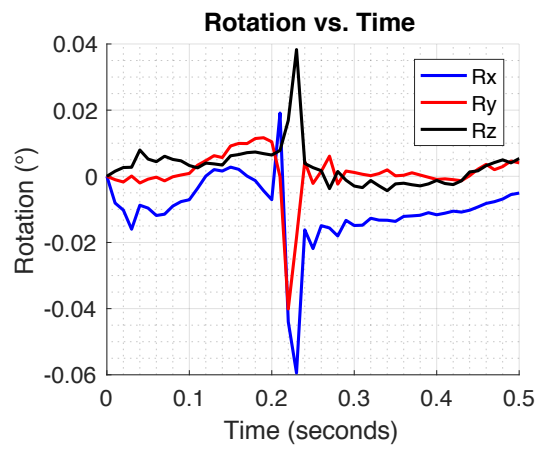
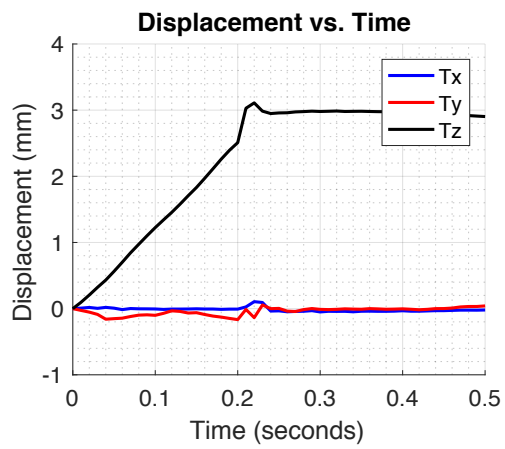
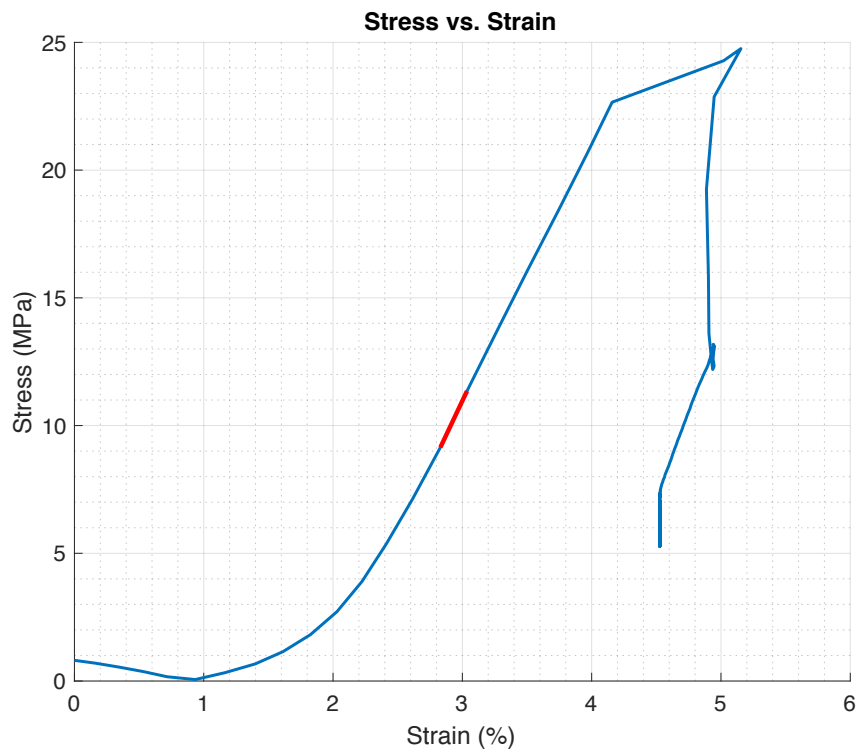
Tx (Start)
Tx (End)

SET POSTURE

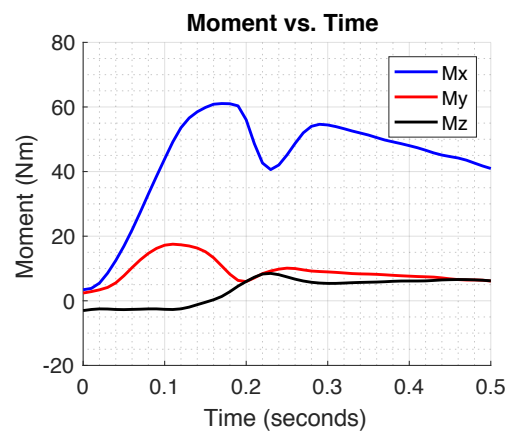
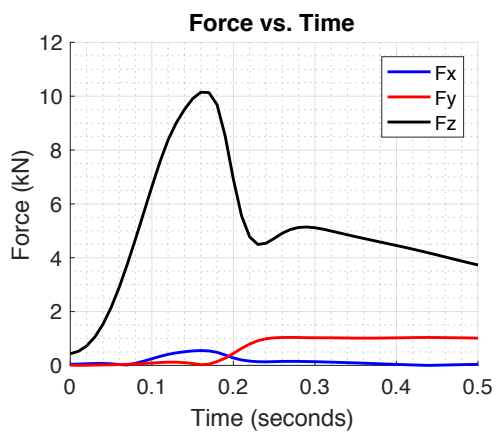
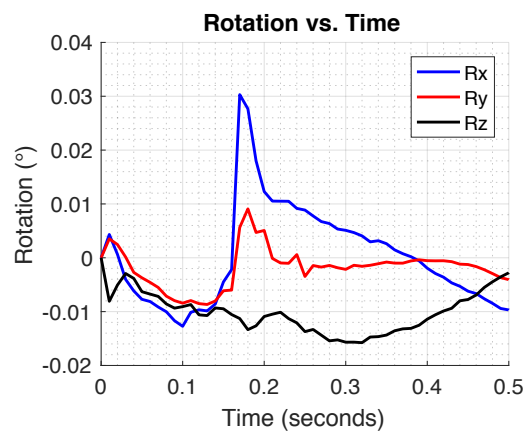
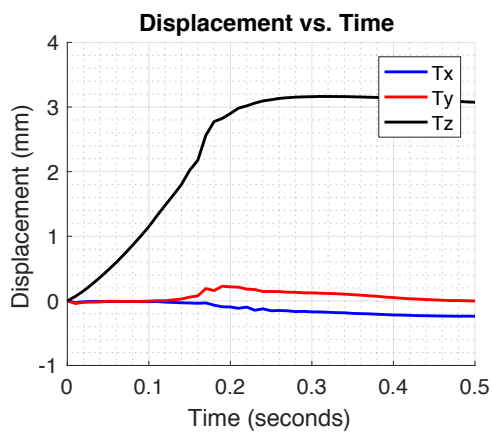
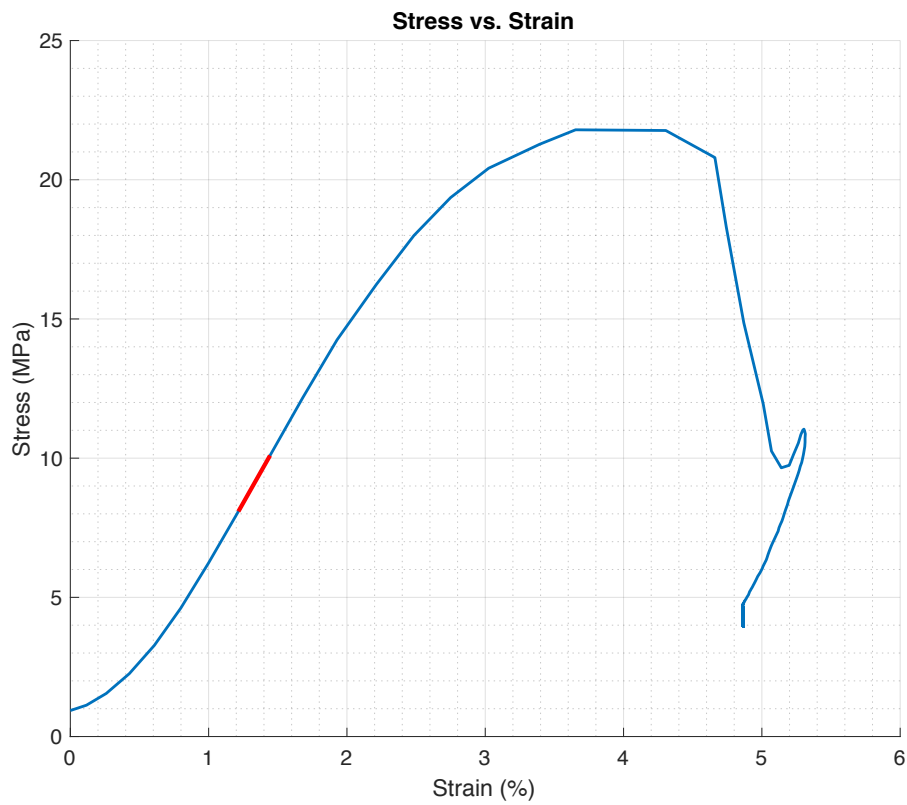
12.3 Appendix 3: Pilot Testing Results

ID	Group	Load (kN)			Tz (mm)	Time (s)	Moments (Nm)			Max Stress (MPa)	Max Strain (%)	Energy Absorption (MJ/m ³)	Modulus (MPa)
		Fx	Fy	Fz			Mx	My	Mz				
SSO1	FL	0.11	2.33	11.21	3.11	0.22	32.81	-8.91	-2.03	24.76	67.45	3.6	78.2
SSO2	LB	0.55	0.03	10.15	2.17	0.16	60.85	13.33	0.33	21.79	67.45	3.6	78.0
SSO3	FL + LB	0.94	1.47	10.21	3.02	0.29	5.23	-34.26	0.81	16.39	41.82	3.7	77.0
SSO4	FL	0.25	0.80	8.27	2.33	0.16	-8.35	17.98	2.91	33.45	80.07	3.7	29.3
SSO5	FL	0.00	0.74	4.03	2.82	0.26	9.09	10.41	-2.85	9.45	64.22	3.3	90.1
SSO6	FL	0.04	1.03	6.29	2.00	0.14	-11.12	-2.08	0.43	18.62	68.84	3.4	18.0

Specimen 1 – SSO1

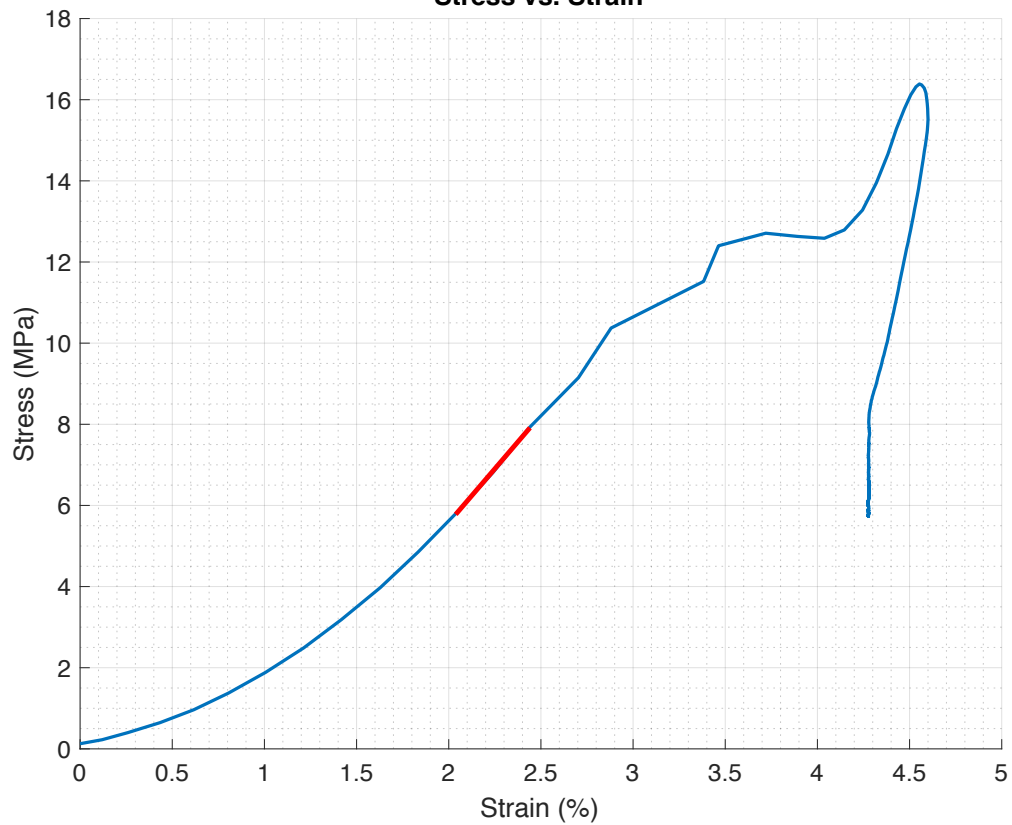


Specimen 2 – SSO2

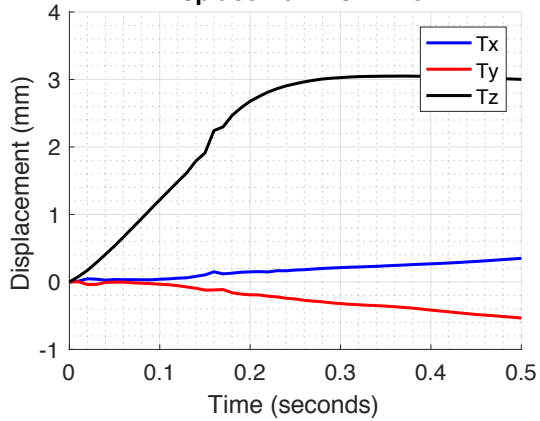


Specimen 3 – SSO3

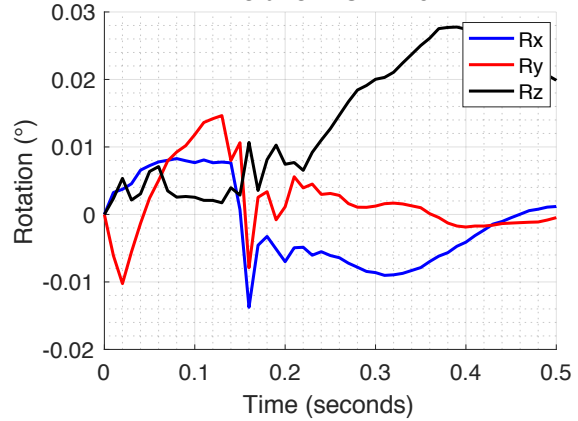
Stress vs. Strain



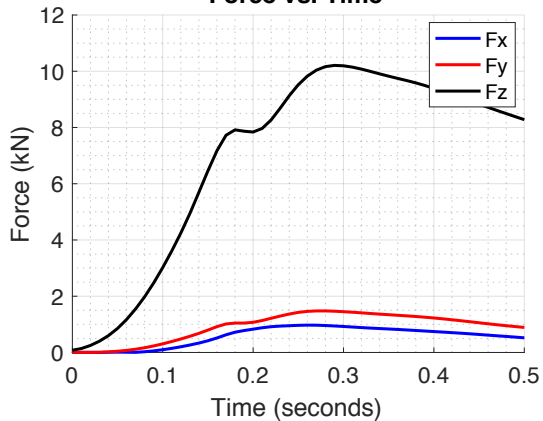
Displacement vs. Time



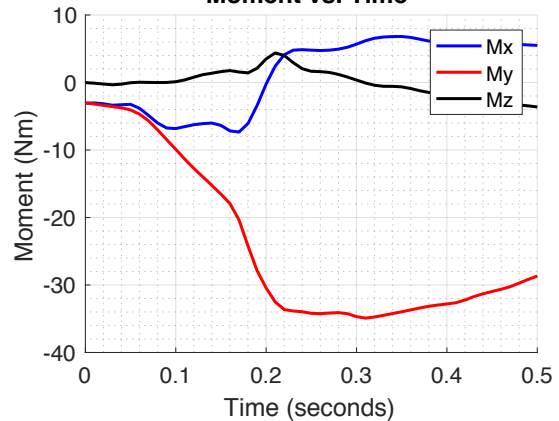
Rotation vs. Time



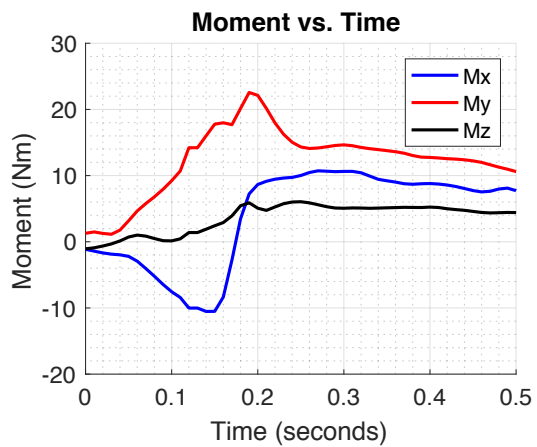
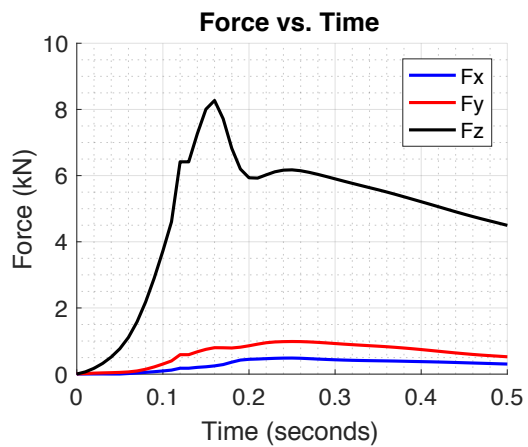
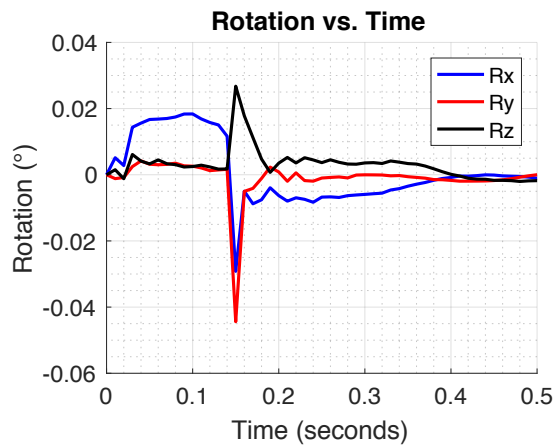
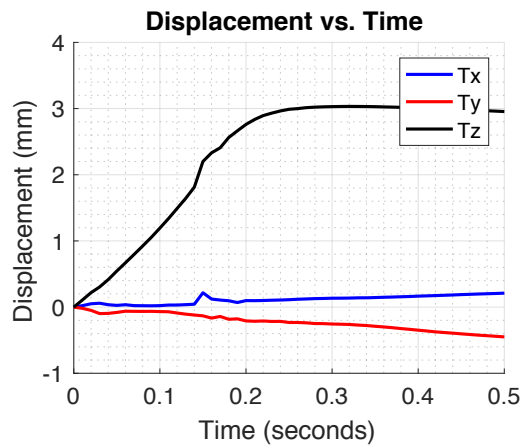
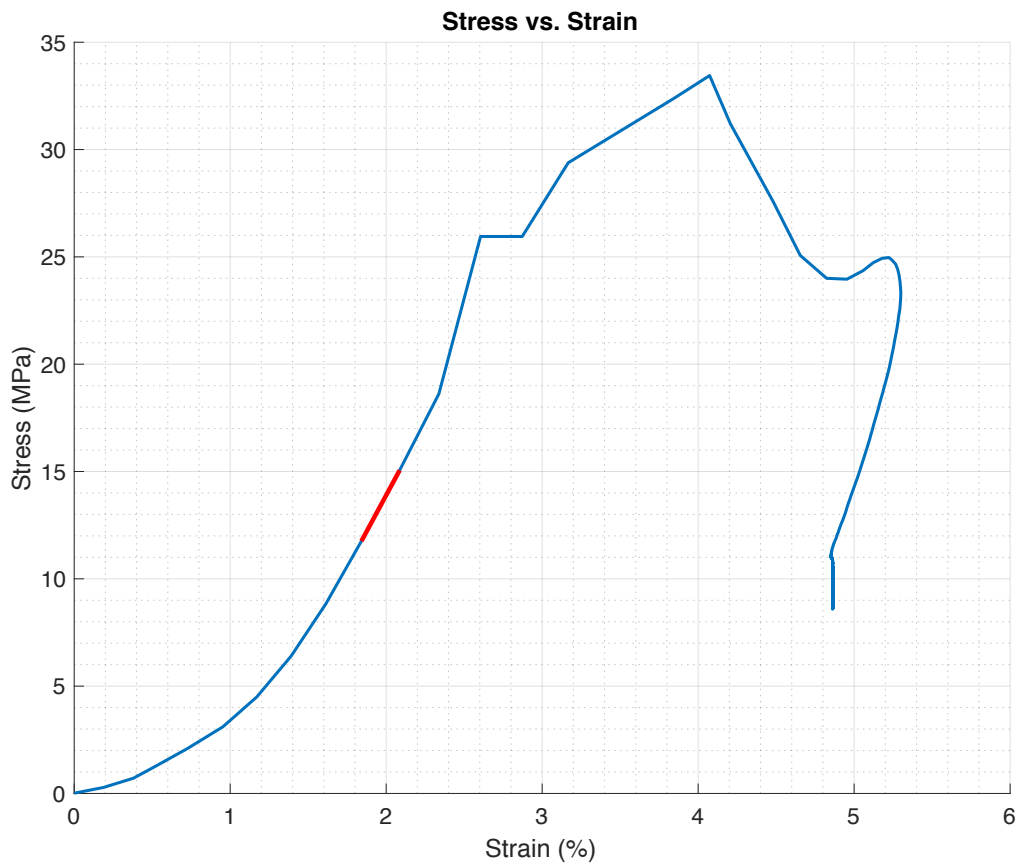
Force vs. Time



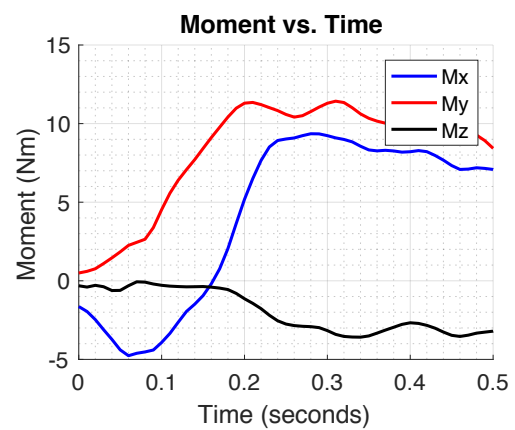
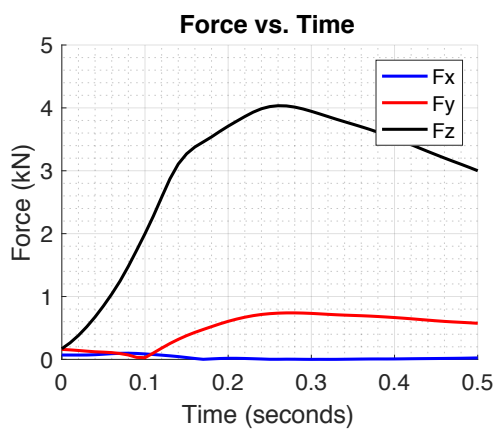
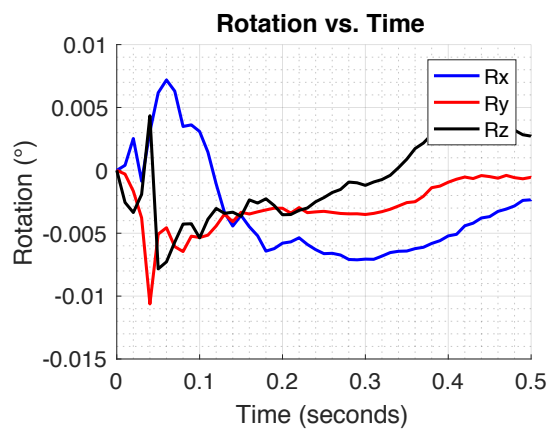
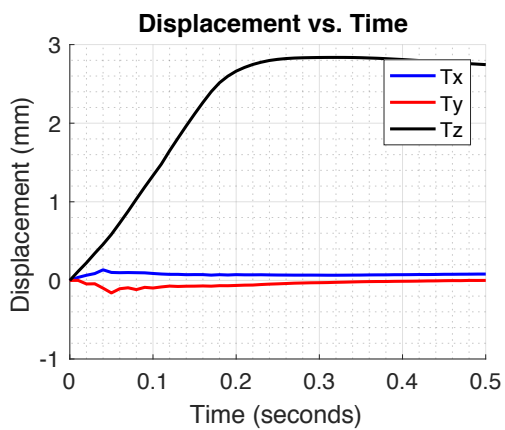
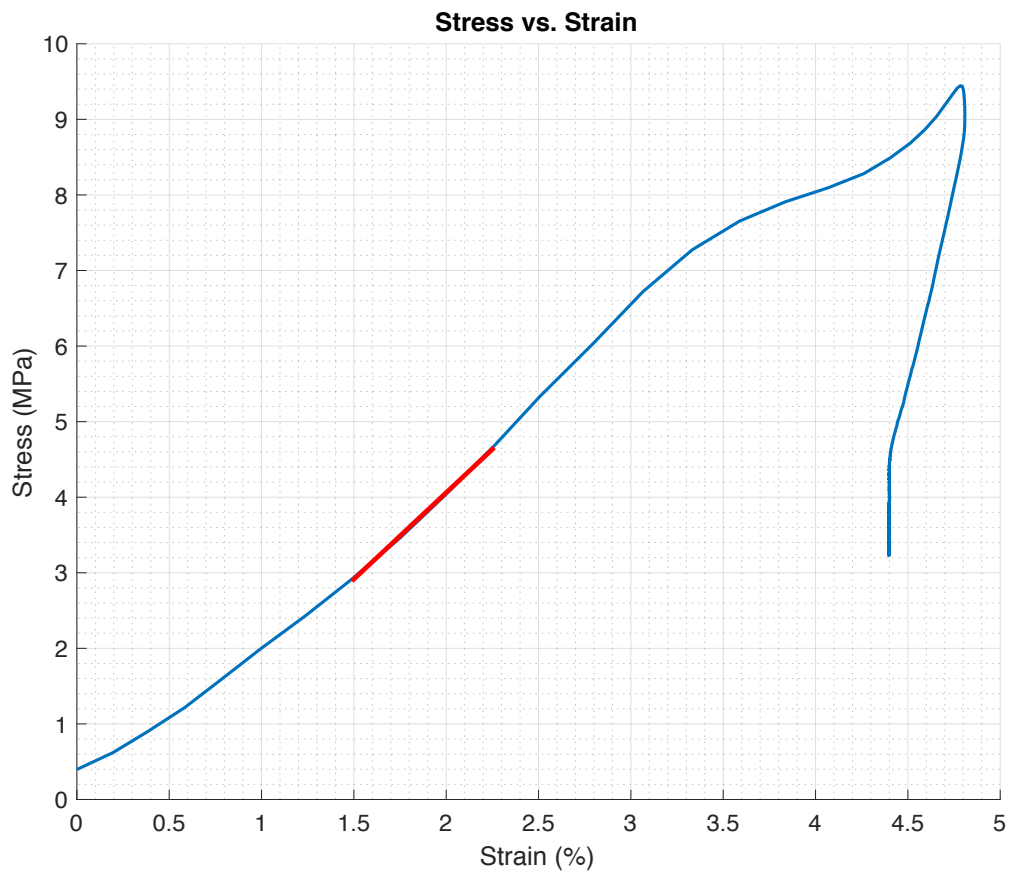
Moment vs. Time



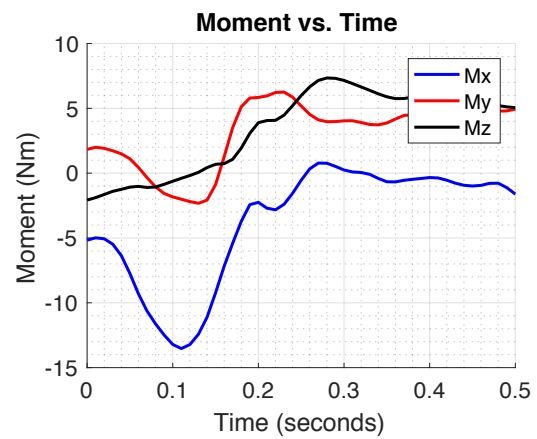
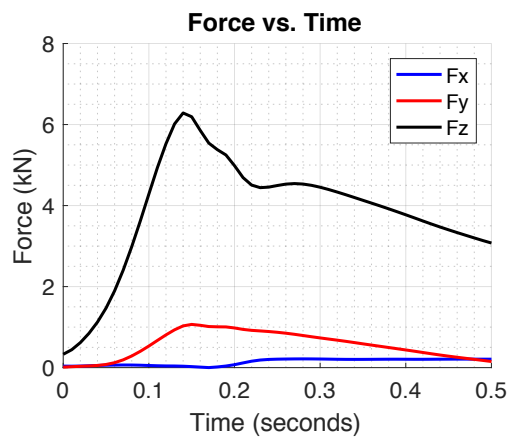
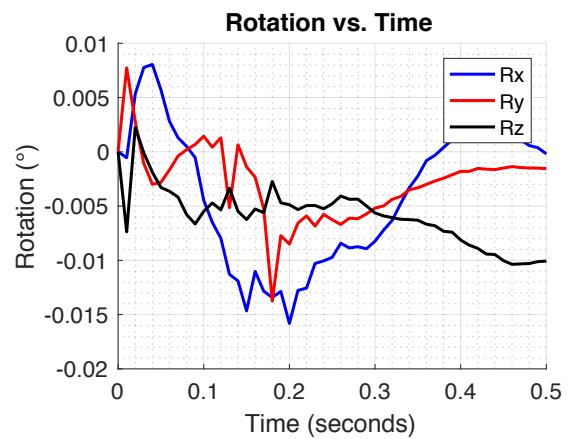
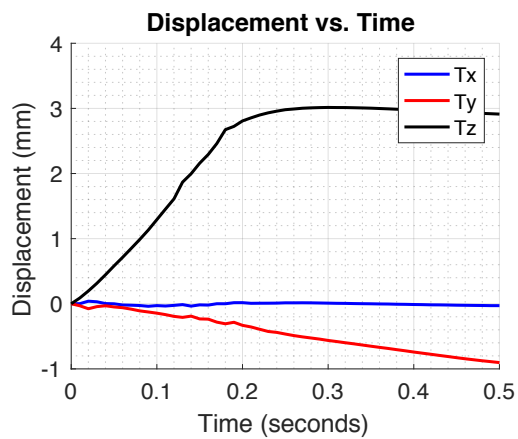
Specimen 4 – SSO4



Specimen 5 – SSO5



Specimen 6 – SSO6



12.4 Appendix 4: Matlab Code

```
%%%%%%%%%%%%%%%%%%%%%%%%%%%%%%%%%%%%%%%%%%%%%%%%%%%%%%%%%%%%%%%%%%%%%%%%
%Main code 2/10/2017
%
%Reads in position and load files collected during hexapod test
%Outputs load-displacement, stress-strain, modulus, toughness for fail
%Outputs final load/unload cycle, stiffness, phase angle for 6DOF
%
%By Bethany Kamitakahara
%%%%%%%%%%%%%%%%%%%%%%%%%%%%%%%%%%%%%%%%%%%%%%%%%%%%%%%%%%%%%%%%%%%%%%%%

close all; clear;

%Initialises parameters
degreeSymbol = sprintf(char(176));
test = {'Flex' 'LateralBend' 'FlexLateralBend' 'LateralBendAxial'};
xAxis = { 'Translation (mm)', 'Translation (mm)', degreeSymbol , degreeSymbol ,
degreeSymbol ,degreeSymbol , 'Translation (mm)'};
loadCondition={'LateralShear' 'AnteriorPosteriorShear' 'AxialRotation'
'LateralBending' 'FlexionExtension' 'FlexionExtension' 'Compression'};
yAxis = { 'Force (N)' 'Force (N)' 'Moment (Nm)' 'Moment (Nm)' 'Moment (Nm)' 'Moment
(Nm)' 'Force (N)'};
output = {'Tx' 'Ty' 'Tz' 'Rx' 'Ry' 'Rz' 'Fx' 'Fy' 'Fz' 'Mx' 'My' 'Mz'};
ref= {'Tx','Fx'; 'Ty','Fy'; 'Rz','Mz'; 'Ry','My'; 'Rx','Mx'; 'Rx','Mx'; 'Tz','Fz'};
panelAxis={'Displacement (mm)', ['Rotation (' degreeSymbol ')'],'Force (kN)',
'Moment (Nm)'};
panelTitle={'Displacement', 'Rotation','Force' 'Moment'};
stiffLabel={'N/mm', 'N/mm', 'Nm/' degreeSymbol, 'Nm/' degreeSymbol, 'Nm/'
degreeSymbol, 'N/mm'};
degreeSymbol, 'N/mm'};
plotFail=0;
plotCompare=0;
plotAverages=0;
pilot=0;
first=1;
last=32;
counterNotSet=1;
n=1;

%Set figure properties
set(groot, 'defaultLineLineWidth',2);
set(0, 'defaultAxesFontSize',15);

store=1;
%Executes for x number of specimens
for i=first:last
    if i~=10 && i~=4 && i~=31
        filePath=cd('/Users/bethanykamitakahara/Documents/Matlab/Hexapod/Masters
Test');
        if pilot
testType=dlmread(fullfile(['/Users/bethanykamitakahara/Documents/Matlab/Hexapod/Mas
ters Test/SSO' num2str(i) '/SSO' num2str(i) 'test.txt']));
            else
testType=dlmread(fullfile(['/Users/bethanykamitakahara/Documents/Matlab/Hexapod/Mas
ters Test/SO' num2str(i) '/SO' num2str(i) 'test.txt']));
            end

            [data] =
readTextFiles(num2str(i),test{testType(1)},testType(2),testType(4),output,pilot);
%Read in hexapod files

            if testType(2)

[time, fail, startFail, beforeDOF, afterDOF]=failData(data.fail,data.before,data.after,
testType(3),i,loadCondition);
```

```

else
    [time, fail, startFail]=failNObatch(data.fail, testType(3), i, pilot);
end

%----- Failure Data -----%
%Calculate stress and strain
stress=(fail.Fz/(testType(6)/10^(6)))/10^(6);
lo=testType(7);
l=testType(7)-fail.Tz;
strain=abs(((lo-l)/lo)*100);

%Determine maximum force and displacement at failure
[maxStress, index]=max(stress);
maxStrain=strain(index);

%Calculates toughness/energy absorption at failure
tough=trapz(strain(1:index), stress(1:index));
counter=1;

%Stiffness Calculation
for p=1:index
    if stress(p)>0.3*maxStress && stress(p)<0.5*maxStress
        stiff(counter)=p;
        counter=counter+1;
    end
end

xs=strain(stiff); %50% of maximum Stress
ys=stress(stiff); %30% of maximum stress
pvLs = polyfit(xs,ys,1); %Produces line mx+c
bestFits=polyval(pvLs,xs);
failStiffness=pvLs(1);

%Stores specimen failure variables in cell array
if testType(1)==4
    stats(store,1)=i;
    stats(store,2)=testType(1); %Direction load
    stats(store,3)=testType(5); %Facet/no facet
    stats(store,4)=maxStress; %Stress
    stats(store,5)=maxStrain; %Strain
    stats(store,6)=testType(6); %Disc Area
    stats(store,7)=testType(8); %Disc height
    stats(store,8)=tough; %Toughness/energy absorption
    stats(store,9)=failStiffness; %Stiffness
    stats(store,10)=fail.Fz(index)/1000;
    stats(store,11)=fail.Tz(index);
    stats(store,12)=time(index);
    stats(store,13)=fail.Mx(index);
    stats(store,14)=fail.My(index);
    stats(store,15)=fail.Mz(index);
    stats(store,16)=fail.Fx(index)/1000;
    stats(store,17)=fail.Fy(index)/1000;
    compare{store}(1,:)=stress;
    compare{store}(2,:)=strain;

    store=store+1;
end

%----- Failure Plots -----%
if plotFail
    fail.Fz=fail.Fz/1000;
    fail.Fy=fail.Fy/1000;
    fail.Fx=fail.Fx/1000;

    % Tz Vs. Fz
    %Axes('Parent',uitab('Parent', tgroup, 'Title', 'Tz Vs. Fz'));

```

```

figure(1)
hold on;grid on;grid minor;
plot(fail.Tz,abs(fail.Fz));
xlabel('Displacement (mm)');
ylabel('Load (kN)');
title('Load (Fz) vs. Displacement (Tz)');
xlim([0 3.5]);
hold off;

%Stress-Strain Curve
figure(2)
grid on;grid minor;
plot(strain,stress);
xlabel('Strain (%)');
ylabel('Stress (MPa)');
title('Stress vs. Strain');
%xlim([0 0.055]);

%Stress-Strain Curve with toughness stiffness
figure(3)
hold on;grid on;grid minor;
plot(strain,stress);
plot(xs,bestFits,'r','LineWidth',3);
% area(strain(1:index),stress(1:index));
xlabel('Strain (%)');
ylabel('Stress (MPa)');
title('Stress vs. Strain');
hold off;

%6DOF Panel Plots (Translation,rotation,force,moment - x,y,z)
j=1;
figure(4)
for p=1:3:12
    subplot(2,2,j)
    hold on;grid on;grid minor;
    plot(time, fail.(output{p}),'b');
    plot(time, fail.(output{p+1}),'r');
    plot(time, fail.(output{p+2}),'k');
    xlabel('Time (seconds)');
    ylabel(panelAxis{j});
    title([panelTitle{j} ' vs. Time']);
    xlim([0, 0.5]);
    legend(output(p:p+2));
    hold off;
    j=j+1;
end

figure(5)
for l=1:3
    %Translation vs. Force (x,y,z)
    subplot(2,3,l)
    hold on;grid on;grid minor;
    plot(fail.(output{l}),fail.(output{l+6}));
    xlabel('Translation (mm)');
    ylabel('Force (kN)');
    title([output{l} ' vs. ' output{l+6}]);
    hold off;

    %Rotation vs. Moment (x,y,z)
    subplot(2,3,3+l)
    hold on; grid on; grid minor;
    plot(fail.(output{l+3}),fail.(output{l+9}));
    xlabel(['Rotation (', degreeSymbol,')']);
    ylabel('Moment (Nm)');
    title([output{l+3} ' vs. ' output{l+9}]);
    hold off;
end

```

```

        figure(6)
        hold on; grid on; grid minor;
        plot(time, fail.Fx,'b');
        plot(time, fail.Fy,'r');
        plot(time, fail.Fz,'k');
        xlabel('Time (seconds)');
        ylabel('Force (kN)');
        title('Force vs. Time');
        xlim([0, 1]);
        legend(output(7:9));
        hold off;
    end
end

% Plot stress-strain curves by group
count=1;
if plotCompare
    for i=first:last
        if stats(i,2)==2 && stats(i,3)==1 %Flexion & Facet
            figure (1)
            hold on;grid minor;grid on;
            plot(compare{i}(2,:),compare{i}(1,:),colour);
            xlabel('Strain (%)');
            ylabel('Stress (MPa)');
            title('Stress-Strain Curves of Intact FSUs in Flexion and Lateral
Bend','FontSize',18);
            l=legend('SO3','SO8','SO13','SO28');
            l.FontSize=15;
            hold off;
            spec(count)=i;
            count=count+1;
        end
    end
end

%Save fail parameters to table for SPSS analysis
failNames={'Specimen','FSU','Direction','Stress','Strain','Modulus','Toughness'};
DOFNames={'Specimen','FSU','Direction','DOF','ARStif','LBStiff','FlexStiff','Compre
ssStiff','ARPhaseAngle','LBPhaseAngle','FlexPhaseAngle','CompressPhaseAngle'};
failSPSS=table(stats(:,1),stats(:,3),stats(:,2),stats(:,4),stats(:,5),stats(:,9),st
ats(:,8),'VariableNames',failNames);
writetable(failSPSS,'failSPSSnoAR.txt','Delimiter',' ');
type 'failSPSSnoAR.txt';

%%%%%%%%%%%%%%%%%%%%%%%%%%%%%%%%%%%%%%%%%%%%%%%%%%%%%%%%%%%%%%%%%%%%%%%%
% ReadTextFiles 2/10/2017
%
% Takes in specimen number, direction of loading, whether 6DOF or position
% data was recorded and if it was a pilot test or not
% Outputs data in a struct
% Struct variables includes 'before' = first 6DOF, 'after' =
% second 6DOF, 'fail'=fail data
%
% Each struct variables contains data on Tx, Ty, Tz, Rx, Ry, Rz, Mx, My,
% Mz, Fx, Fy, Fz
%
%By Bethany Kamitakahara
%%%%%%%%%%%%%%%%%%%%%%%%%%%%%%%%%%%%%%%%%%%%%%%%%%%%%%%%%%%%%%%%%%%%%%%%

function [data] = readTextFiles(x,test,batch,posRecorded,output,pilot)

cd (strcat(['SO' x]));
compress=dir('*/Tz1E1M*');
loadCondition={'LateralShear' 'AnteriorPosteriorShear' 'AxialRotation'

```



```

'LateralBending' 'FlexionExtension' 'Compression'];

% Read data from text files in the set directoy and store them in their groups
if batch
    for i=1:6
        if str2double(x)<10
            comp=compress(4).name(4:10);
        else
            comp=compress(4).name(5:14);
        end

        direction={'B6E1Ty5E2' 'B6E1Tx5E2' 'B003Rz5E2' 'B004Ry5E2' 'B003Rx5E2'
comp};
        beforeLoad=dlmread(fullfile(cd, ['/Before/SO' x direction{i} '_L.txt']));
        beforePos=dlmread(fullfile(cd, ['/Before/SO' x direction{i} '_P.txt']));
        beforeTotal=[beforePos; beforeLoad];
        afterLoad=dlmread(fullfile(cd,['/After/SO' x '-fail' direction{i}
'_L.txt' ]));
        afterPos=dlmread(fullfile(cd,['/After/SO' x '-fail' direction{i}
'_P.txt' ]));
        afterTotal=[afterPos; afterLoad];

        for j=1:length(output)
            data.before.(loadCondition{i}).(output{j})=beforeTotal(j,:);
            data.after.(loadCondition{i}).(output{j})=afterTotal(j,:);
        end
    end
end

fs=100; %Sample rate (Hz)
Ts=1/fs; %Time per sample (seconds)
data.time=0.01:Ts:10.2; %Time vector

% Only if position data recorded during rotation to specified angle
if posRecorded
    for j=1:length(output)
        positionLoad=dlmread(fullfile(cd, ['SO' x test '_L.txt']));
        positionPos=dlmread(fullfile(cd, ['SO' x test '_P.txt']));
        positionTotal=[positionPos; positionLoad];
        data.position.(output{j})(:)=positionTotal(j,:);
    end
end

% Only for pilot data
if pilot
    for j=1:length(output)
        failLoad=dlmread(fullfile(cd, ['SSO' x 'Fail_L.txt']));
        failPos=dlmread(fullfile(cd, ['SSO' x 'Fail_P.txt']));
        failTotal=[failPos; failLoad];
        data.fail.(output{j})=failTotal(j,:);
    end
else
    for j=1:length(output)
        failLoad=dlmread(fullfile(cd, ['SO' x 'Fail_L.txt']));
        failPos=dlmread(fullfile(cd, ['SO' x 'Fail_P.txt']));
        failTotal=[failPos; failLoad];
        data.fail.(output{j})=failTotal(j,:);
    end
end

cd('/Users/bethanykamitakahara/Documents/Matlab/Hexapod/Masters Test');
end

```

```

%%%%%%%%%%%%%%%%%%%%%%%%%%%%%%%%%%%%%%%%%%%%%%%%%%%%%%%%%%%%%%%%%%%%%%%%
% failNObatch 2/10/2017
%
% Adjusts raw data to the start of the test
% Adjusts sampling frequency for S01-S04
% Calculates displacement rather than raw translation values
%
%By Bethany Kamitakahara
%%%%%%%%%%%%%%%%%%%%%%%%%%%%%%%%%%%%%%%%%%%%%%%%%%%%%%%%%%%%%%%%%%%%%%%%

function [timeVector,failed,startFail]=failNObatch(fail,Hz,num,pilot)

%Input variables for failure
fs=Hz;           %Sample rate (Hz)
Ts=1/fs;        %Time per sample (seconds)

if pilot && num==1
    t=30;        %Pilot test 1 recorded for 30 seconds
else
    t=20;        %Total time (seconds) %20 LB, 30 Flex
end

startNotFound=1;

% Adjusting sampling frequency for S01-S04 (conducted at 500Hz)
% Fixing stepped results as sampling frequency of hexapod 5 times less than
% load cell sampling frequency
counter=1;
if ~pilot
    if num==1 || num==2 || num==3 || num==4 %To filter for the 500Hz
        temp.Tx=fail.Tx;
        temp.Ty=fail.Ty;
        temp.Tz=fail.Tz;
        temp.Rx=fail.Rx;
        temp.Ry=fail.Ry;
        temp.Rz=fail.Rz;
        temp.Mx=fail.Mx;
        temp.My=fail.My;
        temp.Mz=fail.Mz;
        temp.Fx=fail.Fx;
        temp.Fy=fail.Fy;
        temp.Fz=fail.Fz;
        fail.Tx=[];
        fail.Ty=[];
        fail.Tz=[];
        fail.Rx=[];
        fail.Ry=[];
        fail.Rz=[];
        fail.Fx=[];
        fail.Fy=[];
        fail.Fz=[];
        fail.Mx=[];
        fail.My=[];
        fail.Mz=[];

        for p=1:5:length(temp.Fz)
            fail.Tx(counter)=temp.Tx(p);
            fail.Ty(counter)=temp.Ty(p);
            fail.Tz(counter)=temp.Tz(p);
            fail.Rx(counter)=temp.Rx(p);
            fail.Ry(counter)=temp.Ry(p);
            fail.Rz(counter)=temp.Rz(p);
            fail.Fx(counter)=temp.Fx(p);
            fail.Fy(counter)=temp.Fy(p);
            fail.Fz(counter)=temp.Fz(p);
            fail.Mx(counter)=temp.Mx(p);
            fail.My(counter)=temp.My(p);
            fail.Mz(counter)=temp.Mz(p);
            counter=counter+1;
        end
    end
end

```

```

        end
        fs=100;           %Sample rate (Hz)
        Ts=1/fs;         %Time per sample (seconds)end
    end
end

% Adjusting plots to the start of the test
factor=[30,30,30,30,110,30,50,30,30,30,30,45,50,30,30,50,35,30,30,30,40,40,45,100,3
0,50,30,50,30,30,30,30];

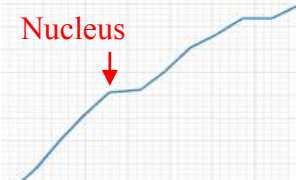

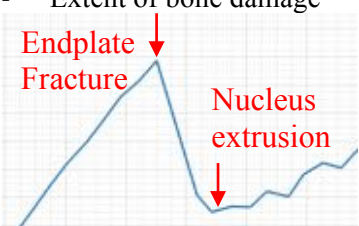



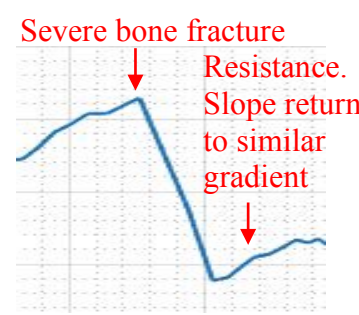



% Calculating Displacement in x,y,z from translations
for j=1:length(fail.Fz)
    if abs(fail.Fz(1)-fail.Fz(j)) >factor(num) && startNotFound
        startFail=j;
        startNotFound=0;
    end
end

timeVector=(0:Ts:t-(Ts*startFail));
counter=1;

for j=startFail:length(fail.Tz)
    failed.Tx(counter)=fail.Tx(startFail)-fail.Tx(j);
    failed.Ty(counter)=fail.Ty(startFail)-fail.Ty(j);
    failed.Tz(counter)=fail.Tz(startFail)-fail.Tz(j);
    failed.Rx(counter)=fail.Rx(startFail)-fail.Rx(j);
    failed.Ry(counter)=fail.Ry(startFail)-fail.Ry(j);
    failed.Rz(counter)=fail.Rz(startFail)-fail.Rz(j);
    failed.Fx=abs(fail.Fx(startFail:end));
    failed.Fy=abs(fail.Fy(startFail:end));
    failed.Fz=abs(fail.Fz(startFail:end));
    failed.Mx=fail.Mx(startFail:end);
    failed.My=fail.My(startFail:end);
    failed.Mz=fail.Mz(startFail:end);
    counter=counter+1;
end
end

```

12.5 Appendix 5: Assessing Modes of Failure

		Identifier	
	Mode of Failure	Load vs. Displacement	Test Observations
1	Annular herniation	<ul style="list-style-type: none"> - Decrease load vs. displacement slope - Indicates Tz displacement increasing while nuclear material slowly extrudes and there's less resistance to load 	<ul style="list-style-type: none"> - Visible extrusion of nuclear material 
2	Endplate fracture	<ul style="list-style-type: none"> - Sharp decrease in load as bone fractures, less resistance to load and displacement increases - Reaches a point of resistance to load where - Followed by sharp increase in load as bone - Extent of bone damage 	<ul style="list-style-type: none"> - Typically, at inferior vertebra disc interface 
3	Facet joint failure		<ul style="list-style-type: none"> - Facet joint capsule torn 
4	Vertebral body fracture		<ul style="list-style-type: none"> - Typically, inferior vertebral body fracture 
5	Pedicle fracture		<ul style="list-style-type: none"> - Fracture at left/right pedicle 

12.6 Appendix 6: Specimen Results

Glossary for Specimen Results

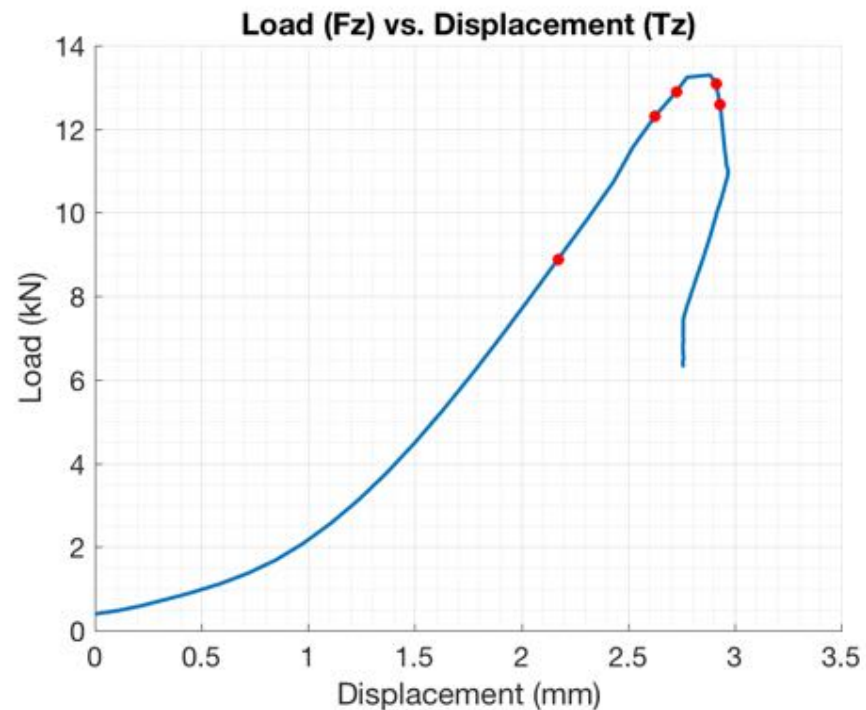
Observation Type	Abbreviation	Meaning
General	POS	Posterior
	L-POS	Left postero-lateral
	R-POS	Right postero-lateral
	ANT	Anterior
	INF	Inferior
	SUP	Superior
Test	AS	Audible cracking/popping sound at failure
	POS-RAIL	XY table AP rail translate posteriorly
	ANT-RAIL	XY table AP rail translate anteriorly
	R-RAIL	XY table lateral rail translate right
	L-RAIL	XY table lateral rail translate left
	EXT	Visible nuclear extrusion filmed
Disc	NE	Visible nuclear extrusion upon examination
	B	Disc bulging
	EPJF	Endplate junction failure
Vertebra	PED	Pedicle fracture
	LAM	Lamina fracture
	EP	Endplate fracture
	F	Facet failure
Classification	HER	Annular herniation
	EPJF	Endplate junction failure
	VER	Vertebral failure
	EP-VER	Endplate vertebra fracture
	IN	Inconclusive

Specimen ID: SO1

Group: Facet Flexion

Date tested: 1/8/2017

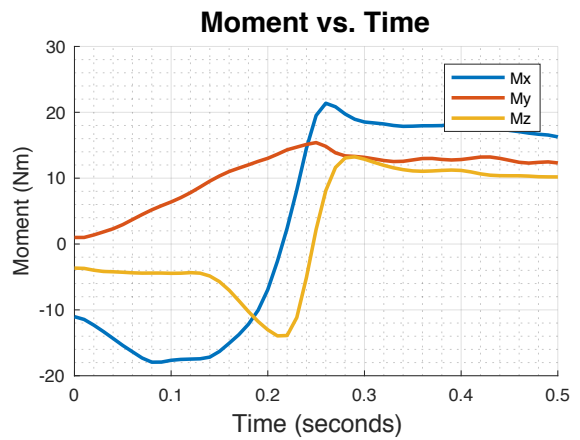
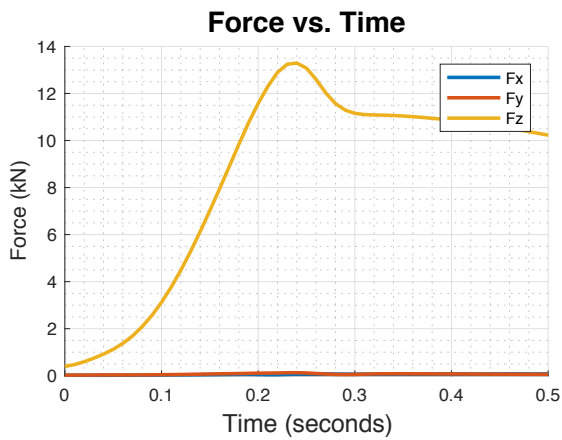
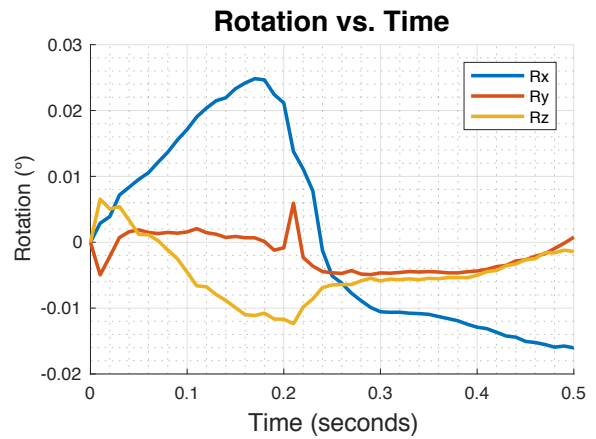
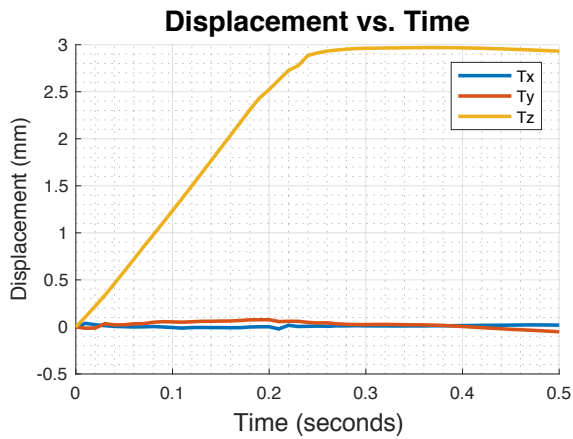
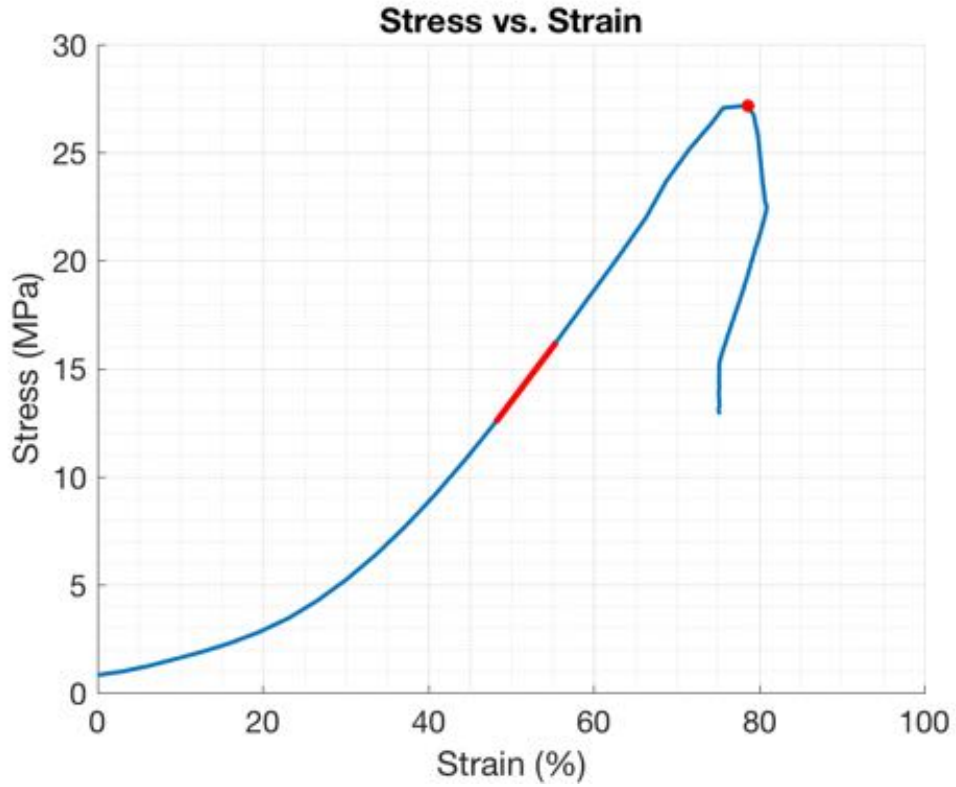
Failure load (kN)	Tz at failure (mm)	Time (s)	Moments (Nm)			Max Stress (MPa)	Max Strain (%)	Modulus (MPa)	Toughness (MJ/m ³)	Observations		
			Mx	My	Mz					Test	Disc	Vertebra
13.30	2.89	0.24	14.56	15.12	-5.07	27.18	78.62	50.6	8.5	AS, POS-RAIL	R-POS NE	-

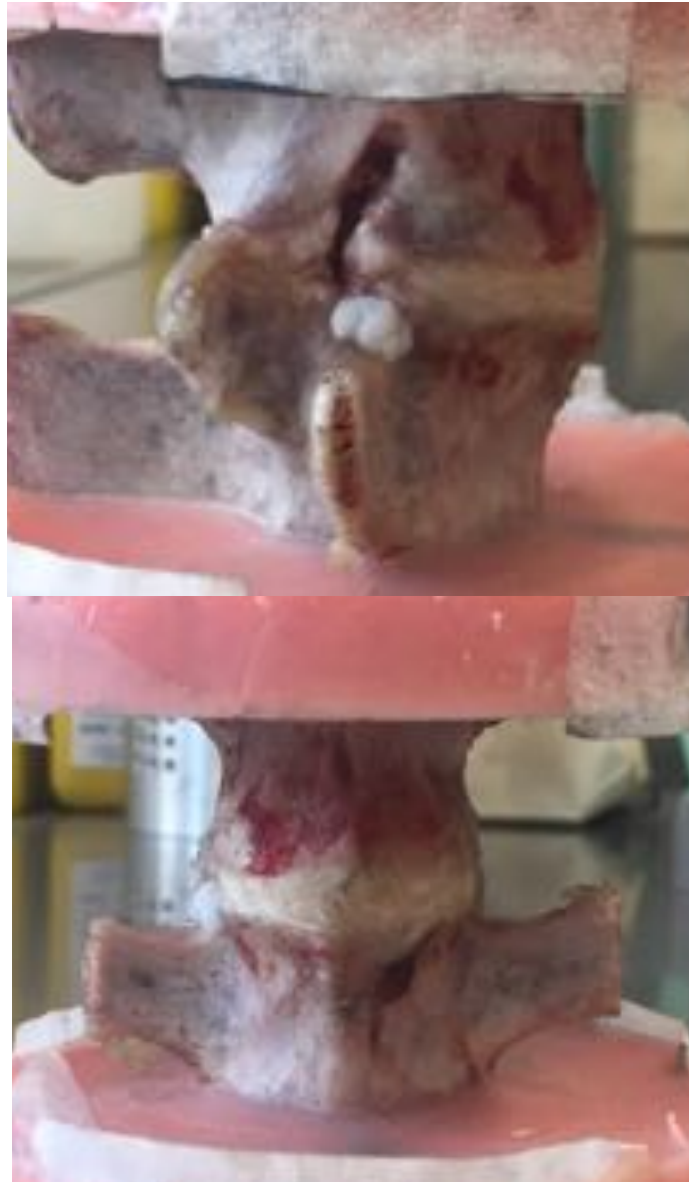


Identification of events by video & load vs. displacement comparison

Note: Failure not captured in video (anterior-right herniation)

Event	Video		Load vs. Displacement	
	Time (s)	Description	Time (s)	Description
1	0.1715	Small compress	0.22	Change in slope
2	0.215	Sound spike	0.23	Change in slope as it plateaus
3	0.2285	Sound spike	0.24	Highest peak
4	0.2465	Bulge left	0.25	Start of declining slope
5	0.255	Sound spike		

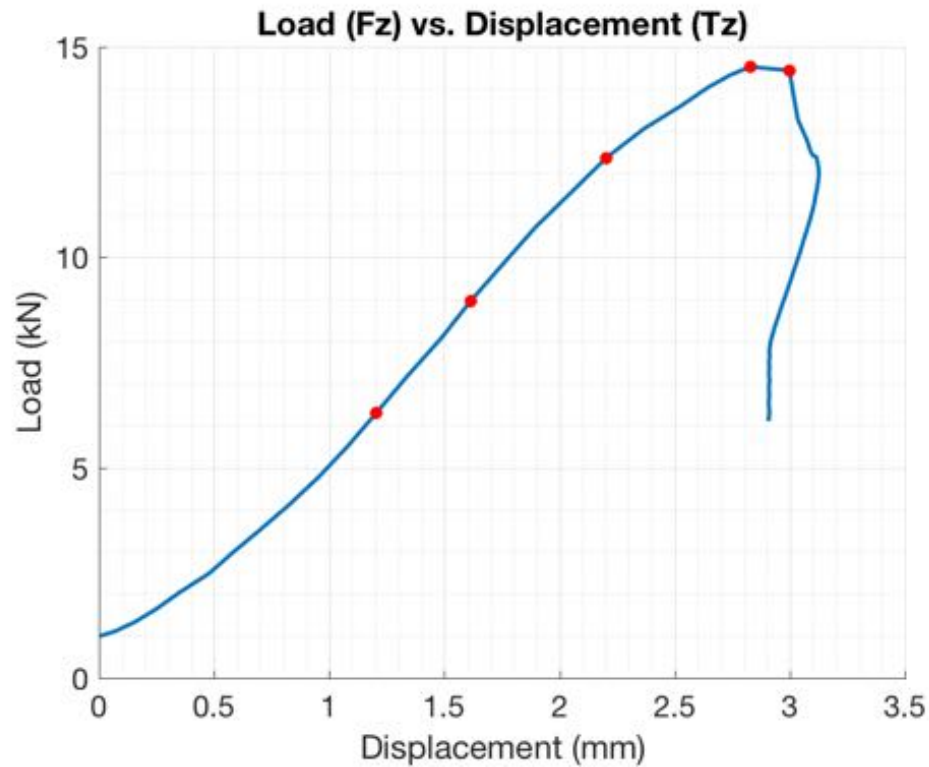




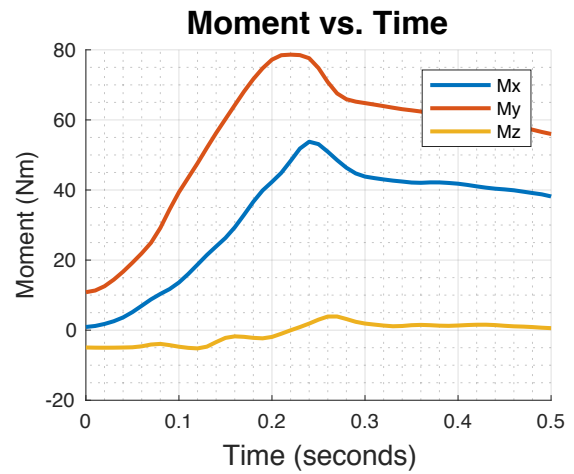
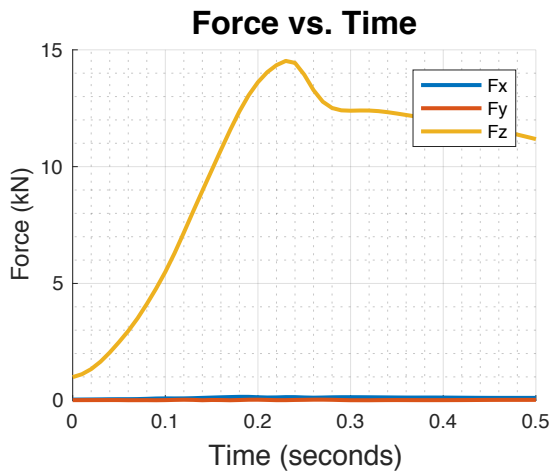
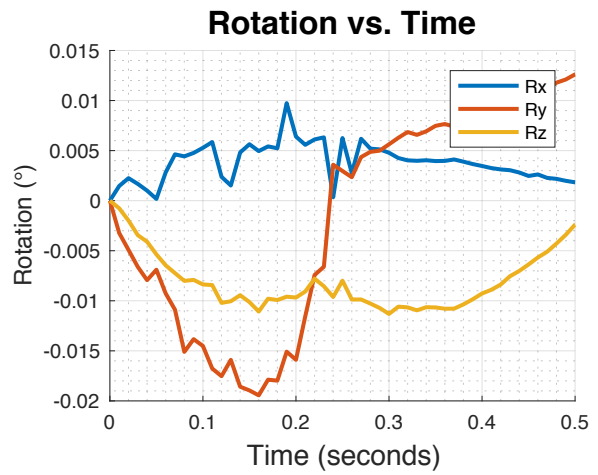
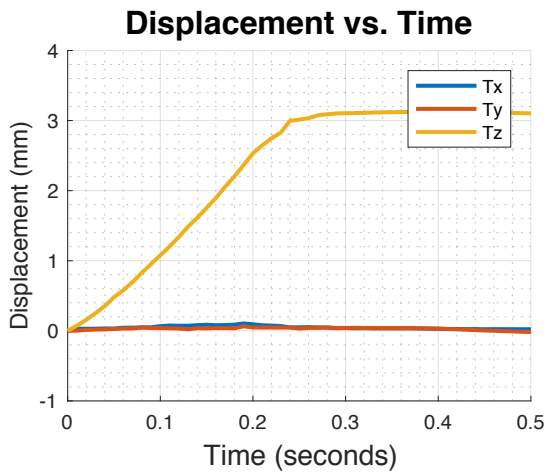
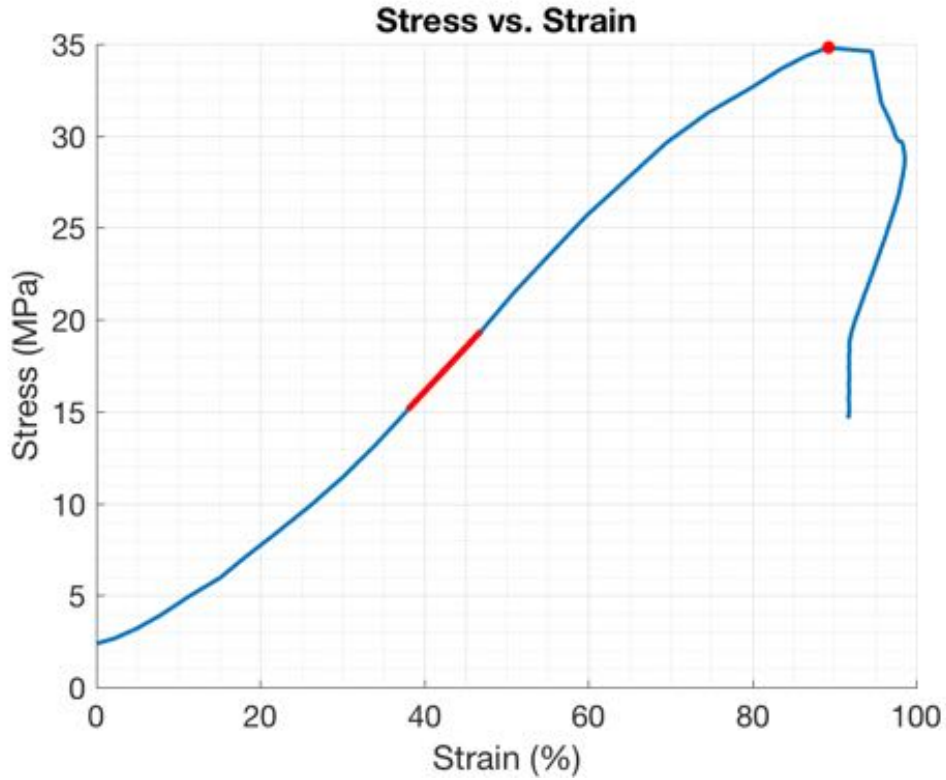
Failure Mode Assessment Summary			
	Load-displacement and video assessment	Photographic indicators	Classification
SO1	Plateau and sound at peak	R-POS NE	HER (R-POS)

Specimen ID: SO2
Group: Facet Right Lateral Bending
Date tested: 2/8/2017

Failure load (kN)	Tz at failure (mm)	Time (s)	Moments (Nm)			Failure Stress (MPa)	Failure Strain (%)	Modulus (MPa)	Toughness (MJ/m ³)	Observations		
			Mx	My	Mz					Test	Disc	Vertebra
14.53	2.83	0.23	51.82	78.49	0.88	34.80	89.24	47.9	16.5	AS, L-RAIL	POS NE in spinal canal + L-POS NE	-



Identification of events by video & load vs. displacement comparison				
	Video		Load vs. Displacement	
Event	Time (s)	Description	Time (s)	Description
1	0.1083	Compress + loud sound – facet collision?	0.1	Change in slope – steeper incline
2	0.135	Sound spike	0.19	Change in slope - decrease
3	0.18	Compress followed by sound spike	0.23	Highest peak
4	0.2285	Sound spike	0.24	Point before declining slope
5	0.24	Sound spike		





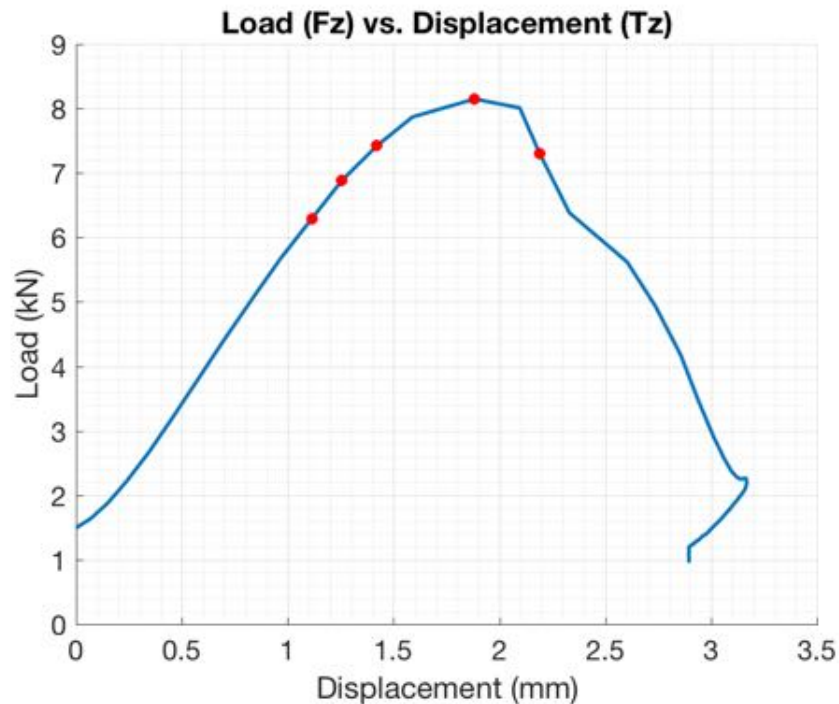
Failure Mode Assessment Summary			
	Load-displacement and video assessment	Photographic indicators	Classification
SO2	Gradual decline in slope up to peak. Plateau and sound at peak	POS-NE	HER (POS)

Specimen ID: SO3

Group: Facet Flexion & Right Lateral Bending

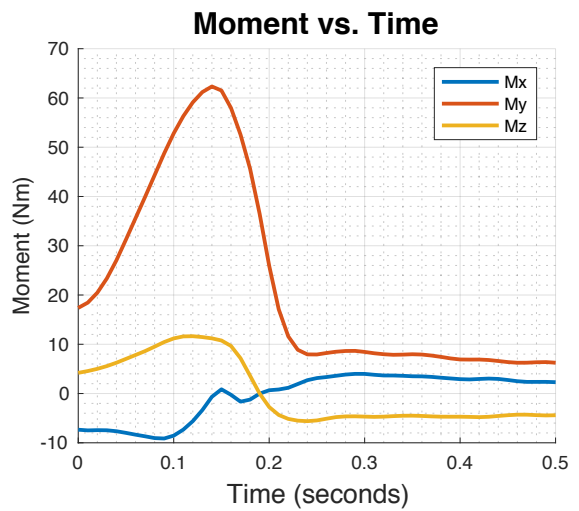
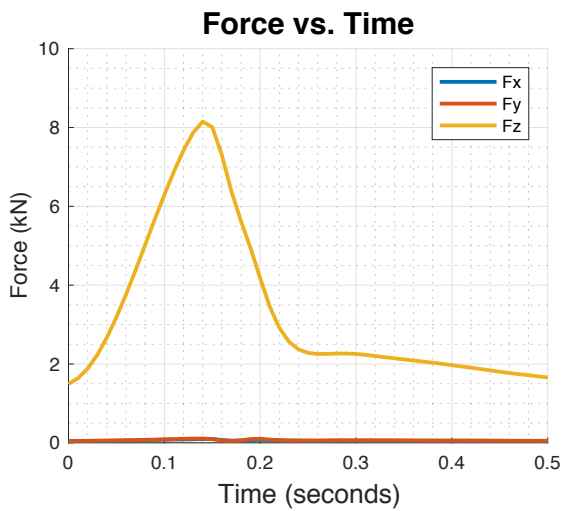
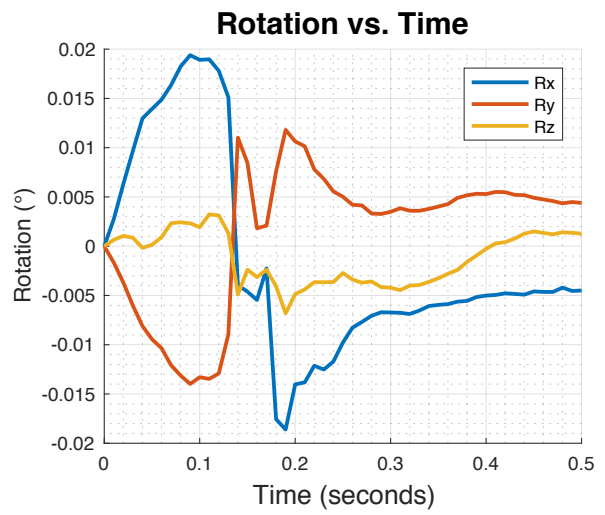
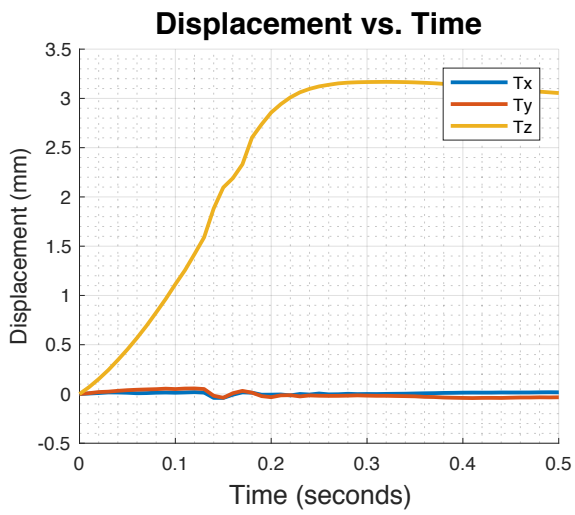
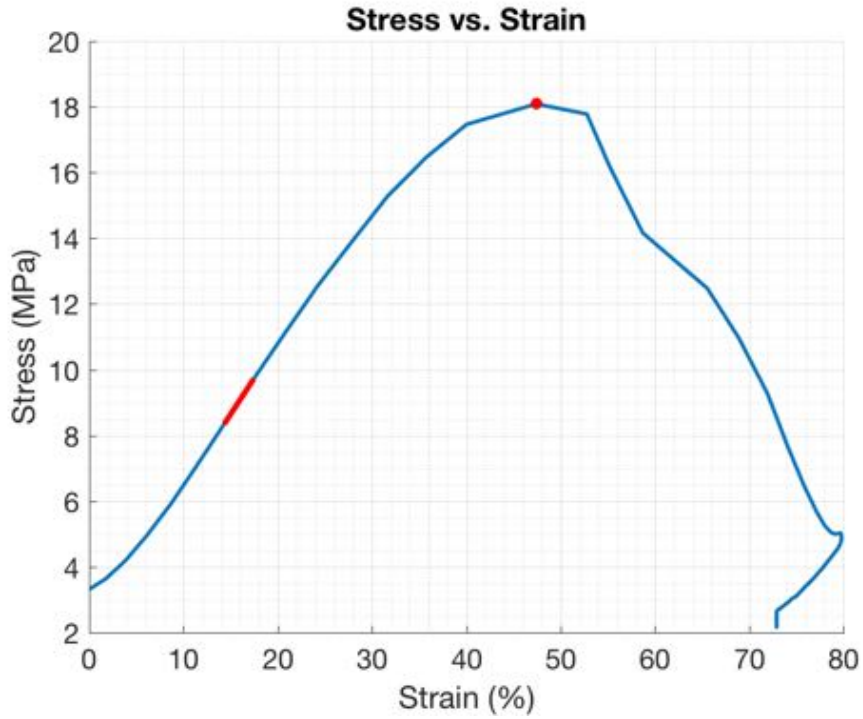
Date tested: 2/8/2017

Failure load (kN)	Tz at failure (mm)	Time (s)	Moments (Nm)			Max Stress (MPa)	Max Strain (%)	Modulus (MPa)	Toughness (MJ/m ³)	Observations		
			Mx	My	Mz					Test	Disc	Vertebra
8.15	1.88	0.14	-0.66	62.33	11.20	18.09	47.41	43.9	5.5	AS, POS-RAIL, L-RAIL	-	SUP R-LAM, L-INF EP torn from INF VER



Identification of events by video & load vs. displacement comparison

Event	Video		Load vs. Displacement	
	Time (s)	Description	Time (s)	Description
1	0.095	Sound spike	0.13	Change in slope
2	0.108	Left postero lateral tear	0.14	Highest peak and plateau
3	0.123	Sound spike	0.15	Point before steep long decline
4	0.14	Further tearing at left endplate? And posterior element fail and sound		
5	0.163	Loud sound followed by further shear forward		

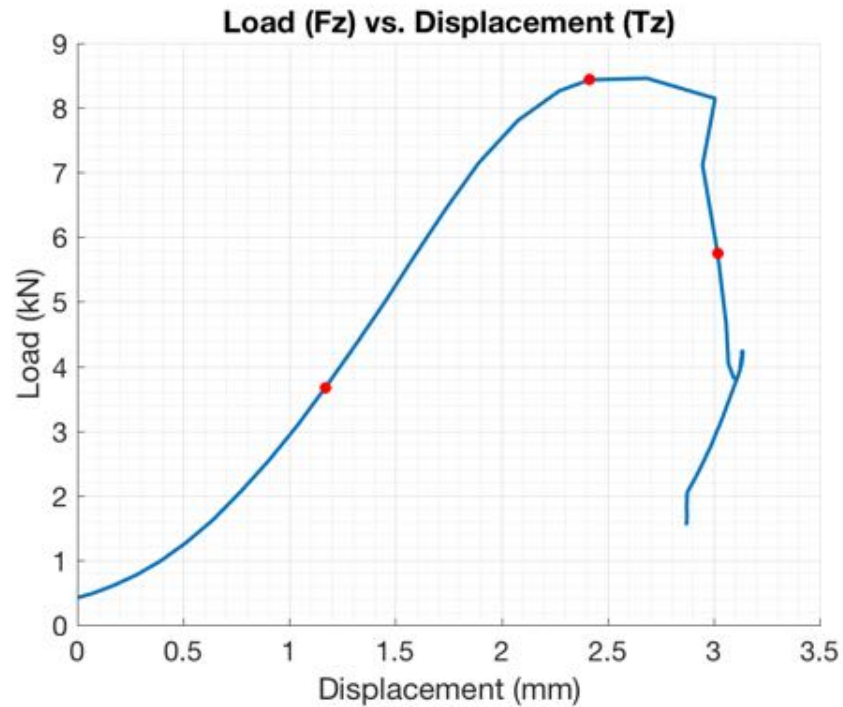




Failure Mode Assessment Summary			
	Load-displacement and video assessment	Photographic indicators	Classification
SO3	- Tear at left inferior endplate-vertebra interface with plateau as plot reaches peak	- Left side of inferior endplate torn from inferior vertebra. - Right lamina fracture	EP-VER

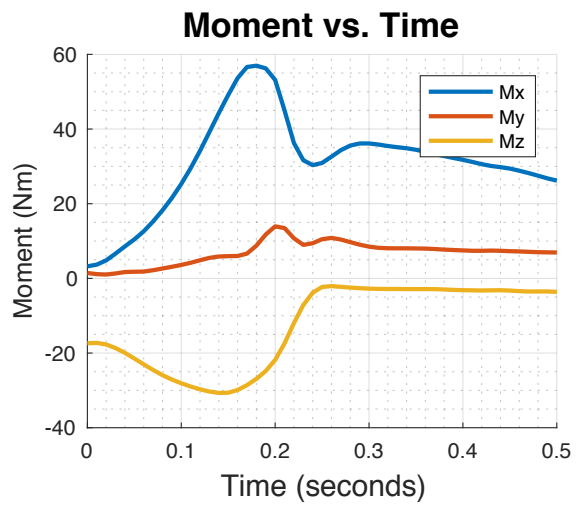
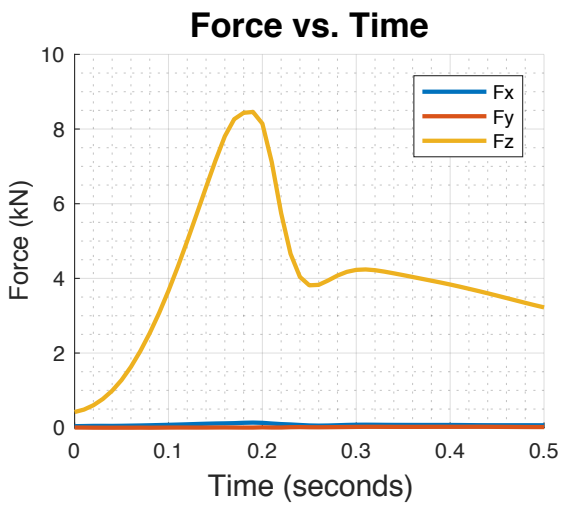
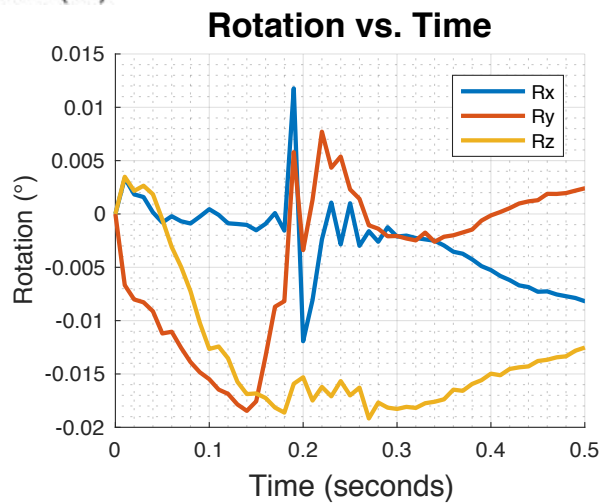
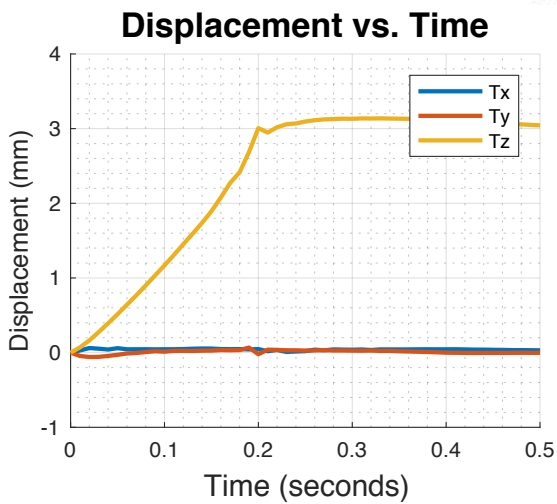
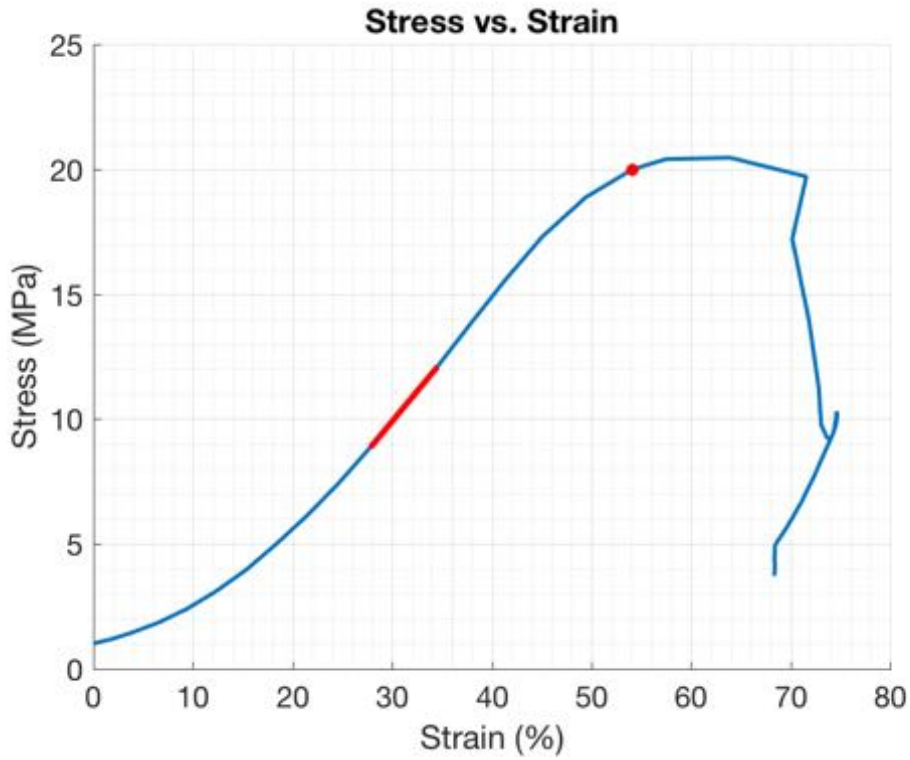
Specimen ID: SO4
Group: Facet Right Lateral Bending & Right Axial Rotation
Date tested: 2/8/2017

Failure load (kN)	Tz at failure (mm)	Time (s)	Moments (Nm)			Max Stress (MPa)	Max Strain	Modulus (MPa)	Toughness (MJ/m ³)	Observations		
			Mx	My	Mz					Test	Disc	Vertebra
8.26	2.27	0.19	56.62	6.64	-28.60	19.99	54.12	48.0	5.1	AS, L-RAIL	Large L-POS NE	ANT SUP VER



Identification of events by video & load vs. displacement comparison

Event	Video		Load vs. Displacement	
	Time (s)	Description	Time (s)	Description
1	0.105	Postero-lateral left extrusion	0.1	Slight change in slope
2	0.175	Sound as superior and inferior posterior elements collide	0.17	Change in slope as reaches peak and plateaus
3	0.22	Louder sound	0.19	Highest peak
4			0.2	Steep decline

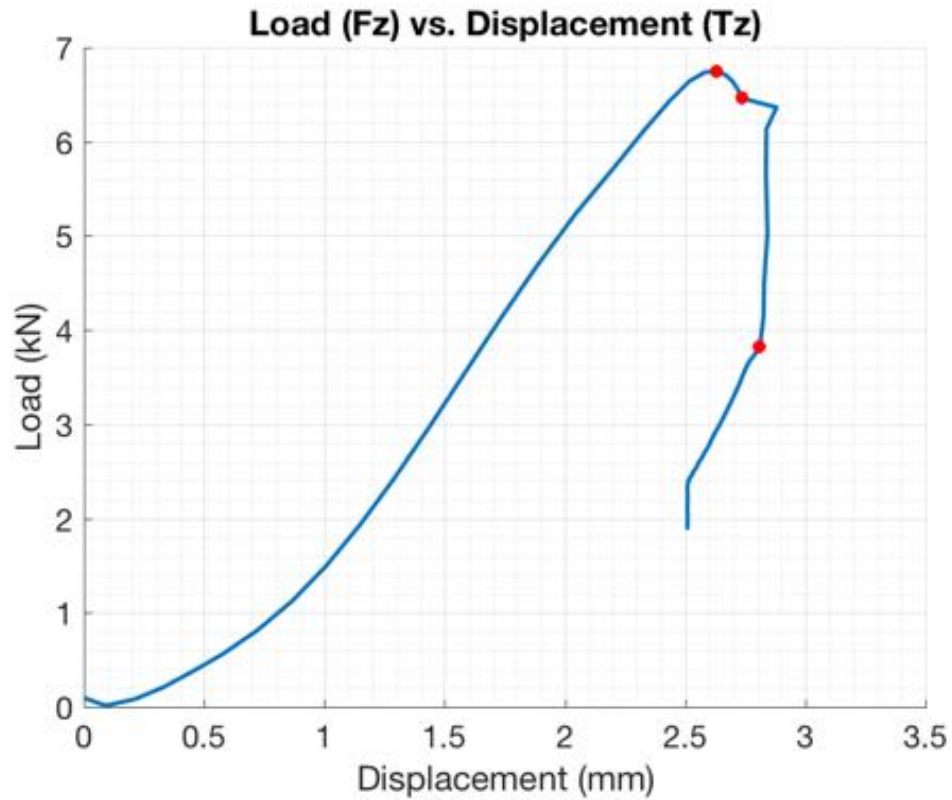




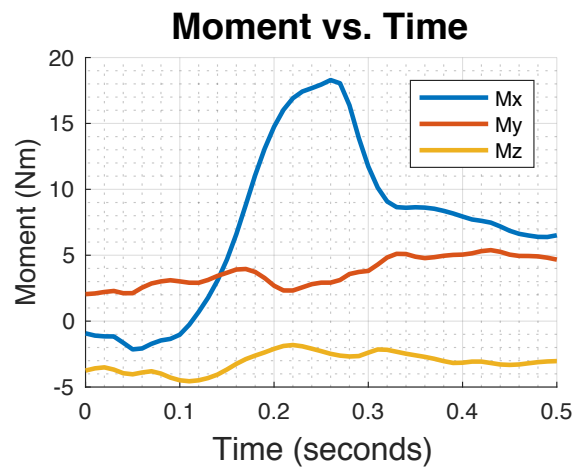
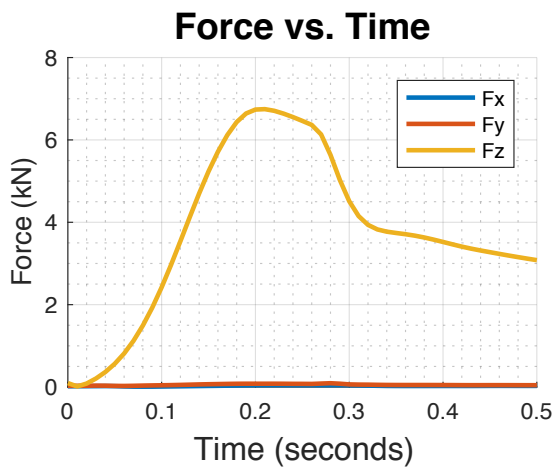
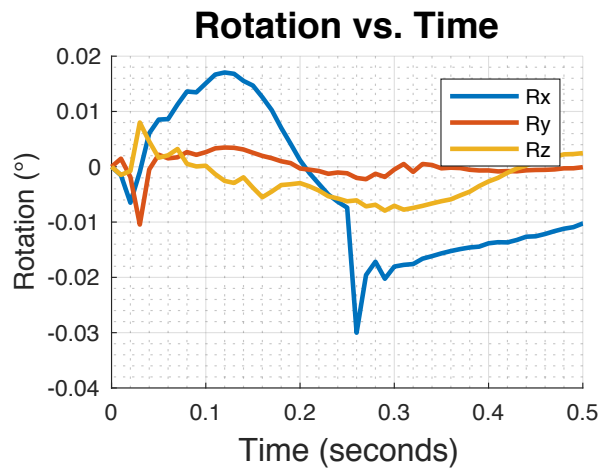
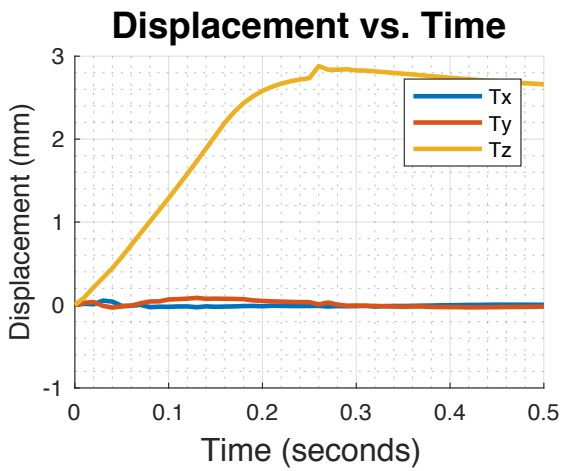
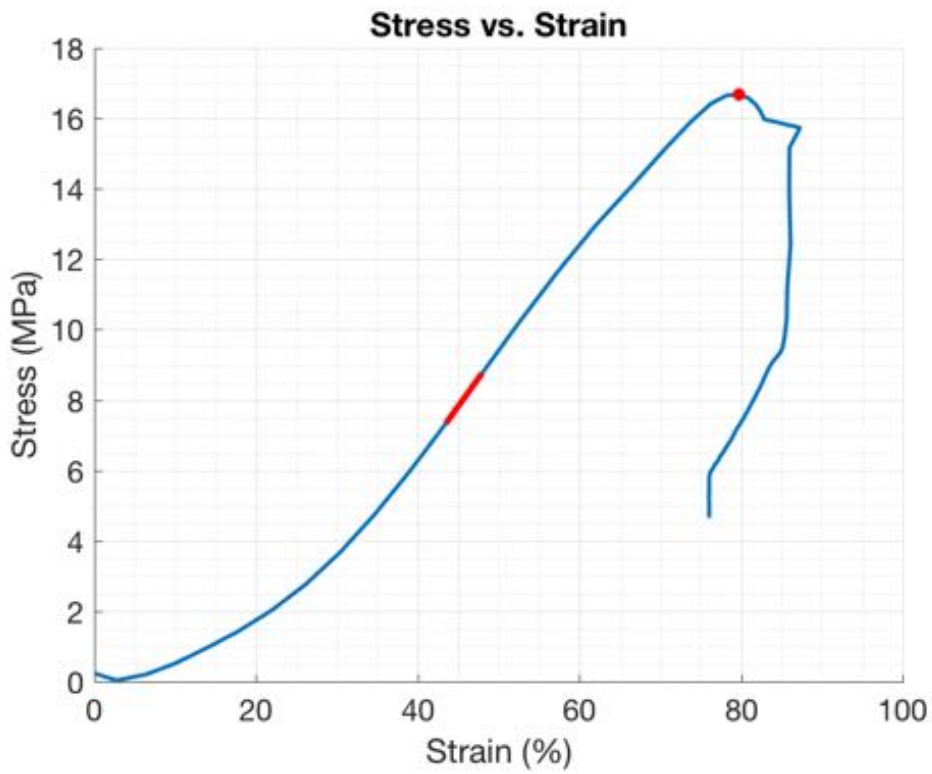
Failure Mode Assessment Summary			
	Load-displacement and video assessment	Photographic indicators	Classification
SO4	- Visible nucleus extrusion on left postero-lateral side with slight change in load-displacement slope	- Anterior fracture on the superior vertebra	HER (L-POS)

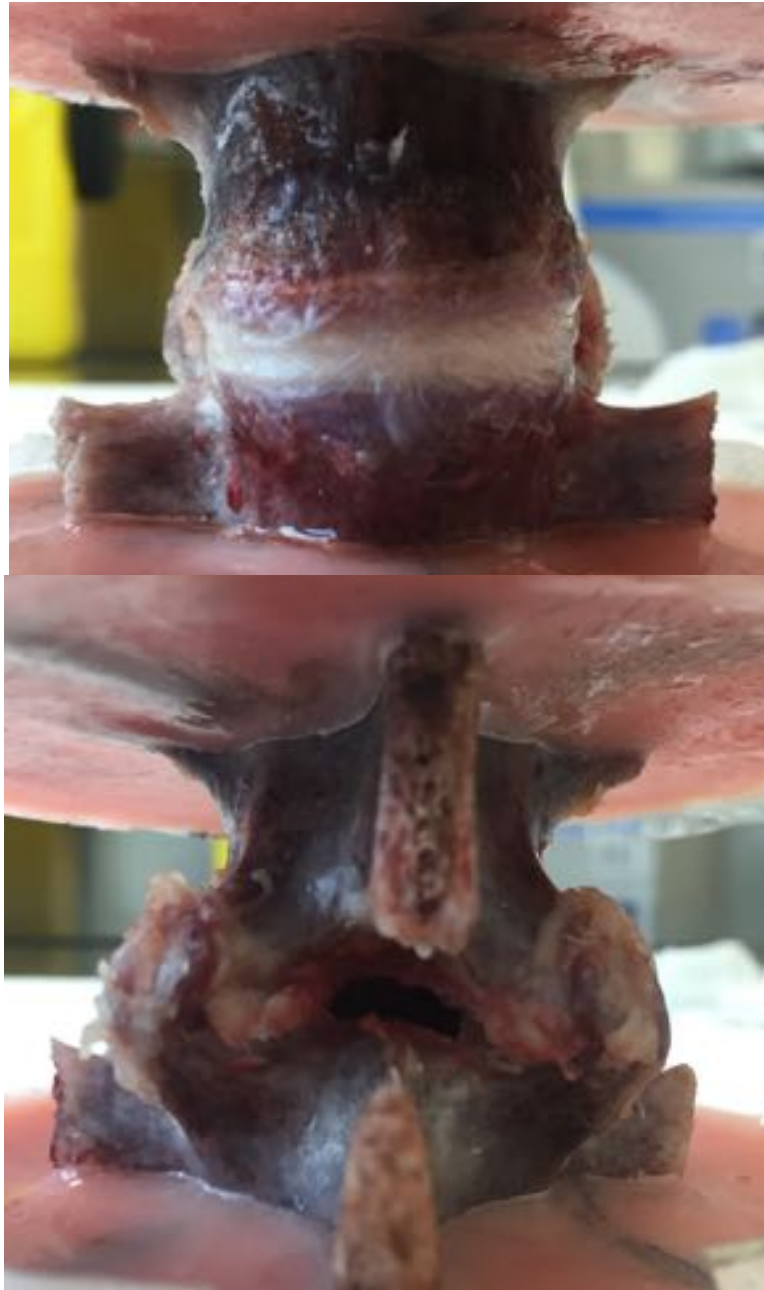
Specimen ID: SO5
Group: Facet Flexion
Date tested: 3/8/2017

Failure load (kN)	Tz at failure (mm)	Time (s)	Moments (Nm)			Stress (MPa)	Strain (%)	Modulus (MPa)	Toughness (MJ/m ³)	Observations		
			Mx	My	Mz					Test	Disc	Vertebra
6.75	2.63	0.21	16.03	2.33	-1.88	16.68	79.71	31.8	5.7	AS, POS-RAIL	-	-



Event	Video		Load vs. Displacement	
	Time (s)	Description	Time (s)	Description
1	0.208	Sound spike	0.21	Smooth and highest peak
2	0.25	Sound spike	0.26	Steep decline
3	0.332	Sound spike	0.33	Decline at slower rate and plateau

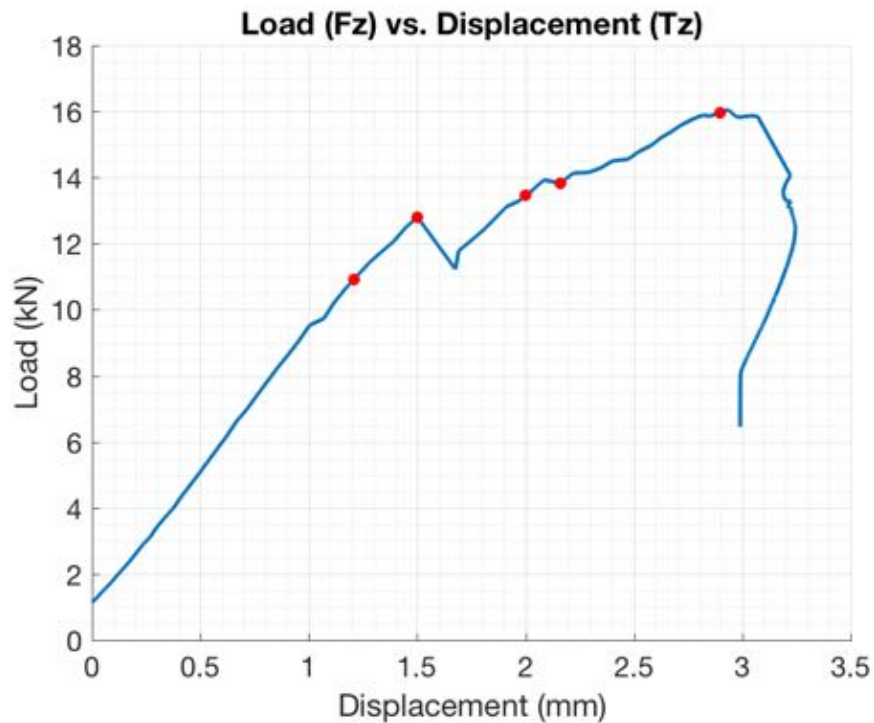




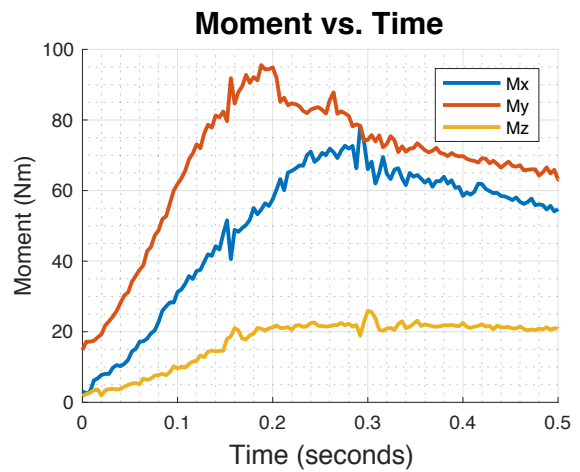
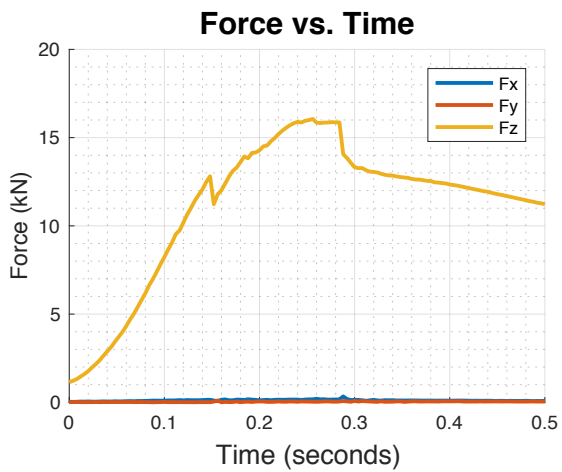
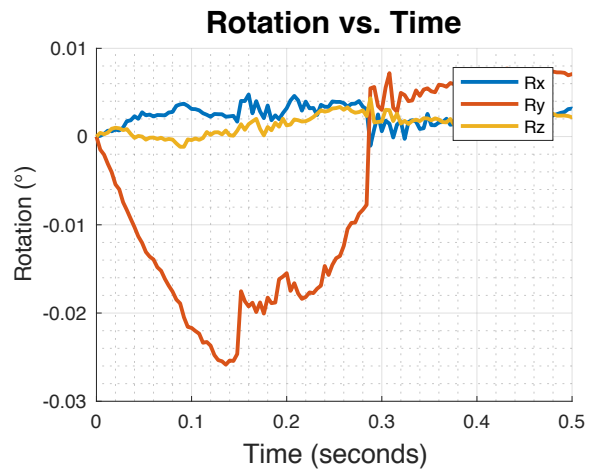
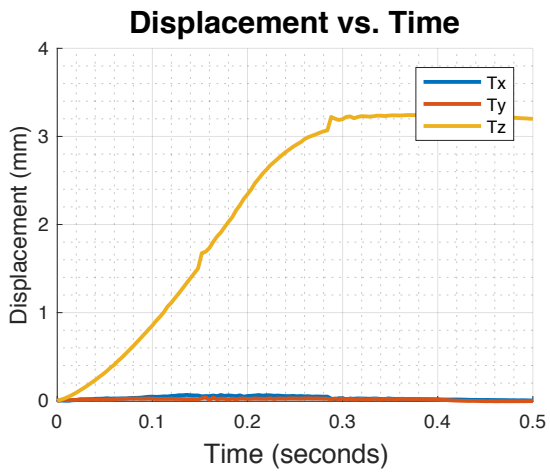
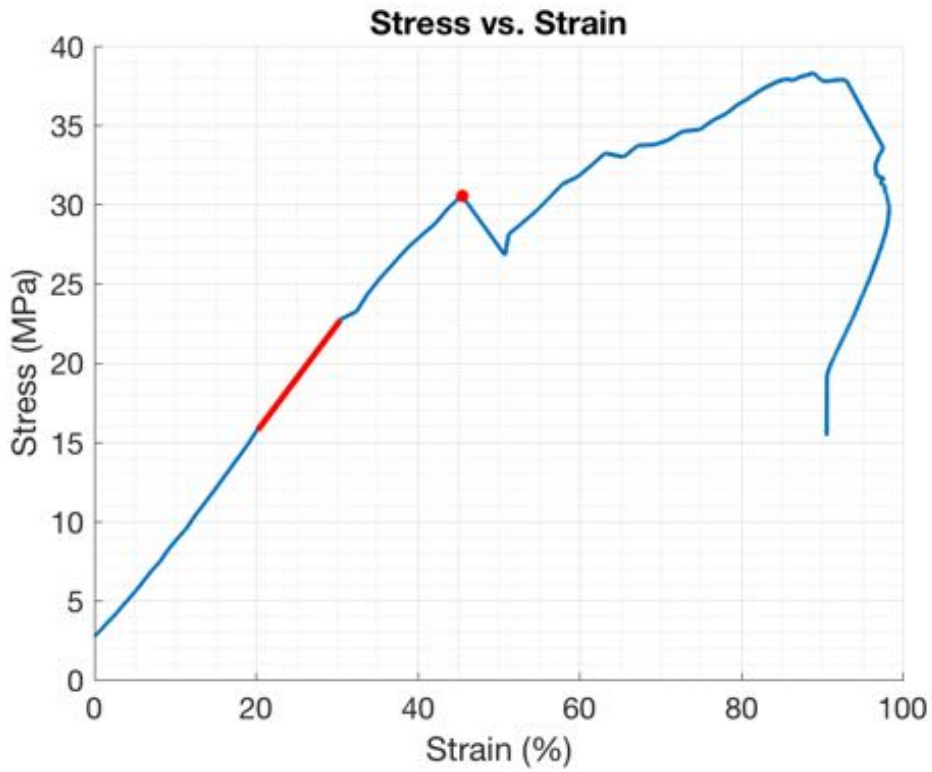
Failure Mode Assessment Summary			
	Load-displacement and video assessment	Photographic indicators	Classification
SO5	- Inconclusive	- No evidence of damage	IN

Specimen ID: SO6
Group: Facet Right Lateral Bending
Date tested: 3/8/2017

Failure load (kN)	Tz at failure (mm)	Time (s)	Moments (Nm)			Max Stress (MPa)	Max Strain (%)	Modulus (MPa)	Toughness (MJ/m ³)	Observations		
			Mx	My	Mz					Test	Disc	Vertebra
12.81	1.50	0.256	47.73	82.40	14.63	30.56	45.47	67.9	7.8	AS, POS-RAIL	L-POS NE	-



Identification of events by video & load vs. displacement comparison				
	Video		Load vs. Displacement	
Event	Time (s)	Description	Time (s)	Description
1	0.127	Sound spike	0.112	Small plateau
2	0.148	Left nucleus extrude	0.148	Small peak and sharp decline
3	0.178	More extrusion	0.184	Small plateau
4	0.1883	Sound spike	0.256	Highest force & plateau
5	0.25	Further compression		

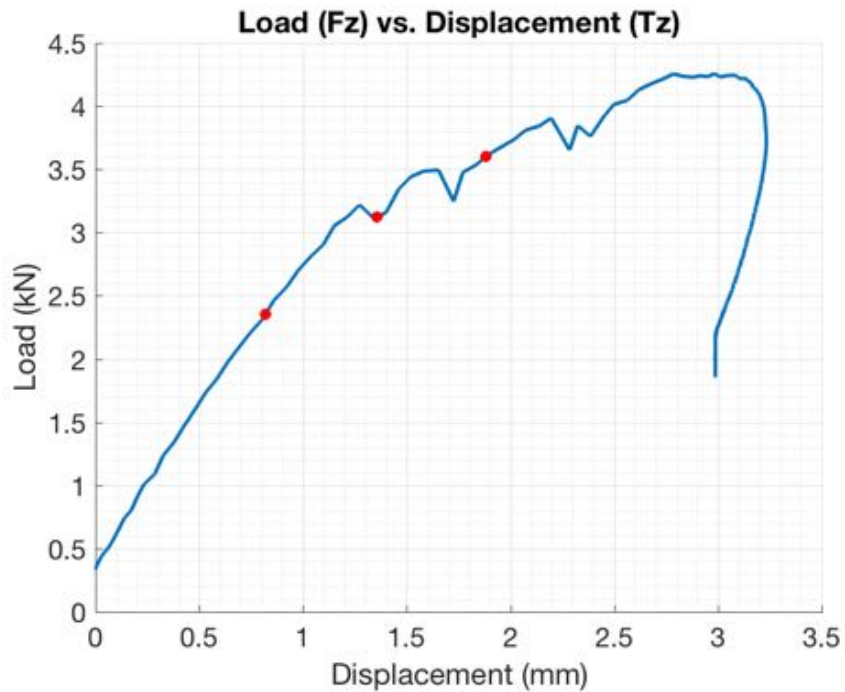




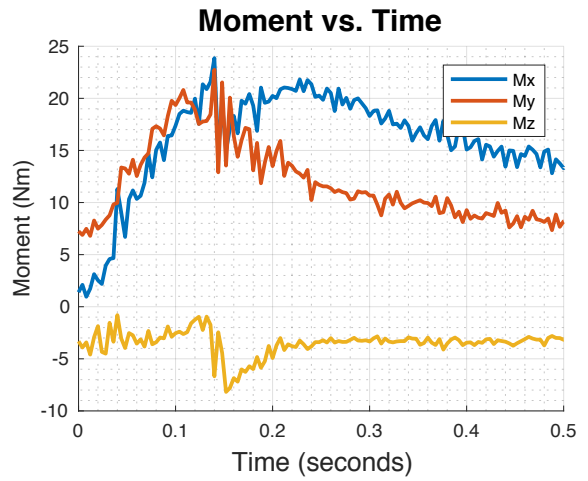
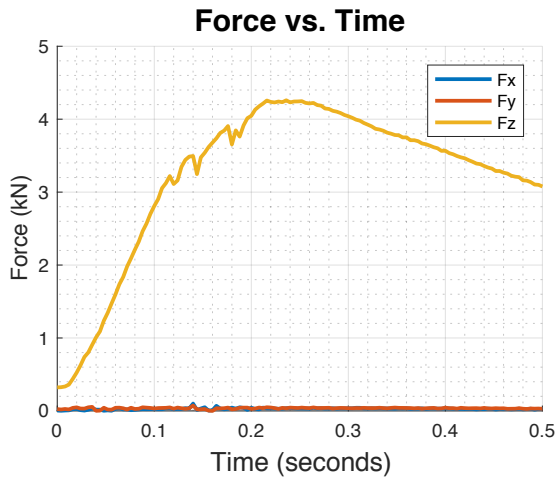
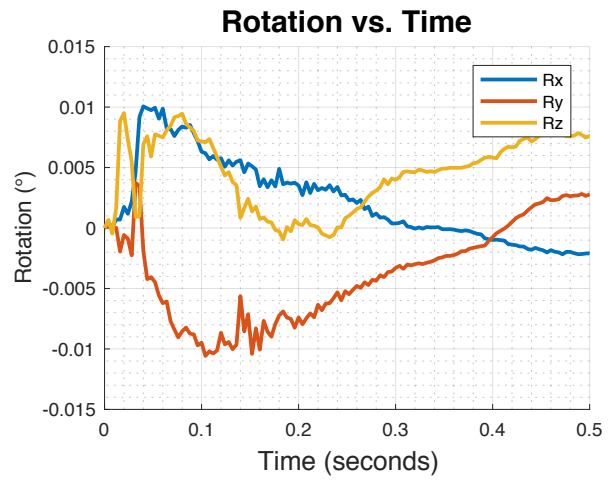
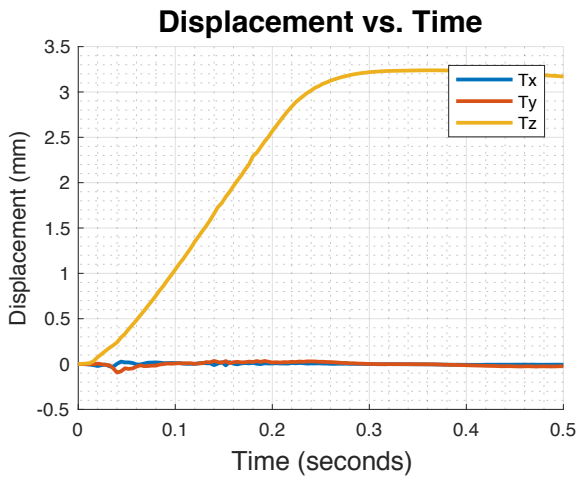
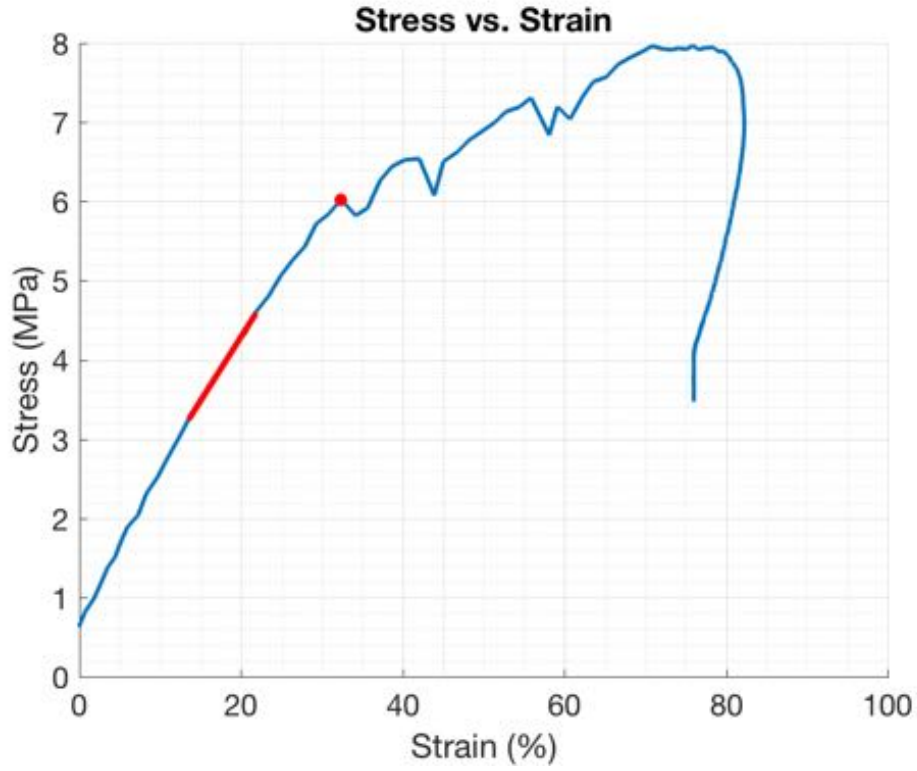
Failure Mode Assessment Summary			
	Load-displacement and video assessment	Photographic indicators	Classification
SO6	- White nucleus extruded on left at first peak of load-displacement curve	- Large nuclear extrusion - No vertebral damage	HER (L-POS)

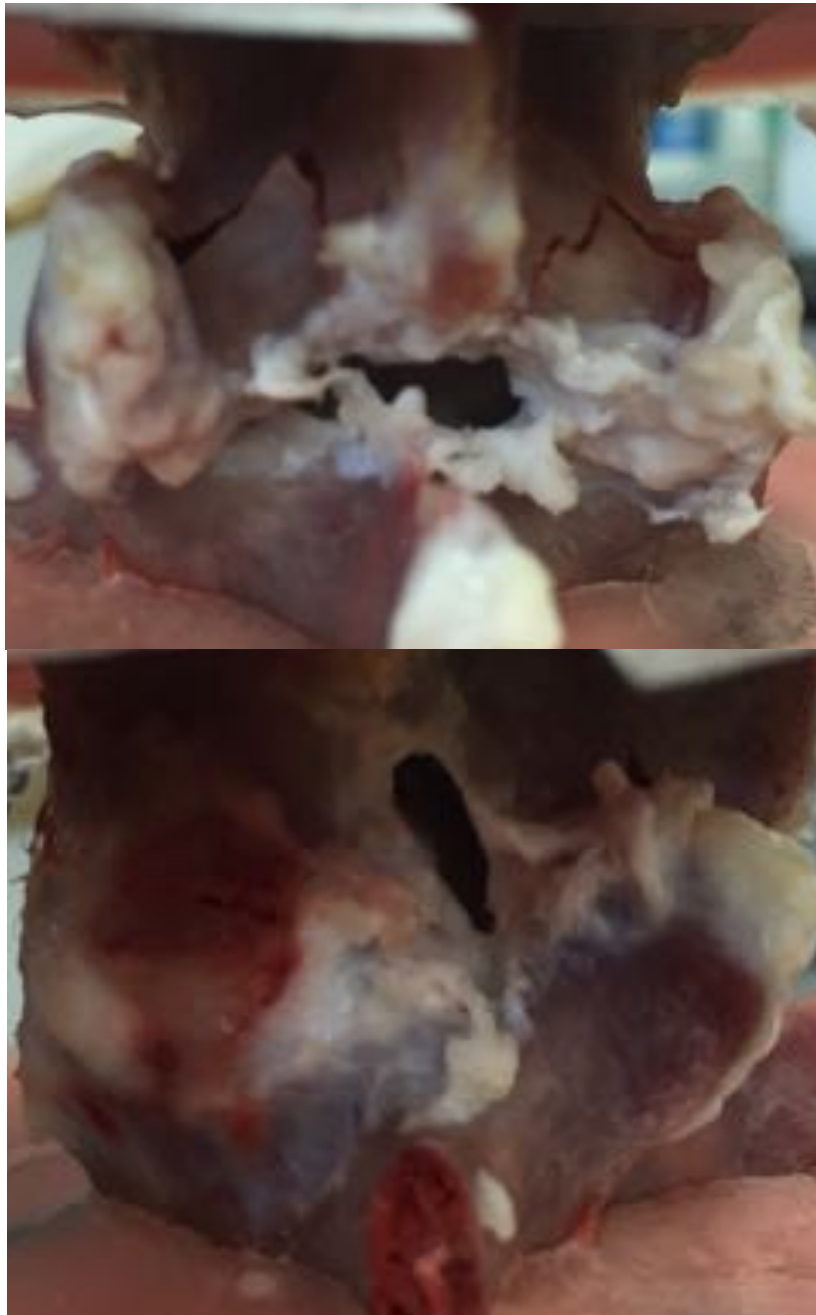
Specimen ID: SO7
Group: Facet Right Lateral Bending
Date tested: 4/8/2017

Failure load (kN)	Tz at failure (mm)	Time (s)	Moments (Nm)			Max Stress (MPa)	Max Strain (%)	Modulus (MPa)	Toughness (MJ/m ³)	Observations		
			Mx	My	Mz					Test	Disc	Vertebra
3.22	1.27	0.228	18.60	19.60	-1.59	6.03	32.38	16.0	1.2	AS, L-RAIL	L-POS NE	R+L LAM



Identification of events by video & load vs. displacement comparison					
		Video		Load vs. Displacement	
Event	Time (s)	Description	Time (s)	Description	
1	0.077	Lamina break	0.116	First small peak	
2	0.113	Lamina break more	0.14	Second small peak	
3	0.147	Loud sound – compress further	0.176	Third small peak	
4			0.216	Highest peak and plateau	





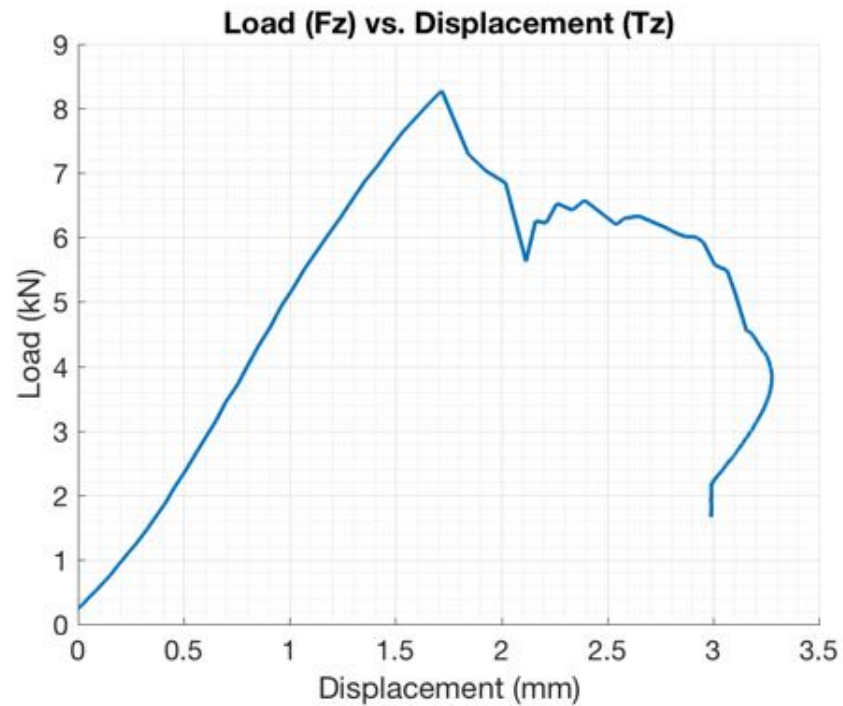
Failure Mode Assessment Summary			
	Load-displacement and video assessment	Photographic indicators	Classification
SO7	<ul style="list-style-type: none"> - Right and left lamina fracture 	<ul style="list-style-type: none"> - Right and left lamina fracture - Small amount of nucleus extruded (left postero-lateral) - Existing damage to disc and vertebra left superior? 	ERROR – pre-existing damage HER(L-POS) + R/L LAM

Specimen ID: SO8

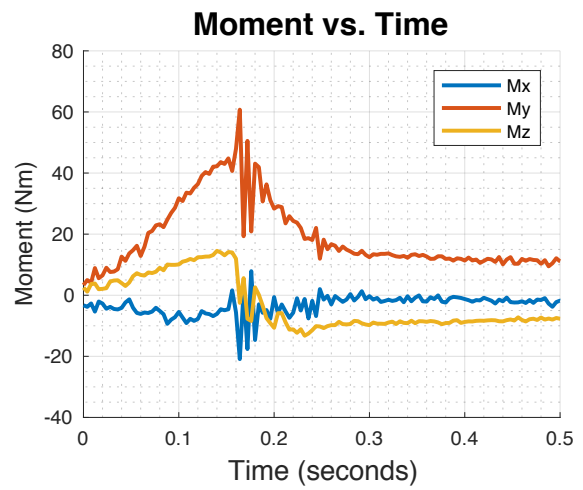
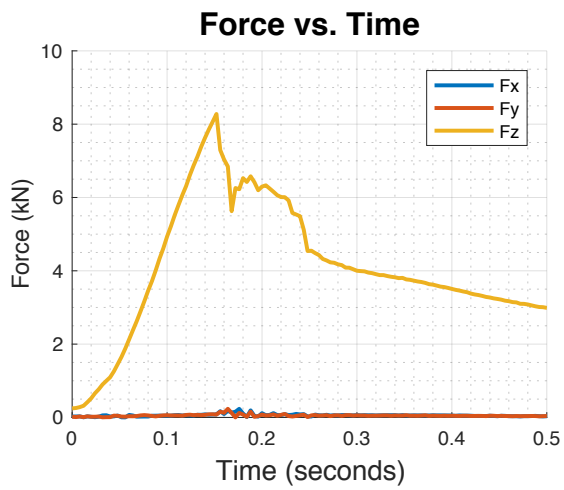
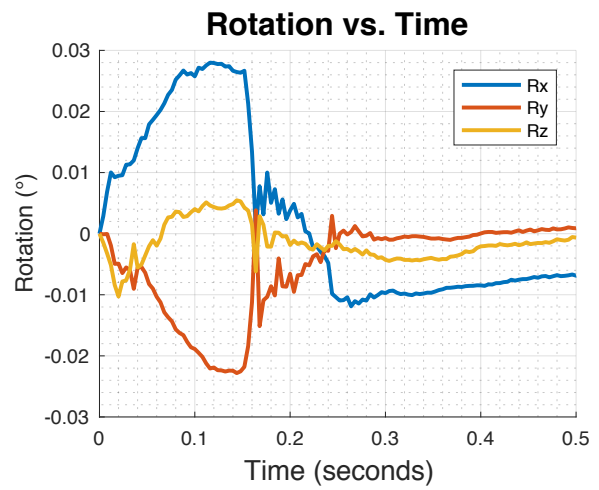
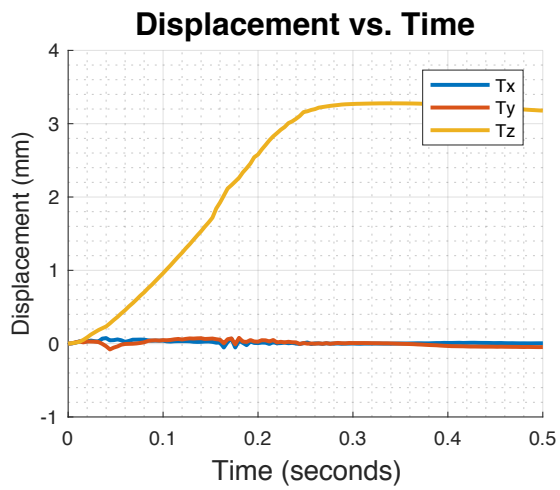
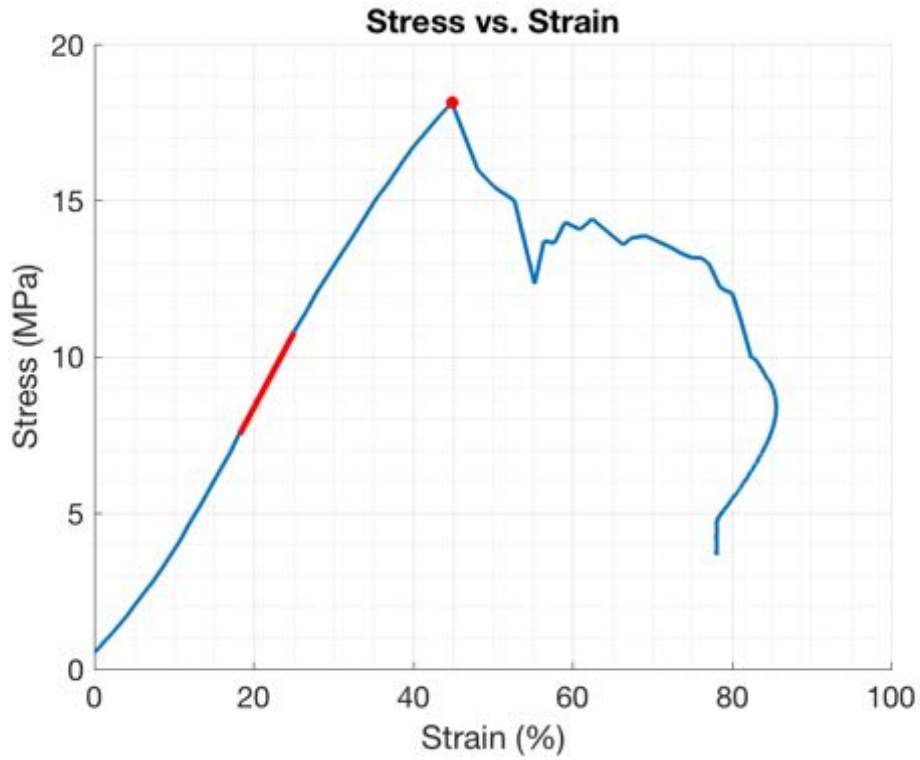
Group: Facet Flexion & Right Lateral Bending

Date tested: 4/8/2017

Failure load (kN)	Tz at failure (mm)	Time (s)	Moments (Nm)			Max Stress (MPa)	Max Strain (%)	Modulus (MPa)	Toughness (MJ/m ³)	Observations		
			Mx	My	Mz					Test	Disc	Vertebra
8.28	1.72	0.152	-4.59	44.81	14.15	18.13	44.86	47.8	4.2	AS, POS-RAIL, L-RAIL	L-POS NE	L-EP shear from INF-VER



NOTE: Video file corrupt

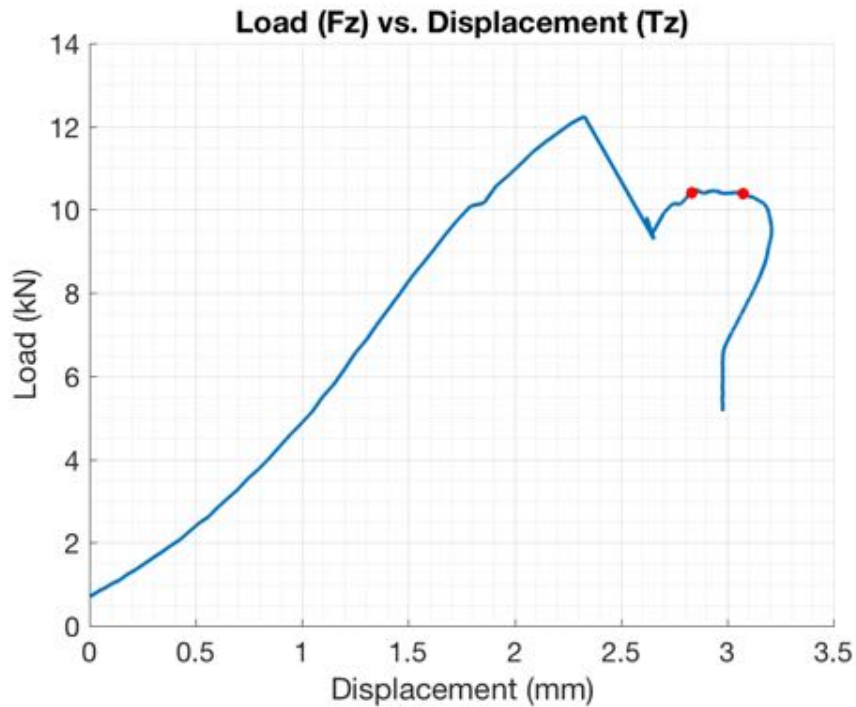




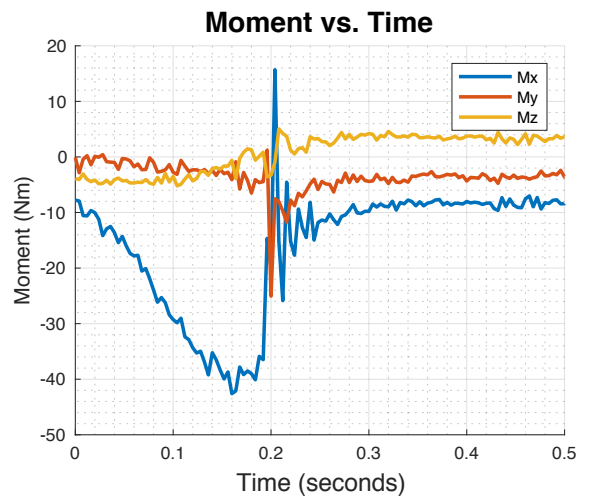
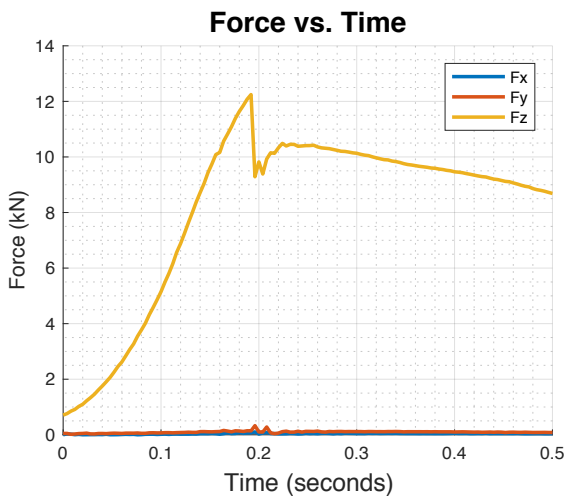
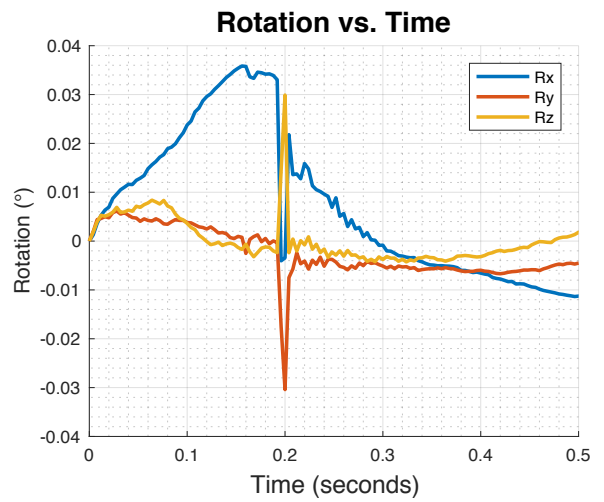
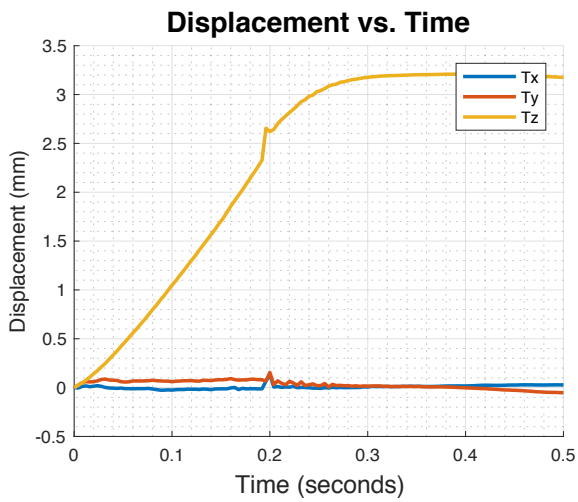
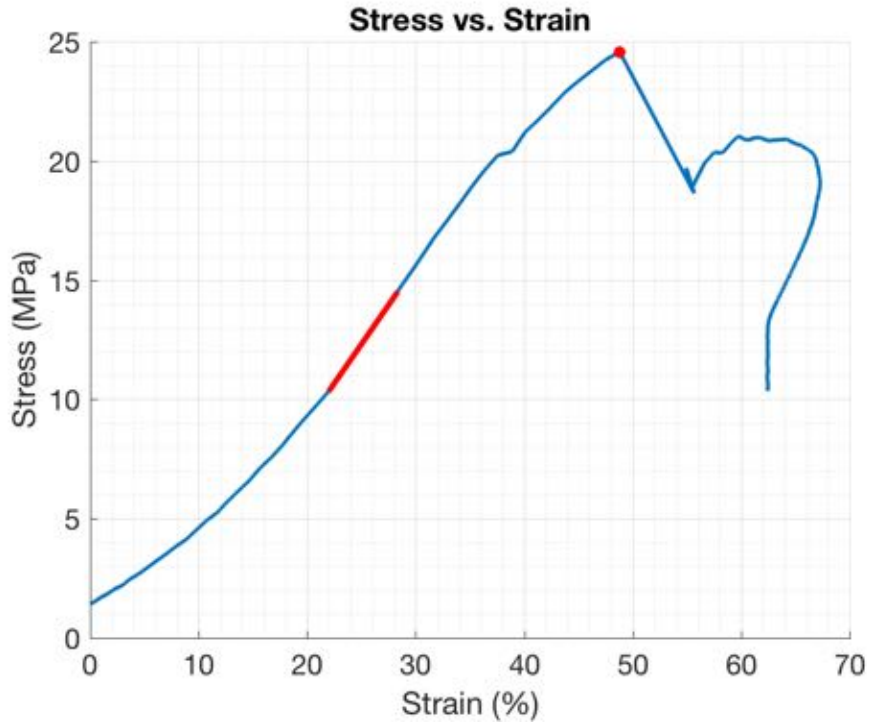
Failure Mode Assessment Summary			
	Load-displacement and video assessment	Photographic indicators	Classification
SO8	-	<ul style="list-style-type: none"> - Left postero-lateral nuclear extrusion - Left side of inferior endplate torn from inferior vertebra. 	HER(L-POS) + EP VER (L)

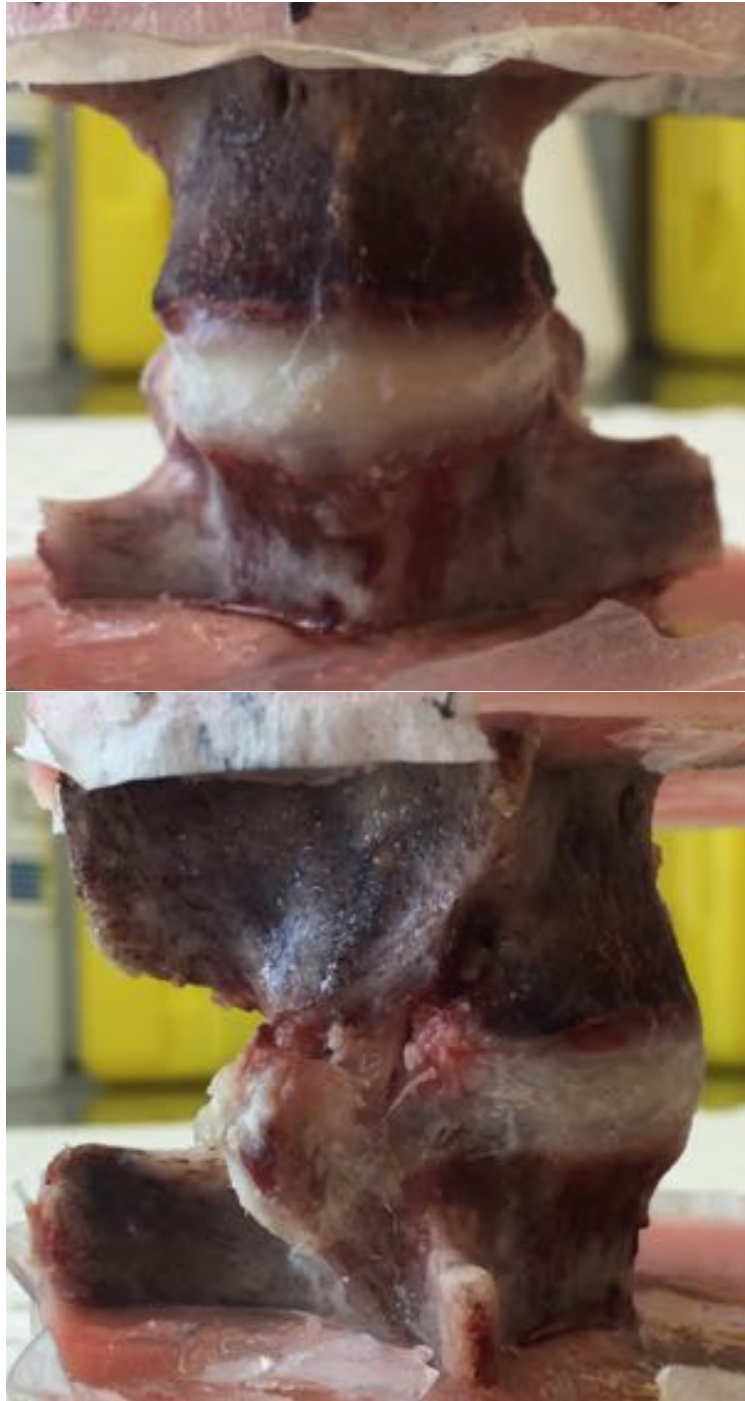
Specimen ID: SO9
Group: Facet Flexion
Date tested: 4/8/2017

Failure load (kN)	Tz at failure (mm)	Time (s)	Moments (Nm)			Max Stress (MPa)	Max Strain (%)	Modulus (MPa)	Toughness (MJ/m ³)	Observations		
			Mx	My	Mz					Test	Disc	Vertebra
12.24	2.33	0.192	-36.48	-4.45	0.85	24.57	48.80	65.7	6.1	AS, POS-RAIL	R-POS NE	-



Identification of events by video & load vs. displacement comparison				
Event	Video		Load vs. Displacement	
	Time (s)	Description	Time (s)	Description
1	0.222	Sound spike – possible facet collision	0.156	Small plateau
2	0.258	Sound spike – possible second facet collision	0.192	Highest peak followed by steep decline
3			0.2	Second peak - small
4			0.212	Gradual bumpy incline plateauing





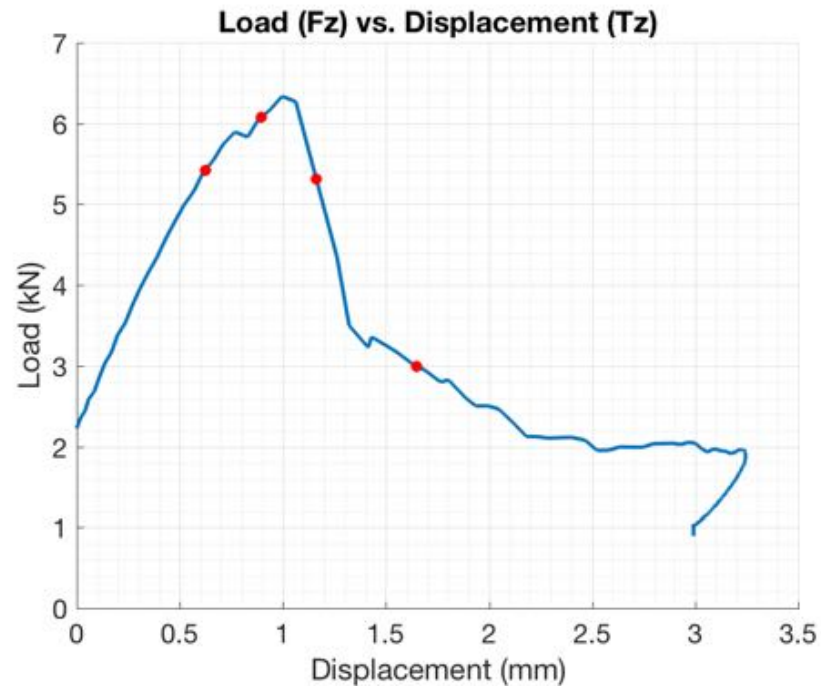
Failure Mode Assessment Summary			
	Load-displacement and video assessment	Photographic indicators	Classification
SO9	-	<ul style="list-style-type: none"> - Small nuclear extrusion on right postero-lateral side - No other evidence of damage 	HER(R-POS)

Specimen ID: SO10

Group: Facet Flexion & Right Lateral Bending

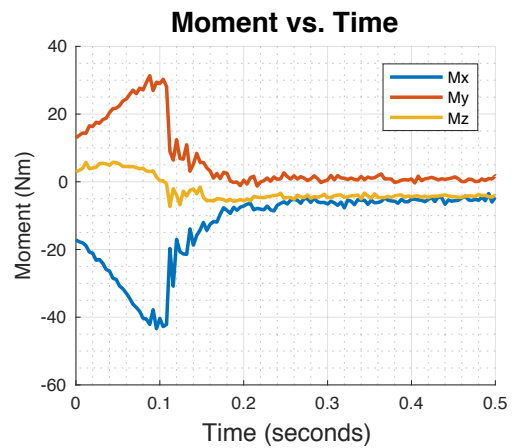
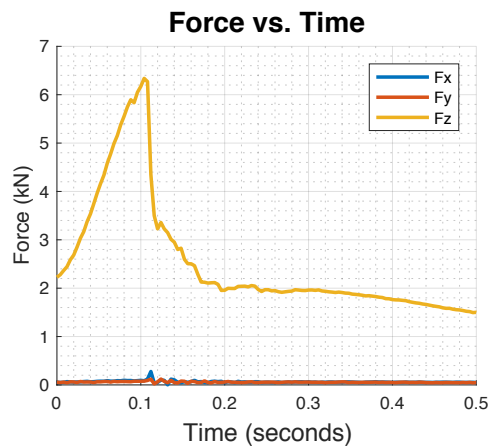
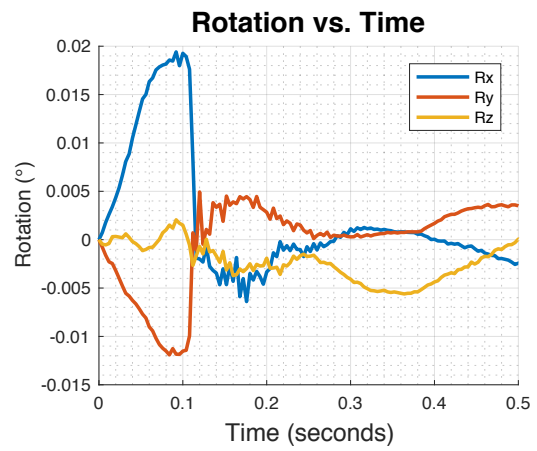
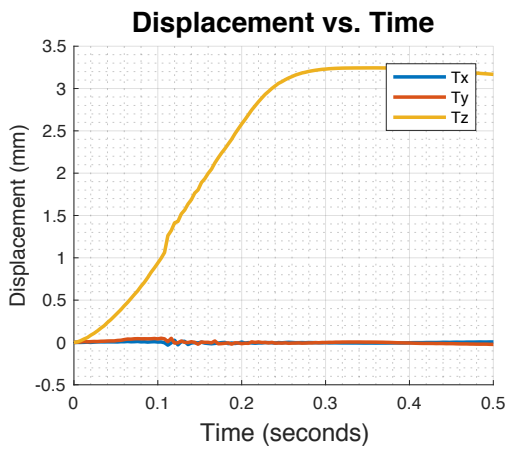
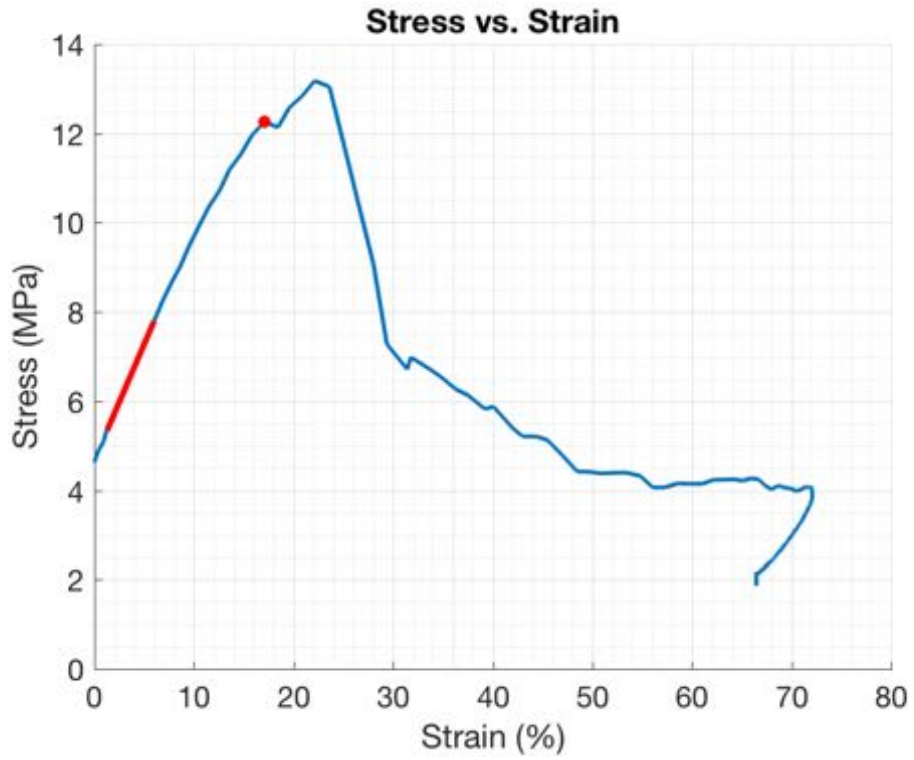
Date tested: 4/8/2017

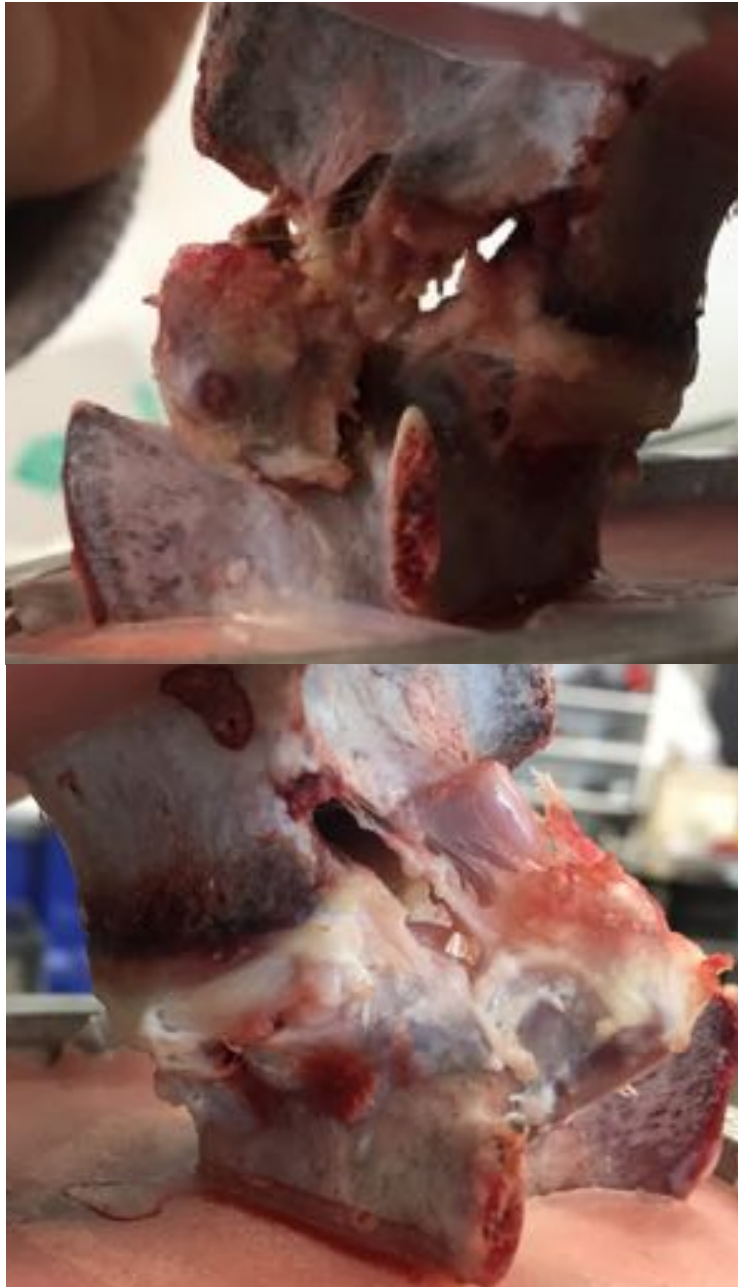
Failure load (kN)	Tz at failure (mm)	Time (s)	Moments (Nm)			Max Stress (MPa)	Max Strain (%)	Modulus (MPa)	Toughness (MJ/m ³)	Observations		
			Mx	My	Mz					Test	Disc	Vertebra
5.90	0.77	0.104	-42.14	31.34	3.04	12.26	17.05	52.0	1.5	HIGH Fz error, AS L-RAIL, POS-RAIL	L-POS NE	FAC, L+R SUP-PED, ANT INF-EP



Identification of events by video & load vs. displacement comparison

Event	Video		Load vs. Displacement	
	Time (s)	Description	Time (s)	Description
1	0.077	Loud sound + possible nucleus extrude left	0.088	Small peak and plateau
2	0.097	Loud sound 2	0.104	Highest peak before steep decline
3	0.11	Facet fail and compress		
4	0.137	Shear forward		





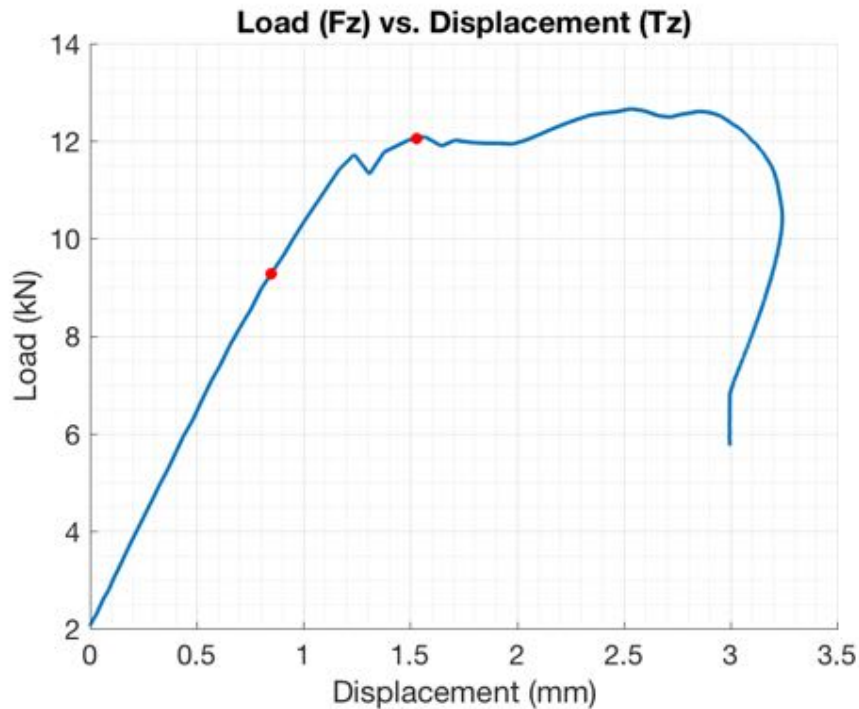
Failure Mode Assessment Summary			
	Load-displacement and video assessment	Photographic indicators	Classification
SO10	-	- Catastrophic failure of vertebra, posterior elements, disc	ERROR

Specimen ID: SO11

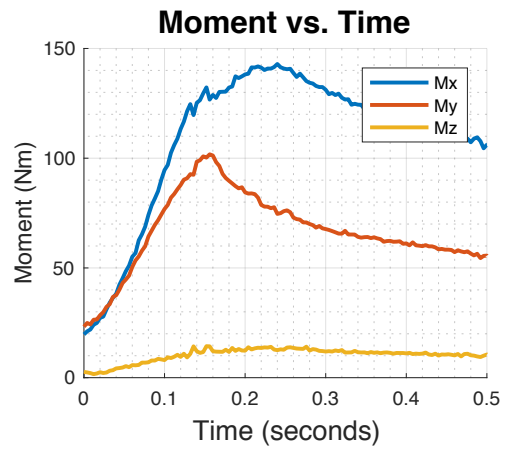
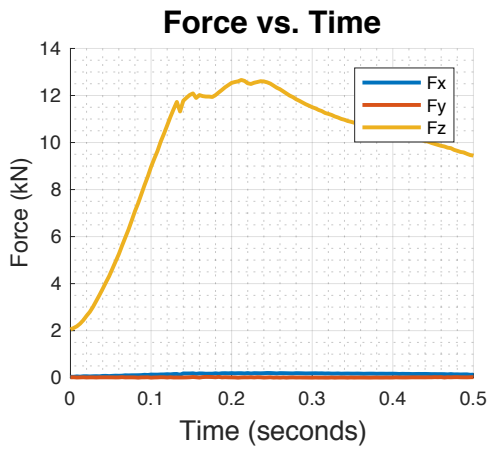
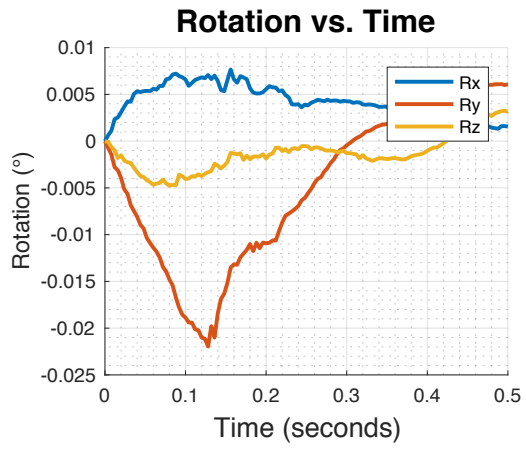
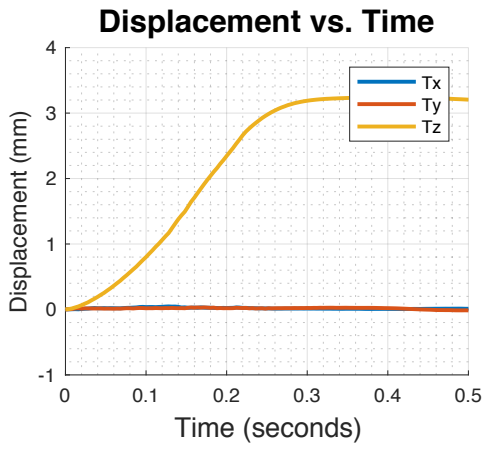
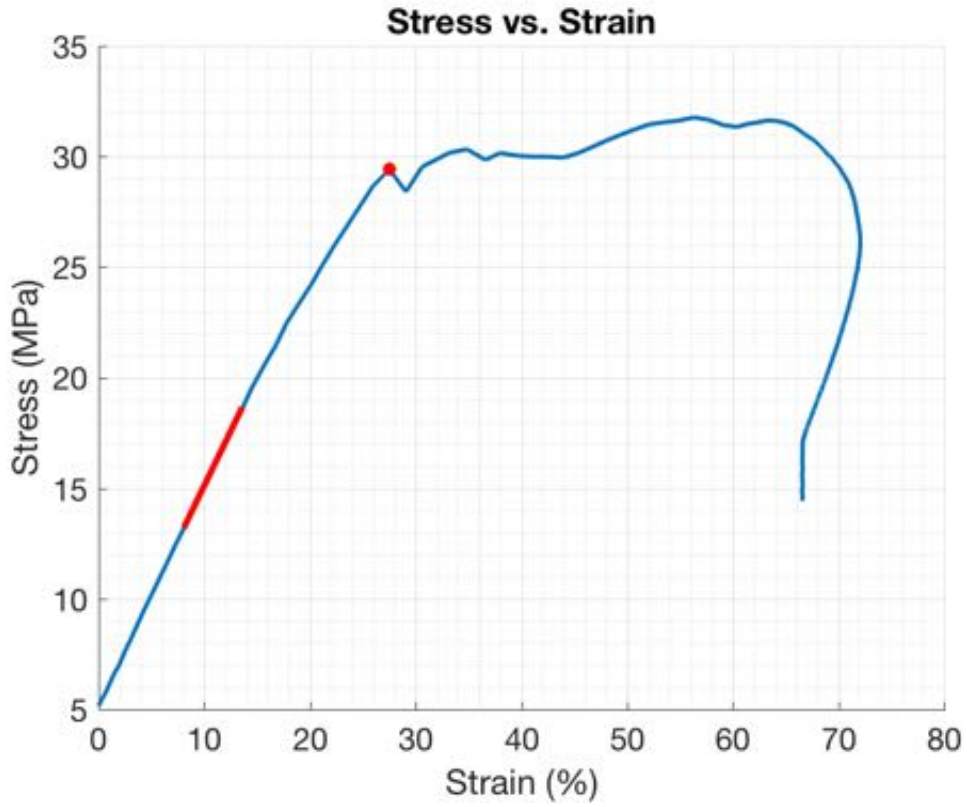
Group: Facet Right Lateral Bending

Date tested: 7/8/2017

Failure load (kN)	Tz at failure (mm)	Time (s)	Moments (Nm)			Max Stress (MPa)	Max Strain (%)	Modulus (MPa)	Toughness (MJ/m ³)	Observations		
			Mx	My	Mz					Test	Disc	Vertebra
11.73	1.24	0.212	124.64	92.73	10.87	29.42	27.51	98.4	5.0	AS, L-RAIL, POS-RAIL	L-POS NE	EP?



Identification of events by video & load vs. displacement comparison				
Event	Video		Load vs. Displacement	
	Time (s)	Description	Time (s)	Description
1	0.1035	Loud sound + left disc bulge	0.132	First small peak
2	0.152	Loud noise 2 - Left nucleus extrude?	0.152	Second small peak and plateau followed by very gradual incline





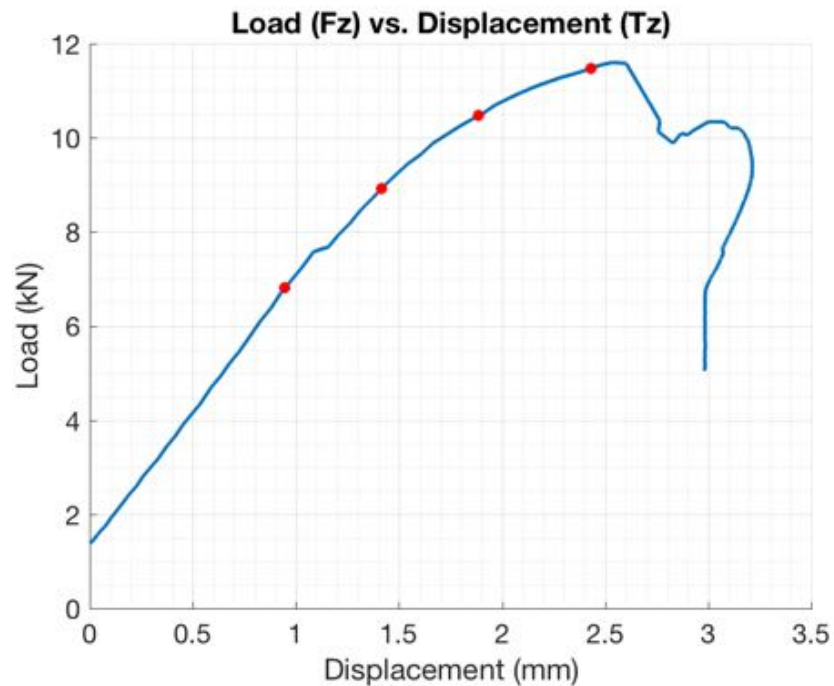
Failure Mode Assessment Summary			
	Load-displacement and video assessment	Photographic indicators	Classification
SO11	<ul style="list-style-type: none"> - Sound spikes, nuclear extrusion on left side corresponding to second peak on load-displacement curve 	<ul style="list-style-type: none"> - Left postero-lateral nuclear extrusion - No other damage evident 	HER (L-POS)

Specimen ID: SO12

Group: Facet Flexion

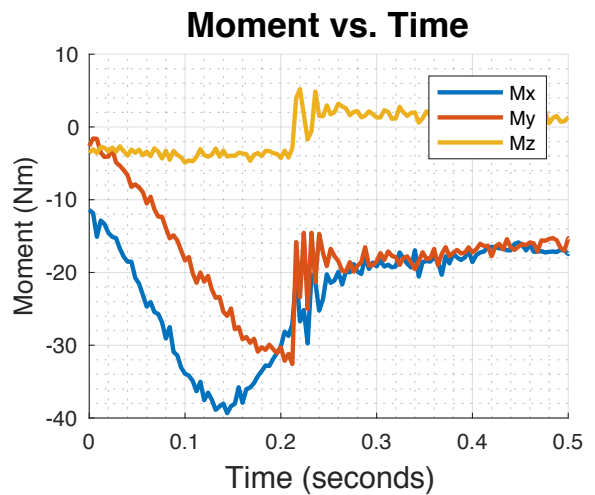
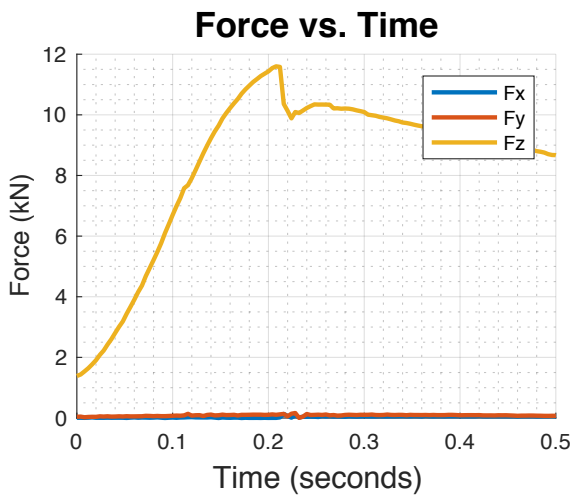
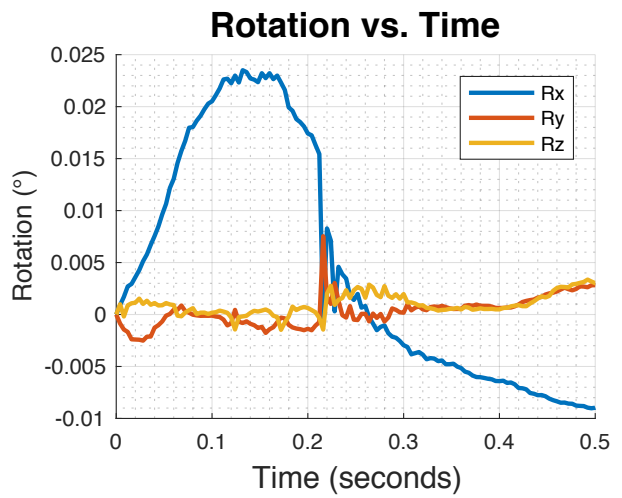
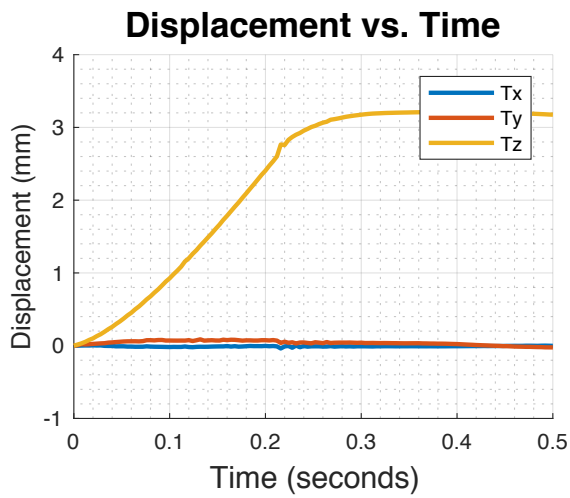
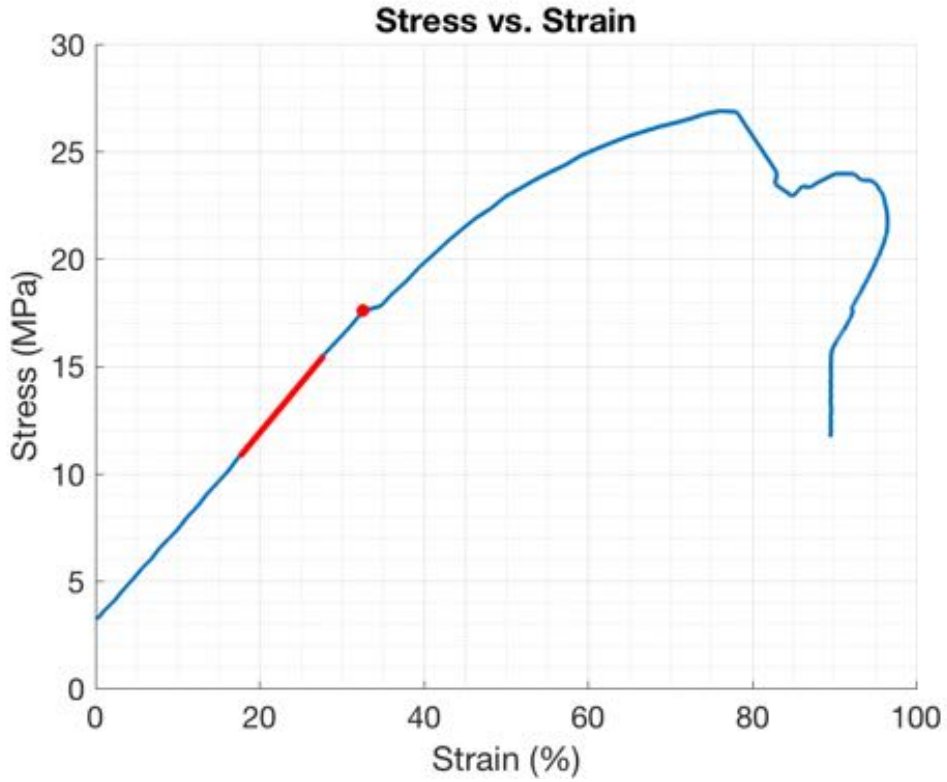
Date tested: 7/8/2017

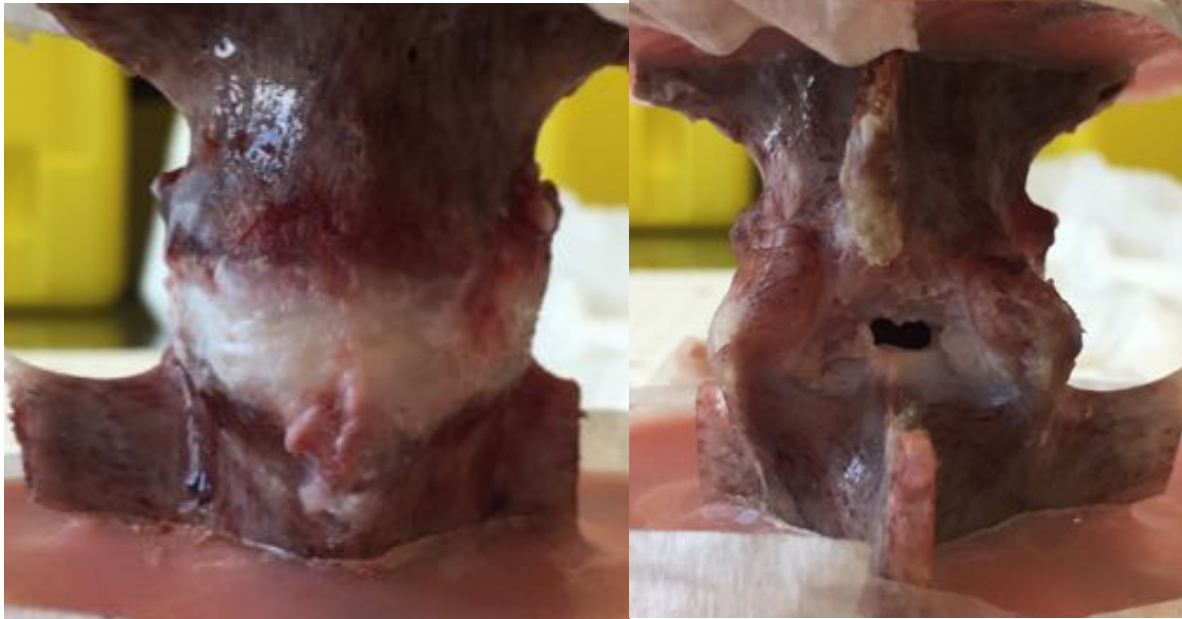
Failure load (kN)	Tz at failure (mm)	Time (s)	Moments (Nm)			Max Stress (MPa)	Max Strain (%)	Modulus (MPa)	Toughness (MJ/m ³)	Observations		
			Mx	My	Mz					Test	Disc	Vertebra
7.58	1.09	0.212	-36.32	-21.41	-4.11	17.57	32.62	45.9	3.4	AS, POS-RAIL	SUP L-POS NE	-



Identification of events by video & load vs. displacement comparison

Event	Video		Load vs. Displacement	
	Time (s)	Description	Time (s)	Description
1	0.1015	Small shear forward + loud noise	0.124	Small plateau/ change slope
2	0.135	Shear forward	0.176	Change in slope as plateau at peak
3	0.1665	Shear + bulge	0.224	Peak
4	0.2015	Shear forward + loud noise		





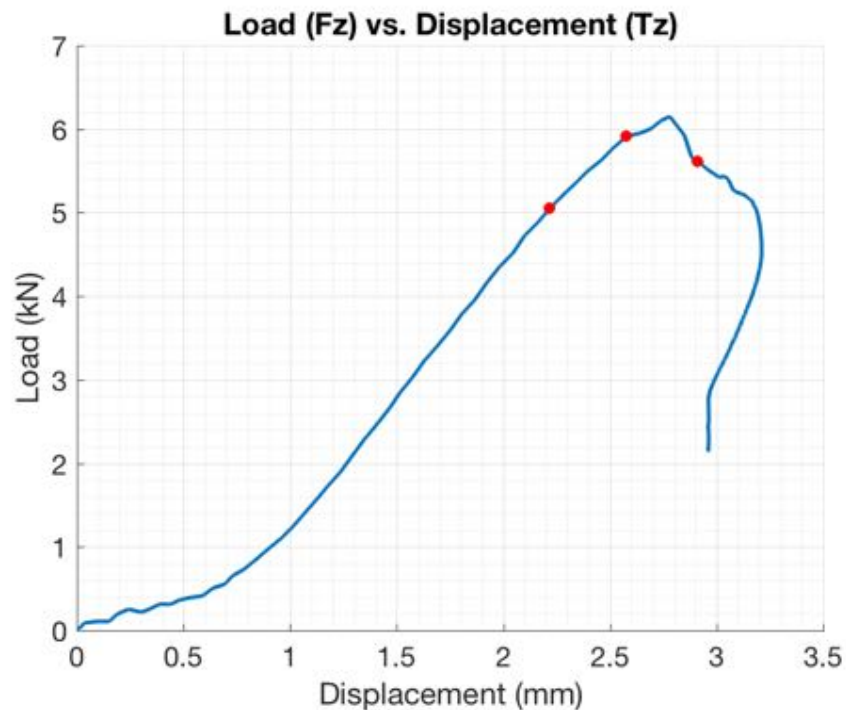
Failure Mode Assessment Summary			
	Load-displacement and video assessment	Photographic indicators	Classification
SO12	- No correlation	<ul style="list-style-type: none"> - No posterior damage to vertebra - Pre-existing cut where nuclear material extruding? – at superior vertebra. 	ERROR

Specimen ID: SO13

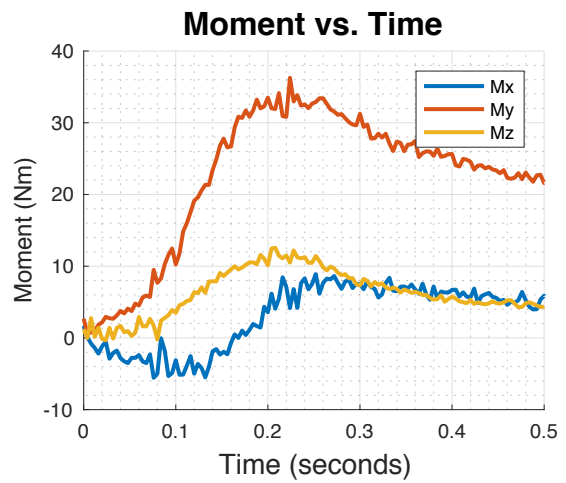
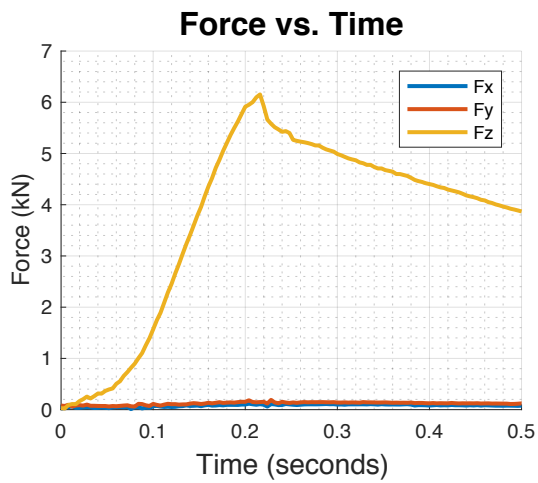
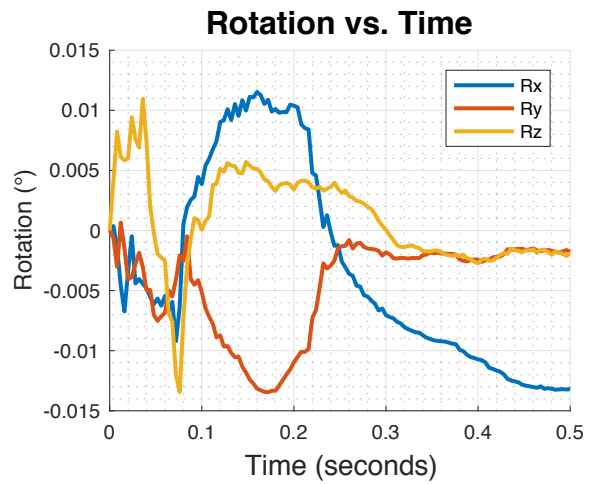
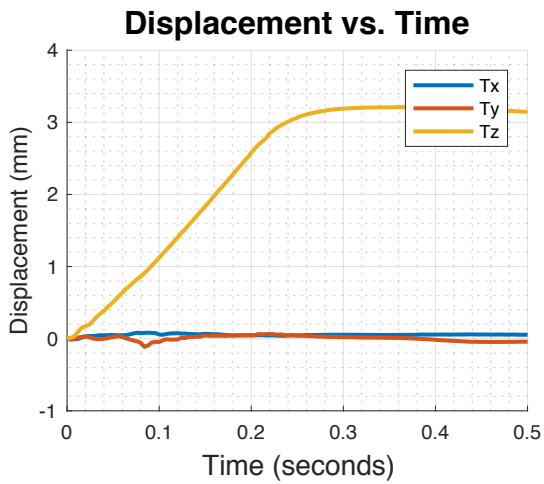
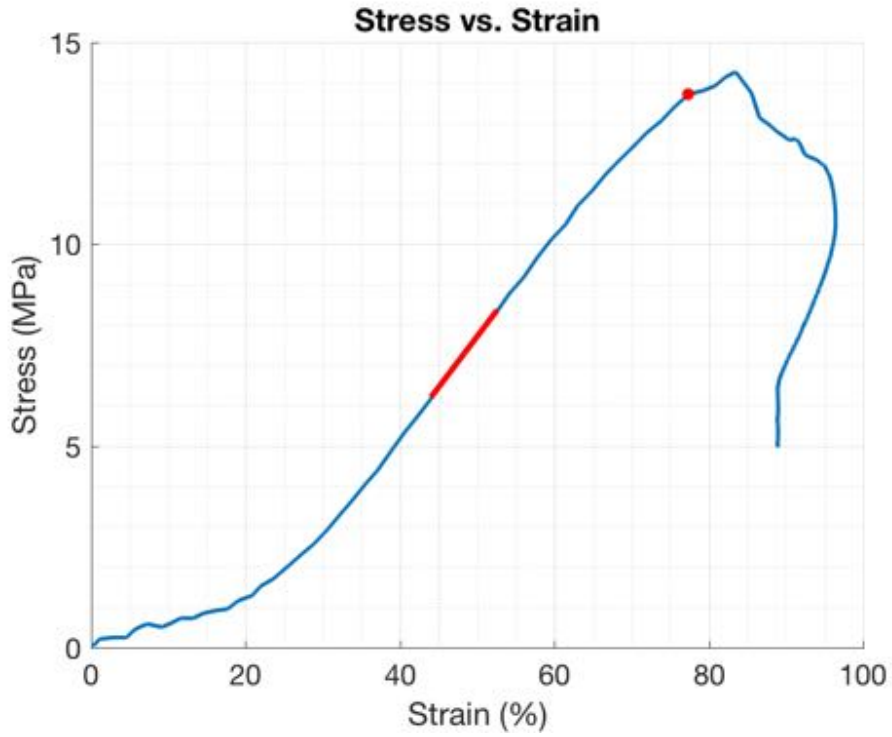
Group: Facet Flexion & Right Lateral Bending

Date tested: 7/8/2017

Failure load (kN)	Tz at failure (mm)	Time (s)	Moments (Nm)			Max Stress (MPa)	Max Strain (%)	Modulus (MPa)	Toughness (MJ/m ³)	Observations		
			Mx	My	Mz					Test	Disc	Vertebra
5.91	2.58	0.216	3.59	33.49	10.12	13.72	77.38	25.2	4.4	AS, POS-RAIL, L-RAIL	Small L-POS NE	-



Identification of events by video & load vs. displacement comparison					
		Video		Load vs. Displacement	
Event	Time (s)	Description	Time (s)	Description	
1	0.176	Shear forward / compress	0.176	Small change slope	
2	0.2	Shear / compress and bulge + loud sound	0.2	Plateau before peak	
3	0.2265	Loud noise + no motion	0.216	Highest peak followed by gradual decline and end of test	

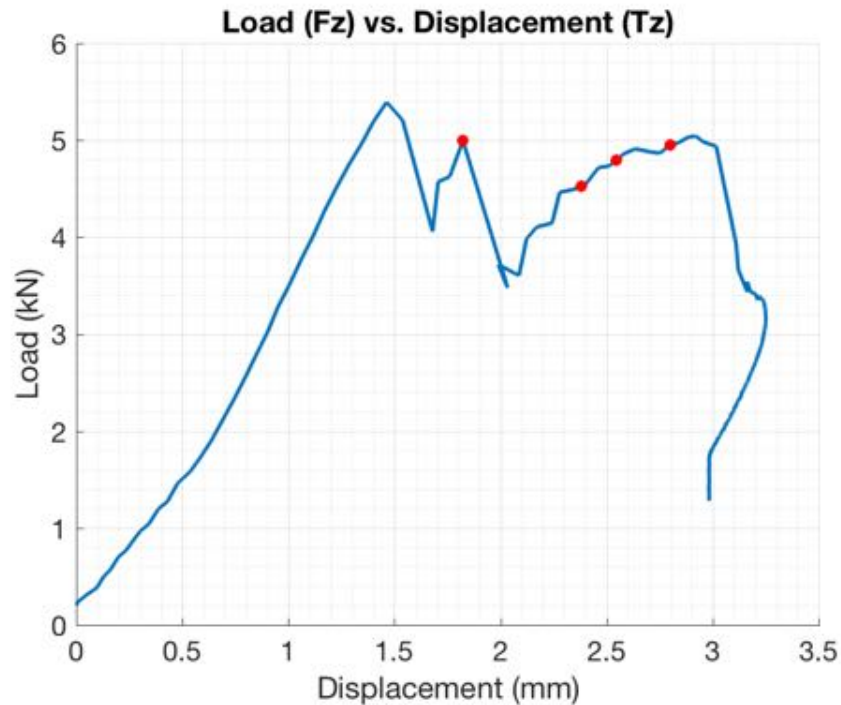




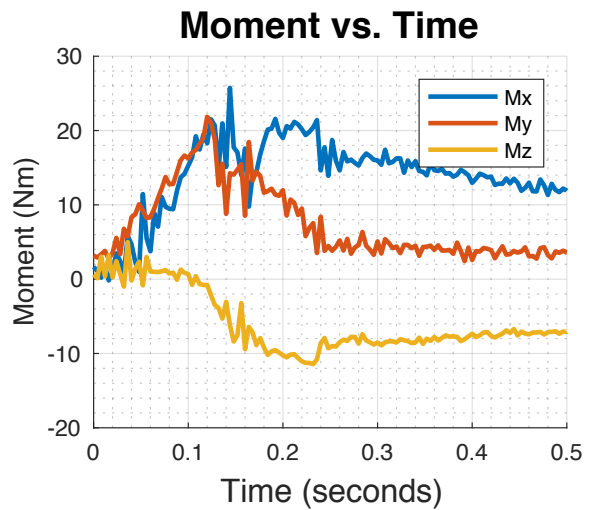
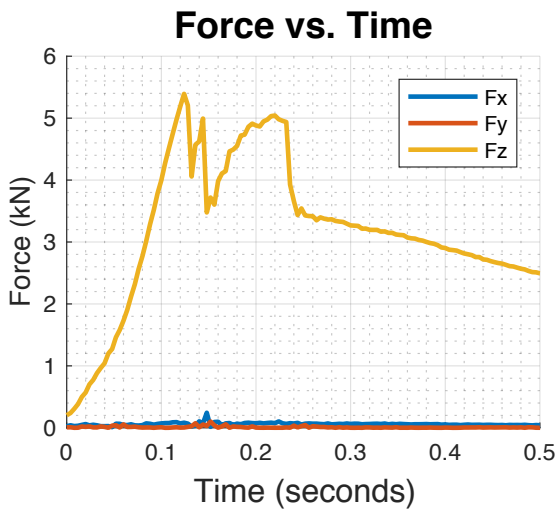
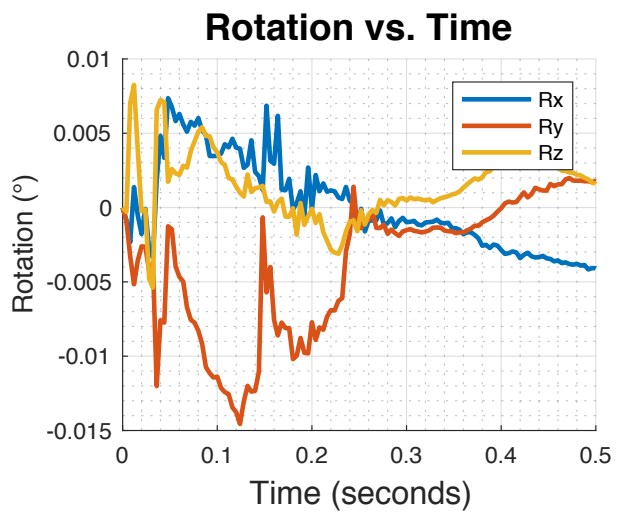
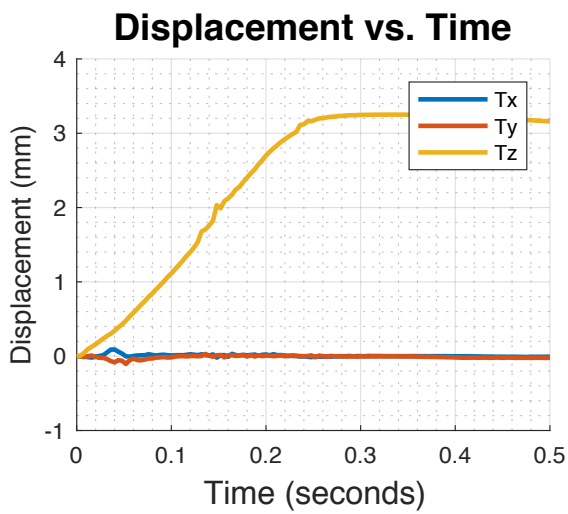
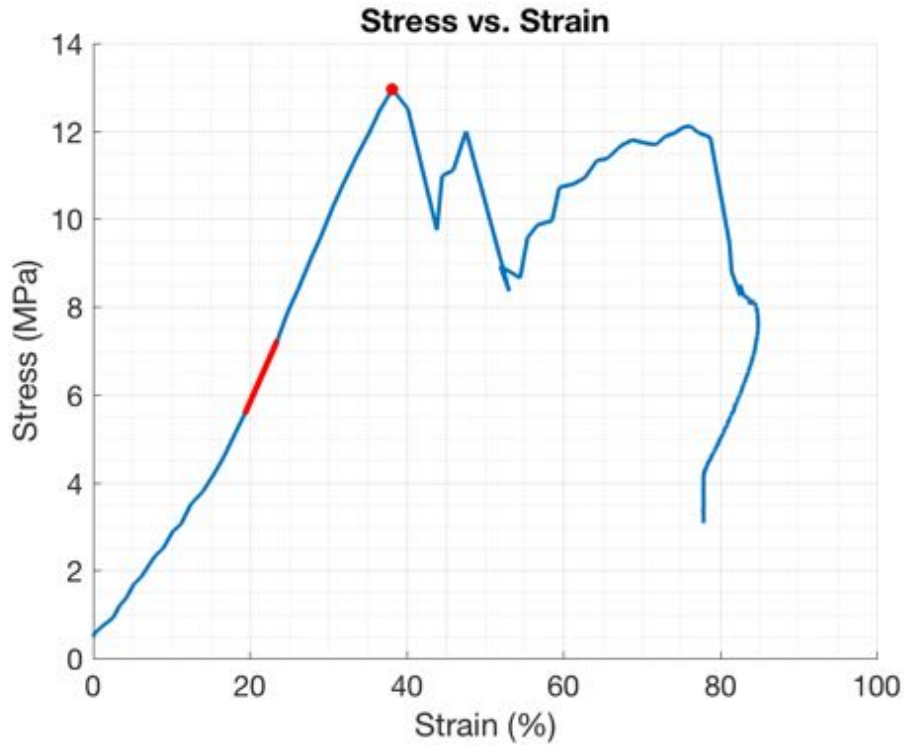
Failure Mode Assessment Summary			
	Load-displacement and video assessment	Photographic indicators	Classification
SO13	<ul style="list-style-type: none"> - Bulging and possible nuclear extrusion (left-postero-lateral) at 0.2 seconds seen in video and load-displacement curve at plateau 	<ul style="list-style-type: none"> - Small nuclear extrusion left postero-lateral region - No other evidence of damage 	HER(L-POS)

Specimen ID: SO14
Group: No Right Lateral Bending
Date tested: 8/8/2017

Failure load (kN)	Tz at failure (mm)	Time (s)	Moments (Nm)			Max Stress (MPa)	Max Strain (%)	Modulus (MPa)	Toughness (MJ/m ³)	Observations		
			Mx	My	Mz					Test	Disc	Vertebra
5.39	1.46	0.124	+21.51	+21.03	-2.152	12.96	38.20	40.3	2.3	AS, POS-RAIL, L-RAIL	Large POS NE	Shear EP from R INF VER



Identification of events by video & load vs. displacement comparison				
Event	Video		Load vs. Displacement	
	Time (s)	Description	Time (s)	Description
1	0.145	Bulging, nucleus extrude near superior vertebra posterior + right inferior tear?	0.124	Highest peak
2	0.1785	Bulging	0.144	Second peak and steep decline
3	0.19	Sound – no motion	0.18	Gradual bumpy incline for remainder of test
4	0.208	Nucleus extrude more + sound + right inferior side tear more		





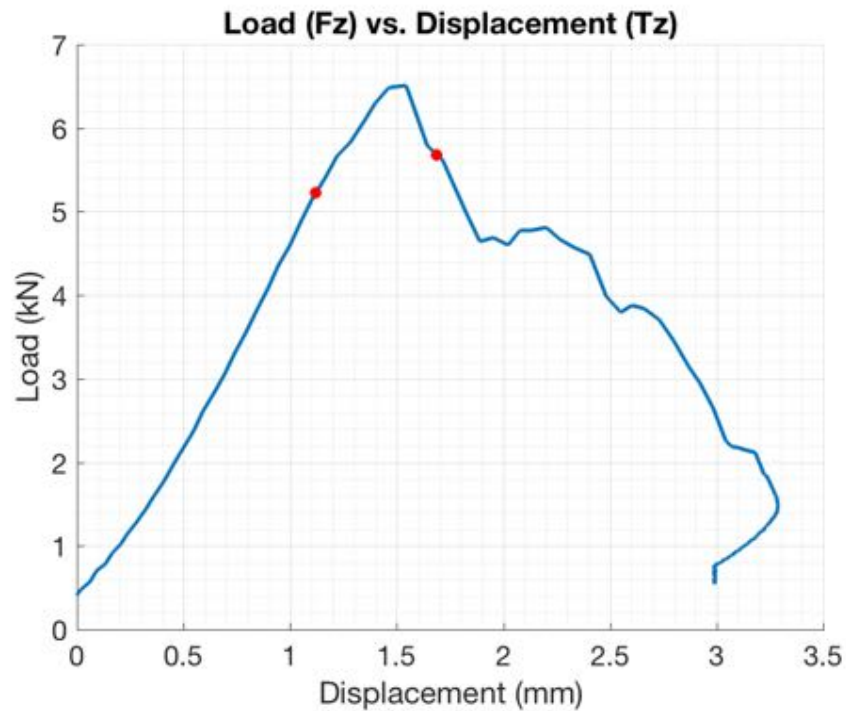
Failure Mode Assessment Summary			
	Load-displacement and video assessment	Photographic indicators	Classification
SO14	<ul style="list-style-type: none"> - Nucleus extrusion seen in video and correlated to second peak of load-displacement 	<ul style="list-style-type: none"> - Large nucleus extrusion in posterior region - Shearing at right inferior endplate-vertebra interface 	HER(POS) + EP-VER (R)

Specimen ID: SO15

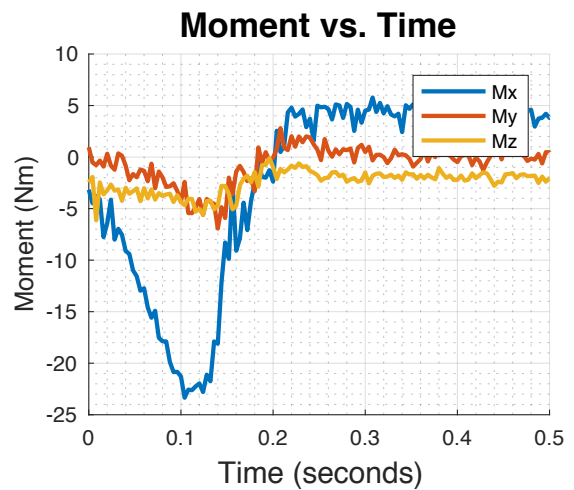
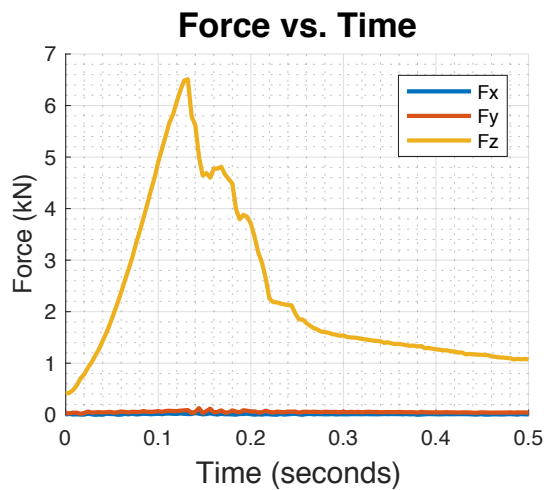
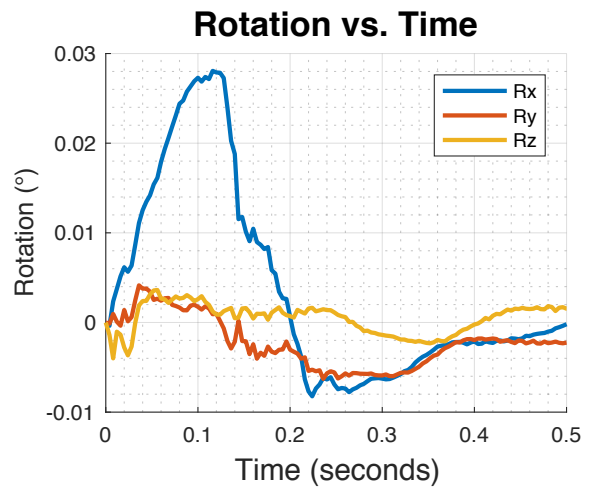
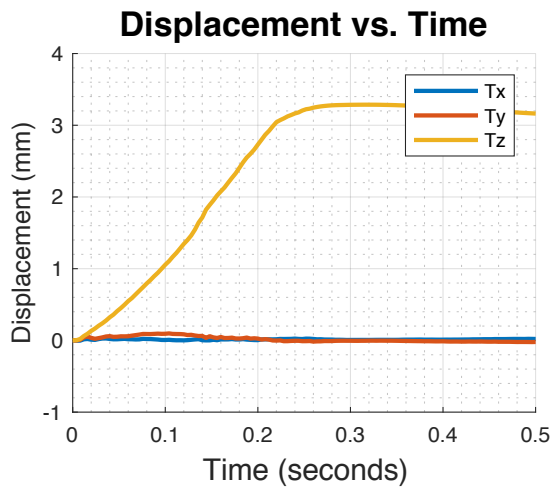
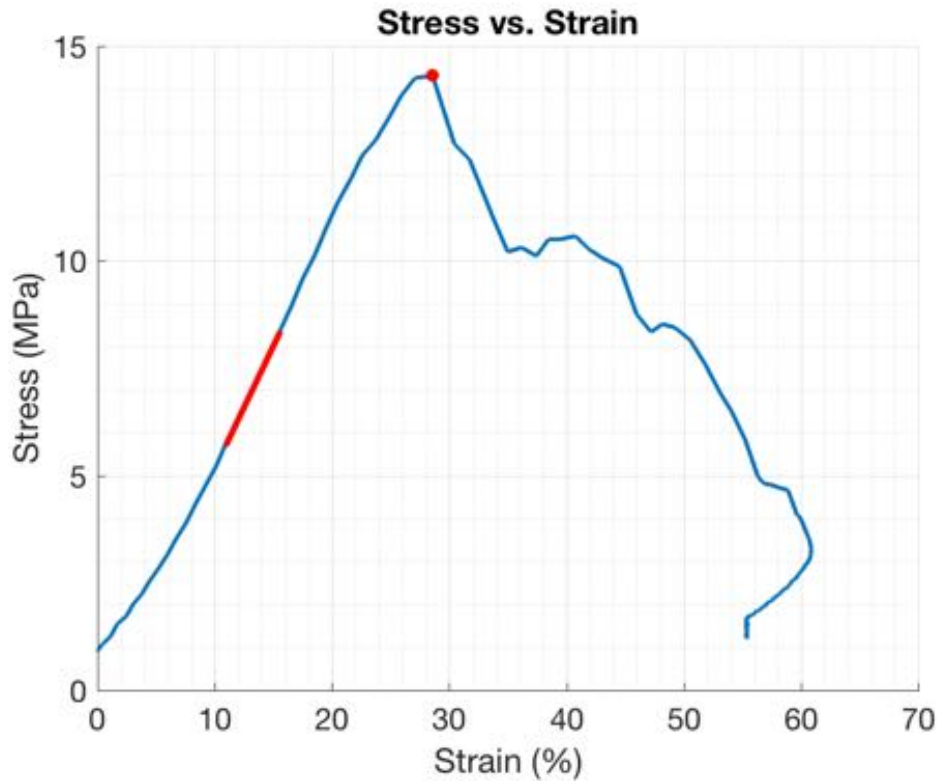
Group: No Facet Flexion

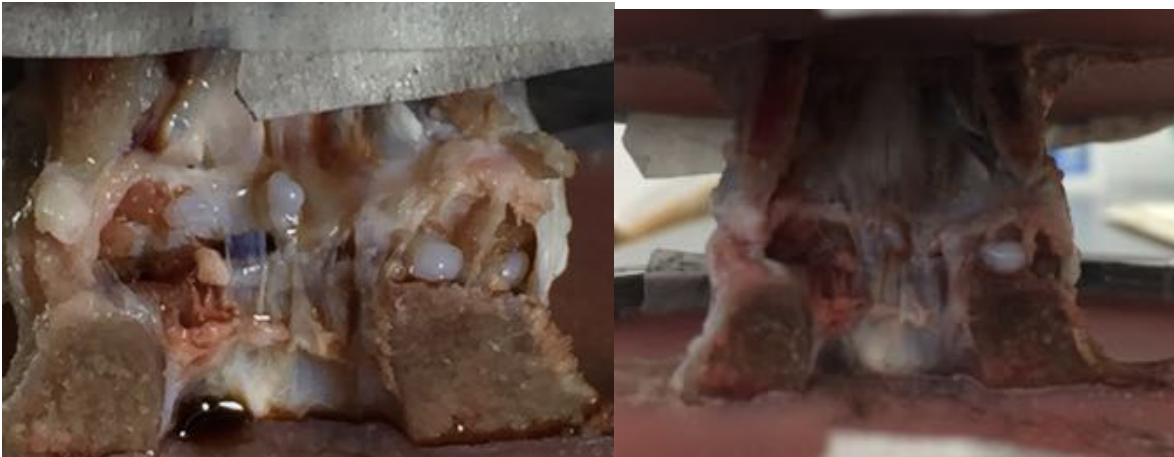
Date tested: 8/8/2017

Failure load (kN)	Tz at failure (mm)	Time (s)	Moments (Nm)			Max Stress (MPa)	Max Strain (%)	Modulus (MPa)	Toughness (MJ/m ³)	Observations		
			Mx	My	Mz					Test	Disc	Vertebra
6.51	1.54	0.132	-21.75	-4.37	-4.23	14.31	28.58	57.2	2.2	AS, POS-RAIL	POS NE, R-POS NE	Shear EP torn from INF-VER



Identification of events by video & load vs. displacement comparison				
		Video	Load vs. Displacement	
Event	Time (s)	Description	Time (s)	Description
1	0.105	Start shear forward	0.136	Slight slope change
2	0.1385	Shear forward & possible nucleus material posterior right	0.152	Plateau at peak fail
3			0.156	Peak and massive decline





Failure Mode Assessment Summary

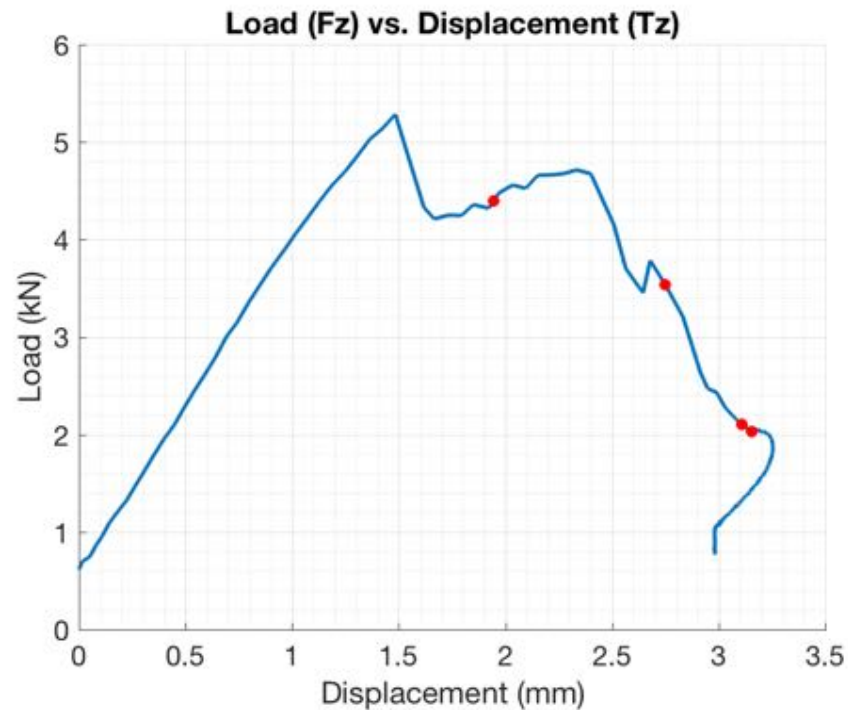
	Load-displacement and video assessment	Photographic indicators	Classification
SO15	<ul style="list-style-type: none"> - Gradual shearing of superior vertebra forward - Nuclear material extruded posteriorly 	<ul style="list-style-type: none"> - Significant inferior endplate shear off inferior vertebra - Nucleus extruded posteriorly in several locations 	HER (POS + EP-VER)

Specimen ID: SO16

Group: No Facet Flexion & Right Lateral Bending

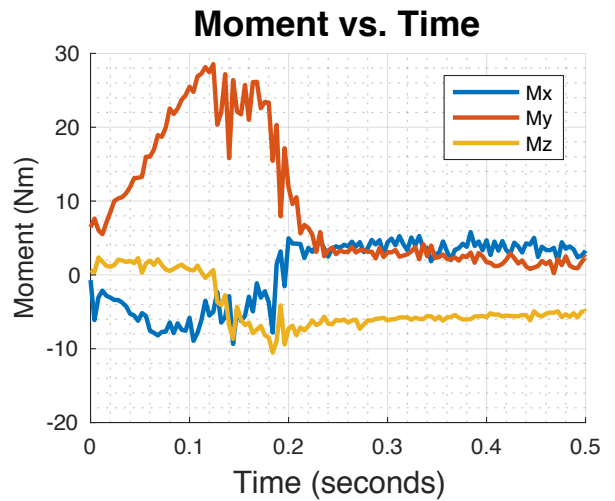
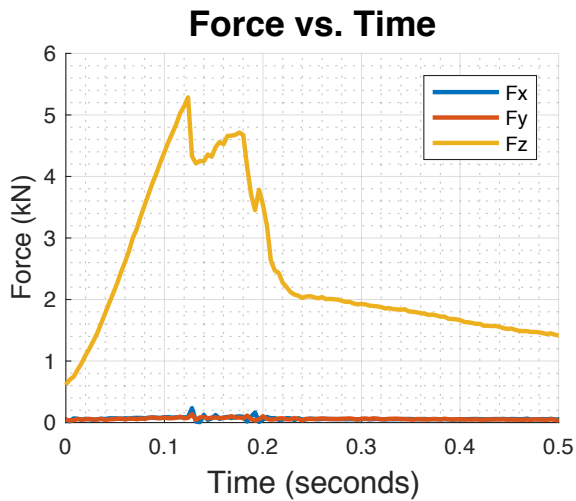
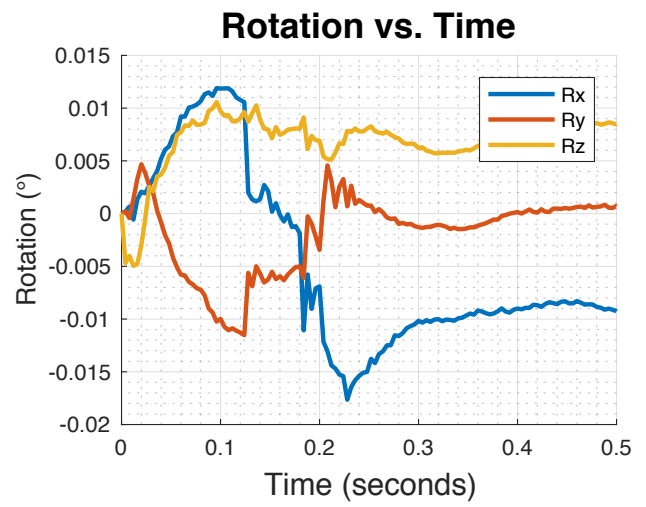
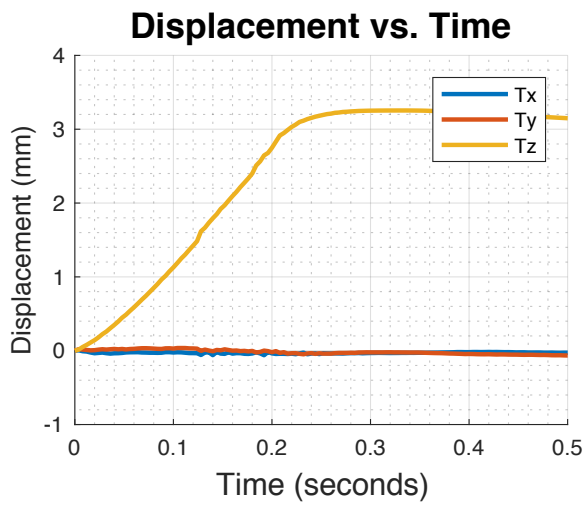
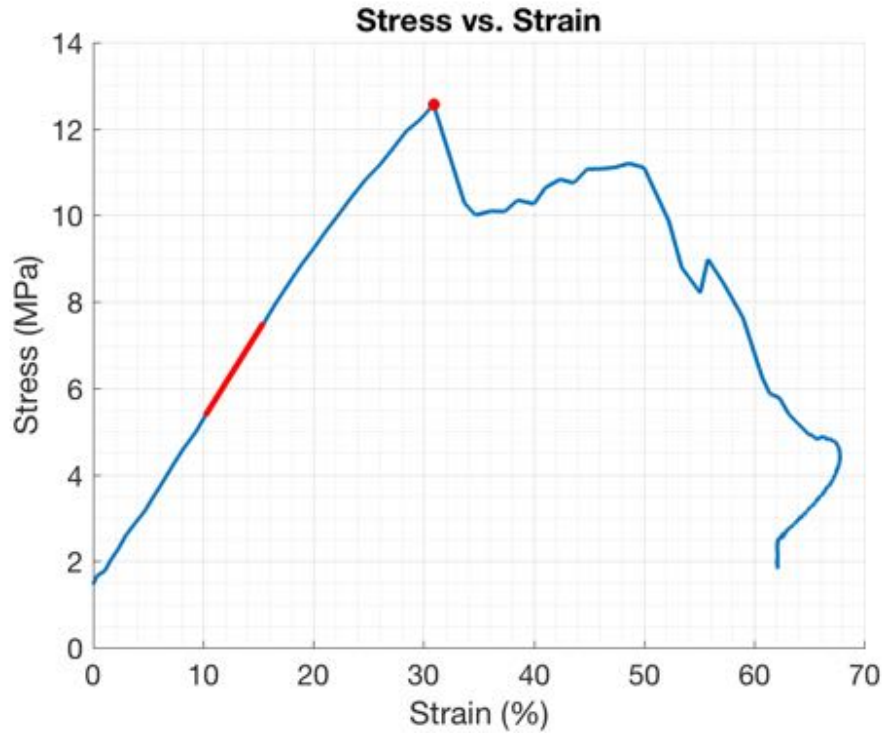
Date tested: 8/8/2017

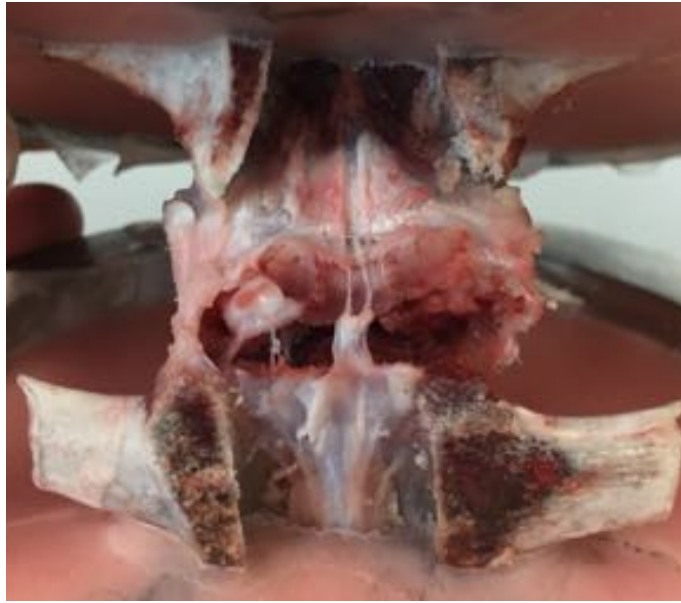
Failure load (kN)	Tz at failure (mm)	Time (s)	Moments (Nm)			Max Stress (MPa)	Max Strain (%)	Modulus (MPa)	Toughness (MJ/m ³)	Observations		
			Mx	My	Mz					Test	Disc	Vertebra
5.29	1.48	0.124	-5.01	28.54	0.66	12.56	30.91	40.7	2.3	AS, L-RAIL, POS-RAIL	L-POS NE	Shear EP torn from INF-VER



Identification of events by video & load vs. displacement comparison

Event	Video		Load vs. Displacement	
	Time (s)	Description	Time (s)	Description
1	0.15	Postero-lateral left endplate tear	0.168	Peak load
2	0.2	Sound	0.2	Bumpy gradual slope to peak – Maybe herniating?
3	0.23	Louder sound	0.224	Second peak
4	0.24	Shear slip anterior	0.24	Third peak then decline

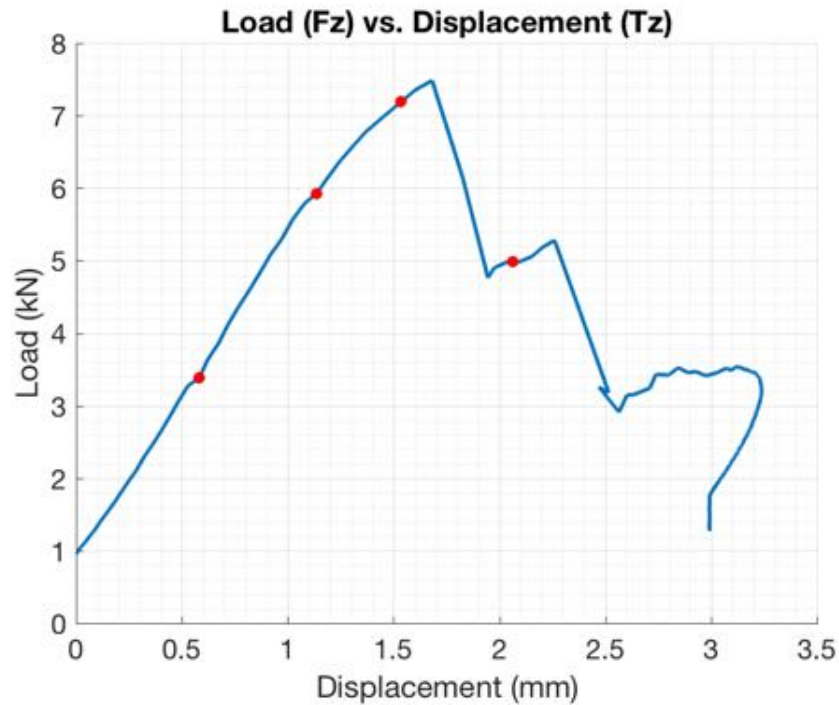




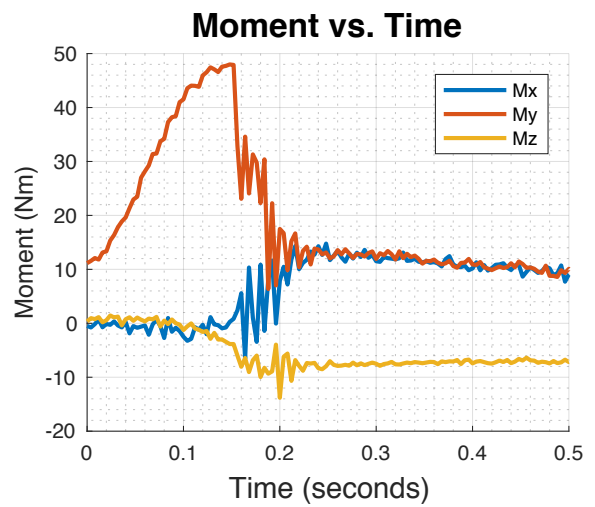
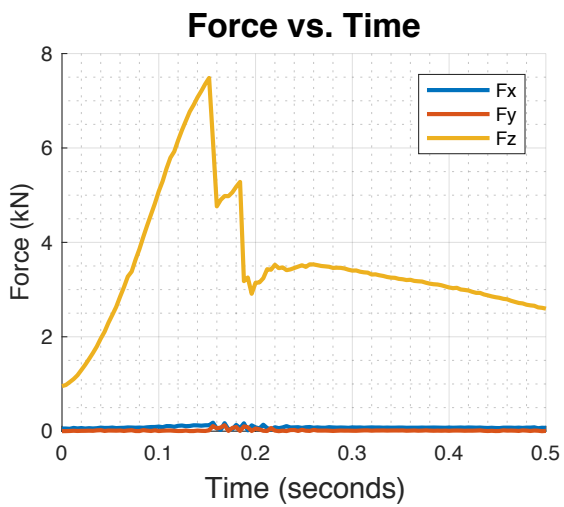
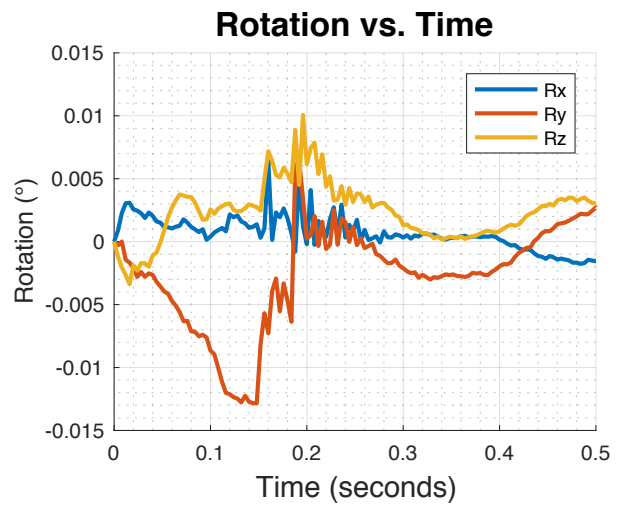
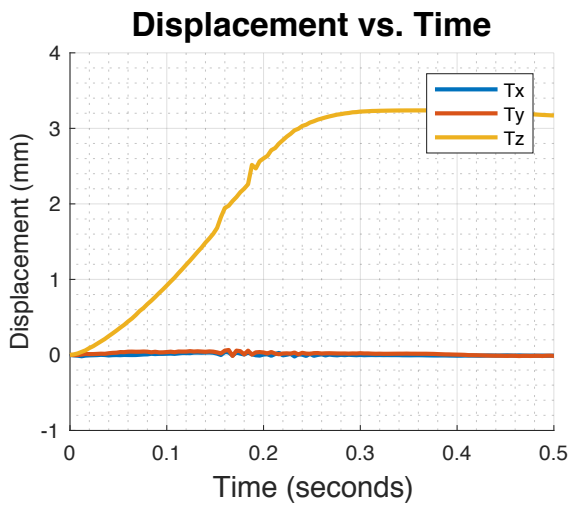
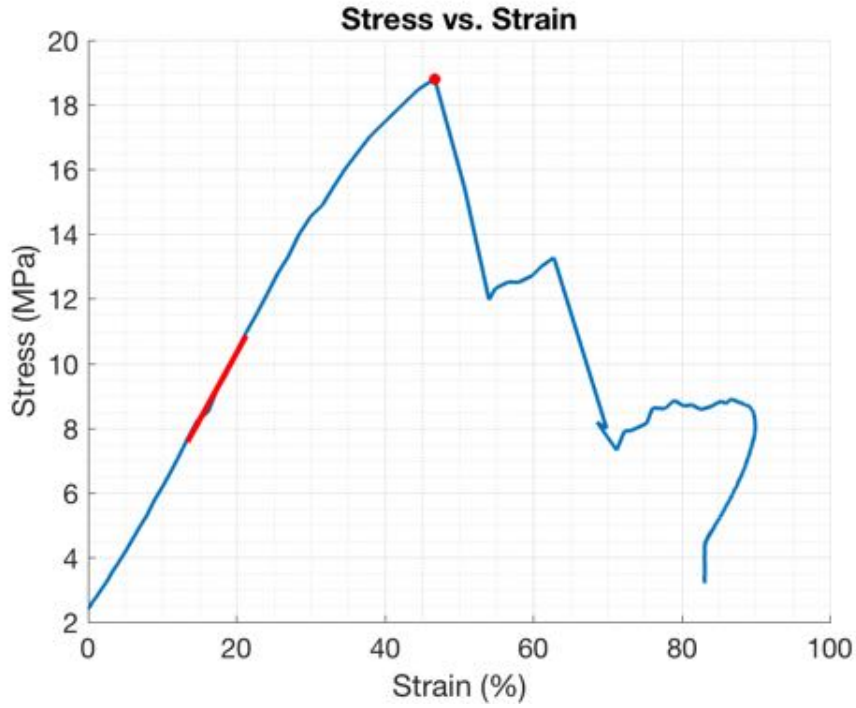
Failure Mode Assessment Summary			
	Load-displacement and video assessment	Photographic indicators	Classification
SO16	- Shear tear of inferior endplate/vertebra first event in video and load-displacement	- Significant shear tear at inferior endplate and vertebra interface - Nucleus material extruded left postero-laterally	EP-VER + HER(L-POS)

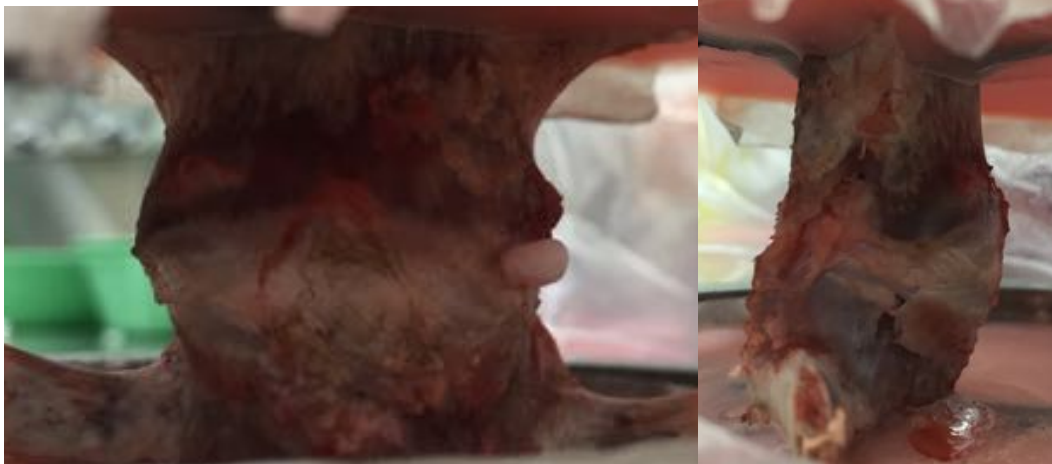
Specimen ID: SO17
Group: No Right Lateral Bending
Date tested: 8/8/2017

Failure load (kN)	Tz at failure (mm)	Time (s)	Moments (Nm)			Max Stress (MPa)	Max Strain (%)	Modulus (MPa)	Toughness (MJ/m ³)	Observations		
			Mx	My	Mz					Test	Disc	Vertebra
7.48	1.68	0.152	0.82	47.90	-3.85	18.81	46.72	41.5	5.3	AS, L-RAIL, POS-RAIL	L-POS NE	R INF VER fracture



Identification of events by video & load vs. displacement comparison				
	Video		Load vs. Displacement	
Event	Time (s)	Description	Time (s)	Description
1	0.072	Compress FSU	0.072	Small plateau 1
2	0.116	Nucleus extrude postero-lateral left – Sound spike	0.116	Small plateau 2
3	0.1435	Superior VB shear forward – sound spike	0.156	Peak force
4	0.17	Superior VB shear forward further	0.188	Second peak





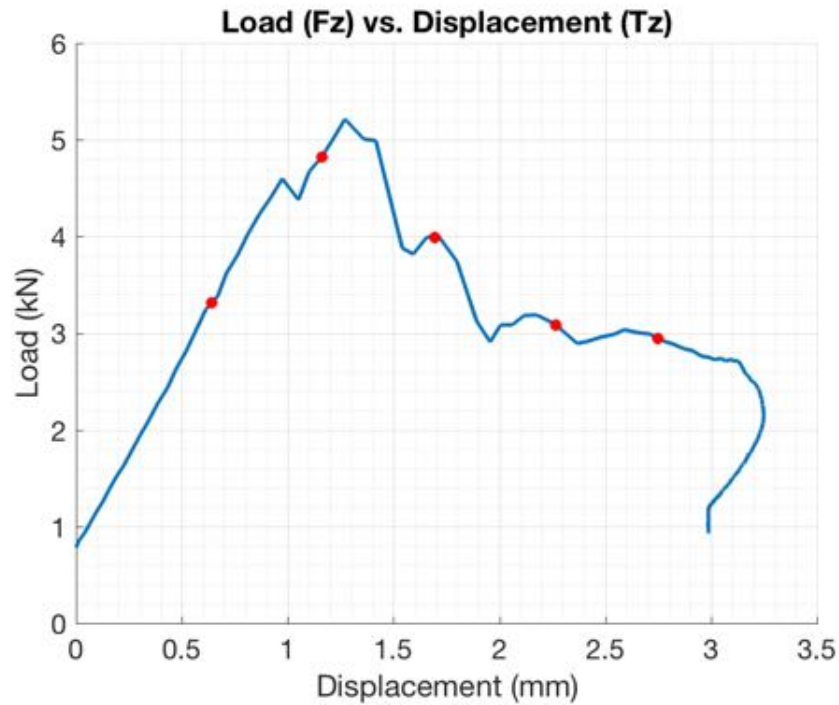
Failure Mode Assessment Summary			
	Load-displacement and video assessment	Photographic indicators	Classification
SO17	- Nucleus extruded at second plateau of load-displacement curve	- Left postero-lateral nuclear extrusion - Small shear of the inferior vertebra	HER(L-POS) + EP-VER

Specimen ID: SO18

Group: No Facet Flexion & Right Lateral Bending

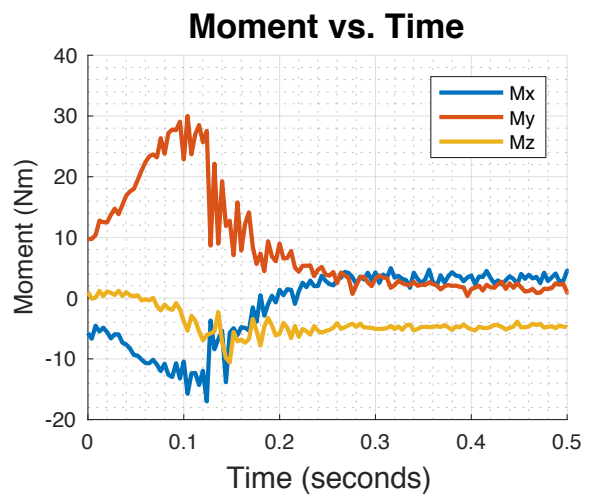
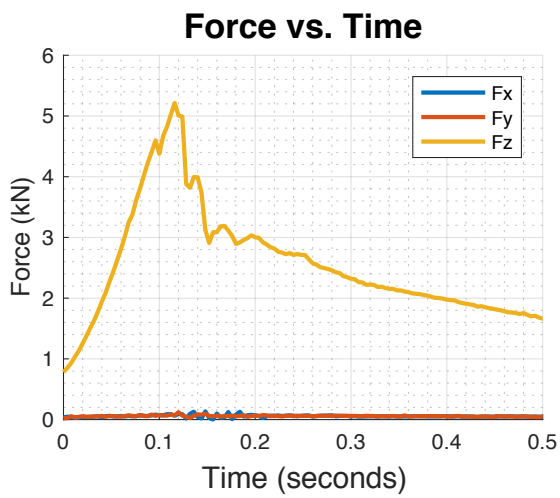
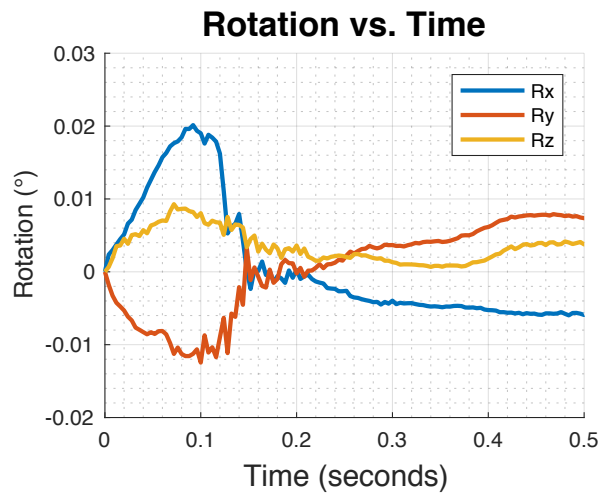
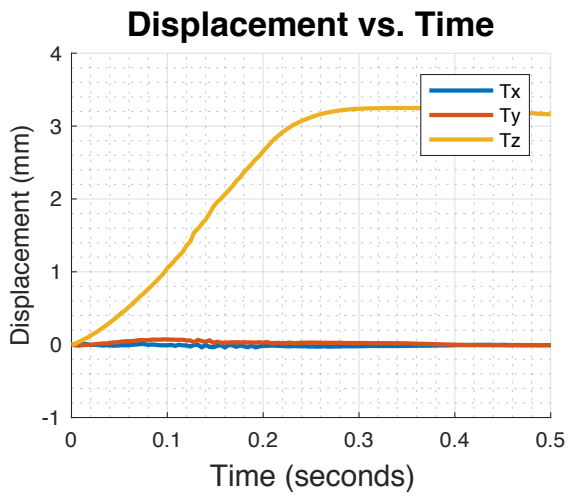
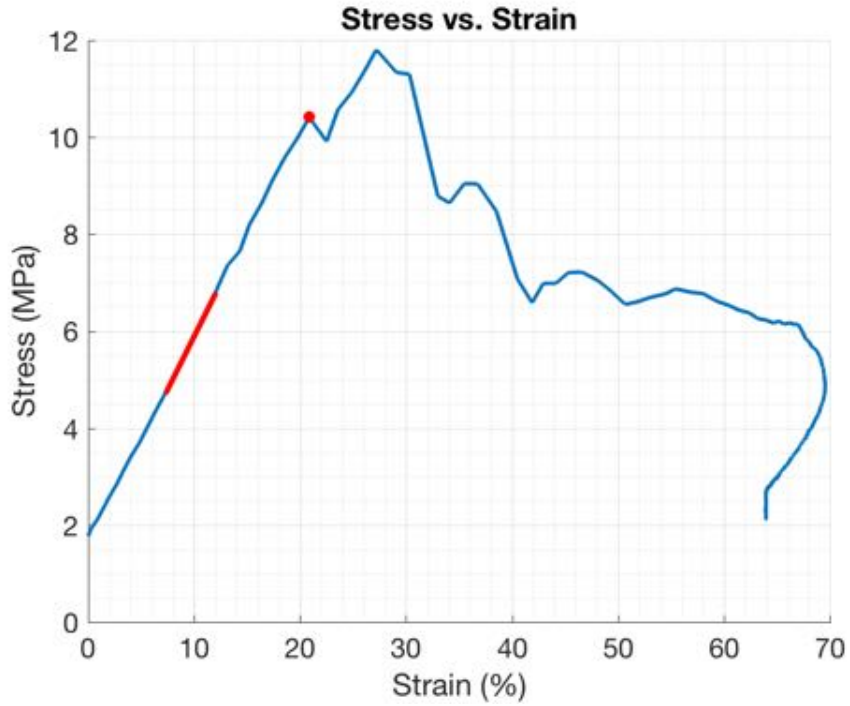
Date tested: 9/8/2017

Failure load (kN)	Tz at failure (mm)	Time (s)	Moments (Nm)			Max Stress (MPa)	Max Strain (%)	Modulus (MPa)	Toughness (MJ/m ³)	Observations		
			Mx	My	Mz					Test	Disc	Vertebra
4.60	0.97	0.116	-13.23	29.06	-1.87	10.41	20.86	43.8	1.3	AS, L-RAIL, POS-RAIL	L-POS NE	Shear EP torn from R INF-VER



Identification of events by video & load vs. displacement comparison

Event	Video		Load vs. Displacement	
	Time (s)	Description	Time (s)	Description
1	0.07	FSU compression & shear	0.084	Small plateau
2	0.108	FSU compression & shear	0.108	Peak 1
3	0.1385	Postero-lateral left endplate inferior tear	0.128	Peak 2 highest
4	0.1735	Shear forward	0.152	Plateau
5	0.2065	Shear forward	0.18	Drop





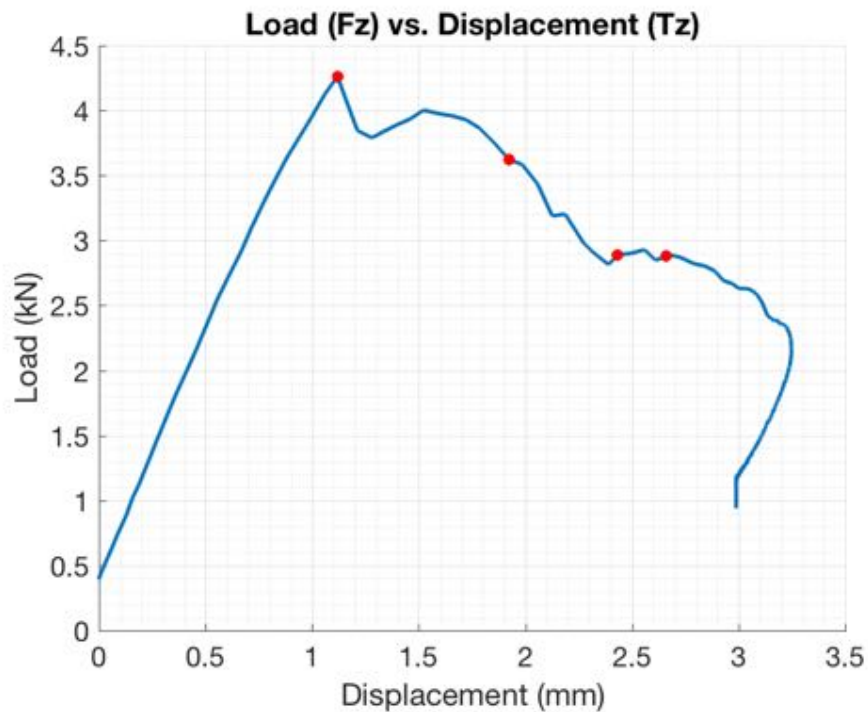
Failure Mode Assessment Summary			
	Load-displacement and video assessment	Photographic indicators	Classification
SO18	- No clear correlation	<ul style="list-style-type: none"> - Shearing of superior vertebra with respect to inferior. - Endplate tear at right and left endplate/inferior vertebra interface 	HER (L-POS) + EP-VER

Specimen ID: SO19

Group: No Facet Right Lateral Bending

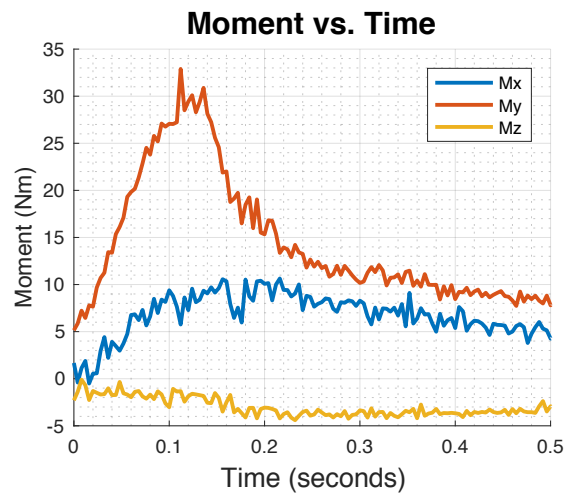
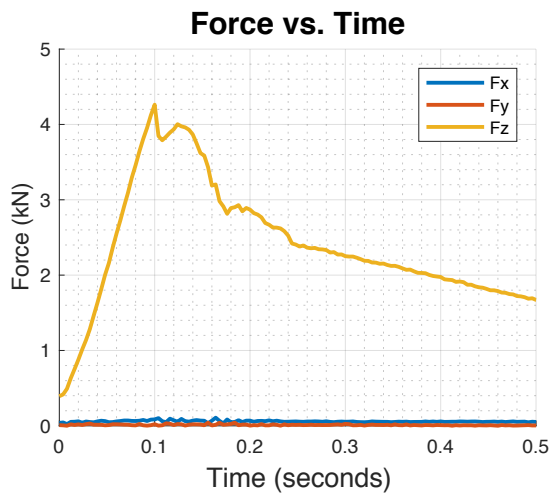
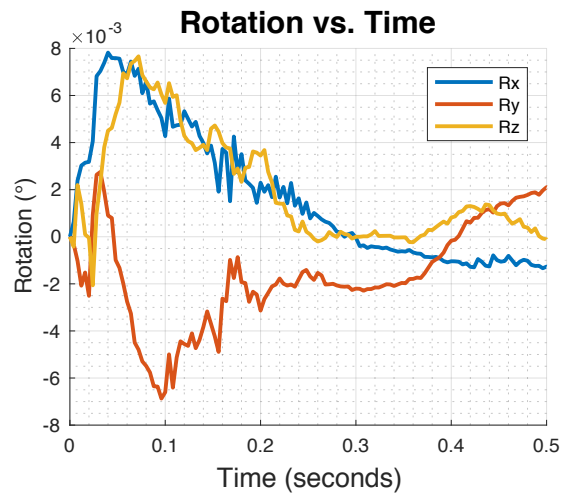
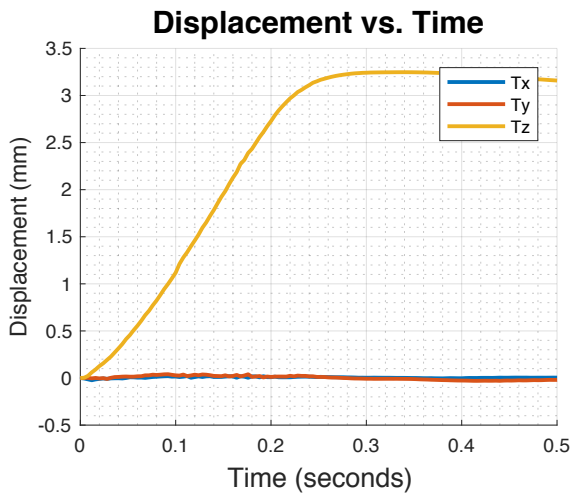
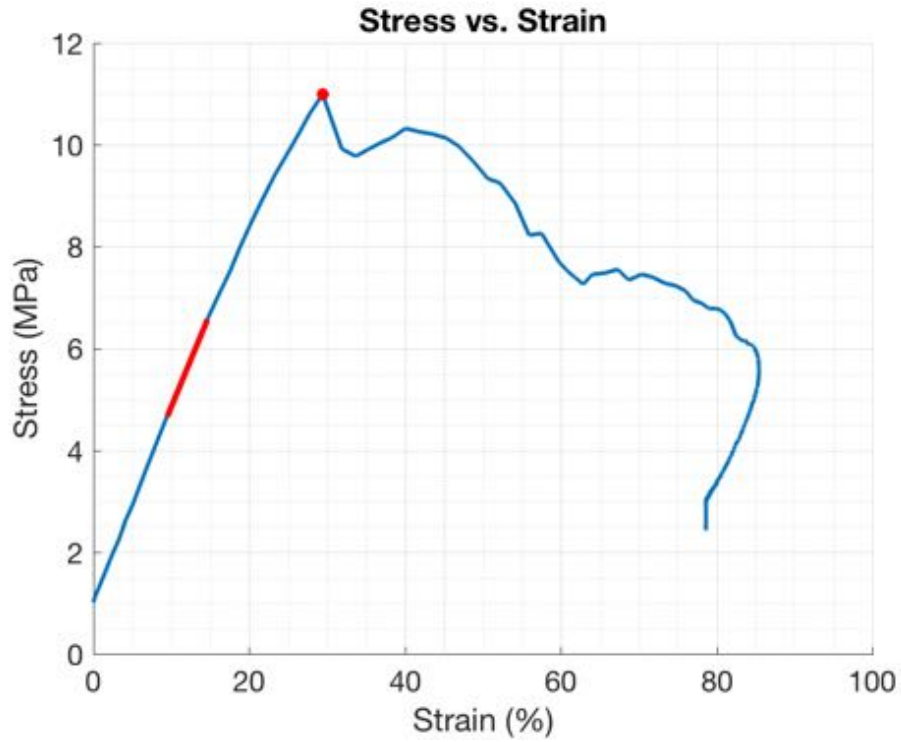
Date tested: 9/8/2017

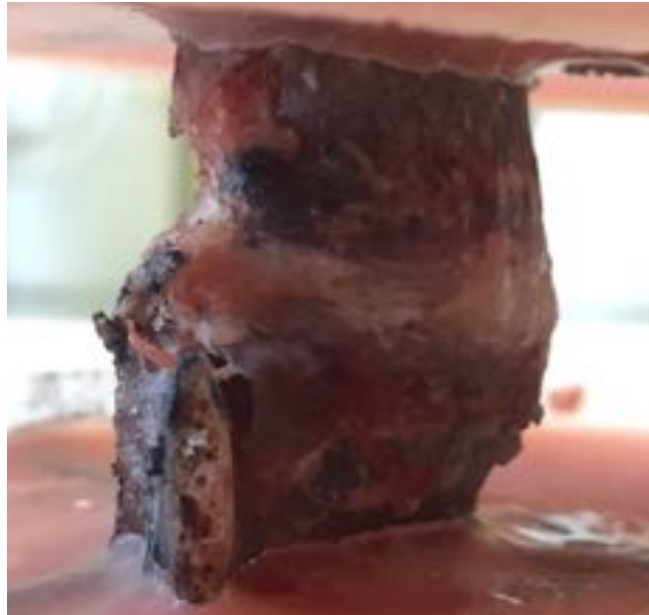
Failure load (kN)	Tz at failure (mm)	Time (s)	Moments (Nm)			Max Stress (MPa)	Max Strain (%)	Modulus (MPa)	Toughness (MJ/m ³)	Observations		
			Mx	My	Mz					Test	Disc	Vertebra
4.26	1.12	0.1	9.39	27.07	-3.03	10.99	29.43	36.9	1.9	AS, L-RAIL, POS-RAIL	-	-



Identification of events by video & load vs. displacement comparison

Event	Video		Load vs. Displacement	
	Time (s)	Description	Time (s)	Description
1	0.1	Small shear	0.1	Highest peak
2	0.148	Small shear	0.148	Small plateau
3	0.18	Shear to right front	0.16	Second small plateau
4	0.195	Loud noise – no motion	0.188	Small peak followed by gradual declining slope





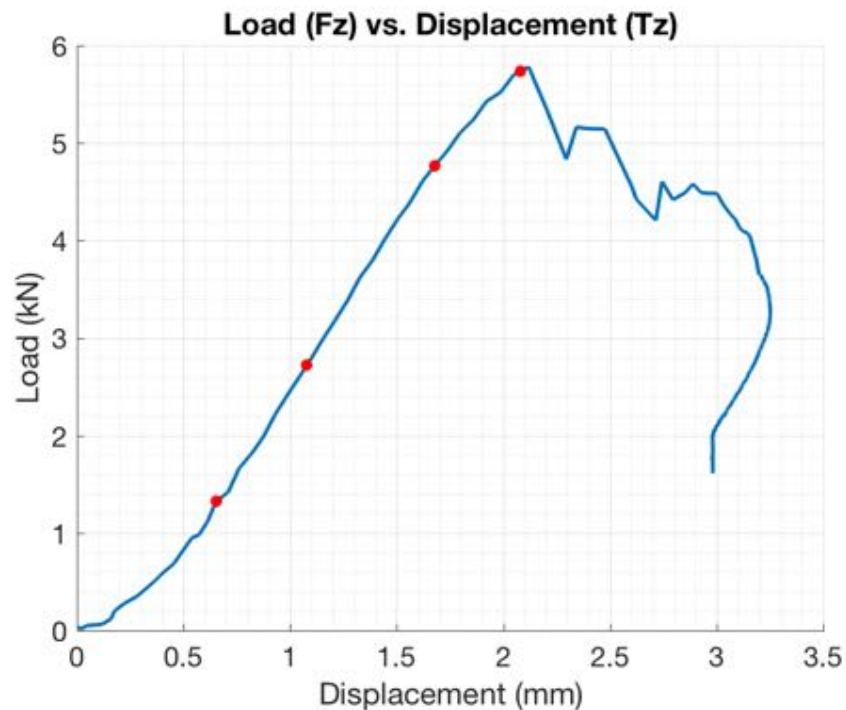
Failure Mode Assessment Summary			
	Load-displacement and video assessment	Photographic indicators	Classification
SO19	- No Clear evidence	- Right inferior shear at endplate/vertebra interface	EP-VER

Specimen ID: SO20

Group: No Facet Flexion

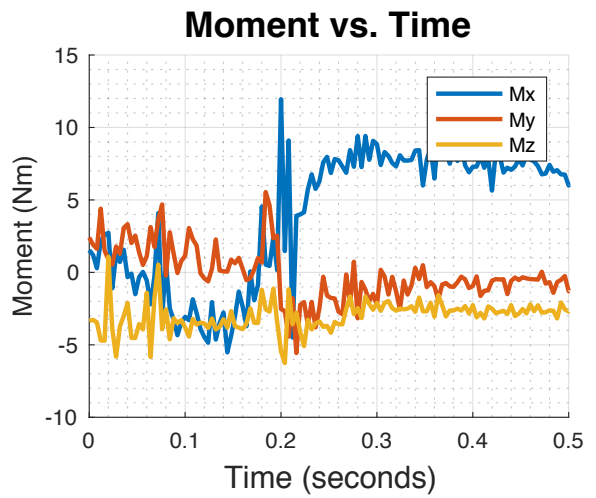
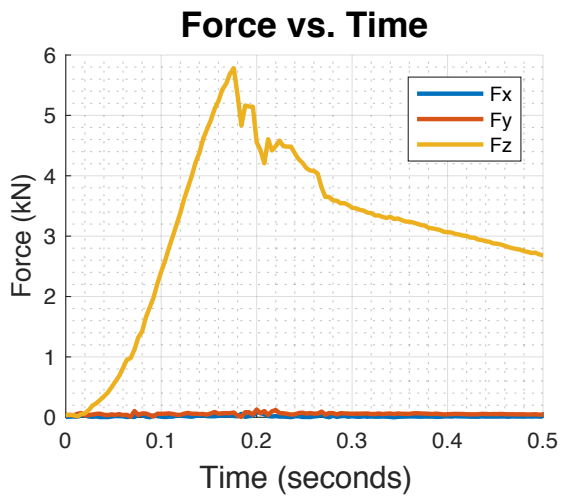
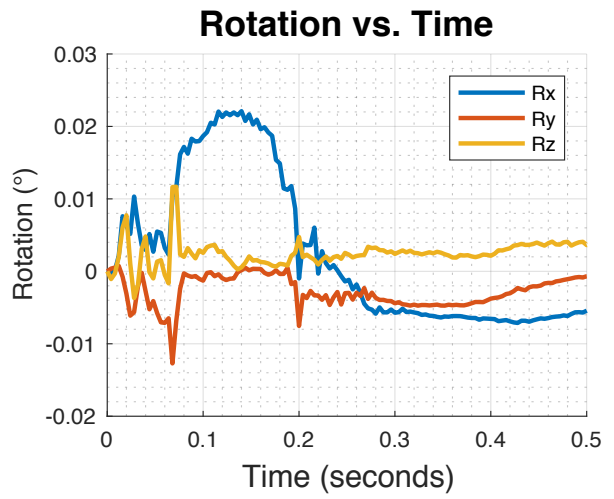
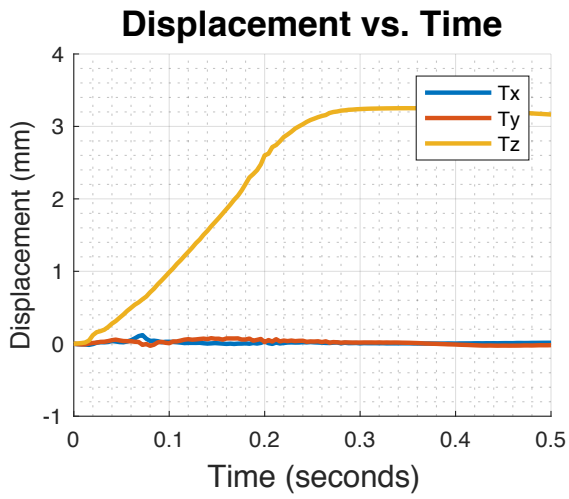
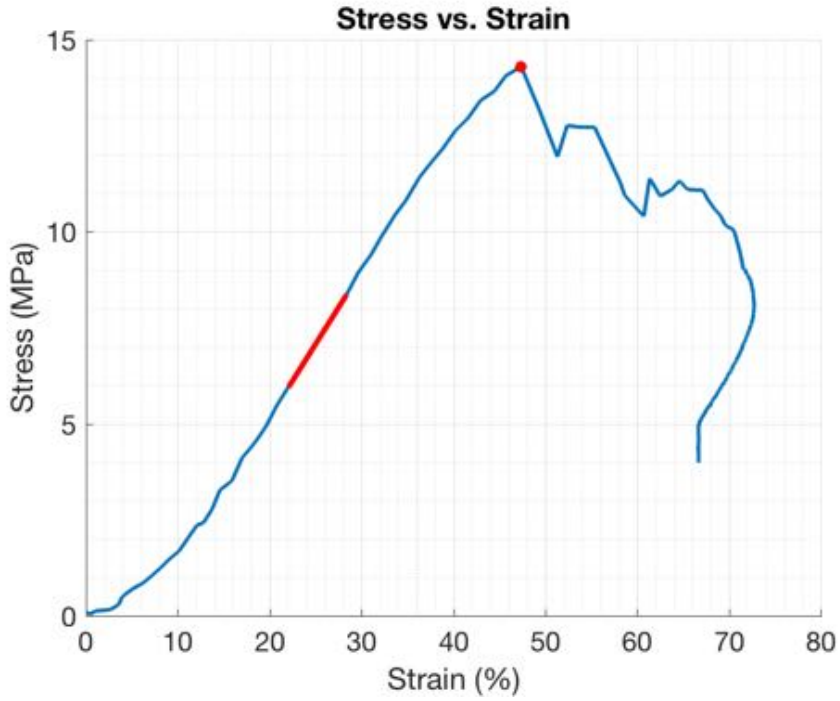
Date tested: 9/8/2017

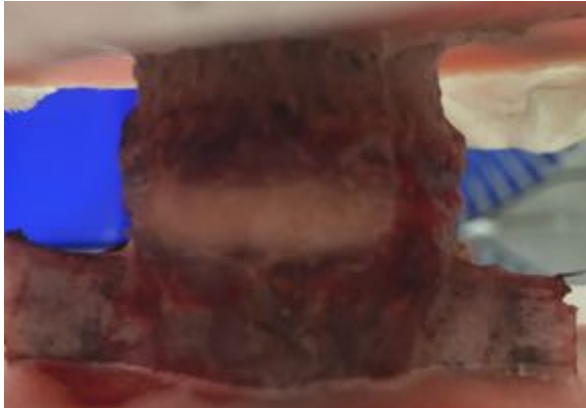
Failure load (kN)	Tz at failure (mm)	Time (s)	Moments (Nm)			Max Stress (MPa)	Max Strain (%)	Modulus (MPa)	Toughness (MJ/m ³)	Observations		
			Mx	My	Mz					Test	Disc	Vertebra
5.78	2.12	0.176	-0.86	1.00	-3.49	14.30	47.38	38.1	3.2	AS, POS-RAIL	-	VER SHEAR R



Identification of events by video & load vs. displacement comparison

Event	Video		Load vs. Displacement	
	Time (s)	Description	Time (s)	Description
1	0.076	Small shear forward	0.076	Small change in slope
2	0.1065	Shear	0.148	Small change in slope near peak
3	0.148	Loud noise – no motion	0.176	Highest peak
4	0.1735	Loud noise and shear forward	0.188	Plateau then decline





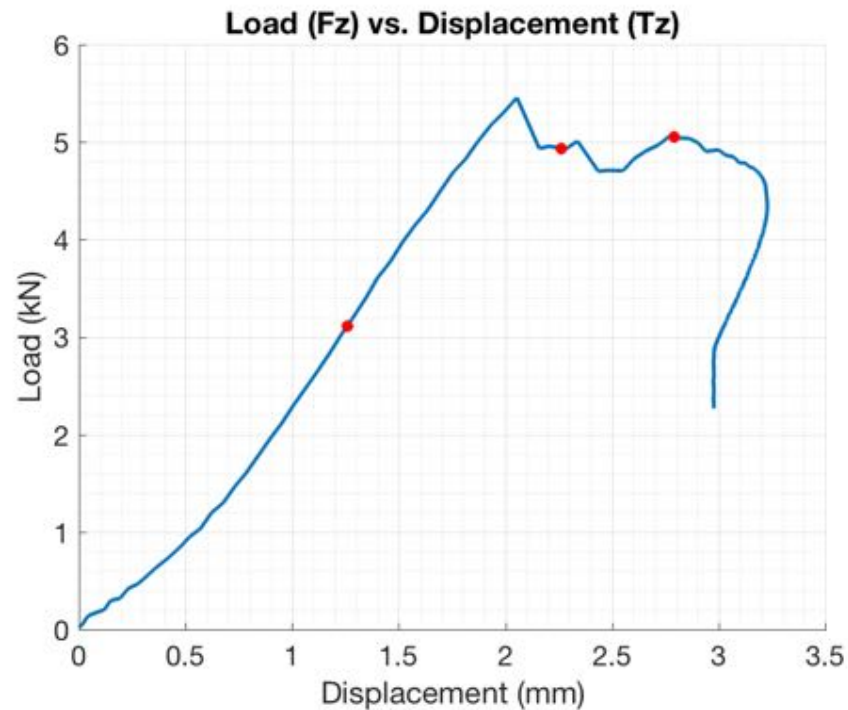
Failure Mode Assessment Summary			
	Load-displacement and video assessment	Photographic indicators	Classification
SO20	- No clear evidence	- Superior vertebra shear forward	EP-VER

Specimen ID: SO21

Group: No Facet Flexion & Right Lateral Bending

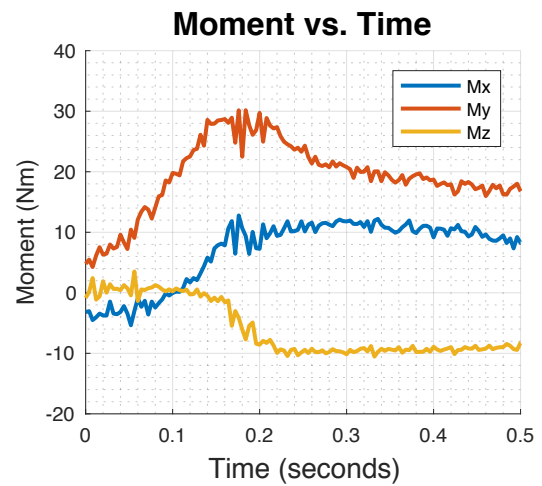
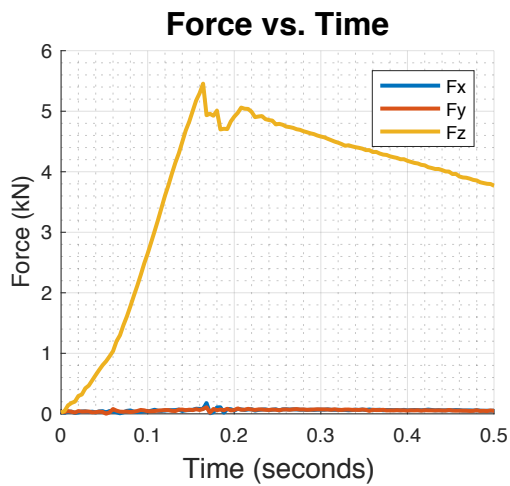
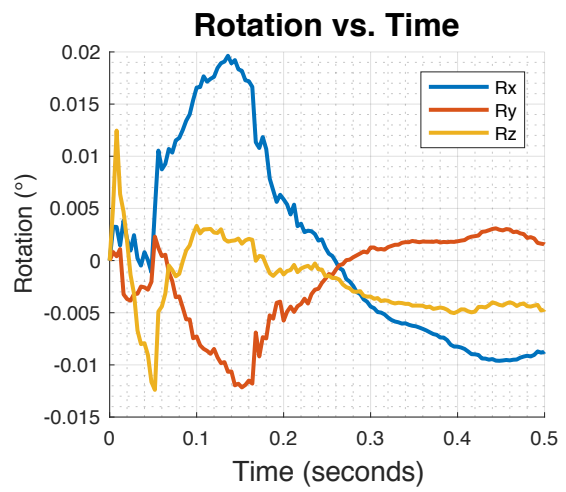
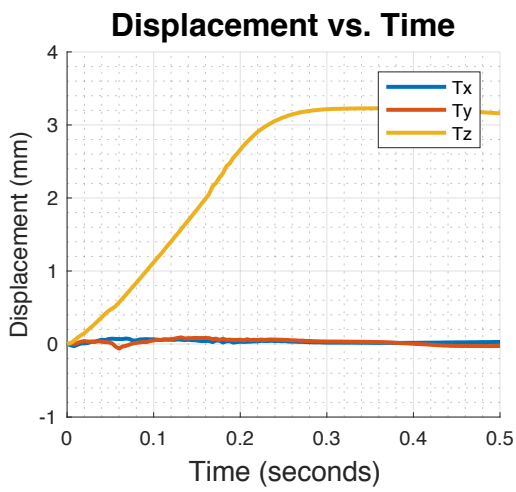
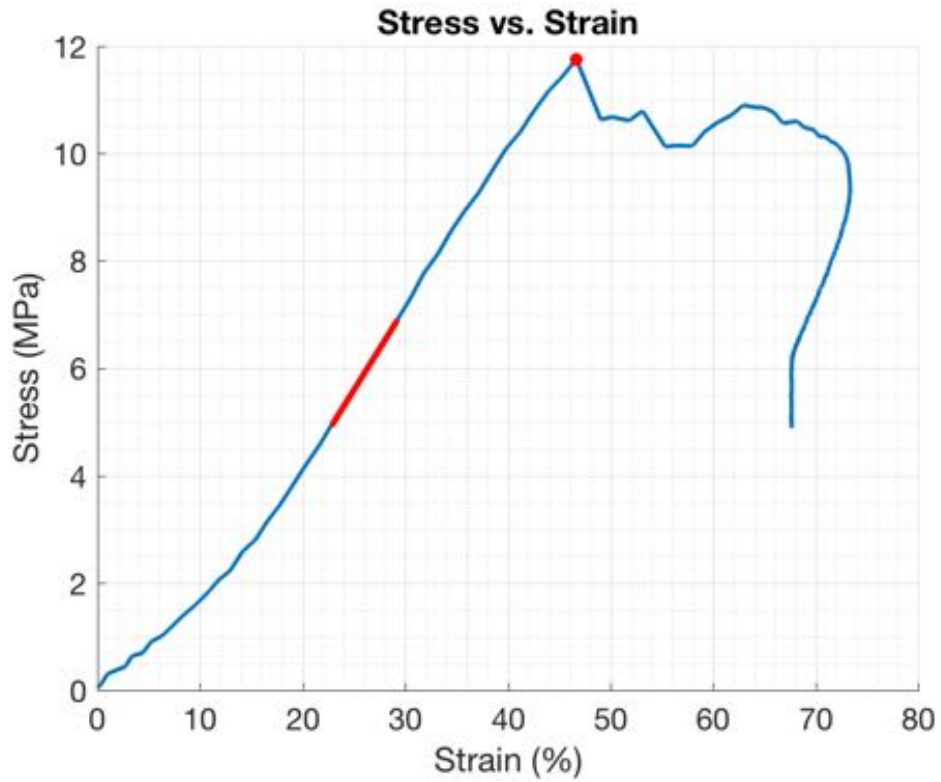
Date tested: 10/8/2017

Failure load (kN)	Tz at failure (mm)	Time (s)	Moments (Nm)			Max Stress (MPa)	Max Strain (%)	Modulus (MPa)	Toughness (MJ/m ³)	Observations		
			Mx	My	Mz					Test	Disc	Vertebra
5.46	2.05	0.164	10.63	28.08	-1.27	11.75	46.67	30.7	2.5	AS, L-RAIL, POS-RAIL	Small L-NE	Shear EP torn from R INF-VER



Identification of events by video & load vs. displacement comparison

Event	Video		Load vs. Displacement	
	Time (s)	Description	Time (s)	Description
1	0.11	Small shear	0.172	Highest peak
2	0.175	Larger shear and sound – hole appear at posterior right side near inferior vertebra	0.216	Third peak
3	0.21	Loud sound		





Failure Mode Assessment Summary

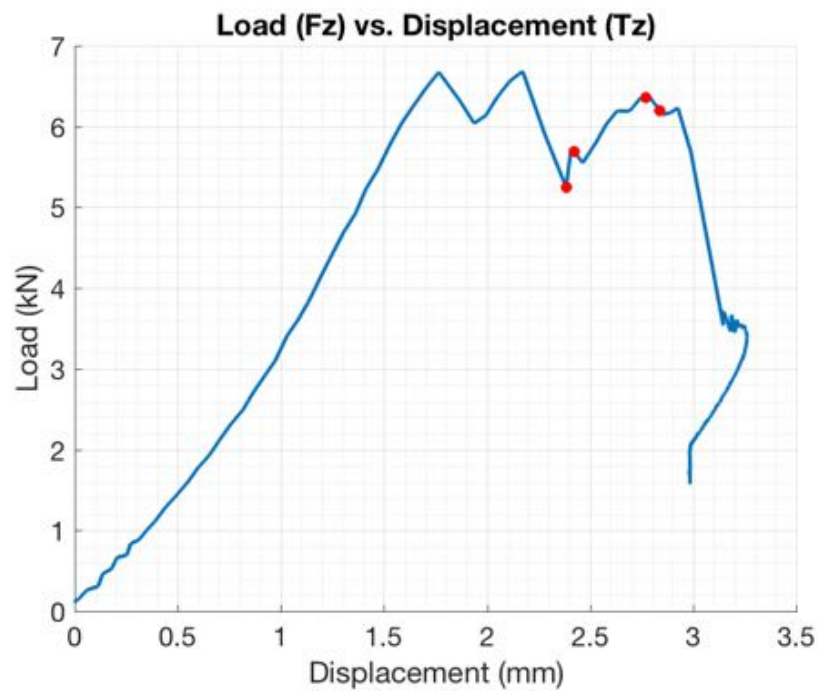
	Load-displacement and video assessment	Photographic indicators	Classification
SO21	<ul style="list-style-type: none"> - Highest peak of load-displacement curve correlate with shear tear at inferior endplate/vertebra interface 	<ul style="list-style-type: none"> - Rupture of tissue at the endplate/vertebra interface - Small nuclear extrusion left postero-lateral region of disc 	HER (L-POS) + EP-VER

Specimen ID: SO22

Group: No Facet Right Lateral Bending

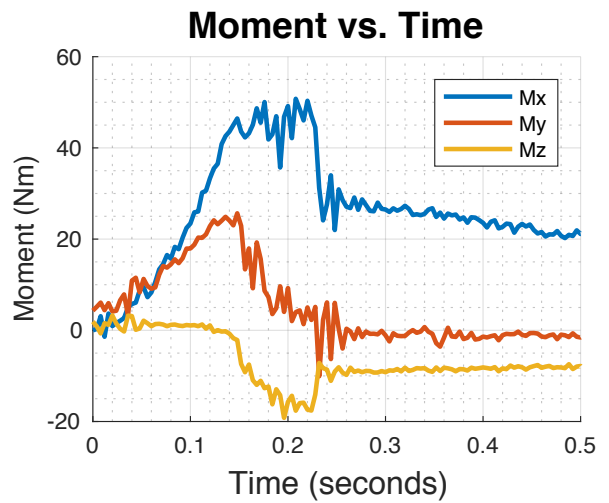
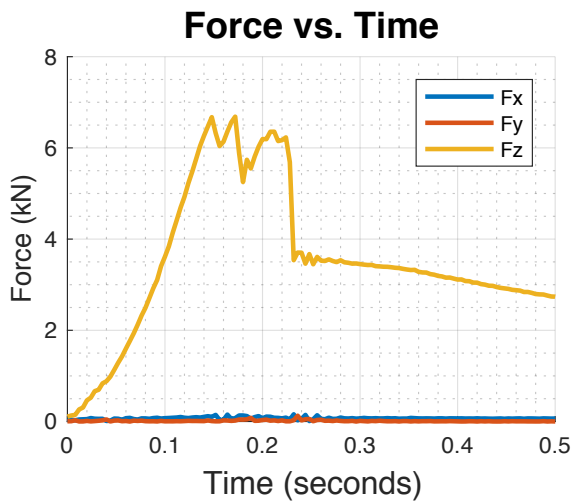
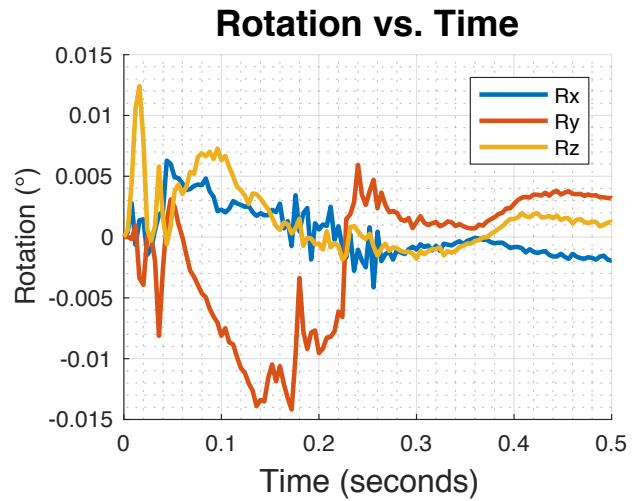
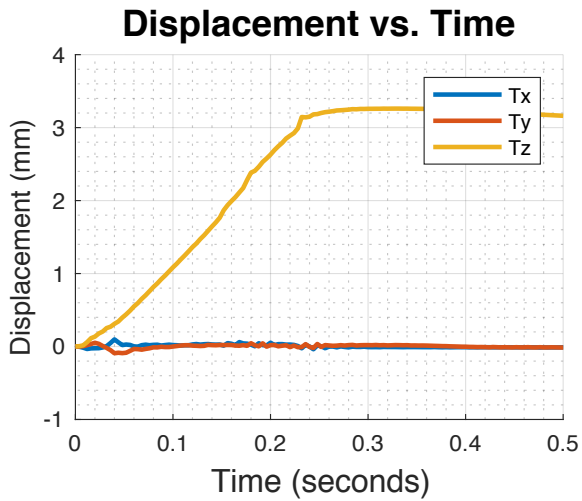
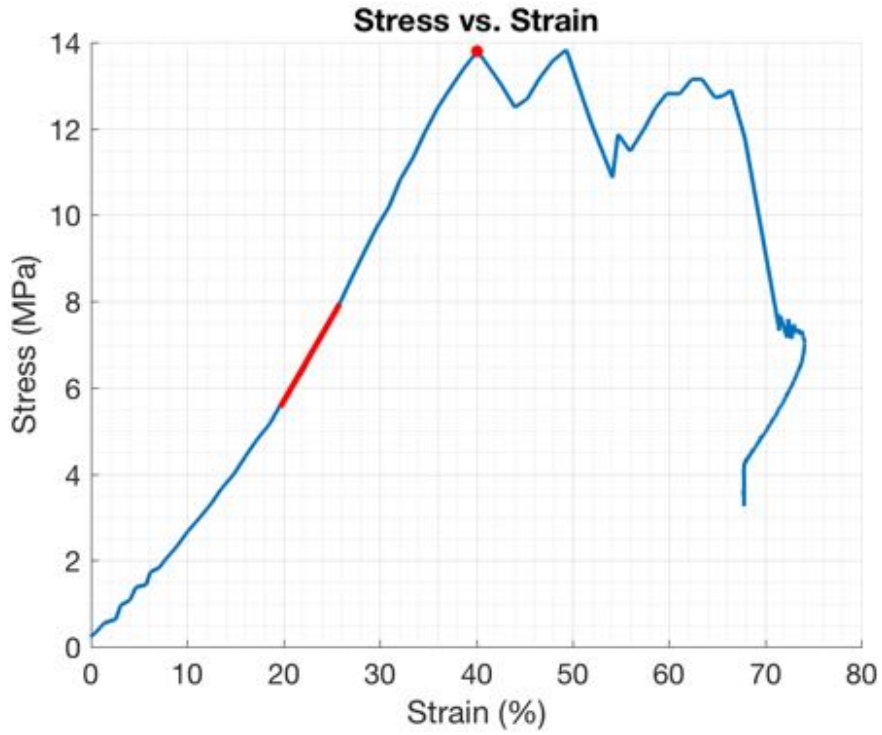
Date tested: 10/8/2017

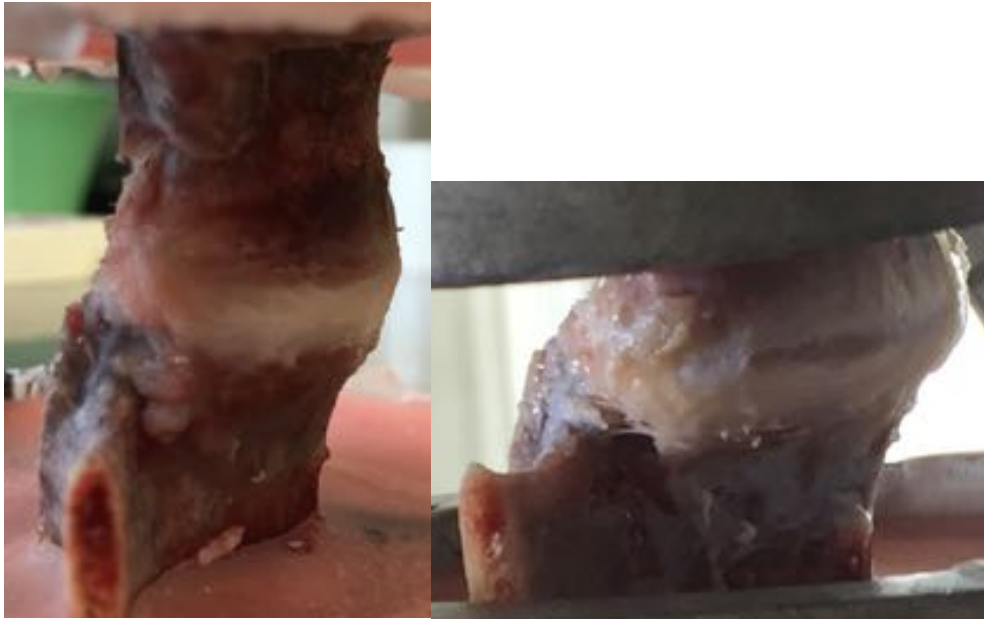
Failure load (kN)	Tz at failure (mm)	Time (s)	Moments (Nm)			Max Stress (MPa)	Max Strain (%)	Modulus (MPa)	Toughness (MJ/m ³)	Observations		
			Mx	My	Mz					Test	Disc	Vertebra
6.67	1.77	0.172	46.45	25.66	-2.14	13.81	40.13	38.7	2.5	AS, R-RAIL, POS-RAIL	R-POS at INF-VER	Shear EP torn from R INF-VER



Identification of events by video & load vs. displacement comparison

Event	Video		Load vs. Displacement	
	Time (s)	Description	Time (s)	Description
1	0.18	Small anterior shear	0.15	First small peak
2	0.185	Loud sound – no motion	0.174	Second small peak
3	0.21	Second loud sound – no motion	0.186	Small peak
4	0.215	Small shear forward	0.202	Plateau
5			0.214	Small peak





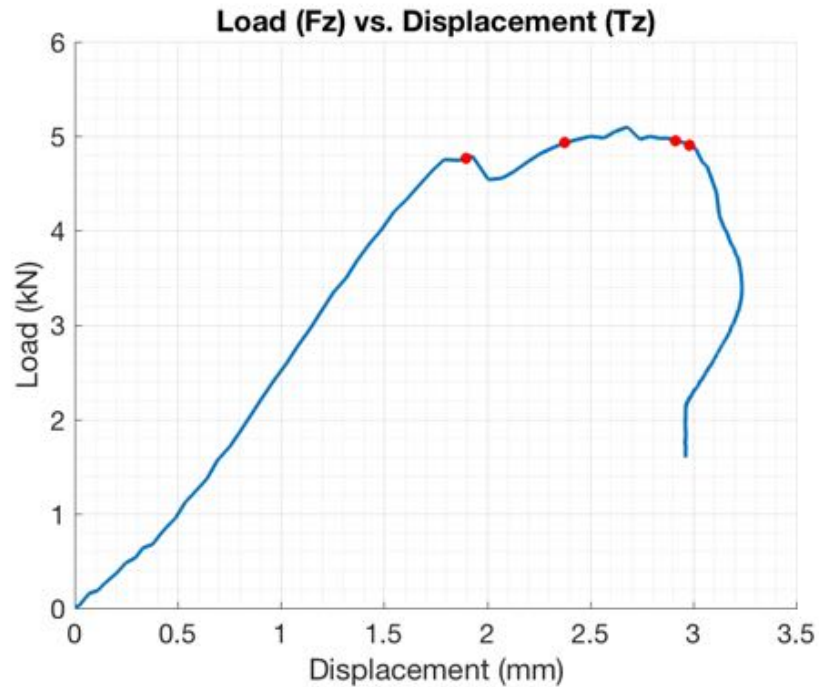
Failure Mode Assessment Summary			
	Load-displacement and video assessment	Photographic indicators	Classification
SO22	- No clear evidence	- Right inferior endplate-vertebra interface	HER (R-POS) + EP-VER

Specimen ID: SO23

Group: No Facet Flexion & Right Lateral Bending

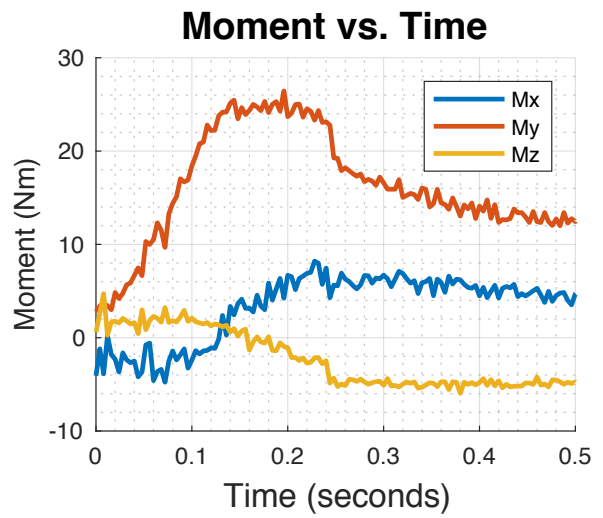
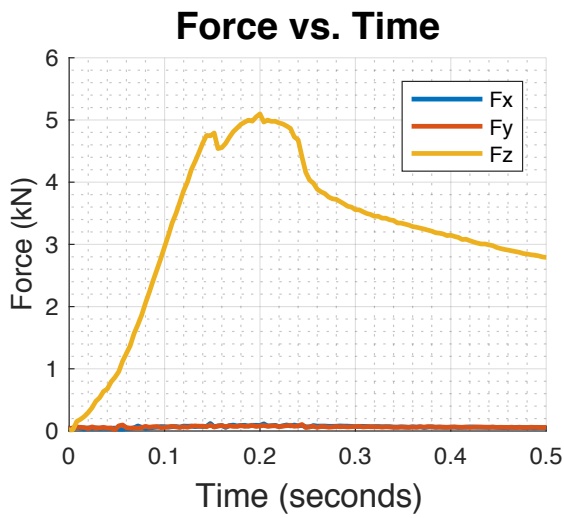
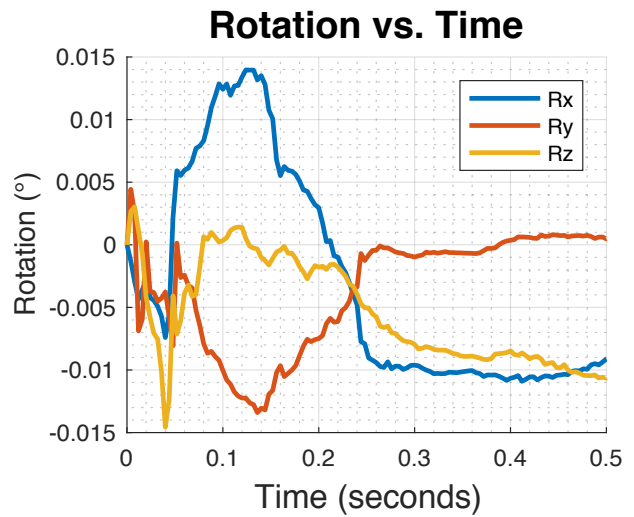
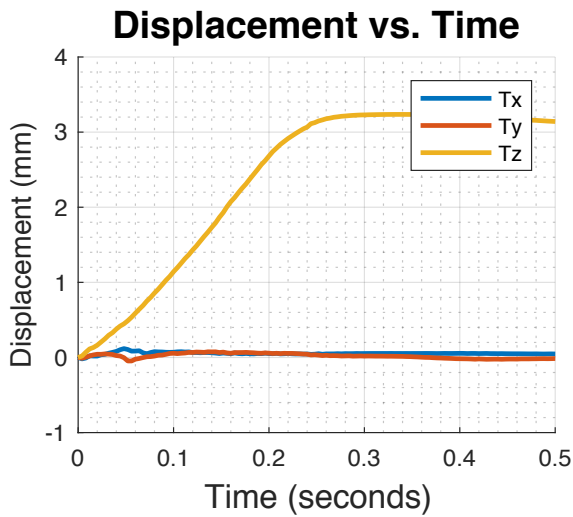
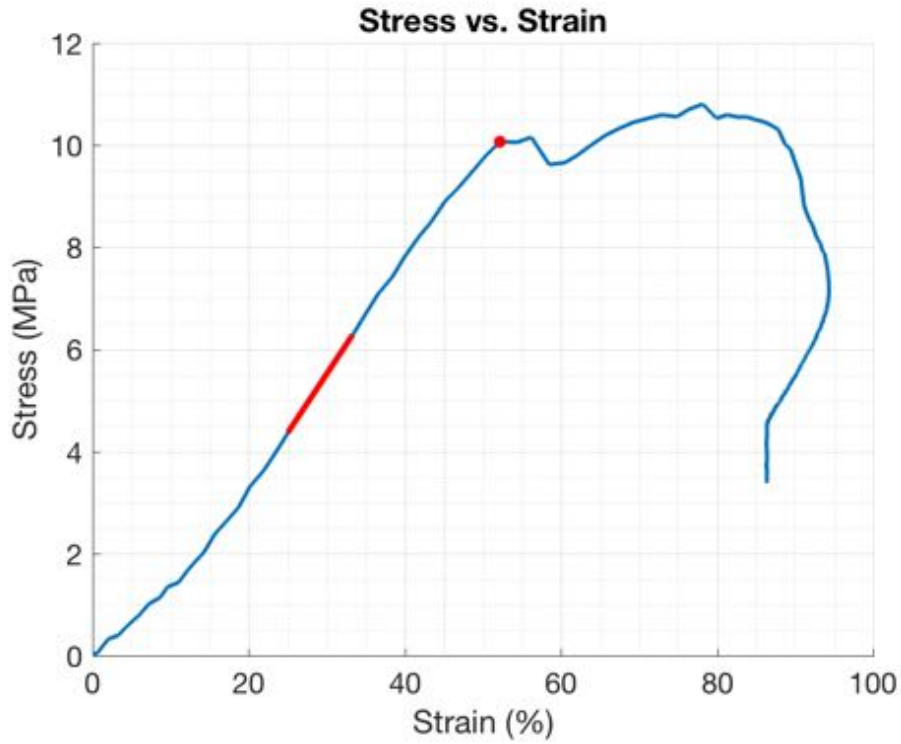
Date tested: 10/8/2017

Failure load (kN)	Tz at failure (mm)	Time (s)	Moments (Nm)			Max Stress (MPa)	Max Strain (%)	Modulus (MPa)	Toughness (MJ/m ³)	Observations		
			Mx	My	Mz					Test	Disc	Vertebra
4.75	1.79	0.2	2.44	25.45	0.98	10.07	52.22	23.1	2.5	AS, POS-RAIL, L-RAIL	-	R EP torn from INF VER



Identification of events by video & load vs. displacement comparison

Event	Video		Load vs. Displacement	
	Time (s)	Description	Time (s)	Description
1	0.15	Small shear forward	0.144	Small plateau and peak
2	0.18	Small shear forward	0.2	Small peak and highest peak
3	0.22	Loud sound – no motion	0.228	Decline slope
4	0.25	Small shear forward/ compress		

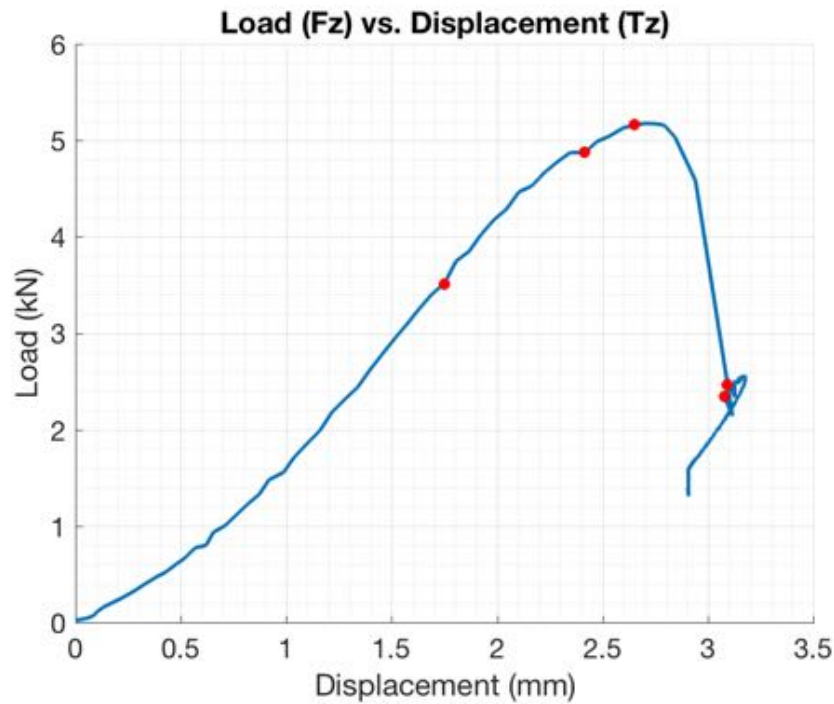




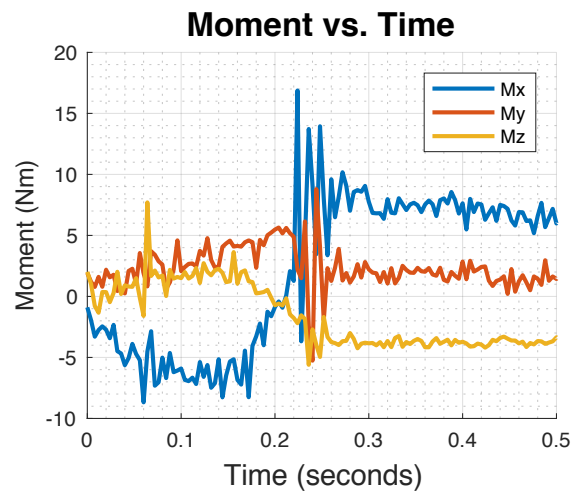
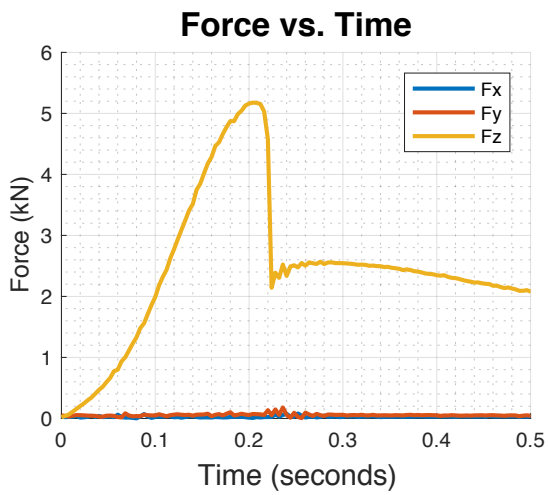
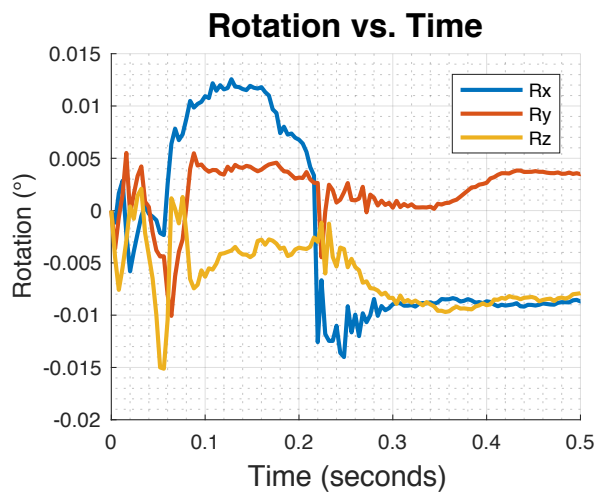
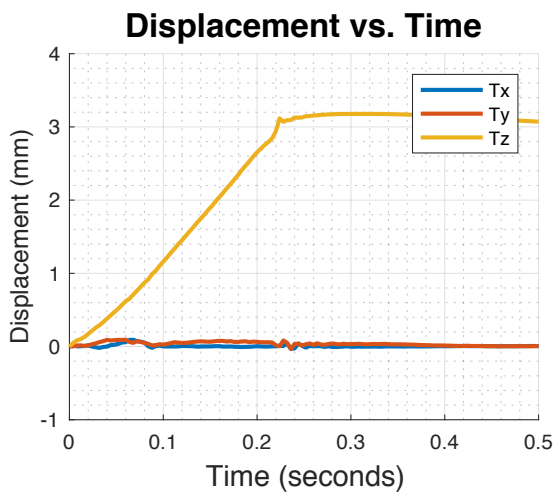
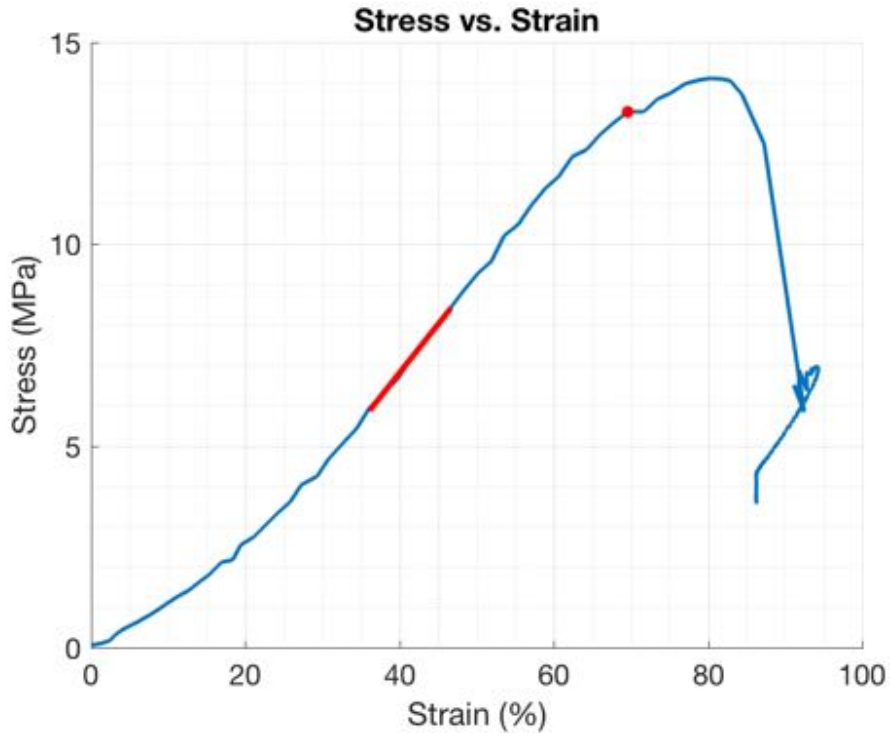
Failure Mode Assessment Summary			
	Load-displacement and video assessment	Photographic indicators	Classification
SO23	<ul style="list-style-type: none"> - FSU shear forward at plateau of load-displacement curve 	<ul style="list-style-type: none"> - Rupture of tissue at right side of inferior endplate vertebra interface - No disc extrusion 	EP-VER

Specimen ID: SO24
Group: No Facet Flexion
Date tested: 10/8/2017

Failure load (kN)	Tz at failure (mm)	Time (s)	Moments (Nm)			Max Stress (MPa)	Max Strain (%)	Modulus (MPa)	Toughness (MJ/m ³)	Observations		
			Mx	My	Mz					Test	Disc	Vertebra
4.87	2.35	0.204	-3.27	2.35	0.25	13.28	69.62	24.1	4.2	AS, POS-RAIL	ANT-BUL	INF end of INF-VER fracture



Identification of events by video & load vs. displacement comparison				
	Video		Load vs. Displacement	
Event	Time (s)	Description	Time (s)	Description
1	0.14	Shear forward	0.148	Small change in slope
2	0.17	Shear forward	0.184	Small plateau
3	0.205	Big shear forward + nucleus bulge + transverse process cracking	0.2	Larger plateau at peak of curve
4	0.23	Sound	0.22	Decline
5	0.235	Large sound + inferior VB break	0.232	Following decline, next small peak

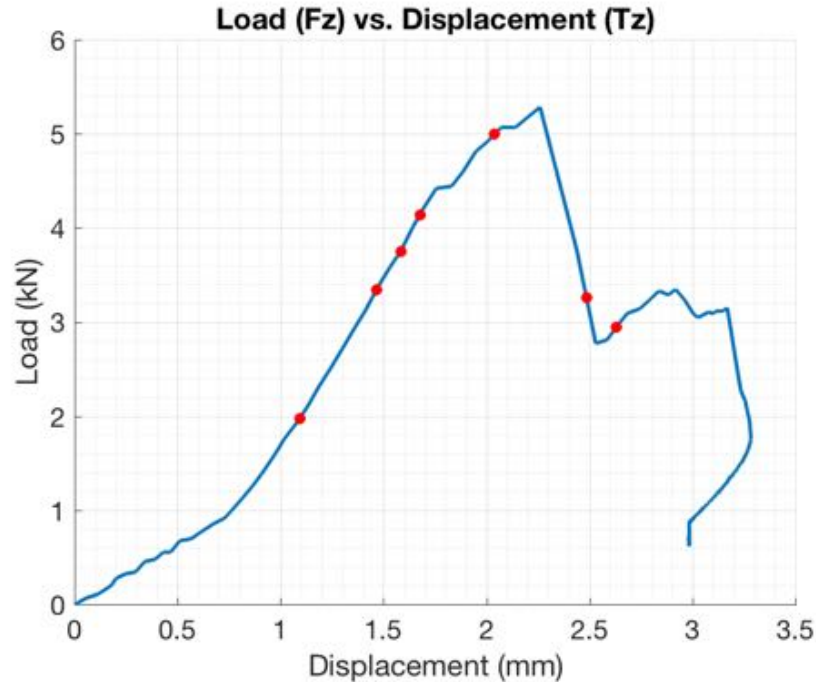




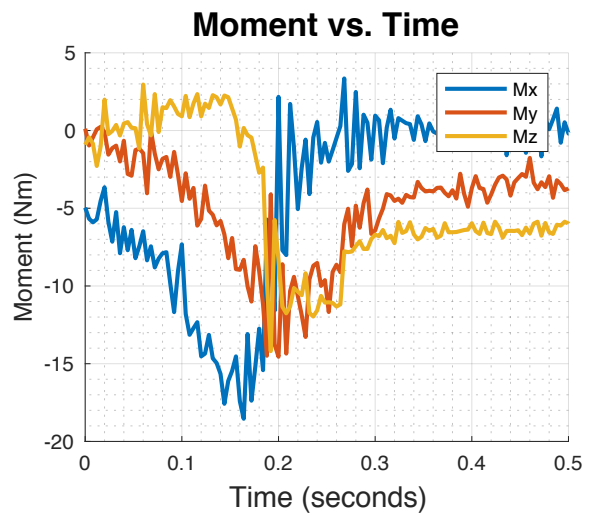
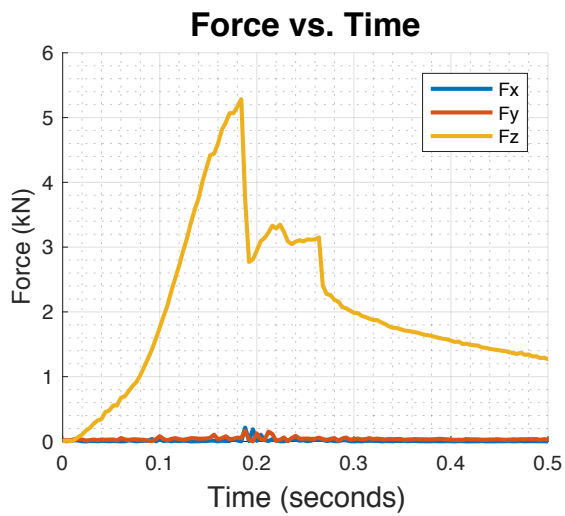
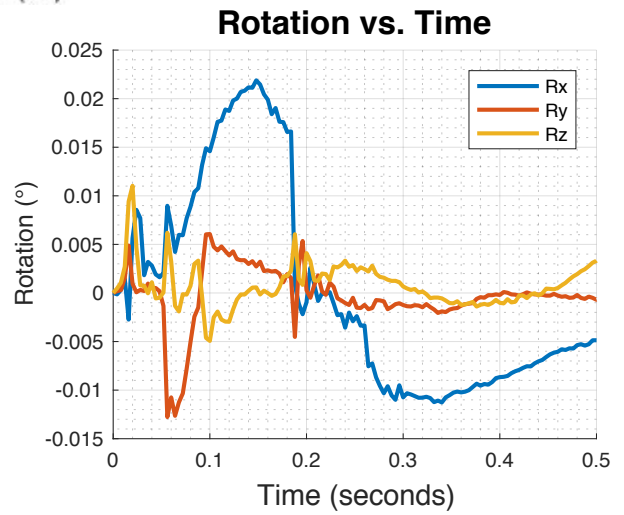
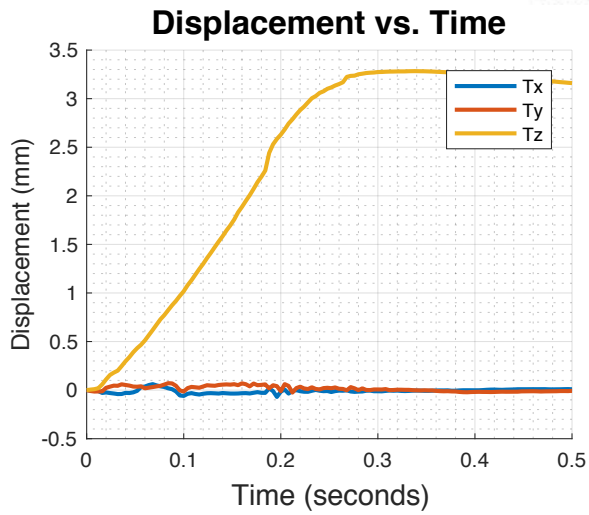
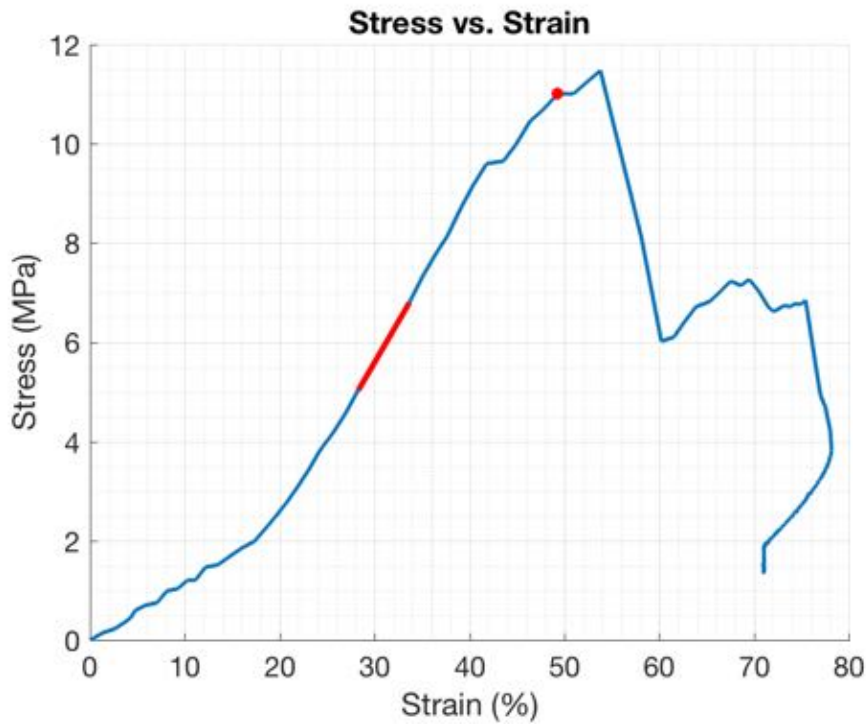
Failure Mode Assessment Summary			
	Load-displacement and video assessment	Photographic indicators	Classification
SO24	- Plateau and shearing of FSU followed by catastrophic fracture of inferior vertebra	- Inferior vertebra fracture	VER

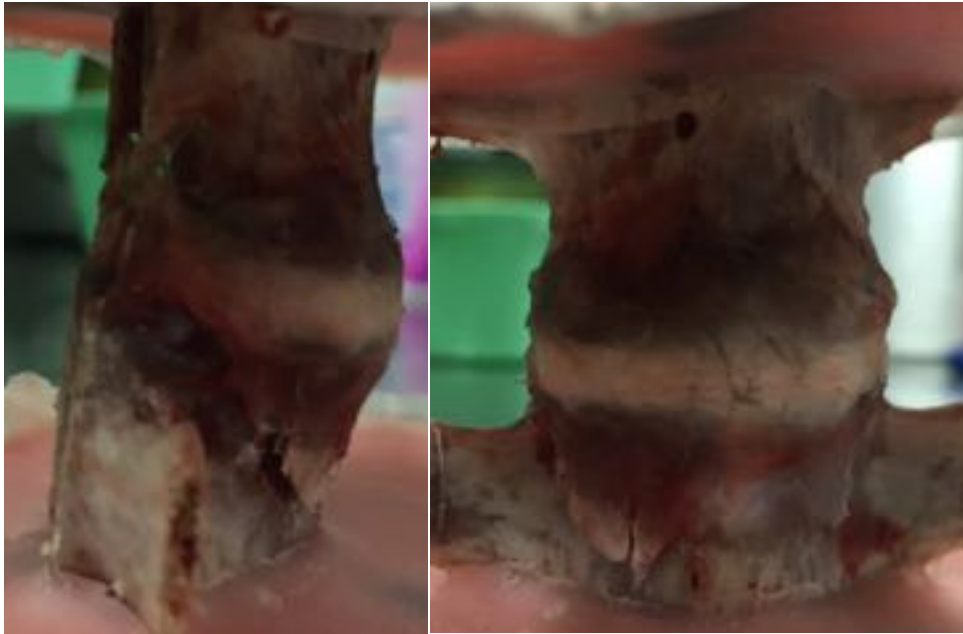
Specimen ID: SO25
Group: No Facet Flexion
Date tested: 10/8/2017

Failure load (kN)	Tz at failure (mm)	Time (s)	Moments (Nm)			Max Stress (MPa)	Max Strain (%)	Modulus (MPa)	Toughness (MJ/m ³)	Observations		
			Mx	My	Mz					Test	Disc	Vertebra
5.07	2.07	0.184	-17.38	-11.00	-0.45	11.01	49.33	32.8	2.3	AS, POS-RAIL	POS-NE	Shear EP torn from INF-VER



Identification of events by video & load vs. displacement comparison				
	Video		Load vs. Displacement	
Event	Time (s)	Description	Time (s)	Description
1	0.105	Small shear forward	0.128	Small change in slope
2	0.1315	Small sound – no motion	0.144	Small plateau
3	0.14	Small shear forward	0.164	Second small plateau
4	0.1465	Larger sound – no motion	0.176	Highest peak before decline
5	0.17	Small shear forward and sound	0.196	Small change in upward slope
6	0.19	Sound – no motion	0.208	Small plateau
7	0.2035	Larger shear forward	0.216	Small peak





Failure Mode Assessment Summary

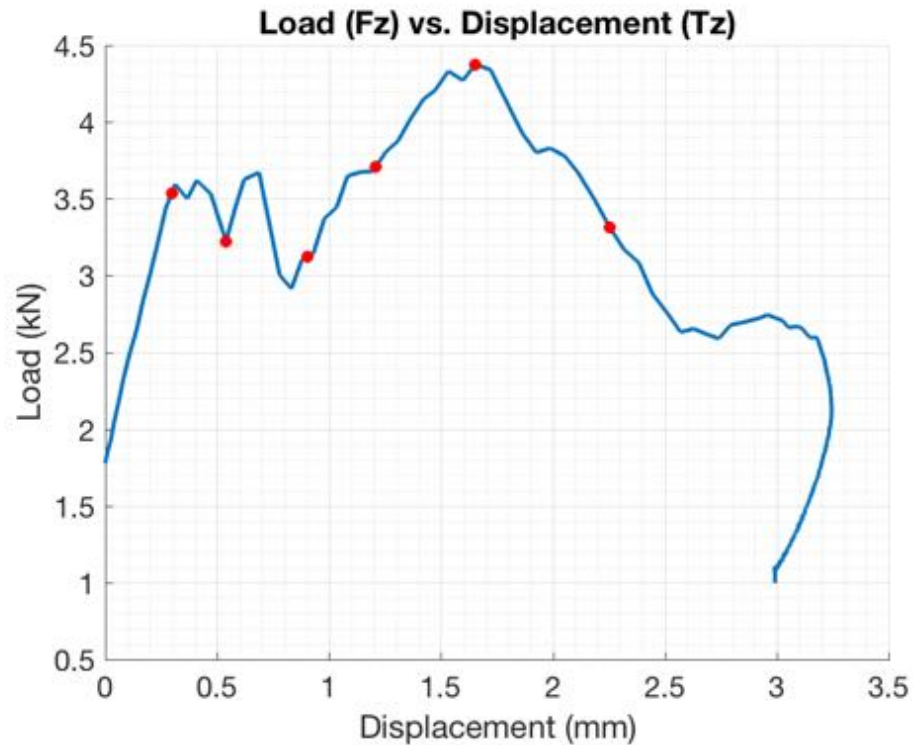
	Load-displacement and video assessment	Photographic indicators	Classification
SO25	- Gradual shearing of the vertebra before catastrophic shear fracture of inferior vertebra	- Anterior shear fracture on inferior vertebra	HER (POS) + EP-VER

Specimen ID: SO26

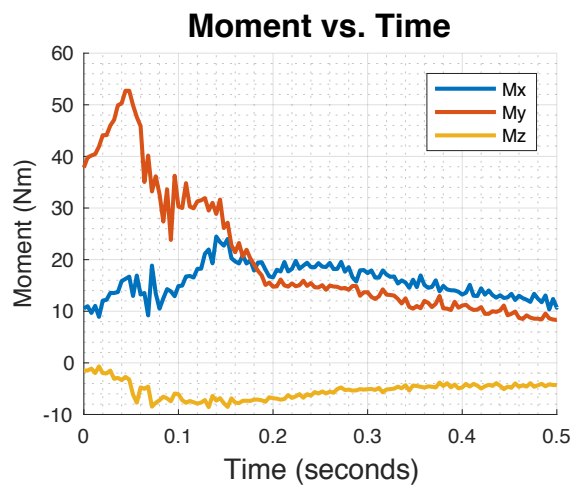
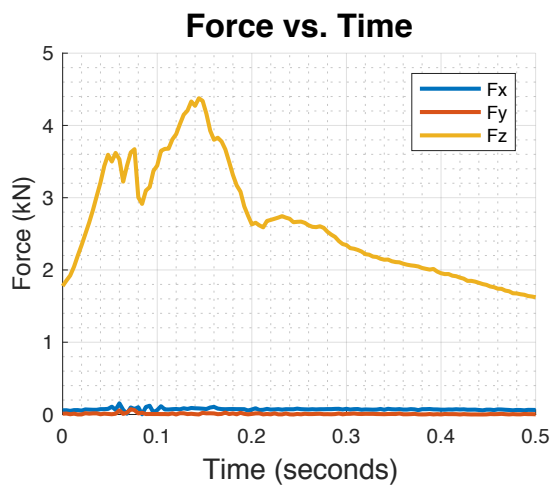
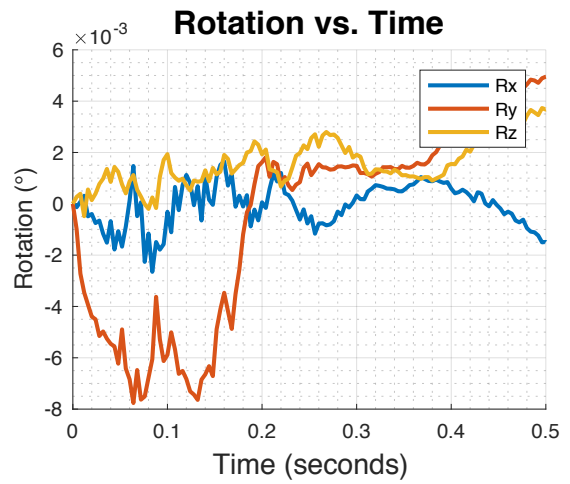
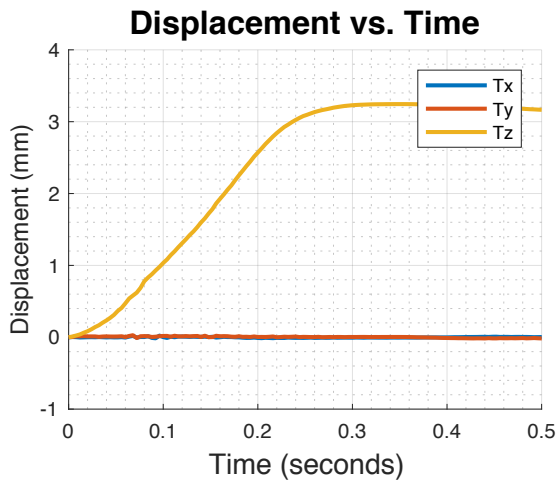
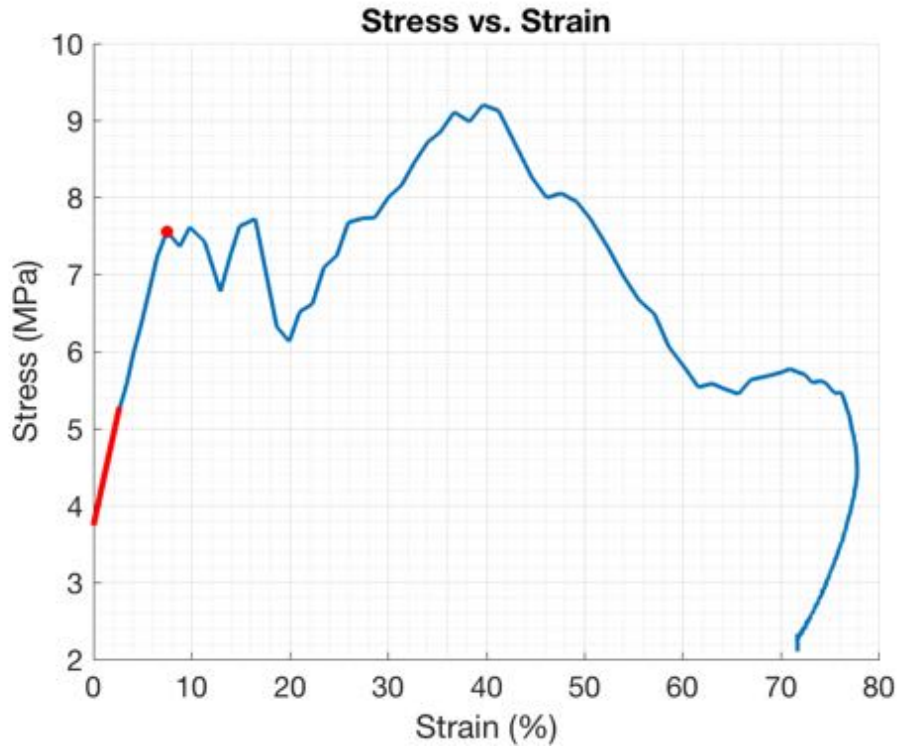
Group: No Facet Right Lateral Bending

Date tested: 11/8/2017

Failure load (kN)	Tz at failure (mm)	Time (s)	Moments (Nm)			Max Stress (MPa)	Max Strain (%)	Modulus (MPa)	Toughness (MJ/m ³)	Observations		
			Mx	My	Mz					Test	Disc	Vertebra
3.59	0.31	0.144	16.71	52.72	-3.22	7.56	7.48	57.9	4.3	AS, L-RAIL	BUL	Shear EP torn from INF-VER



Identification of events by video & load vs. displacement comparison				
	Video		Load vs. Displacement	
Event	Time (s)	Description	Time (s)	Description
1	0.0465	Compression + bulging of disc	0.056	First small peak
2	0.067	Loud noise – no damage	0.064	Second small peak
3	0.09	Loud noise – no damage	0.084	Third small peak then drop
4	0.115	Shear forward	0.112	Small plateau as climbing to peak
5	0.1435	Shear forward	0.144	Highest peak
6	0.18	Shear forward	0.176	Small plateau downward





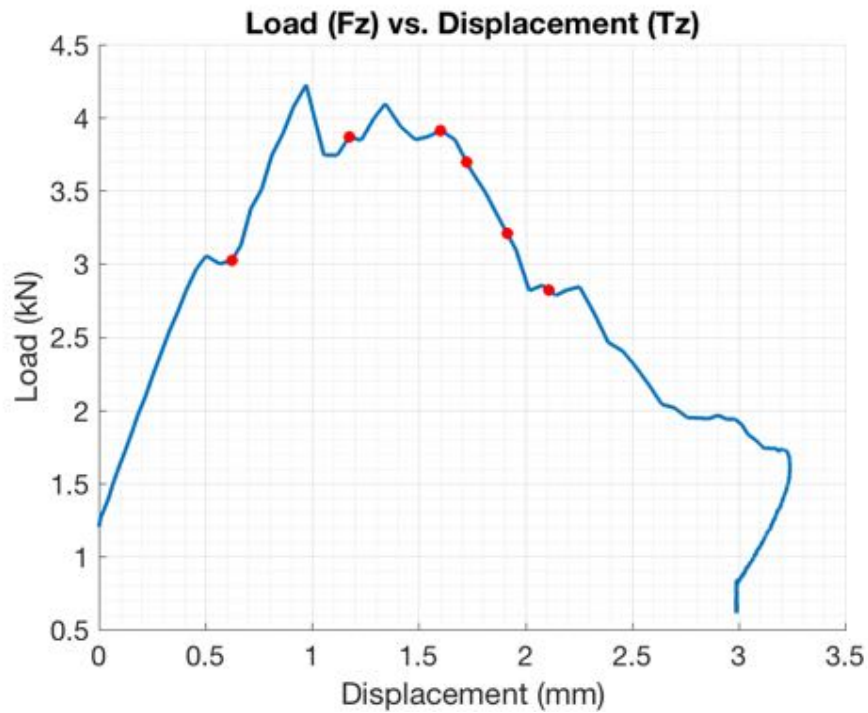
Failure Mode Assessment Summary			
	Load-displacement and video assessment	Photographic indicators	Classification
SO26	- Gradual continual shearing forward of FSU	- Tear at endplate/vertebra interface	EP-VER

Specimen ID: SO27

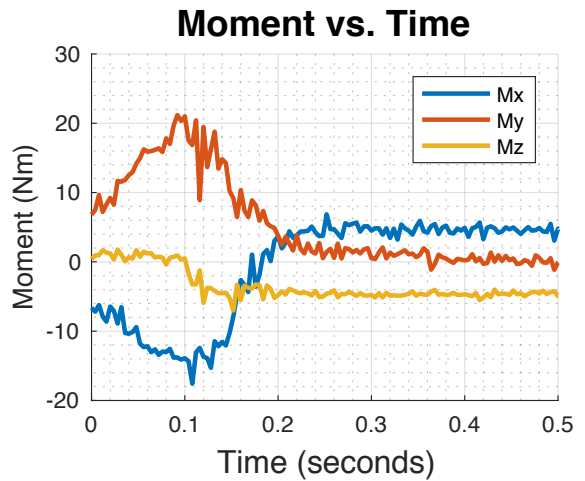
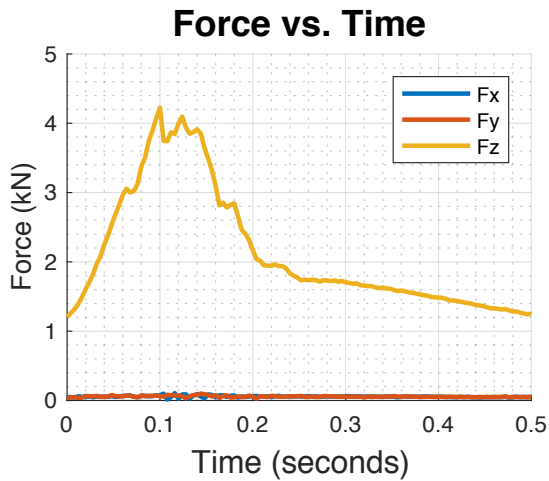
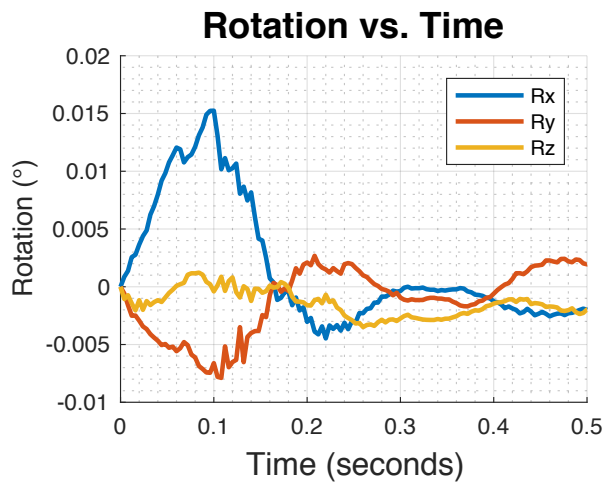
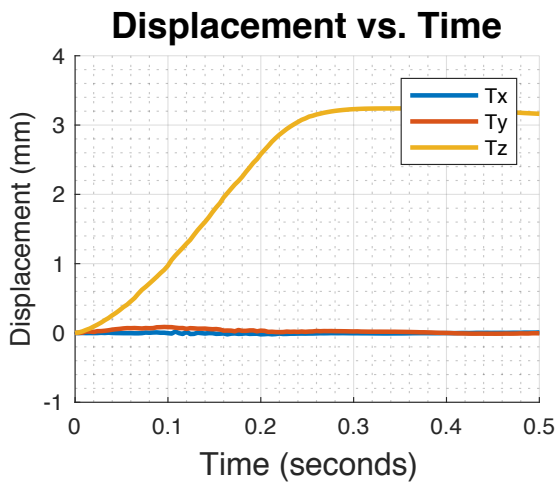
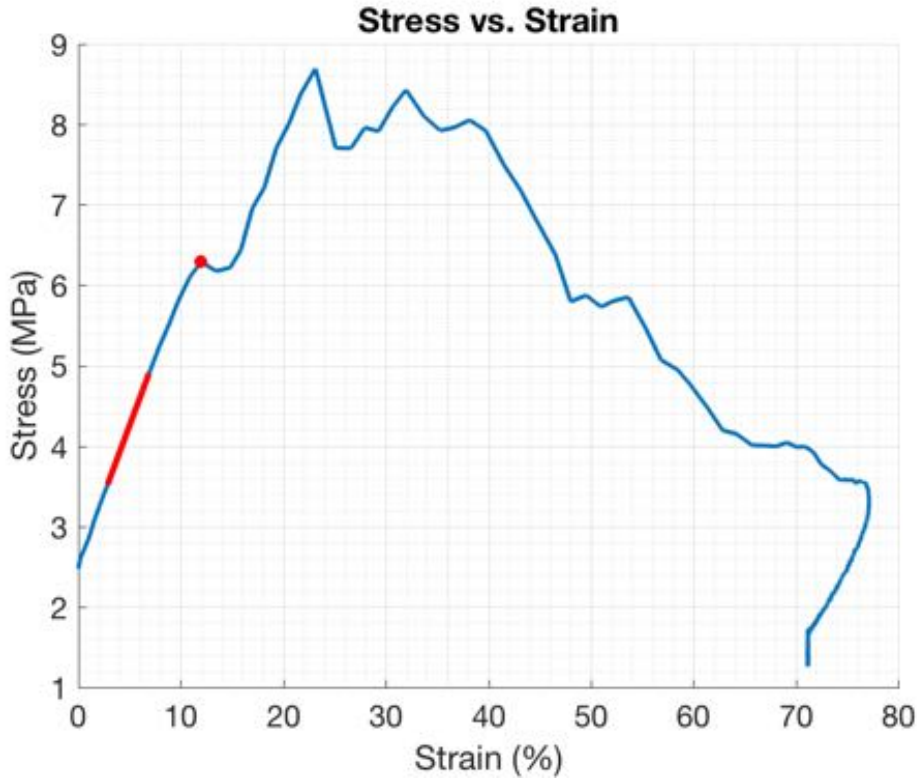
Group: No Facet Flexion & Right Lateral Bending

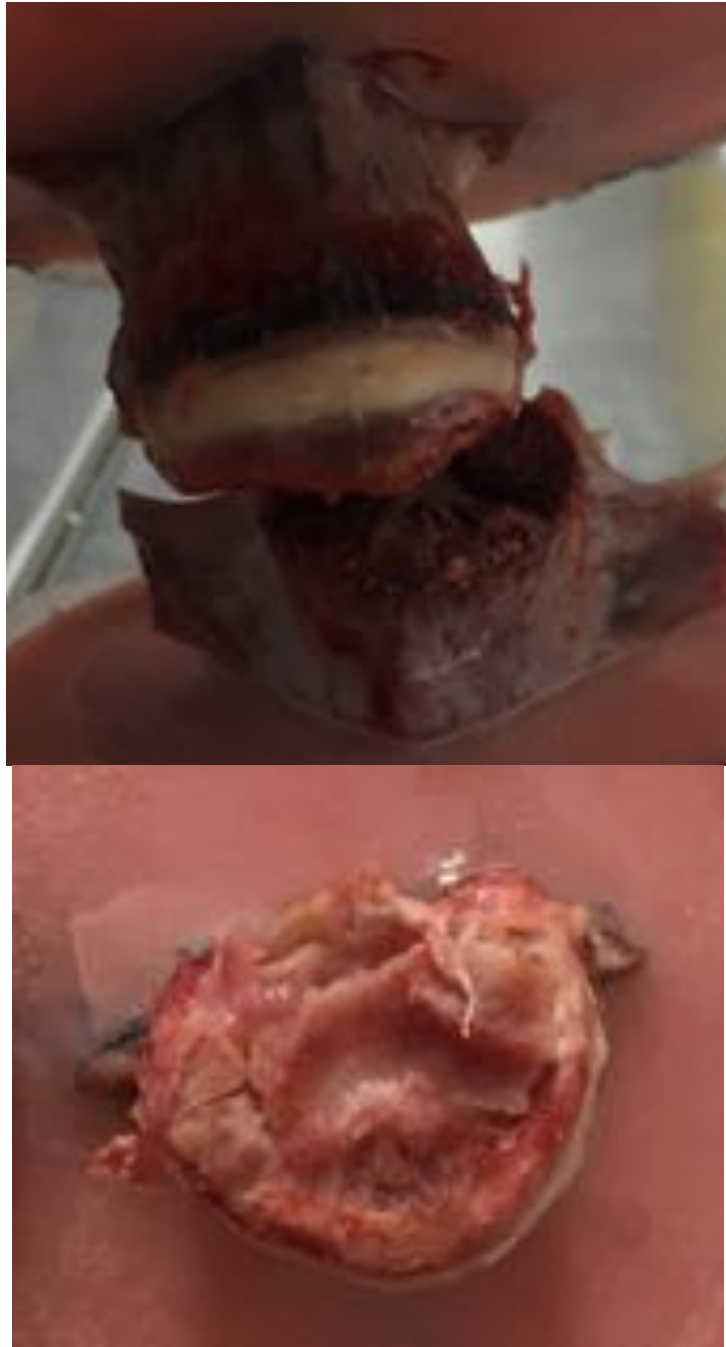
Date tested: 11/8/2017

Failure load (kN)	Tz at failure (mm)	Time (s)	Moments (Nm)			Stress (MPa)	Strain (%)	Modulus (MPa)	Toughness (MJ/m ³)	Observations		
			Mx	My	Mz					Test	Disc	Vertebra
3.06	0.50	0.1	-13.04	15.99	1.25	6.29	11.98	34.2	5.4	AS, POS-RAIL, L-RAIL	R-POS	Shear EP torn from INF-VER



Identification of events by video & load vs. displacement comparison				
	Video		Load vs. Displacement	
Event	Time (s)	Description	Time (s)	Description
1	0.072	Shear forward	0.064	Abrupt plateau
2	0.112	Loud noise + bulge	0.1	Highest peak
3	0.14	Large shear forward	0.124	Second peak
4	0.147	Loud sound	0.14	Third peak before decline
5	0.158	Loud sound	0.164	Bumpy plateau
6	0.17	Large shear forward	0.18	Final decline





Failure Mode Assessment Summary

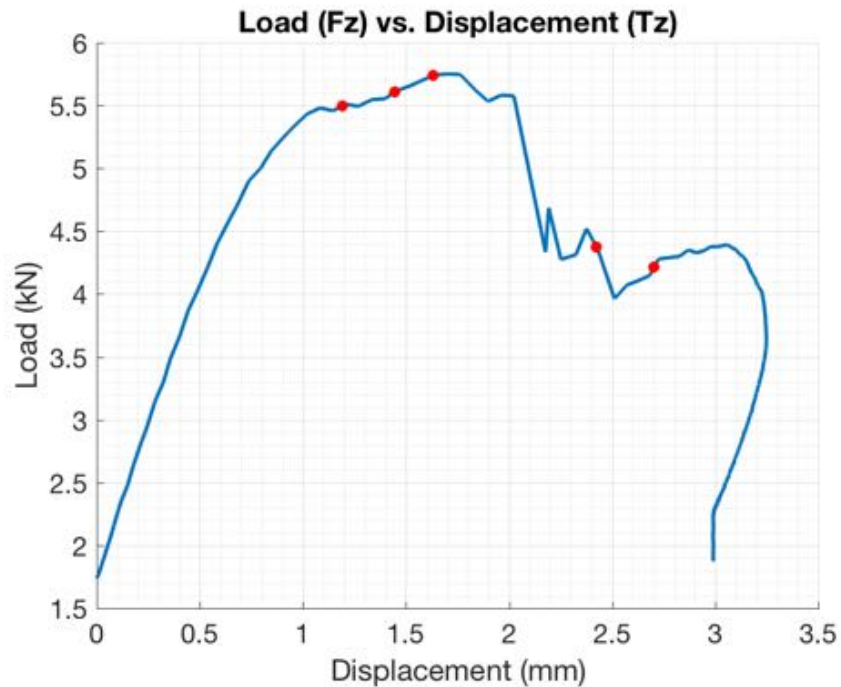
	Load-displacement and video assessment	Photographic indicators	Classification
SO27	- No clear evidence – gradual shearing	- Inferior vertebra sheared in two - When separated, damage at the endplate, nucleus extruding	HER (POS) + EP-VER

Specimen ID: SO28

Group: Facet Flexion & Right Lateral Bending

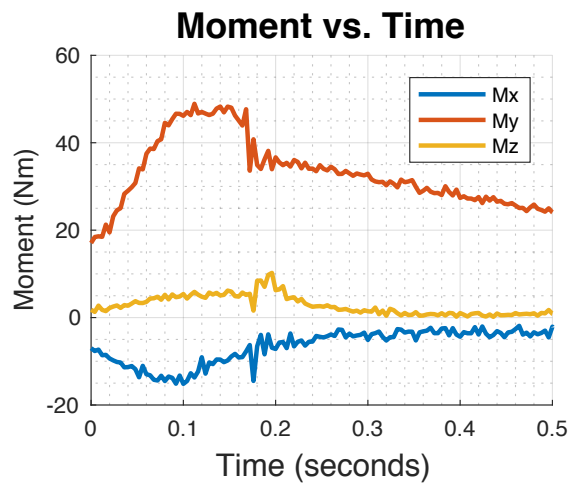
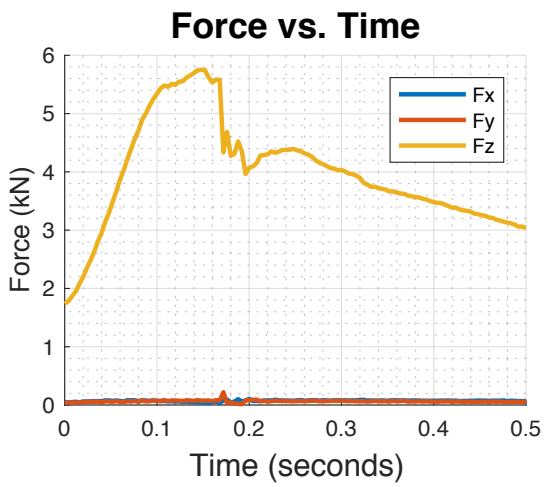
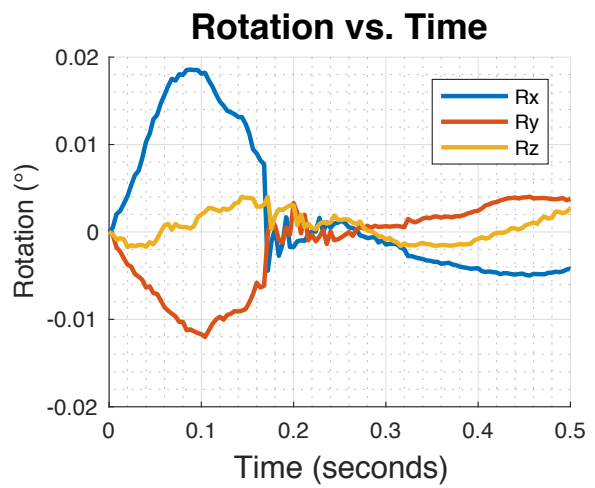
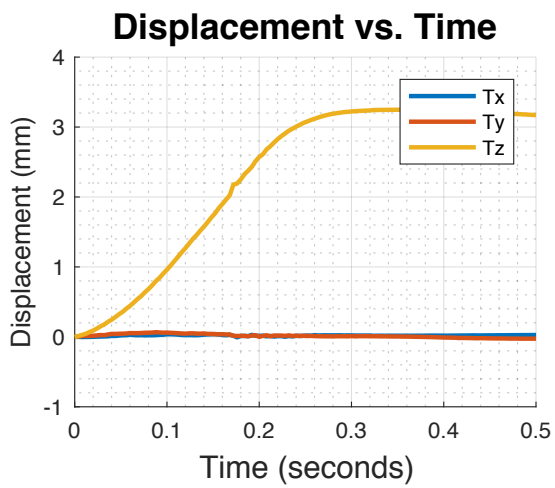
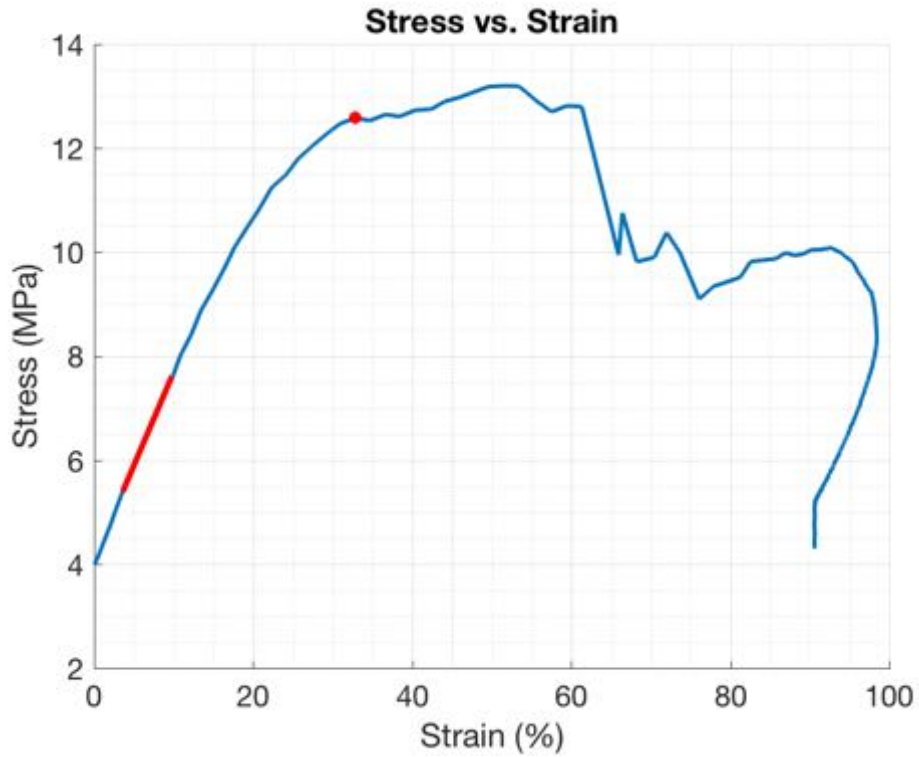
Date tested: 11/8/2017

Failure load (kN)	Tz at failure (mm)	Time (s)	Moments (Nm)			Stress (MPa)	Strain	Modulus (MPa)	Toughness (MJ/m ³)	Observations		
			Mx	My	Mz					Test	Disc	Vertebra
5.48	1.08	0.148	-12.74	46.32	5.20	12.58	32.81	35.8	3.0	AS, POS-RAIL, L-RAIL		-



Identification of events by video & load vs. displacement comparison

Event	Video		Load vs. Displacement	
	Time (s)	Description	Time (s)	Description
1	0.115	Small shear forward	0.115	Start of plateau
2	0.1315	Loud sound – no movement	0.13	Bumpy plateau before peak
3	0.1435	Small shear forward	0.16	First highest peak followed by small decline
4	0.1915	Loud sound – no movement	0.18	Second peak then big decline
5	0.21	Small shear forward	0.188	Next peak then decline

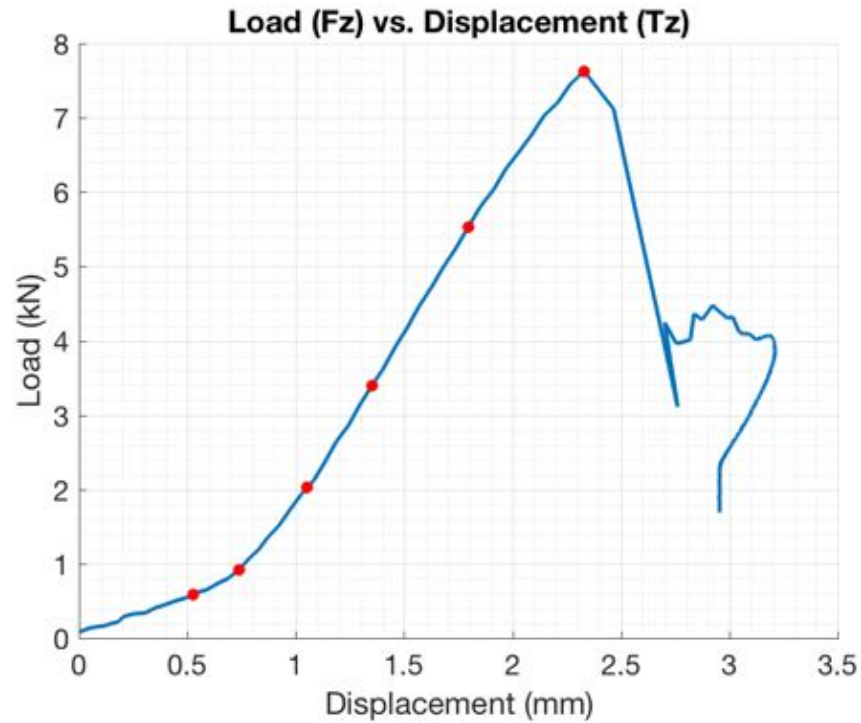




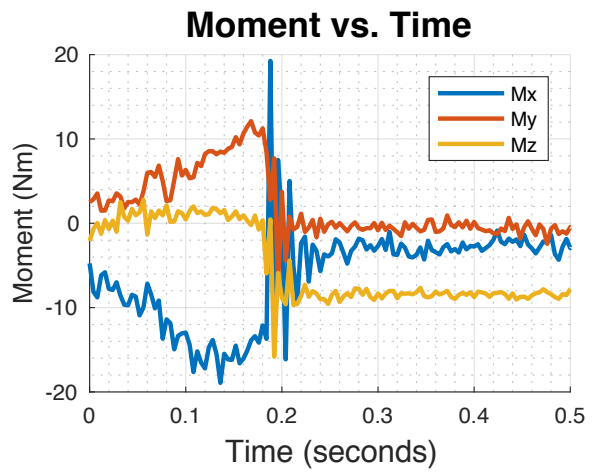
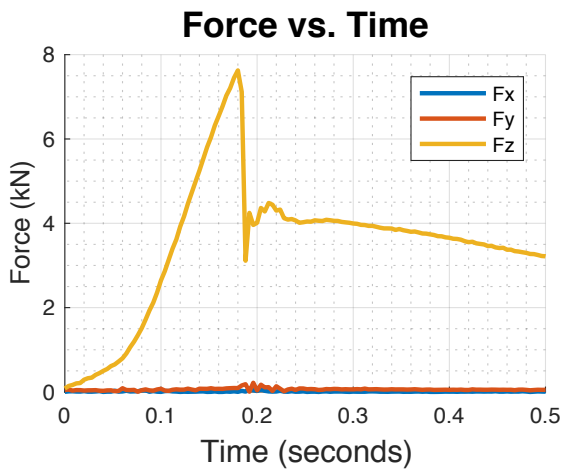
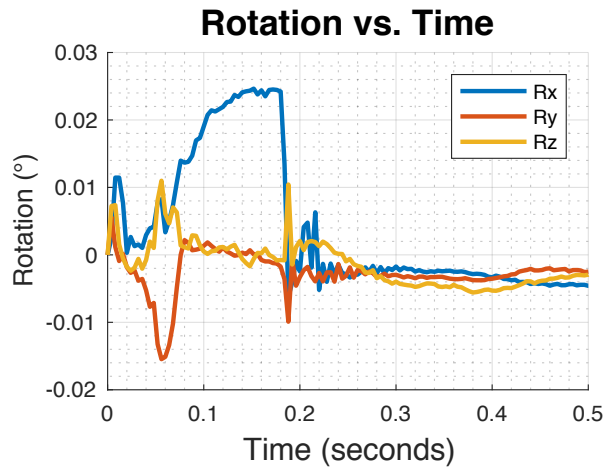
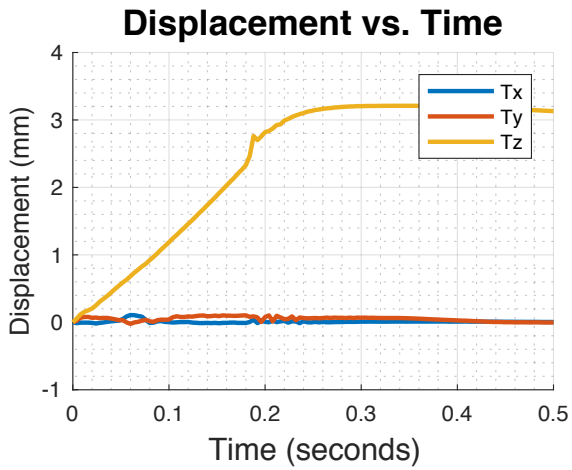
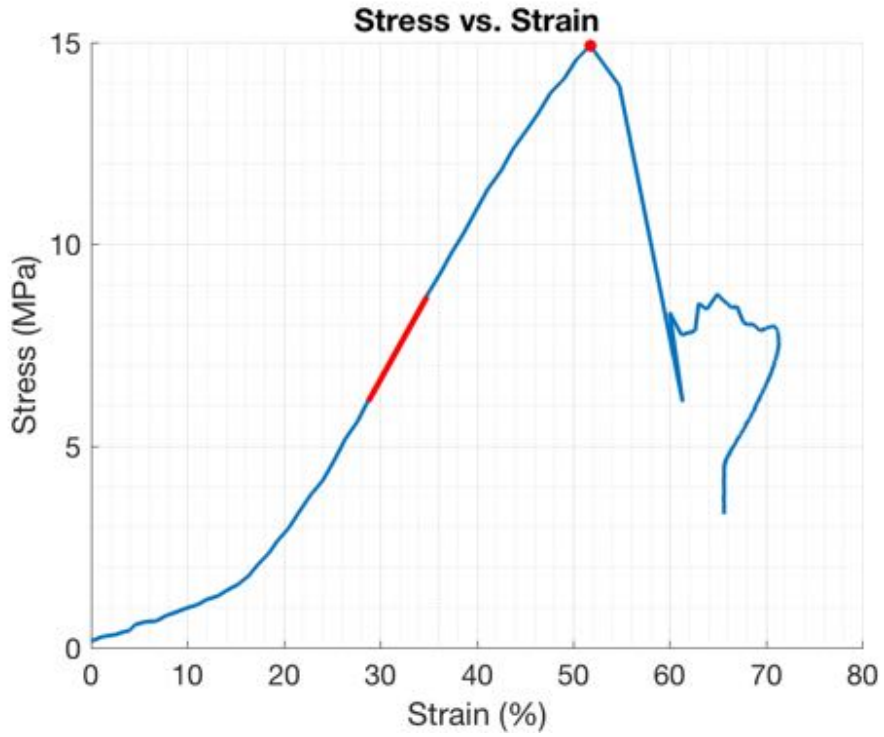
Failure Mode Assessment Summary			
	Load-displacement and video assessment	Photographic indicators	Classification
SO28	<ul style="list-style-type: none"> - Long plateau and then decline - No visible evidence 	<ul style="list-style-type: none"> - No visible evidence of damage 	IN

Specimen ID: SO29
Group: No Facet Flexion
Date tested: 11/8/2017

Failure load (kN)	Tz at failure (mm)	Time (s)	Moments (Nm)			Max Stress (MPa)	Max Strain	Modulus (MPa)	Toughness (MJ/m ³)	Observations		
			Mx	My	Mz					Test	Disc	Vertebra
7.63	2.33	0.18	-12.11	11.26	0.36	14.92	51.78	42.7	3.1			



		Video	Load vs. Displacement	
Event	Time (s)	Description	Time (s)	Description
1	0.0465	Compression + bulging of disc	0.056	First small peak
2	0.064	Loud noise – no damage	0.064	Second small peak
3	0.09	Loud noise – no damage	0.084	Third small peak then drop
4	0.112	Shear forward	0.112	Small plateau as climbing to peak
5	0.144	Shear forward	0.144	Highest peak
6	0.18	Shear forward	0.176	Small plateau downward

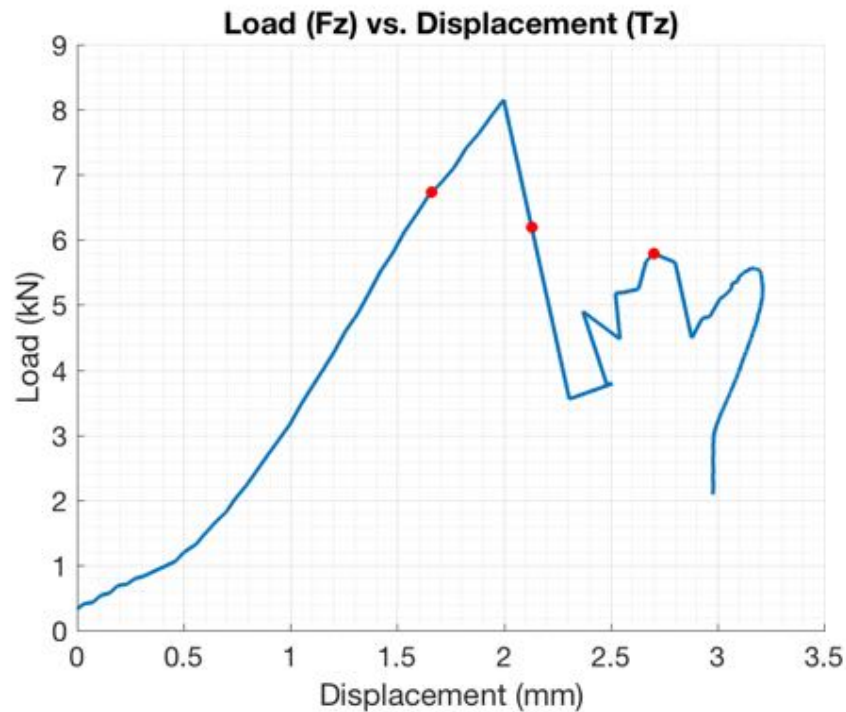




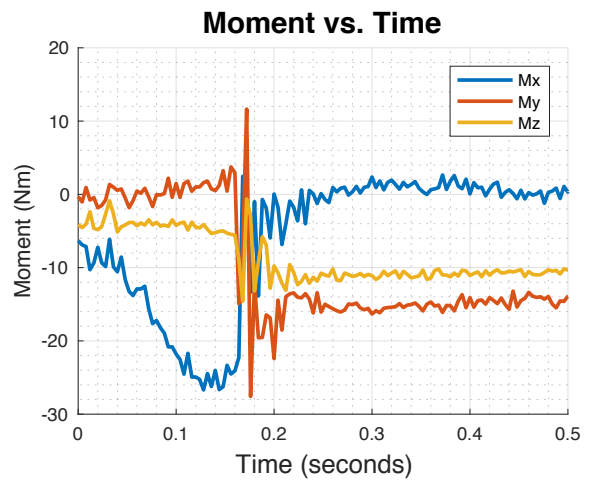
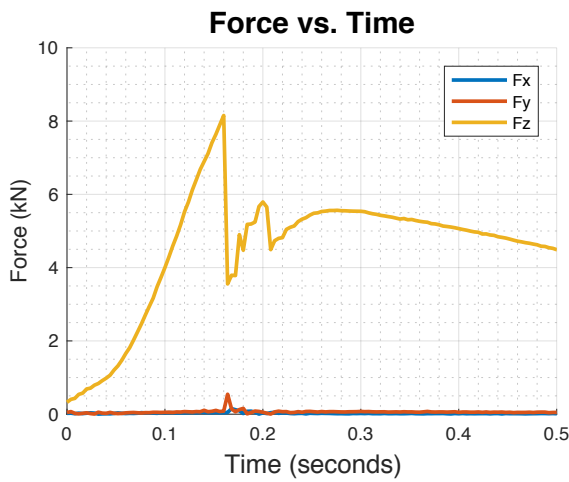
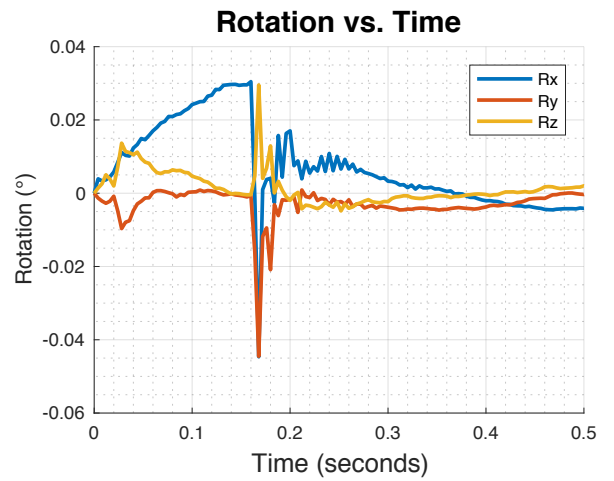
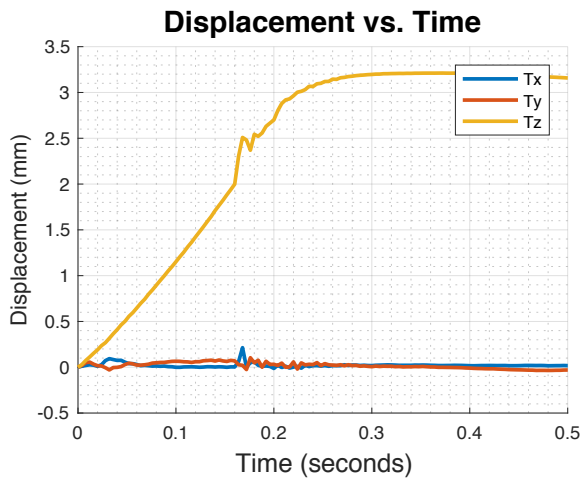
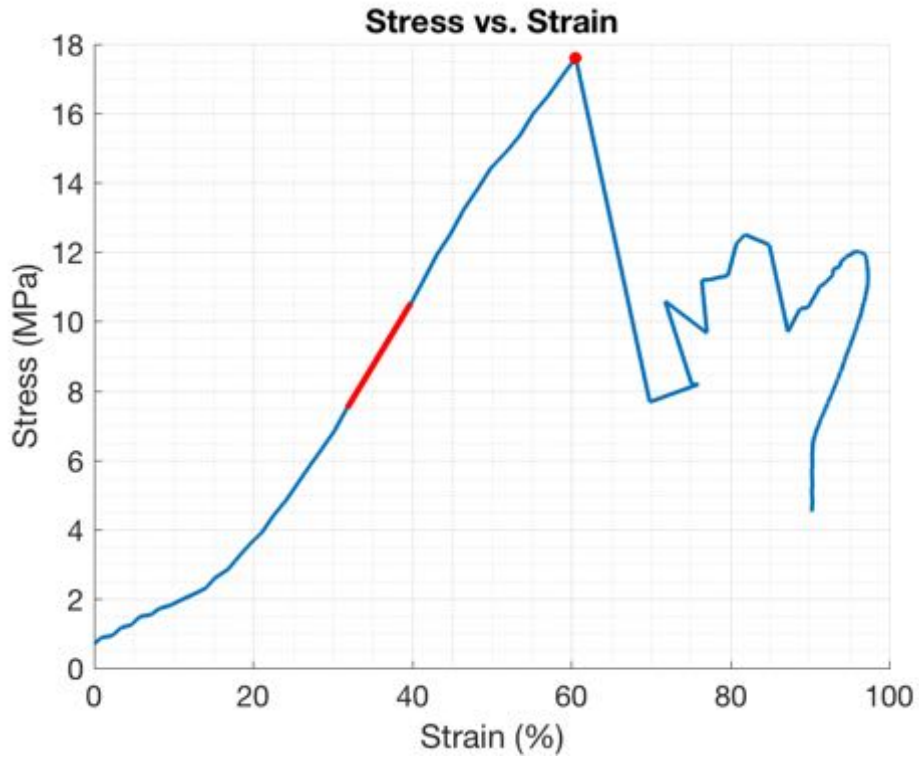
Failure Mode Assessment Summary			
	Load-displacement and video assessment	Photographic indicators	Classification
SO29	<ul style="list-style-type: none"> - Gradual shearing of FSU forward - No conclusive evidence 	<ul style="list-style-type: none"> - Right shear endplate-vertebra interface 	EP-VER

Specimen ID: SO30
Group: Facet Flexion
Date tested: 11/8/2017

Failure load (kN)	Tz at failure (mm)	Time (s)	Moments (Nm)			Stress (MPa)	Strain (%)	Modulus (MPa)	Toughness (MJ/m ³)	Observations		
			Mx	My	Mz					Test	Disc	Vertebra
8.15	2.00	0.16	-24.08	2.95	-5.55	17.61	60.56	37.8	4.7	AS, POS-RAIL	-	R-ANT INF-VER



Identification of events by video & load vs. displacement comparison				
Event	Video		Load vs. Displacement	
	Time (s)	Description	Time (s)	Description
1	0.137	Loud sound	0.136	Change in slope
2	0.1617	Loud sound 2	0.16	Peak before steep decline
3	0.20	Loud sound 3	0.2	Final peak before test end





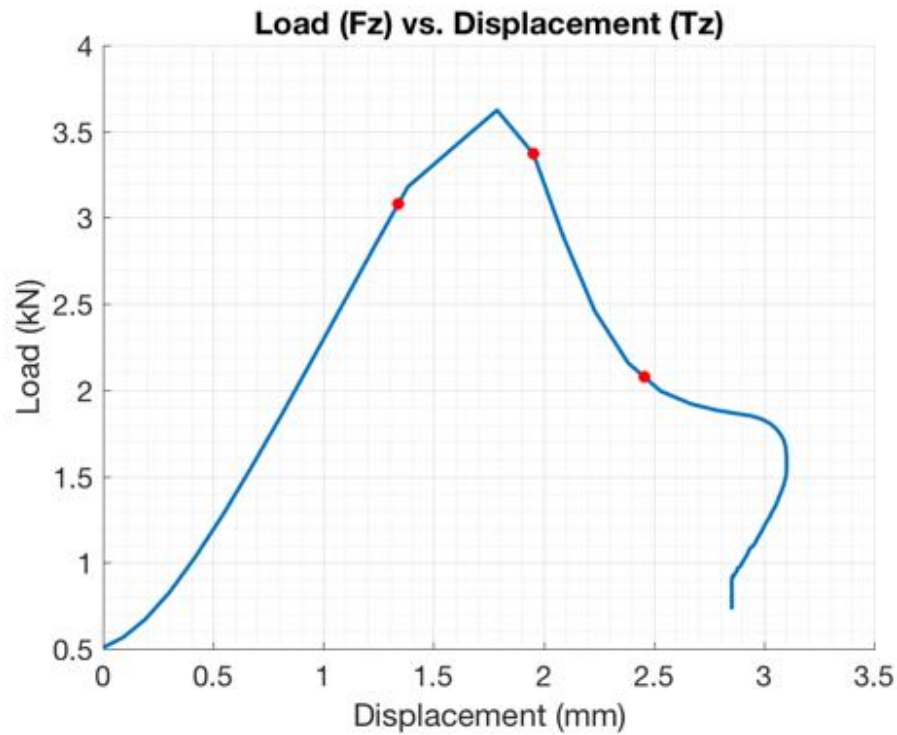
Failure Mode Assessment Summary			
	Load-displacement and video assessment	Photographic indicators	Classification
SO30	- No correlation	<ul style="list-style-type: none"> - Anterior shear fracture of inferior vertebra - Possible nucleus extrusion in spinal canal but inconclusive 	VER(ANT-SHEAR)

Specimen ID: SO31

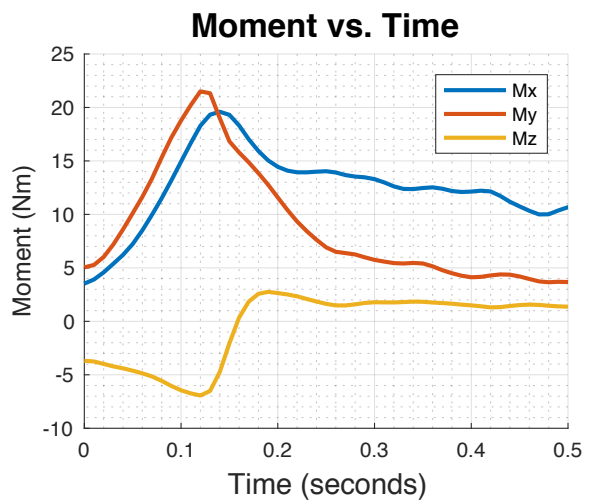
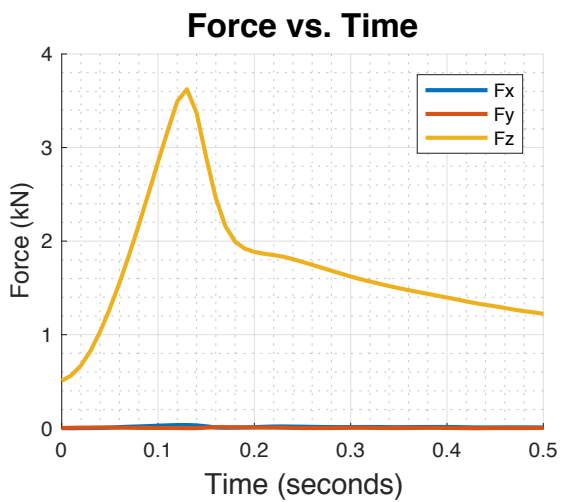
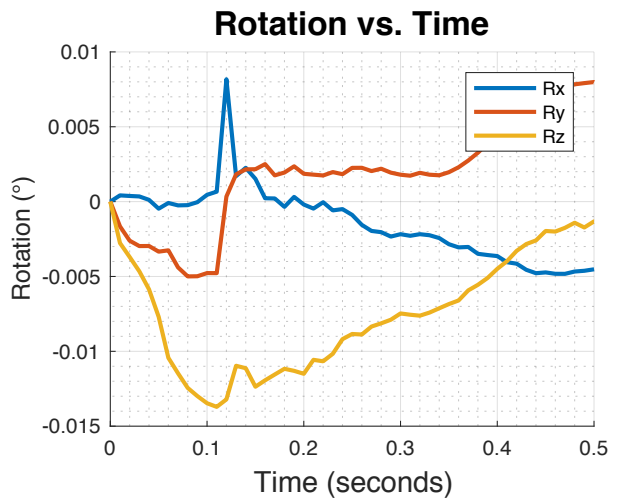
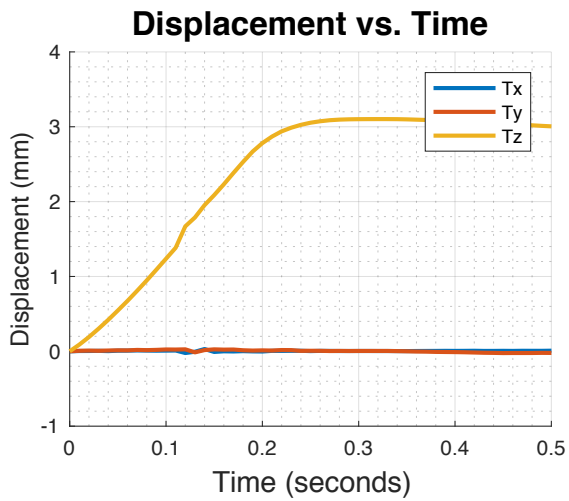
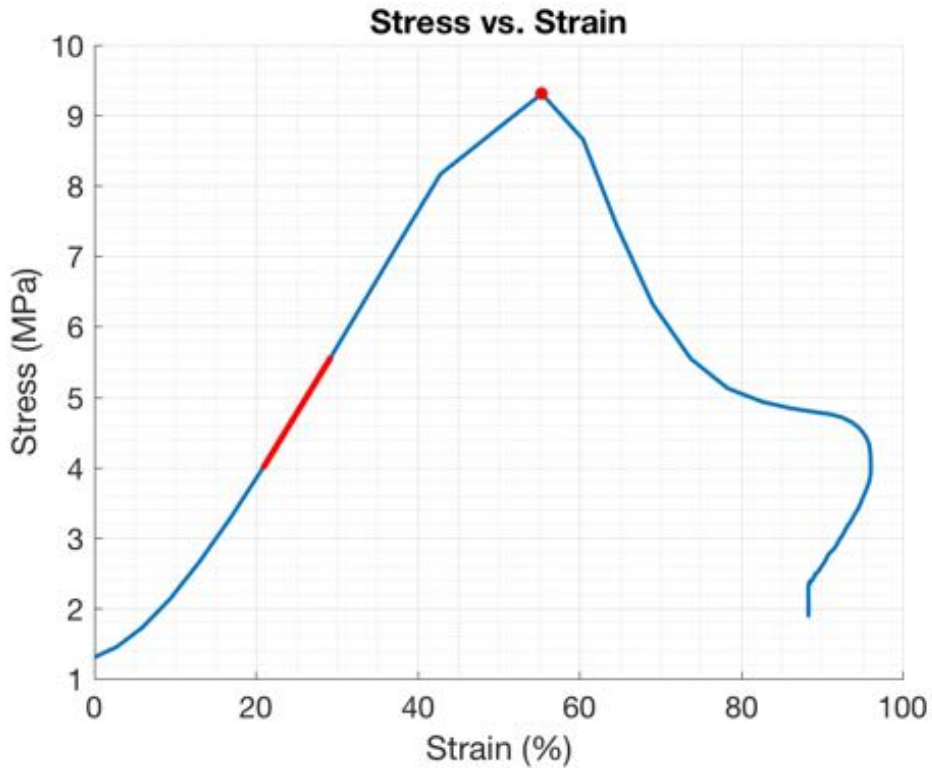
Group: No Facet Right Lateral Bending & Right Axial Rotation

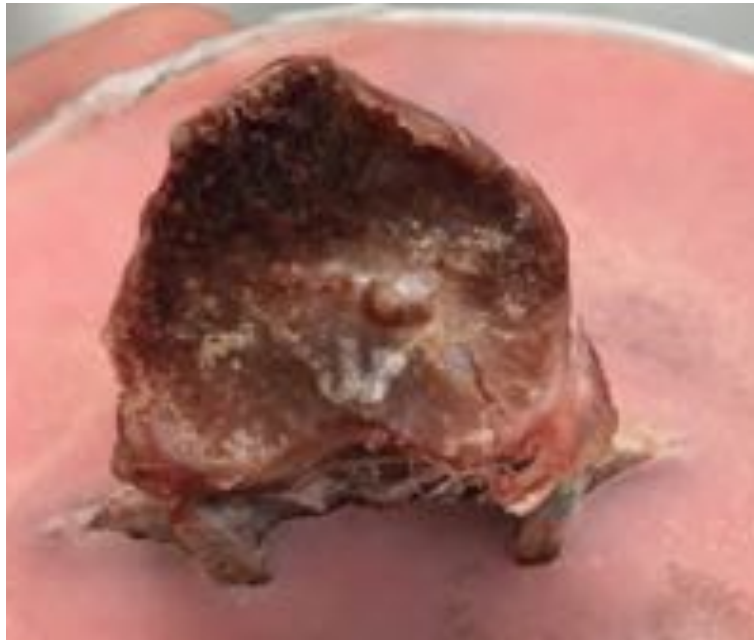
Date tested: 14/8/2017

Failure load (kN)	Tz at failure (mm)	Time (s)	Moments (Nm)			Max Stress (MPa)	Max Strain	Modulus (MPa)	Toughness (MJ/m ³)	Observations		
			Mx	My	Mz					Test	Disc	Vertebra
3.62	1.79	0.13	19.33	21.33	-6.51	9.31	55.36	2.9	293.08	AS	INF-EPJF	INF EP shear off INF VER



Identification of events by video & load vs. displacement comparison				
	Video		Load vs. Displacement	
Event	Time (s)	Description	Time (s)	Description
1	0.107	Bulge	0.12	Change in slope - decrease
2	0.14	Shear forward + loud sound 1	0.13	Highest peak
3	0.175	Shear forward	0.14	Declining slope

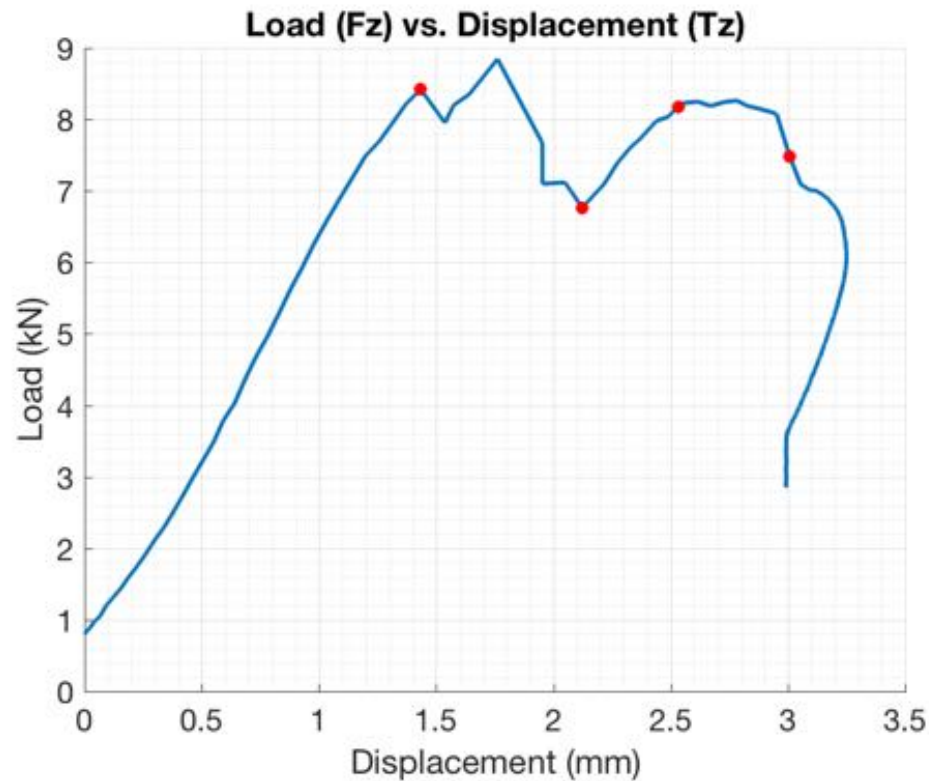




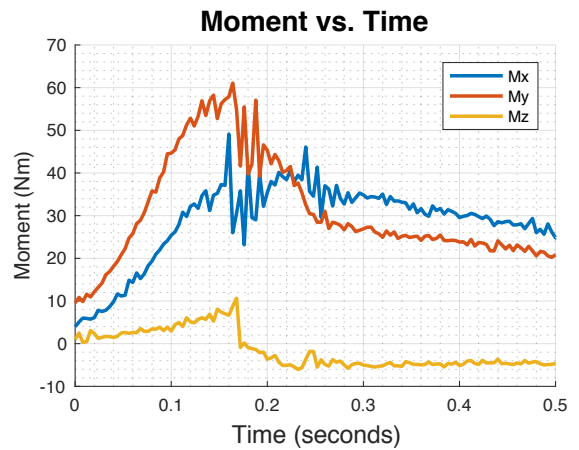
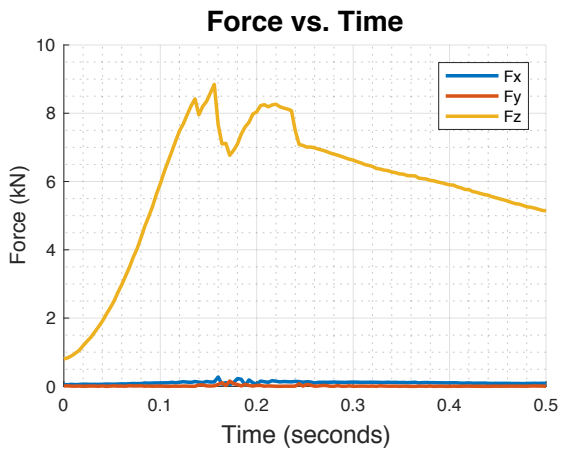
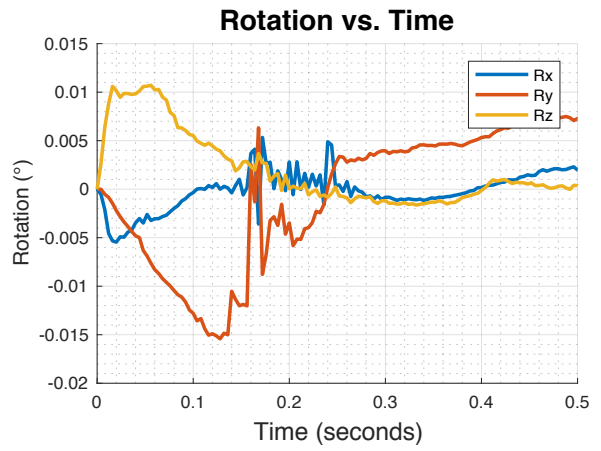
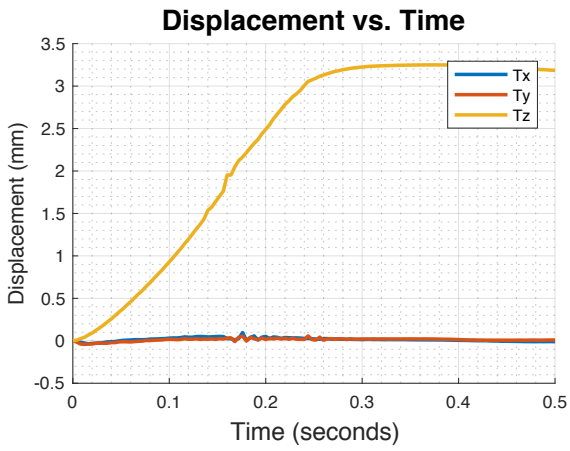
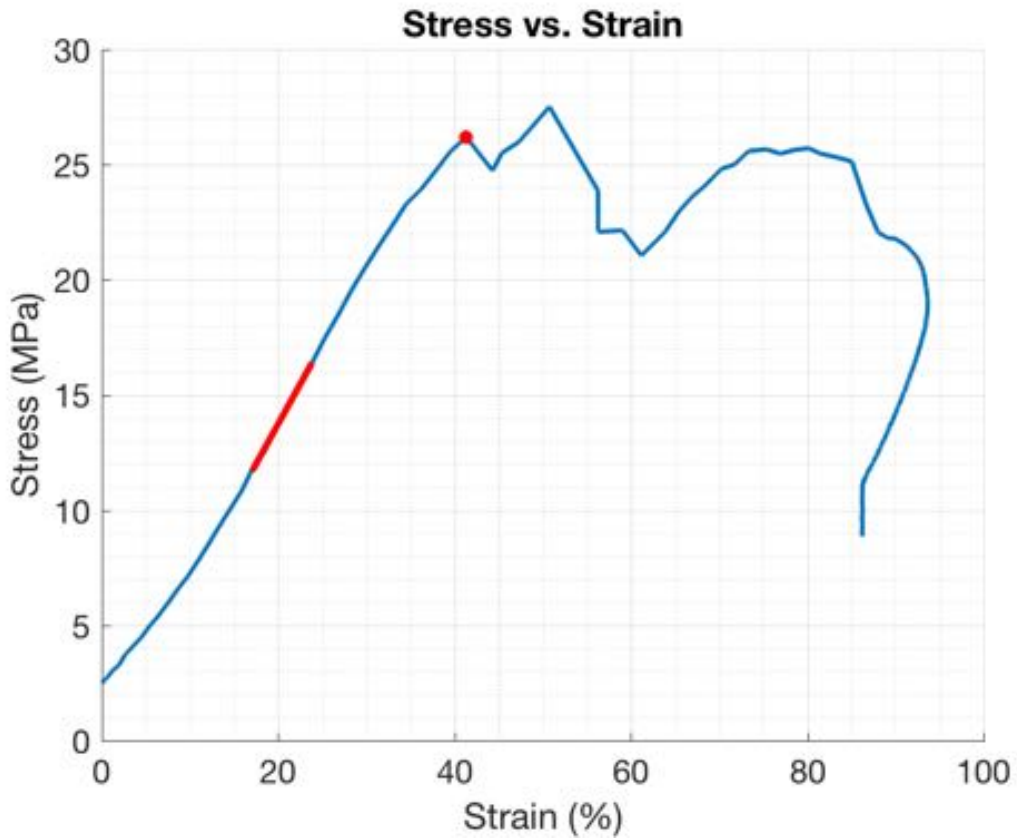
Failure Mode Assessment Summary			
	Load-displacement and video assessment	Photographic indicators	Classification
SO31	- Shearing of disc with respect to inferior vertebra	- Shearing of inferior endplate and inferior vertebra interface - Endplate fracture evident with nuclear material – consequent of shearing?	HER (POS) + EP-VER

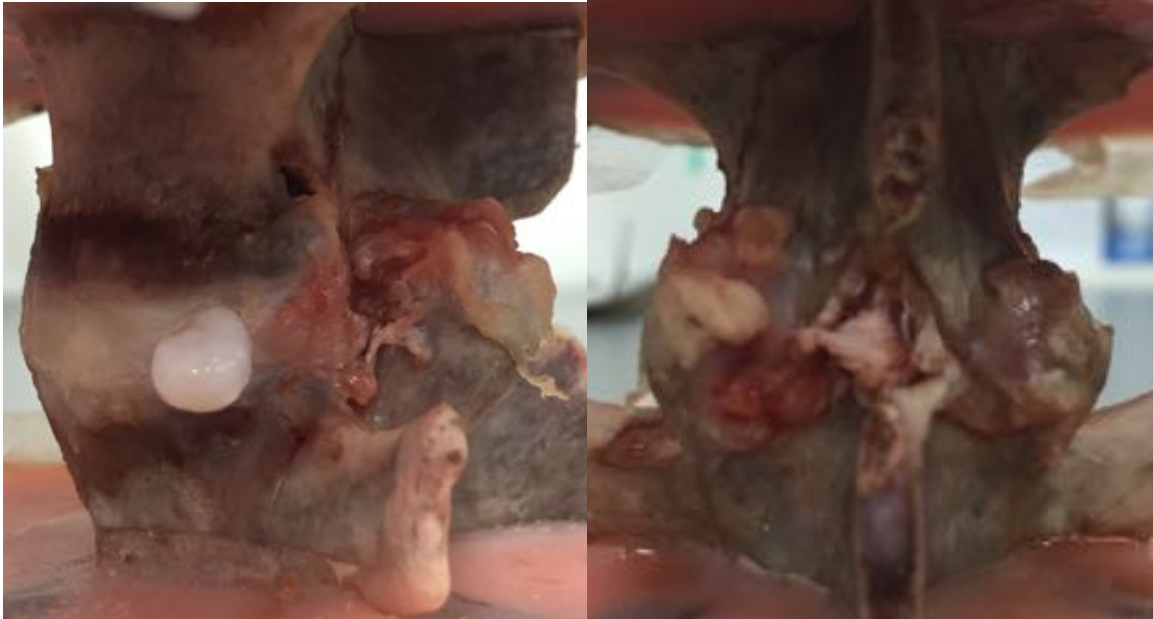
Specimen ID: SO32
Group: Facet Right Lateral Bending
Date tested: 14/8/2017

Failure load (kN)	Tz at failure (mm)	Time (s)	Moments (Nm)			Stress (MPa)	Strain	Modulus (MPa)	Toughness (MJ/m ³)	Observations		
			Mx	My	Mz					Test	Disc	Vertebra
8.42	1.43	0.156	35.83	53.48	5.68	26.19	41.34	69.2	5.9	AS, L-RAIL, POS-RAIL	L-POS	R+L PED



Identification of events by video & load vs. displacement comparison				
Event	Video		Load vs. Displacement	
	Time (s)	Description	Time (s)	Description
1	0.136	Left nucleus extrude + small sound	0.136	First small peak
2	0.172	Further bulging, more nucleus extrude, loud sound	0.156	Highest peak
3	0.203	Loud sound	0.172	Trough
4	0.24	Sound + shear forward / tear	0.216	Plateau before end of test





Failure Mode Assessment Summary			
	Load-displacement and video assessment	Photographic indicators	Classification
SO32	- Peak at 0.36 seconds and nucleus extrude at 0.4 seconds	- Massive left postero-lateral herniation and superior pedicle failure	HER(L-POS)

12.7 Appendix 7: Results Summary

Intact FSU Groups

ID	Posture	Failure Load (kN)	Tz at Failure (mm)	Moments			Max stress (MPa)	Max Strain (%)	Modulus (MPa)	Toughness (MJ/m ³)	Mode of failure
				Mx (Nm)	My (Nm)	Mz (Nm)					
SO1	FL	13.30	2.89	14.56	15.12	-5.07	27.18	78.62	50.6	8.52	HER (R-POS)
SO5	FL	6.75	2.63	16.03	2.33	-1.88	16.68	79.71	31.8	5.68	IN
SO9	FL	12.24	2.33	-36.48	-4.45	0.85	24.57	48.80	65.7	6.1	HER(R-POS)
SO12	FL	7.58	1.09	-36.32	-21.41	-4.11	17.57	32.62	45.9	3.4	ERROR
SO30	FL	8.15	2.00	-24.08	2.95	-5.55	17.61	60.56	37.8	4.7	VER (ANT)
SO2	LB	14.53	2.83	51.82	78.49	0.88	34.80	89.24	47.9	16.5	HER (POS)
SO6	LB	12.81	1.50	47.73	82.40	14.63	30.56	45.47	67.9	7.8	HER(L-POS)
SO7	LB	3.22	1.27	18.60	19.60	-1.59	6.03	32.38	16.0	1.2	ERROR
SO11	LB	11.73	1.24	124.64	92.73	10.87	29.42	27.51	98.4	5.0	HER(L-POS)
SO32	LB	8.42	1.43	35.83	53.48	5.68	26.19	41.34	69.2	5.9	HER(L-POS)
SO3	FL+LB	8.15	1.88	-0.66	62.33	11.20	18.09	47.41	43.9	5.5	EP-VER
SO8	FL+LB	8.28	1.72	-4.59	44.81	14.15	18.13	44.86	47.8	4.2	HER(L-POS) + EP-VER
SO10	FL+LB	5.90	0.77	-42.14	31.34	3.04	12.26	17.05	52.0	1.5	ERROR
SO13	FL+LB	5.91	2.58	3.59	33.49	10.12	13.72	77.38	25.2	4.4	HER(L-POS)
SO28	FL+LB	5.48	1.08	-12.74	46.32	5.20	12.58	32.81	35.8	3.0	IN
SO4	LB+AR	8.26	2.27	56.62	6.64	-28.60	19.99	54.12	48.0	5.1	HER(L-POS)

Isolated Disc Groups

ID	Posture	Failure Load (kN)	Tz at Failure (mm)	Moments			Max stress (MPa)	Max Strain (%)	Modulus (MPa)	Toughness (MJ/m ³)	Mode of failure
				Mx (Nm)	My (Nm)	Mz (Nm)					
SO15	FL	6.51	1.54	-21.75	-4.37	-4.23	14.31	28.58	57.2	2.2	HER (POS) + EP-VER
SO20	FL	5.78	2.12	-0.86	1.00	-3.49	14.30	47.38	38.1	3.2	EP-VER
SO24	FL	4.87	2.35	-3.27	2.35	0.25	13.28	69.62	24.1	4.2	VER
SO25	FL	5.07	2.07	-17.38	-11.00	-0.45	11.01	49.33	32.8	2.3	HER (POS) + EP-VER
SO29	FL	7.63	2.33	-12.11	11.26	0.36	14.92	51.78	42.7	3.1	EP-VER
SO14	LB	5.39	1.46	21.51	21.03	-2.15	12.96	38.20	40.3	2.3	HER(POS) + EP-VER
SO17	LB	7.48	1.68	0.82	47.90	-3.85	18.81	46.72	41.5	5.3	HER(L-POS) + EP-VER
SO19	LB	4.26	1.12	9.39	27.07	-3.03	10.99	29.43	36.9	1.9	EP-VER
SO22	LB	6.67	1.77	46.45	25.66	-2.14	13.81	40.13	38.7	2.5	HER (R-POS) + EP-VER
SO26	LB	3.59	0.31	16.71	52.72	-3.22	7.56	7.48	57.9	4.3	HER (R-POS) + EP-VER
SO16	FL+LB	5.29	1.48	-5.01	28.54	0.66	12.56	30.91	40.7	2.3	HER (L-POS) + EP-VER
SO18	FL+LB	4.60	0.97	-13.23	29.06	-1.87	10.41	20.86	43.8	1.3	HER (L-POS) + EP-VER
SO21	FL+LB	5.46	2.05	10.63	28.08	-1.27	11.75	46.67	30.7	2.5	HER (L-POS) + EP-VER
SO23	FL+LB	4.75	1.79	2.44	25.45	0.98	10.07	52.22	23.1	2.5	EP-VER
SO27	FL+LB	3.06	0.50	-13.04	15.99	1.25	6.29	11.98	34.2	5.4	HER (POS) + EP-VER
SO31	LB+AR	3.62	1.79	19.33	21.33	-6.51	9.31	55.36	18.7	2.9	HER (POS) + EP-VER

12.8 Appendix 8: Modes of Failure Statistics

Chi-Squared Likelihood Ratio test to assess correlation of variables with fail mode			
Inclusion Criteria	Category 1	Category 2	Significance (p-value)
All	Specimen type (intact/isolated)	Fail mode (herniation/vertebral)	0.001*
Intact	Direction of loading (FL, LB, FL+LB, LB+AR)	Fail mode (herniation/vertebral)	0.078
Isolated	Direction of loading (FL, LB, FL+LB, LB+AR)	Fail mode (herniation/vertebral)	0.471
Flexion	FSU (intact/isolated)	Fail modes	0.050*
Lateral bend	FSU (intact/isolated)	Fail modes	0.002*
Flexion and lateral bend	FSU (intact/isolated)	Fail modes	0.229
Lateral bend and axial rotation	FSU (intact/isolated)	Fail modes	0.096
Fail mode: Herniation	Direction of loading (FL, LB, FL+LB, LB+AR)	Site of failure (right postero-lateral, posterior, left postero-lateral)	0.055*

One-way ANOVA tests to compare modes of failure			
Inclusion Criteria	Grouping Variable	Dependent Variables	Significance (p-value)
Intact Flexion	Failure mode (herniation/vertebral)	Stress Strain Modulus Toughness	0.17 0.923 0.365 0.434
Intact Flexion and lateral bend	Failure Modes (herniation/herniation and endplate-vertebra shear)	Stress Strain Modulus Toughness	0.005* 0.045* 0.105 0.728
Isolated Flexion	Failure Modes (herniation/herniation and endplate-vertebra shear/vertebral)	Stress Strain Modulus Toughness	0.591 0.264 0.507 0.003*
Isolated Lateral bending	Failure Modes (herniation and endplate-vertebra/endplate-vertebra)	Stress Strain Modulus Toughness	0.687 0.862 0.497 0.755
Isolated Flexion and lateral bend	Failure Modes (herniation and endplate-vertebra/endplate-vertebra)	Stress Strain Modulus Toughness	0.958 0.236 0.122 0.469
Flexion and lateral bend Failure mode: Herniation and endplate-vertebra	Specimen type (intact/isolated)	Stress Strain Modulus Toughness	0.020* 0.173 0.141 0.016*

12.9 Appendix 9: Failure Parameters Statistics

Stress: Univariate two-way ANOVA analysis

Overall FSU and direction effect on stress	
Independent variable	p-value (2-tailed)
FSU	0.000**
Direction	0.000**
FSU*Direction	0.002**

Pairwise comparisons Directions		
Independent variable 1	Independent variable 2	P-value
Flexion	Lateral bend	0.032**
Flexion	Flexion and lateral bend	0.041**
Lateral bend	Flexion and lateral bend	0.000**

Pairwise comparisons FSU*Direction			
Direction	Independent variable 1	Independent variable 2	P-value
Flexion	Intact	Isolated	0.003*
Lateral bend	Intact	Isolated	0.000*
Flexion and lateral bend	Intact	Isolated	0.027*

Pairwise comparisons FSU*Direction			
FSU	Independent variable 1	Independent variable 2	P-value
Intact	Flexion	Lateral bend	0.001**
Intact	Flexion	Flexion and lateral bend	0.110**
Intact	Lateral bend	Flexion and lateral bend	0.000**
Isolated	Flexion	Lateral bend	1.000
Isolated	Flexion	Flexion and lateral bend	0.405
Isolated	Lateral bend	Flexion and lateral bend	0.720

Strain: Univariate two-way ANOVA analysis

Overall FSU and direction effect on Strain	
Independent variable	p-value (2-tailed)
FSU	0.038**
Direction	0.233
FSU*Direction	0.878

Modulus: Univariate two-way ANOVA analysis

Overall FSU and direction effect on Modulus	
Independent variable	p-value (2-tailed)
FSU	0.012**
Direction	0.007**
FSU*Direction	0.113

Pairwise comparisons Directions		
Independent variable 1	Independent variable 2	P-value
Flexion	Lateral bend	0.064*
Flexion	Flexion and lateral bend	0.854
Lateral bend	Flexion and lateral bend	0.006**

Pairwise comparisons FSU*Direction			
Direction	Independent variable 1	Independent variable 2	P-value
Flexion	Intact	Isolated	0.361
Lateral bend	Intact	Isolated	0.003*
Flexion and lateral bend	Intact	Isolated	0.664

Pairwise comparisons FSU*Direction			
FSU	Independent variable 1	Independent variable 2	P-value
Intact	Flexion	Lateral bend	0.024*
Intact	Flexion	Flexion and lateral bend	1.000
Intact	Lateral bend	Flexion and lateral bend	0.004*
Isolated	Flexion	Lateral bend	1.000
Isolated	Flexion	Flexion and lateral bend	1.000
Isolated	Lateral bend	Flexion and lateral bend	0.866

Toughness

Kruskal-Wallis H tests to compare failure parameters			
Inclusion Criteria	Grouping Variable	Dependent Variables	Significance (p-value)
All	Specimen type (intact/isolated)	Toughness	0.000*
Intact	Direction of loading (FL, LB, FL+LB)	Toughness	0.089
Isolated	Direction of loading (FL, LB, FL+LB)	Toughness	0.370
Intact	LB / FL+LB	Toughness	0.043*
Intact	FL / LB	Toughness	0.327
Intact	FL / FL+LB	Toughness	0.142
Isolated	LB / FL+LB	Toughness	0.602
Isolated	FL / LB	Toughness	0.465
Isolated	FL / FL+LB	Toughness	0.117